Hydropower in a changing climate : coupled modeling of hydrological and electricity systems for adaptation and mitigation

Laure Baratgin

INSTITUT POLYTECHNIQUE DE PARIS

NNT : 2024IPPAX078

Thèse de doctorat

Hydropower in a changing climate: coupled modeling of hydrological and electricity systems for adaptation and mitigation

Thèse de doctorat de l'Institut Polytechnique de Paris
préparée à l'École polytechnique

École doctorale n°626 École doctorale de l'Institut Polytechnique de Paris (EDIPP)
Spécialité de doctorat : Mécanique des fluides et des solides, acoustique

Thèse présentée et soutenue à Palaiseau, le 18 novembre 2024, par

LAURE BARATGIN

Composition du Jury :

Nathalie Voisin Professeure, Pacific Northwest National Laboratory	Rapportrice
Eric Martin Directeur de recherche, INRAE	Rapporteur
Anna Créti Professeure, Université Paris Dauphine	Présidente du jury
Sylvie Parey Ingénieure, EDF Lab Paris-Saclay	Examinatrice
Jan Polcher Directeur de recherche CNRS, Ecole polytechnique	Directeur de thèse
Philippe Quirion Directeur de recherche CNRS, CIRED	Co-directeur de thèse
Patrice Dumas Chercheur, CIRAD	Invité

Résumé détaillé

L'hydroélectricité joue aujourd'hui un rôle clé dans le paysage énergétique français, couvrant plus de 10% de la demande électrique nationale et contribuant significativement aux besoins de flexibilité du système électrique, notamment infra-journaliers. Toutefois, la production hydroélectrique française sera exposée à d'importants changements dans les années à venir. D'une part le réchauffement climatique accentue les contrastes saisonniers de précipitations et augmente la demande évaporative, modifiant ainsi les débits des rivières et donc la ressource disponible pour les centrales hydroélectriques. D'autre part, l'intégration croissante d'énergies renouvelables variables prévue par les politiques d'atténuation des émissions modifie les besoins de flexibilités du système électrique. Enfin, la gestion des réservoirs hydroélectriques dépend également des autres usages de l'eau et sera donc influencée par leur évolution.

Dans cette thèse, nous proposons une approche intégrée de modélisation pour quantifier et analyser ces différents effets et leur interaction. Notre méthodologie repose sur le couplage d'un modèle climatique de surface continentale (LSM) et d'un modèle d'optimisation du système électrique (PSM).

1. Représenter l'hydroélectricité dans les modèles hydrologiques par une approche basée sur la demande

La première partie du manuscrit décrit une méthode innovante pour représenter la gestion de l'eau pour l'hydroélectricité dans un LSM. La spécificité de notre approche réside dans l'utilisation d'une série temporelle de production cible, définie au niveau national, qui sert de référence pour déterminer les lâchers d'eau de chaque réservoir pour la production d'électricité. Les autres usages des réservoirs sont également pris en compte. Nous représentons notamment les lâchers d'eau nécessaires pour satisfaire les besoins environnementaux et d'irrigation, ainsi que le maintien d'un niveau d'eau minimal en été dans les réservoirs dédiés au tourisme.

Nous implémentons cette méthode dans le modèle ORCHIDEE et considérons le réseau hydroélectrique français comme cas d'étude. Après avoir caractérisé la performance hydrologique du modèle sur les bassins versants français, nous montrons que cette la méthode implémentée simule de façon réaliste l'évolution annuelle du stock hydraulique et la production hydroélectrique nationale. Par ailleurs, elle améliore la simulation des débits des rivières dans les petits bassins versants de montagne fortement impactés par l'hydroélectricité.

2. Représenter des contraintes hydroélectriques dynamiques dans un modèle électrique

Les contraintes sur la flexibilité des centrales hydroélectriques sont représentées grossièrement dans la majorité des modèles électriques. En particulier, ces modèles reposent souvent sur des contraintes statiques, alors que celles-ci évoluent en réalité avec la variabilité météorologique, le climat et l'opération des réservoirs pour les autres usages de l'eau.

La deuxième partie du manuscrit propose d'utiliser les simulations hydrologiques issues du LSM pour définir des contraintes dynamiques à utiliser dans les modèles électriques. Ces contraintes incluent notamment des limites de production horaire minimale et maximale des centrales, qui tiennent compte des lâchers d'eau minimums pour l'environnement et l'irrigation, des variations de hauteur d'eau dans les réservoirs et de la contrainte touristique. En comparant les résultats des simulations aux observations disponibles, nous montrons qu'une telle approche améliore sensiblement la production simulée par le modèle par rapport à la version initiale. Elle permet notamment de tenir compte des changements de production induits par des changements du climat, du mix électrique ou des autres usages de l'eau.

3. Explorer le futur de la production hydroélectrique française

La troisième partie du manuscrit utilise les méthodes développées précédemment pour explorer les scénarios futurs de la production hydroélectrique en France dans le contexte du changement climatique et de l'intégration croissante d'énergies renouvelables variables.

Nous trouvons un effet limité du changement climatique sur la production hydroélectrique à l'échelle annuelle mais des contrastes saisonniers plus marqués, avec une augmentation de la production en hiver et une diminution en été. Par ailleurs, l'intégration d'énergies renouvelables variables modifie le profil de production des centrales réservoirs et augmente la valeur de la flexibilité offerte par les réservoirs hydroélectriques.

Toutefois, notre étude met aussi en évidence une importante incertitude sur les niveaux futurs de production hydroélectrique et les prix de l'électricité. La première incertitude est liée aux projections climatiques, et provient notamment des difficultés des modèles à représenter la précipitation dans les régions montagneuses. La seconde est due aux incertitudes des coûts de production des centrales thermiques décarbonées, qui seront nécessaires pour couvrir les besoins de flexibilité d'un mix énergétique neutre en carbone.

Remerciements

Voici venu le moment d'écrire les derniers mots de ce manuscrit, qui clôturent trois années de thèse. Une aventure que je termine comme je l'ai commencée avec une articulation dans le plâtre ! Ce fut un voyage riche en émotions et apprentissages.

Je voudrais commencer par remercier mes directeurs de thèse, Jan et Philippe, qui m'ont accompagnée tout au long de ce parcours, depuis l'élaboration du sujet jusqu'à la soutenance. Merci pour votre disponibilité et vos conseils, tant sur volet académique qu'humain. Je souhaite également remercier très chaleureusement Patrice, qui m'a aussi guidée pendant ces trois ans. Merci pour nos discussions en visio et tes commentaires toujours très pertinents. Je m'estime très chanceuse d'avoir pu bénéficier de l'encadrement de votre trio, et je pense qu'on a formé une bonne équipe !

Un grand merci à mes collègues, qu'ils soient à l'ouest ou à l'est de Paris ! Merci aux jeunes chercheurs et ingénieurs du LMD à Polytechnique pour l'ambiance conviviale du labo, et les traditionnels gâteaux du mercredi après-midi. Même si je suis venue moins fréquemment vers la fin de ma thèse, j'ai toujours apprécié ces moments partagés avec vous ! Merci également à mes collègues du CIRED pour la joyeuse atmosphère qu'il y règne. Les parties de ping-pong, les week-ends de glisse (estivale et hivernale), et les verres au Rosa Bonheur ou à Paris, ont été des instants précieux qui m'ont aidé à rester motivée tout au long la thèse.

Enfin, je remercie ma famille et mes amis pour leur présence et leur soutien. Je remercie particulièrement ma maman qui a eu le courage de relire le manuscrit. Et merci enfin à Charles, pour m'avoir soutenue et supportée pendant ces trois ans et avoir préparé de délicieux repas pendant que je "lançais des simulations" :).

Contents

1 Introduction **1**
- 1.1 Hydropower in the French Energy system . . . 2
  - 1.1.1 Several types of hydropower plant . . . 2
  - 1.1.2 French energy policies . . . 3
  - 1.1.3 Managing the variability of renewables . . . 4
  - 1.1.4 Modeling future power systems . . . 5
- 1.2 The impact of climate change on the water-energy nexus . . . 6
  - 1.2.1 Modeling climate change and its impacts on the hydrological cycle 6
  - 1.2.2 Modeling the continental hydrological cycle . . . 7
  - 1.2.3 The hydrological cycle under climate change . . . 10
  - 1.2.4 Climate change and the power sector . . . 14
- 1.3 Contributions and manuscript overview . . . 16
  - 1.3.1 Scientific questions . . . 16
  - 1.3.2 Manuscript overview . . . 17

I Representing hydropower operations in hydrological models - A demand-based approach **21**

2 Presentation of the modeling framework **23**
- 2.1 Introduction . . . 24
  - 2.1.1 Background and motivation . . . 24
  - 2.1.2 Objectives . . . 25
- 2.2 Presentation of the modeling approach . . . 25
  - 2.2.1 Definition of a routing network that includes hydropower connections 26
  - 2.2.2 Dams and reservoir parametrization . . . 28
  - 2.2.3 Water demands . . . 31
  - 2.2.4 Validation diagnostics . . . 33
  - 2.2.5 Calibration . . . 34
- 2.3 Summary . . . 35

3 Implementation in the ORCHIDEE model and validation with the French study case **37**
- 3.1 Data and methods for the study case over France . . . 38
  - 3.1.1 ORCHIDEE setup . . . 38
  - 3.1.2 Infrastructure datasets . . . 39
  - 3.1.3 Data for water demands and validation . . . 41

3.2 Assessment of the performance of ORCHIDEE to simulate river discharges in France . . . 43
3.2.1 Bias in average discharge . . . 43
3.2.2 Discharge seasonality . . . 46
3.3 Results . . . 47
3.3.1 Calibration . . . 47
3.3.2 Hydropower operations . . . 50
3.3.3 Effects of hydropower operations on river discharges . . . 53
3.4 Discussion and conclusion . . . 54
3.4.1 Summary of the work . . . 54
3.4.2 Limitations and opportunities for improvements . . . 55
3.4.3 Sources of uncertainties . . . 56
3.4.4 Perspectives . . . 57

4 Supplementary analysis and extended results 59
4.1 Which rule to model the coordinated operation of a hydropower network? - Comparison of different rules . . . 60
4.1.1 Introduction . . . 60
4.1.2 Methods . . . 61
4.1.3 Results . . . 63
4.1.4 Conclusion . . . 67
4.2 Representing the management of pumped hydro storage (PHS) plants . . . 67
4.2.1 Presentation of French PHS plants . . . 67
4.2.2 PHS modeling . . . 68
4.2.3 Results . . . 70
4.2.4 Discussion - Competition with reservoir production . . . 71

II Representing dynamic hydropower constraints in power system models 73

5 Coupling a power system model with a hydrological model improves the representation of hydropower flexibility 75
5.1 Introduction . . . 76
5.2 Model presentation . . . 78
5.2.1 ORCHIDEE land surface model . . . 79
5.2.2 EOLES-Dispatch power system model . . . 80
5.2.3 Coupling approach . . . 81
5.3 Simulation framework . . . 83
5.3.1 ORCH_EOLES - Procedure for coupling the two models . . . 84
5.3.2 Data inputs . . . 84
5.4 Results . . . 86
5.4.1 Improvements in simulated hydropower production . . . 86
5.4.2 Impacts of a change in the power mix on the hydropower generation 89
5.4.3 Impacts on the European power system . . . 91
5.4.4 Identifing the main drivers of the change . . . 92
5.5 Discussion . . . 93
5.5.1 Increasing the complexity while maintaining a simple linear model with a representative reservoir plant . . . 93
5.5.2 Discrepancy between simulated production and historical data . . . 95

5.5.3 Improving reservoir operations in the hydrological model 96
5.6 Conclusion 97
5.7 Supplementary material: Further insights on hydropower modeling in EOLES-Dispatch 97
5.7.1 Simulation area 97
5.7.2 Distinguishing poundage and run-of-river power plants 99

III The future of hydropower in the French power system under climate change 101

6 Exploring the joint impacts of climate change and renewables penetration on French hydropower generation 103
6.1 Introduction 104
6.2 Methods and data 105
6.2.1 Modeling framework 105
6.2.2 Climate scenarios 108
6.2.3 Power system scenarios 108
6.3 Results 110
6.3.1 Stand-alone ORCHIDEE simulations 110
6.3.2 Coupled simulations - Impacts of climate change on reservoir operations in the 2019 power scenario 113
6.3.3 Coupled simulations - Economic consequences of the hydrological changes in the 2019 power scenario 114
6.3.4 Coupled simulations - Joint impacts of renewable energy integration and climate change 116
6.3.5 Coupled simulations - Impact on the overall power system 121
6.4 Discussion 121
6.4.1 Limitations of the study 121
6.4.2 Climate change uncertainties 122
6.4.3 Uncertainties of future power systems 123
6.5 Conclusion 123

7 Uncertainties of climate projections 125
7.1 Sensitivity to radiative concentration scenarios 126
7.1.1 Introduction 126
7.1.2 Results 126
7.2 Role of the bias-correction method 130
7.2.1 Introduction 130
7.2.2 Description of the ADAMONT bias correction method 130
7.2.3 Results 131
7.2.4 Conclusion 135

8 The evolution of pumped hydro storage profitability with the integration of renewable energies 137
8.1 Introduction 138
8.2 The business model of PHS plants 138
8.2.1 Investment costs 138
8.2.2 Various sources of revenue and estimates for 2019 139
8.2.3 Balance 140

8.3 Modeling reserves in power system models . . . 141
8.3.1 Implementation of the reserves mechanism in EOLES-Dispatch model 141
8.3.2 Validation . . . 143
8.4 Evolution of the revenues from PHS plants in 2050 . . . 145
8.4.1 Revenues from reserves . . . 145
8.4.2 Energy market . . . 147
8.4.3 Conclusion . . . 148

9 Conclusions and perspectives **151**
9.1 Main findings . . . 152
9.1.1 How to represent hydropower operation in a climate model considering the needs for power system balancing? . . . 152
9.1.2 How to represent dynamic hydropower constraints in power system models? . . . 152
9.1.3 How will hydropower production evolve in the future French power system under climate change? . . . 153
9.2 Perspectives for future research . . . 154
9.2.1 Towards a better assessment of climate change impacts on power systems . . . 154
9.2.2 Enhancing the representation of water management in land surface models (LSMs) . . . 155
9.2.3 Dealing with climate uncertainties . . . 157
9.3 Broader implications . . . 157

A Supplementary data for Part I **159**
A.1 Building the routing network . . . 159
A.1.1 Locating hydroelectric infrastructures on the river network . . . 159
A.1.2 Adduction network . . . 160
A.2 Alternative precipitation datasets . . . 160
A.2.1 Presentation of the datasets . . . 160
A.2.2 Simulation of hydropower production under SAF_SPAZM . . . 161
A.2.3 Simulation of hydropower production under SAF_COM . . . 161
A.3 Conversion factors for hydropower generation . . . 164

B Supplementary data for Part II **165**
B.1 Convergence of the iterations . . . 165
B.2 Thermal plants assumptions . . . 169
B.3 2050 power mix . . . 169
B.3.1 Power demand . . . 169
B.3.2 Interconnections . . . 170

C Supplementary data for Part III **173**
C.1 Climate simulations . . . 173
C.2 Simulation of electricity prices . . . 177
C.3 Net load pattern . . . 178

Bibliography **179**

CHAPTER 1

Introduction

Since 1850, human-induced greenhouse gas emissions have increased continuously, leading to a significant rise in global temperature (IPCC, 2021b). By 2022, the global annual mean temperature had risen by approximately 1.2 °C compared to 1850. To tackle global warming and its negative impacts, 195 world leaders concluded the Paris Agreement in 2015, in which they committed *"to substantially reduce global greenhouse gas emissions to hold global temperature increase to well below 2°C"*. However, the measures taken thus far are largely insufficient to achieve this objective.

Approximately 90% of global greenhouse gas emissions stem from the combustion of fossil fuels, which account for 66% of final energy consumption. A major strategy for reducing greenhouse gas emissions is therefore to decarbonize energy production, in particular through the electrification and the integration of renewable energy sources, which represents one of the most cost-effective solutions. France, like other European countries, has set ambitious targets for the expansion of solar and wind power plants. As the generation of electricity from these sources is subject to the vagaries of weather, flexible solutions that can bridge the gap between consumption and generation are crucial for the security of the electricity supply. In this context, existing hydropower infrastructure is of particular value due to its low carbon emissions and generation costs.

Concurrently, global warming affects all climate variables such as precipitation, solar radiation and wind, potentially impacting every component of the electricity system — from power generation to electricity demand and the transmission grid. In particular, the observed and expected changes in the hydrological cycle may significantly alter hydropower generation. In addition, human water management is also modifying the availability of water for hydropower production, and climate change may increase competition for water use.

This manuscript aims to investigate how these different effects interact with the production of hydropower. Focusing on the French context, we have developed an interdisciplinary modeling framework to analyze the future role of hydropower. This first chapter introduces the key concepts addressed in the manuscript and the research questions it aims to answer.

Contents

1.1 Hydropower in the French Energy system 2

1.1.1 Several types of hydropower plant 2

1.1.2 French energy policies 3

1.1.3 Managing the variability of renewables 4

1.1.4 Modeling future power systems 5
1.2 The impact of climate change on the water-energy nexus . . 6
1.2.1 Modeling climate change and its impacts on the hydrological cycle 6
1.2.2 Modeling the continental hydrological cycle 7
1.2.3 The hydrological cycle under climate change 10
1.2.4 Climate change and the power sector 14
1.3 Contributions and manuscript overview 16
1.3.1 Scientific questions 16
1.3.2 Manuscript overview 17

1.1 Hydropower in the French Energy system

1.1.1 Several types of hydropower plant

Hydropower harnesses the potential energy of water to generate electricity. This process was developed in France at the end of the 19th century. The mechanism involves water spinning and driving a turbine, which in turn is connected to the generator that produces electricity. Power output P is a function of the efficiency of the plant η, the head h (difference in height between the water source and the plant) and the volumetric flow rate Q (see Eq. 1.1, where ρ is the density of water and g the gravity acceleration).

$$P = \eta \rho g h Q \tag{1.1}$$

Hydroelectric plants are typically distinguished based on their discharge time, which is defined as the theoretical time required to empty the upstream reservoir (if any) when operating at maximum power. This classification delineates various services for the power system. In France, the transmission system operator (TSO) RTE classifies hydropower plants into four types:

- **Run-of-river plants** are mainly situated in flatter areas, along large rivers. They have no or negligible reservoirs (discharge time less than 2 hours) and use the instantaneous flow of the river to provide power. This production is non-dispatchable as the water cannot be stored for later use.
- **Poundage plants** have higher storage capacity and can adjust their production throughout the day or even the week (discharge time up to 400h). This flexibility enables them to follow variations in consumption over these horizons, such as morning and evening consumption peaks, as well as the difference between working days and weekends.
- **Reservoir plants** have greater storage capacity, which allows for seasonal water storage (with a discharge time greater than 400h).
- **Pumped-hydro storage (PHS) plants** are reversible. They can function in pump mode to lift water from a downstream basin to an upstream basin, or in turbine mode to generate electricity. They store thus gravitational energy when electricity prices are low and make it available when they are high.

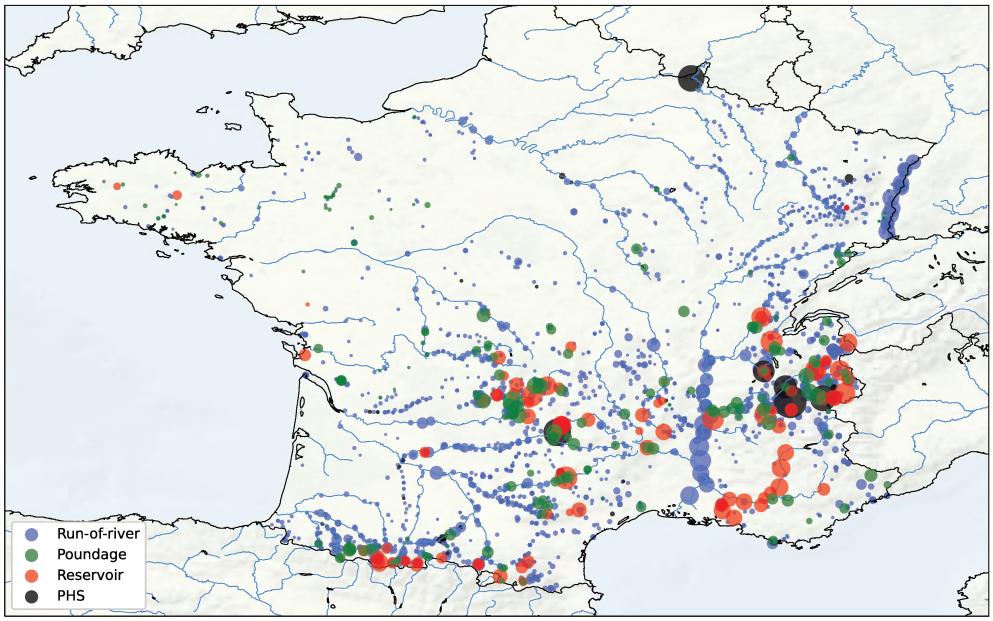

Figure 1.1: Location of French hydropower plants (based on ODRÉ (2022))

	Total	Run-of-river	Poundage	Reservoir	PHS
Installed capacities in GW (ODRÉ, 2022)	25.39	7.79	3.73	8.79	5.06

Table 1.1: Installed capacities by type of plants and annual productions

There are over 2500 hydroelectric power plants in mainland France, with a total installed capacity of 25.7 GW (Fig. 1.1). The breakdown of this total capacity into the different categories of plants is detailed in Table 3.1.

Figure 1.2 shows the annual production in recent years and highlights its significant inter-annual variability. This variability is particularly high for reservoir plants, with a -35.5% decline in annual production in 2022 compared to 2021. In comparison, total hydropower production declined by 20% in 2022 compared to 2021.

1.1.2 French energy policies

France has set ambitious goals for mitigating climate change, aiming to reduce its greenhouse gas emissions by 33% by 2030 relative to 2022 and achieve carbon neutrality by 2050. Currently, two-thirds of France's emissions stem from the combustion of fossil fuels, which still provide 60% of the final energy consumption. In contrast, electricity, accounting for 25% of final energy consumed, boasts a significantly low carbon footprint due to the substantial contribution of nuclear power plants (accounting for 69% of electricity production), hydroelectric facilities (12%), and other renewable sources (10%). To honor its climate commitments, the French strategy, formalized in the SNBC (National Low Carbon Strategy), relies on several drivers:

- Electrification of major fossil fuel-consuming sectors (road transportation, building heating and industry), with a target of 55% of final energy consumption supplied by electricity by 2050 (compared to only 25% in 2021);

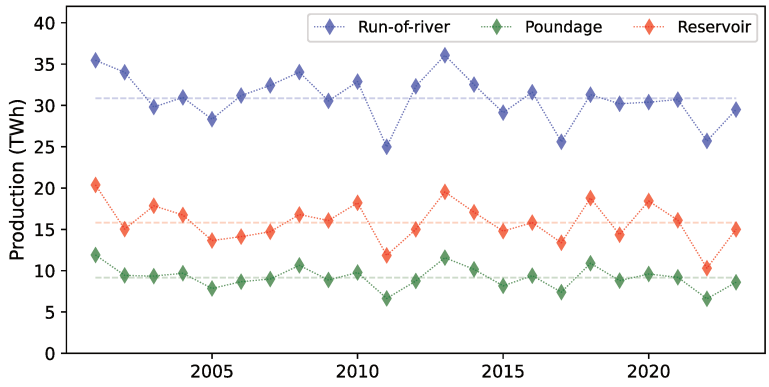

Figure 1.2: Annual production by hydropower plant type (RTE, 2023a).

- Transitioning to decarbonized fuels, including a portion of green hydrogen whose production requires electricity;
- Reducing overall energy consumption through efficiency and sufficiency measures, with a target of a decrease by 40% in final energy consumption between 2020 and 2050.

This results in a projected increase in overall electricity demand, estimated to rise from 500 TWh today to 645 TWh by 2050, according to RTE (2021), necessitating the integration of new electrical production capacities within the national territory. Additionally, a considerable number of existing nuclear power plants are nearing the end of their operational lifespan, further accentuating the need for new capacities in the coming years.

To shed light on this critical issue, RTE (2021) documents the different options and analyzes them along four dimensions: technical, economic, environmental and societal. The study proposes six contrasting scenarios for the future of France's power generation fleet, all capable of managing the necessary energy transition. The scenarios differ in terms of the construction of new nuclear plants. In 2023, the French government decided to build six new reactors, putting France on one of the trajectories with new nuclear defined in RTE (2021).

In all these scenarios, a significant integration of wind and photovoltaic (PV) power plants is foreseen. However, the current rate of their deployment lags behind forecasts. For instance, in December 2023, 1.4 GW of offshore wind power was installed, compared with a target of 2.4 GW set in the law (such objectives are fixed in the *Programmation Pluriannuelle de l'Energie* (PPE)). Concerning hydropower, no significant new installation is planned for run-of-river, poundage, and reservoir power plants. Nevertheless, the modernization of existing facilities and the deployment of small-scale hydroelectricity are expected to lead to a small increase in the installed capacity of these three types of plants, with the PPE forecasting an increase of 0.9 to 1.2 GW by 2028. Conversely, the PPE anticipates the installation of new PHS plants, with a potential of 1.5 GW that should be commissioned between 2030 and 2035. In their scenarios, RTE (2021) project an additional 3 GW in installed capacity of PHS plants.

1.1.3 Managing the variability of renewables

The production of solar PV and wind power plants varies with meteorological conditions and cannot be perfectly forecasted. Thus, maintaining system adequacy – the ability of

a power system to cope with load at all times – becomes a challenge when integrating renewables in power systems (IEA, 2021).

The flexibility of a power system refers to its ability to modify or buffer electricity production or consumption in response to variability, expected or not. Many balancing options can provide flexibility, including dispatchable generators, transmission capacities, energy storage assets, demand-side management and sector coupling. Dispatchable generation, particularly from thermal and hydropower plants, is currently the dominant source of system flexibility for both short- and long-duration timescales.

IEA (2023) explores the relative contribution of the different flexibility options for power mix with a very high share of wind and PV (over 70%) and shows that different mixes of flexibility resources are required to manage variability across timescale (short duration and seasonal) and climate zones. For example, if a high share of PV plants is installed, batteries play a critical role in balancing the hourly and daily variation of solar production. In temperate zones like France, where wind and solar PV have complementary seasonal generation patterns, IEA (2023) finds that thermal and hydropower plants remain the dominant sources of system flexibility for both short and long-duration timescales.

However, even for plants equipped with reservoirs able to store water, hydropower production remains dependent on the hydrological conditions. It is exposed to significant interannual variations (as illustrated in Fig. 1.2) and to potential impacts of climate change. Weather and climate aspects are therefore necessary to address as part of energy infrastructure planning.

1.1.4 Modeling future power systems

To assess the feasibility of future energy systems, modeling tools are required. In particular, operation models have been developed to represent the hourly dispatch of a power system (Emmanuel et al., 2020; Oikonomou et al., 2022). The objective of dispatching is to ensure the security of supply while minimizing the overall system cost. In the context of a developed and complex power system, the responsibility for dispatching usually resides with the TSO. In many countries, this phase takes place on the market. Owners of generating units bid their production onto the market, whereby a merit order is established according to the bid prices. The system operator then dispatches generating units according to residual demand and based on the merit order.

Dispatching models represent the decision-making of TSOs when it comes to dispatch. They have to take into account the generation constraints applying to the different power plants such as starting and ramping constraints of thermal plants. Hydropower production is also subject to some constraints, related to water availability and multi-objective water management priorities such as flood control, water supply, environmental flows, navigation and recreation (Oikonomou et al., 2022). These constraints are challenging to integrate in power system models and various refinements are used depending on the model (Oikonomou et al., 2022; Rheinheimer et al., 2023).

Many dispatching models exist, which have been used in an increasing number of studies. Some examples are PyPSA (Brown et al., 2017; Hörsch et al., 2018), DIETER (Zerrahn et al., 2017), EOLES (Shirizadeh et al., 2021), and PLEXOS (Brinkerink et al., 2021).

1.2 The impact of climate change on the water-energy nexus

Hydropower is embedded in the water cycle (represented in Fig. 1.3), in particular because its production depends on river discharges. Water evaporates from the land and oceans and enters the atmosphere as water vapor. It then condenses into clouds and falls as liquid or solid precipitation. This precipitation is intercepted by vegetation, soaks into the ground, or runs off at the surface. As it flows into groundwater or rivers, water can be abstracted by humans for a variety of uses, including energy production, agriculture, and industry. It can then be returned to the river (non-consumptive use) or evaporated to the atmosphere (consumptive use).

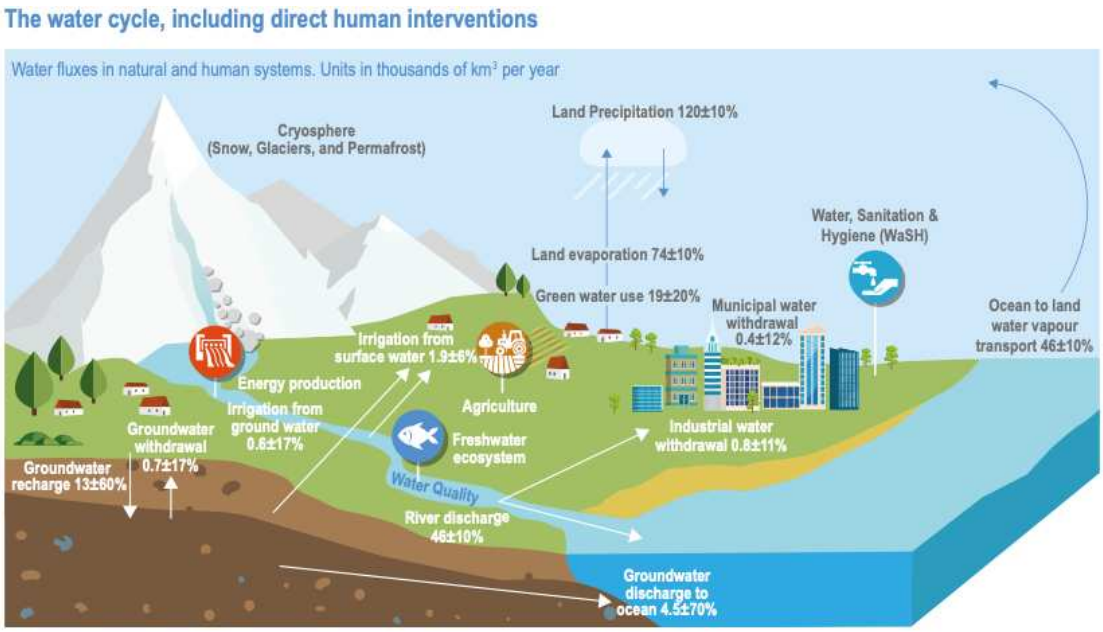

Figure 1.3: The water cycle including direct human interventions (IPCC, 2022a).
Natural water fluxes are shown from IPCC (2021a), and human water withdrawals for various sectors from Hanasaki et al. (2018). Green water use (Abbott et al., 2019) refers to the use of soil moisture for agriculture and forestry. Irrigation water use is not included in green water use.

Human-induced climate change intensifies the water cycle (IPCC, 2021a), threatening water security in various regions. Continued greenhouse gas emissions will lead to increasing global warming, with further impacts on the hydrological cycle.

1.2.1 Modeling climate change and its impacts on the hydrological cycle

1.2.1.1 Modeling chain for impact studies

To enhance our understanding of climate change and its likely impacts on the climate system, global climate models (GCMs) are used. They are complex numerical representations of the major climate system components (atmosphere, land surface, ocean and sea ice), and their interactions. Driven by different scenarios of increased greenhouse gas concentration - also called *Representative concentration pathways (RCPs)* -, they provide projections of future climatic conditions. Such models are run at coarse resolution, typically 100km, which limits the fine representation of the many physical processes that occur on smaller scales, such as cloud formation or land surface processes. To account

for these subgrid-scale processes, GCMs use parametrization, which introduces inherent uncertainty and biases into the model outputs. To deal with the significant uncertainty of such climate projections, the outputs of the various GCMs are compared in collective initiatives such as the Coupled Model Intercomparison Project (CMIP).

To produce climate projections at smaller scales, GCMs are "*downscaled*" using either dynamical or statistical methods. Dynamical downscaling involves using the output of the GCM as the input for a finer regional climate model (RCM) that recalculates climate at a finer scale using local features.

Finally, to study specific climate components, in particular the continental water cycle, an additional model should be used, driven by the climate projection simulated by GCM-RCM couples. In order to be used as an input for process-based impact models, output from climate models is usually post-processed to reduce its systematic biases (i.e., the errors compared to observations over a reference, present-day period) (Ehret et al., 2012). Bias correction techniques are statistical methods that usually employ a transfer function to match the cumulative distribution functions (CDFs) of modeled and observed data.

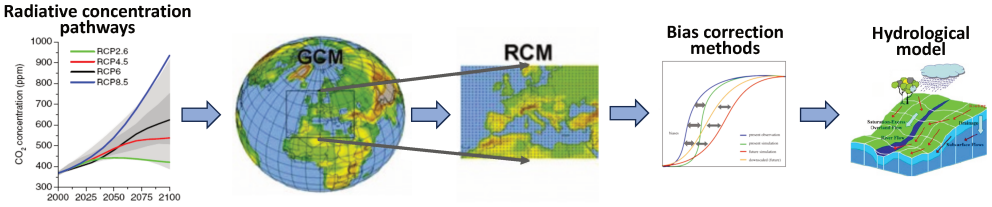

Figure 1.4: Description of the modeling chain for climate impact studies. Source: Author.

Figure 1.4 illustrates the complete modeling chain which allows the simulation of the evolution of river discharges in response to increased human gas emissions. It is important to keep in mind that each step introduces some level of uncertainty and biases to the final output. To better quantify this cascade of uncertainty, it is necessary to multiply the possibilities retained at each step.

The Explore2 project is an application of this modeling chain. Funded by the French Ministry of Ecological Transition and the French Biodiversity Agency, it aims to improve the knowledge of the impacts of climate change on French rivers. This project builds on 9 hydrological models to generate river flow time series, based on 3 contrasting greenhouse gas emission scenarios and a set of 17 climate models that have been corrected by 2 bias correction methods (Sauquet et al., 2022).

1.2.2 Modeling the continental hydrological cycle

Modeling the continental part of the water cycle presented in Fig. 1.3 is key for the monitoring of water resources and the prediction of their evolution under changing climate, land use or water management practices. Different approaches have been developed to build such models. Two categories are usually distinguished.

1.2.2.1 Calibrated parsimonious hydrological models

These models aim at reproducing well but as simply as possible the relationship between discharge and climate variables. Most complexities are aggregated within parameters that are adjusted over the area of study to best fit observed data. The calibrated model can

then be used to extrapolate streamflow to unmonitored areas with similar characteristics or to predict streamflow over the same area in future times.

One example of parsimonious models is the family of models GR (Perrin et al., 2003), which was developed to reproduce streamflow at the catchment level for a daily time step. The catchment is conceptualized as a series of interconnected reservoirs, connected by transfer functions. The dimensions of the reservoirs and the transfer coefficients are then calibrated. These models provide highly accurate catchment discharge models for a variety of contrasting catchments in France and around the world (Oudin et al., 2008).

Parsimonious models are simple to use and accurate to represent streamflow over the period and scale over which they were designed and adjusted. They are very useful to predict streamflow in the short/medium term, or over unmonitored areas for water management purposes. However, they rely on the assumption that the adjusted parameters are invariant and independent of trends in the forcing data. In other words, the system considered is assumed to be stationary, which may be questionable in the face of climate change (Coron et al., 2014; Duethmann et al., 2020).

1.2.2.2 Physical-based distributed hydrological models

These models represent the physical processes based on mathematical equations. They are spatially distributed, decomposing the spatial area into fine grids in each of which the water balance is calculated. Historically, two distinct communities have developed physical-based models to represent water cycle processes (Telteu et al., 2021):

- The climate community has developed **Land Surface models (LSMs)**, initially designed to provide realistic land boundary conditions to GCMs. LSMs contain interconnected computational modules that characterize physical processes related to soil, vegetation, and water, and account for their influence on water, energy and carbon exchanges (Nazemi et al., 2015a). A wide range of LSMs is currently available - some examples being the Community Land Model (CLM) (Oleson, 2010), ISBA (Noilhan et al., 1996), MATSIRO (Takata et al., 2003), and ORCHIDEE (Krinner et al., 2005). Progressive development has been done in representing various components of the hydrological cycle, such as soil moisture, vegetation, snowmelt and evaporation (Stephens et al., 2023).
- The hydrological community has developed **Global Hydrological Models (GHMs)**. Similar to LSMs, they are gridded large-scale models but are typically simpler in their structure, as they mainly focus on representing the water cycle. In particular, the energy budget is not computed within the model, so the potential evapotranspiration is computed based on the exogenous atmospheric variables. They simulate the different water flows, water storage compartments, and human water use sectors. The main focus is streamflow simulation and their ability to reproduce historical observations of these variables. Some examples of existing GHMs are PCR-GLOBWB (Sutanudjaja et al., 2018), VIC (Newman et al., 2017), and WaterGAP2 (Döll et al., 2012).

The offline use of LSMs as independent global hydrological models has emerged in recent decades for the evaluation of water resources and the investigation of climate change impacts at both regional and global scales (Huang et al., 2024). Major developments have been made to enhance their hydrological simulations, in particular through the incorporation of more detailed catchment-scale processes and river routing (how rivers flow through the landscape) (Shaad, 2018; Sheng et al., 2017). These improvements have

notably been driven by the development of RCMs that required a finer representation of hydrological processes (Polcher et al., 2023). LSMs and GHMs can therefore be used similarly driven by climate projections to study the impact of climate change on the water cycle, such as represented in Fig. 1.4. In the remaining part of the chapter, the term *"Hydrological models"* will therefore englobe both GHMs and LSMs used in this purpose.

Physical-based models represent a valuable tool for explicitly representing physical processes that govern water flows and storage. In comparison to parsimonious models, they are better able to account for spatial variability in basin properties and are more robust for simulating outside the range of calibration conditions, such as long-term future scenarios. However, they require extensive input data, including topography, soil properties, and vegetation, and are computationally demanding. Moreover, they necessitate numerous parameters that are challenging to measure directly and must be calibrated.

1.2.2.3 Accounting for the anthropization of the water cycle

As represented in Fig. 1.3, human activities are embedded in the continental water cycle and may exert a significant influence on the water flows (Nazemi et al., 2015a). For instance, surface-water withdrawals for supplying human needs decrease downstream flows, often substantially, and result in a seasonal decline in flows of major rivers (Haddeland et al., 2014). All regions are not equally impacted, as depicted in Fig. 1.5 for Europe. Moreover, dam operations may considerably change the timing and volume of natural streamflow in some areas (Biemans et al., 2011). Representing the effect of human activities on the water cycle within hydrological models is therefore necessary in order to accurately simulate the water cycle.

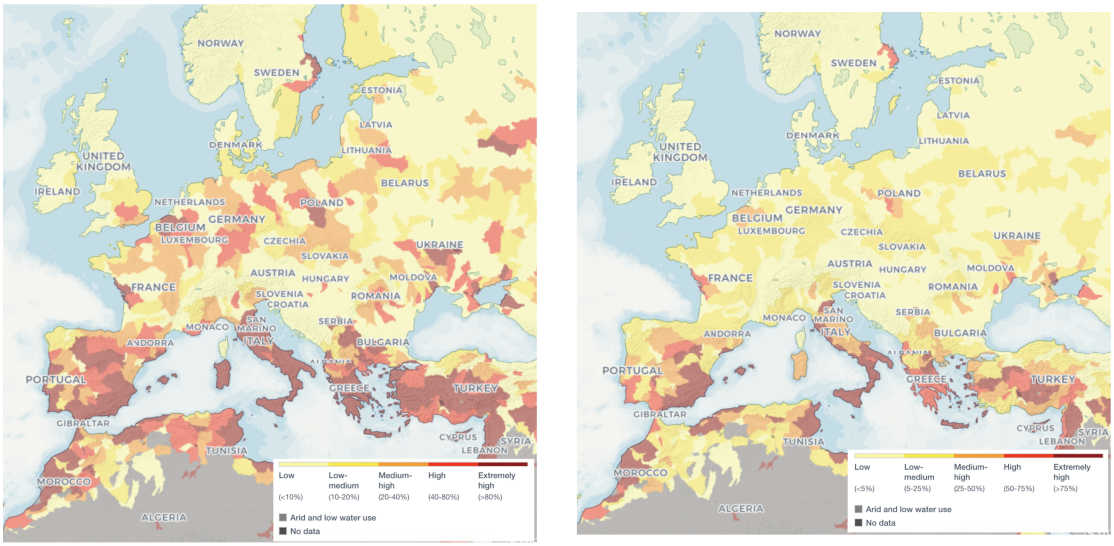

Figure 1.5: Left: Water stress in Europe. Right: Water depletion in Europe.
Water stress measures the ratio of total water demand to available renewable surface and groundwater supplies. Higher values indicate more competition among users. Water depletion is similar to water stress; however, instead of looking at total water demand (consumptive plus nonconsumptive), water depletion is calculated using consumptive withdrawal only. Source: Aqueduc, World Resources Institute.

In the last decade, noteworthy progress has been made to incorporate water manage-

ment in hydrological models (Pokhrel et al., 2016). This has been identified as one of the great challenges in Earth-System modeling by the World Climate Research Programme (WCRP). The challenges lie in modeling water demands and the corresponding water supply and allocation (Nazemi et al., 2015a).

Irrigation is the first process to have been included in hydrological models, as it is the most consumptive human water use. In the majority of cases, the irrigation demand is computed by the model at the grid scale as the water requirement for optimal crop growth assuming no water deficit. Different methods exist. Some models compute the irrigation demand as the water required to bring the soil moisture at the root zone at saturation. Others define the irrigation demand as the difference between the potential and actual evapotranspiration.

Other water withdrawals have been less frequently represented. Water demands for domestic, industrial and energy uses are estimated based on socio-economic factors, in particular population and national GDP. For example, Hanasaki et al. (2008) built gridded datasets of industrial and municipal water withdrawals and uses at the global scale.

Water allocation distributes the available water sources (groundwater, river, lake and reservoir) among the different demands. The majority of allocation schemes assume that grid-based demands can be supplied from the sources available within the local grid. However, as the resolution of models increases, this assumption becomes restrictive as it does not allow for any water transfer. Various modifications have been proposed to overcome this limitation. For example, Hanasaki et al. (2006) assumed that large reservoirs can potentially supply downstream demands that are located within a certain distance range. Alternatively, river routing schemes can provide a more accurate basis for representing the water delivery (Zhou et al., 2021). In order to decide in case of water shortage, different priorities and rules between the competing demands have been defined.

Finally, algorithms have been developed to represent reservoir operations. They are usually classified into two categories (Nazemi et al., 2015a), based on either simulating the reservoir release using a set of prescribed operational rules (Hanasaki et al., 2006) or using search algorithms to find optimal reservoir release (Haddeland et al., 2006). Prescribed operational rules used in the simulation algorithm are a function of reservoir inflow and filling level. They generally do not consider the reservoir's specific purpose, except for irrigation-aimed reservoirs, for which the rules also depend on downstream irrigation demands. On the contrary, in optimization algorithms (Haddeland et al., 2006), the objective function to optimize varies depending on the reservoir's primary purpose.

1.2.3 The hydrological cycle under climate change

All components of the anthropized water cycle presented in Fig. 1.3 are affected by climate change (IPCC, 2021a, 2022a). Analyzing the respective evolution of the different water fluxes is key to understanding how river discharges are evolving and will evolve with climate change.

1.2.3.1 Evapotranspiration

Evapotranspiration (ET) refers to the water transferred to the atmosphere in the form of vapor. This is a complex process that depends on atmospheric conditions, soil type and vegetation states. Three components are usually distinguished (Zhang et al., 2016):

- **Evaporation**. Above open water bodies such as lakes or rivers, there is a dynamic equilibrium between the vapor and liquid phases of water. If the partial pressure of water vapor in the air is less than the saturation vapor pressure, some of the molecules will transition from the liquid to the gaseous phase. The same phenomenon occurs above ground. However, in this case, evaporation is constrained by the upward diffusion of water through the soil layers.

- **Water interception.** Some precipitation is intercepted by plant leaves and directly evaporated.

- **Plant transpiration.** Water is evaporated through leaf stomata, which drives the circulation of sap from roots to leaves and the assimilation of carbon through photosynthesis. It depends on weather conditions, plant cover, plant type, vegetative stage and growth, and the water availability of the soil from which the roots draw.

The modeling of ET often relies on the concept of potential evapotranspiration (PET). PET represents the maximal evapotranspiration under specific atmospheric conditions, i.e. in a system not limited by water availability. It corresponds to the atmospheric demand for water, determined by available energy and aerodynamic resistance (Barella-Ortiz et al., 2013). PET is a conceptual flux that cannot be observed but can be estimated through several methods, such as the Penman–Monteith equation, which is considered the standard method. Four climatological parameters are involved in the computation of PET. The first two are the available radiative energy and the air temperature, which provide the needed energy. The third one is the air humidity, which is key in the vapor pressure gradient between the surface and the atmosphere. The fourth one is the wind speed, which is in charge of generating the turbulence needed to transfer the saturated air to the atmosphere, replacing it with a drier one.

IPCC (2021a) concludes with high confidence that global terrestrial annual ET has increased since the early 1980s, driven by both increasing atmospheric water demand and vegetation greening (i.e. increase in photosynthetic activity driven by CO2 fertilization and global warming). CMIP6 models project an increase in ET over most land areas, except in regions that are projected to become moisture-limited (due to reduced precipitation and increased evaporative demand), such as the Mediterranean region. Furthermore, they project a strong seasonality in many regions, with a larger relative increase in the winter season and a smaller relative change in the summer. However, substantial uncertainties in projections of ET, especially at seasonal and regional scales, remain. In France, there is uncertainty about the future evolution of ET, with some models predicting an increase and others a decrease.

1.2.3.2 Precipitation

The change in global precipitation is driven by increasing moisture in the atmosphere and the energy budget of the troposphere. IPCC (2021a) concludes that annual mean precipitation is increasing in many regions worldwide and decreasing over a smaller area, particularly in the tropics and the Mediterranean region. Furthermore, the contrasts in precipitation amounts between wet and dry seasons are increasing. Finally, reanalysis data indicate a significant reduction in snowfall, with the largest decline over the Alps, where snow water equivalent reductions of about 20 mm per decade were found (Tamang et al., 2020).

Christidis et al. (2022) analyzed the change in precipitation in Europe over the last century and found a decrease in precipitation in the Mediterranean area and an increase

over most other parts of the continent, except for summer, during which drying is more widespread and rainfall increases are mainly concentrated in Scandinavia. In France, Meteo-France finds an unchanged national mean pluviometry between 1981-2010 and 1991-2020 but with seasonal and regional disparities (Soubeyroux, 2023). Precipitations have decreased in the South, while they have increased in the North. Same trends are found by Vicente-Serrano et al. (2019).

CMIP6 models project these global and regional trends to continue in the future. In Europe, a continuation of the drying over the Mediterranean area is projected while an increase in precipitation is projected in the North (Christidis et al., 2022). Seasonal contrasts are expected to increase with a higher increase in precipitation in winter. More generally the variability of precipitation is expected to increase, thereby enhancing the likelihood of extreme events.

In France, large uncertainties among models are found (see Fig. 1.6 for Explore2 projections), with the median projecting an increase in annual precipitation in the North and a decrease in the South, particularly marked over the Pyrenees. Strong seasonal contrasts are obtained with a general increase in winter (except in the Pyrenees) and a decrease in summer in the whole country.

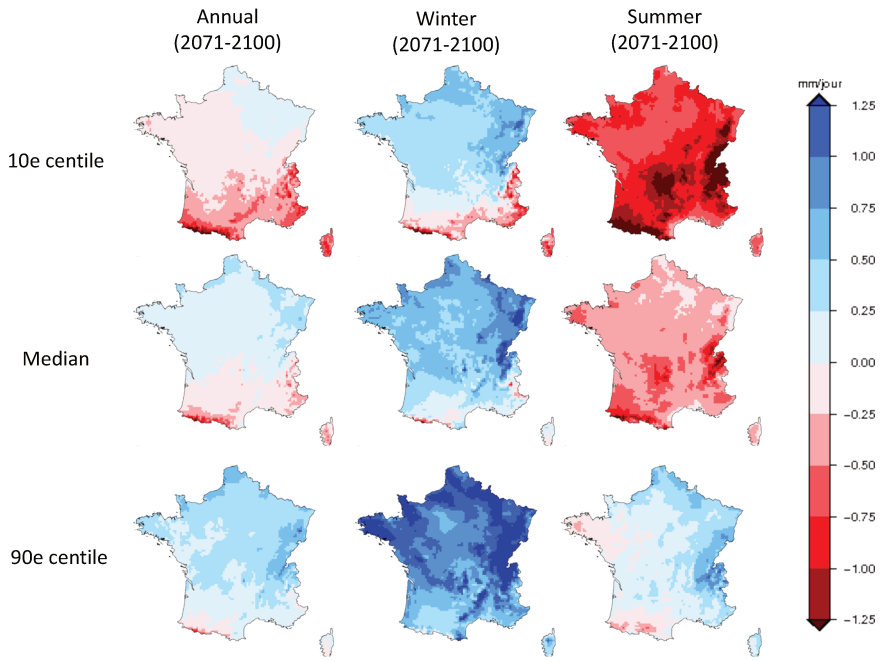

Figure 1.6: Distribution of the changes in precipitation relative to the 1961-2012 reference period projected by Explore2 climate models for the 2071-2100 period (RCP8.5). 17 climate models have been used. Source: Explore2.

1.2.3.3 Glacier runoff

Higher temperatures increase the melting of glaciers, with significant impacts on the runoff. Alpine glaciers have lost almost 50% of their area since the 1850s (Zemp et al., 2006). As glaciers recede, water is released from long-term glacial storage. Thus, annual glacier runoff volume typically increases until a maximum is reached, often referred to as "peak water", beyond which runoff decreases because the reduced glacier area cannot support rising meltwater volumes anymore (Huss et al., 2018). Regarding the Alps

glaciers upstream of French rivers, most studies have found that peak water has already been reached or passed (Laurent et al., 2020). The annual glacier runoff is therefore decreasing with climate change, with its peak being shifted because of earlier glacier melting in the year.

Two effects therefore combine to affect flow rates in the Alps (Laurent et al., 2020). Firstly, there is an increase in rainfall and a decrease in snowfall in winter, which increases river discharges in winter and decreases them in spring/summer. Secondly, there is an increase in glacier melting in summer, which has led to a significant increase in past summer runoff, but will lead to a decrease in future summer runoff due to glacier retreat.

1.2.3.4 River discharges

Observations of river discharges show contrasted changes in Europe, as a result of changes in precipitation, ET, and glacier melting but also human activities. Focusing on near-natural European catchments, Stahl et al. (2010) found negative trends in southern and eastern regions and generally positive trends elsewhere. Regarding seasonality, they found a general increase in winter flows and a decrease in summer. Using regression-based techniques, Vicente-Serrano et al. (2019) showed that climate (precipitation and ET) explains mainly the observed increase in annual streamflows in Northwest Europe, while for Southwest Europe human disturbances better explain both temporal and spatial trends. For the latter, large increases in irrigated areas, agricultural intensification, and natural revegetation of marginal lands are inferred to be the dominant drivers of decreases in streamflow. Collignan et al. (2024 (submitted)) found simular results. They show that over Europe, especially in the South, the dominant explanations for discharge trends are non-climatic factors while in some countries of Northern Europe, climate change seems to be the dominating driver of change.

Fatichi et al. (2015) carried out a high-resolution distributed analysis of climate and anthropogenic changes on the hydrology of the upper Rhone basin, a Swiss catchment that contains reservoirs, river diversions and irrigated areas. They found that changes in the natural hydrology regime imposed by the existing hydraulic infrastructure are likely larger than climate change signals expected by the middle of the 21st century.

Regarding France, Boé et al. (2009) found that despite large uncertainties linked to climate models, some robust signals would already appear in the middle of the 21st century. In particular, a decrease in mean discharge in summer and fall is simulated. The low flows become more frequent but generally weak, and uncertain changes in the intensity of high flows are simulated. Available Explore2 outputs project a general increase in annual discharges in the North and a decrease in the South. However, the hydrological models used for such projections do not account for human action and glacier processes, that modify the river discharges.

1.2.3.5 Water withdrawals in France

The volumes of water withdrawn in France in 2020 and their associated consumptions are presented in Fig. 1.7. Water consumption refers to the part of these withdrawals that is not locally returned to the natural habitat.

Irrigation is the main consumptive use as most of the water withdrawn is evaporated into the atmosphere. In 2020, 58% of the water consumption came from agriculture. However, the total volume of irrigation withdrawals (3.4 billion cubic meters) is low compared to that of Mediterranean countries, with Spain and Greece accounting for 18.9 billion and 8.1 billion cubic meters, respectively. 6.8% of the French agricultural area is

equipped for irrigation (see Fig. 1.8), primarily for corn crops (38%) and wheat (12%). The surface equipped for irrigation has increased by 23% between 2010 and 2020, with more farmers equipping themselves to adapt to climate change. Depending on the region, water is withdrawn from rivers and streams (in the southeast), groundwater (Centre region, Beauce), and reservoirs (southwest). The particularity of irrigation, unlike industrial and energy production activities, is that most water is withdrawn between June and August, when groundwater and river levels are at their lowest. Without any change in cultivation practices, water requirements for irrigated crops will increase with climate change, due to increased atmospheric water demand.

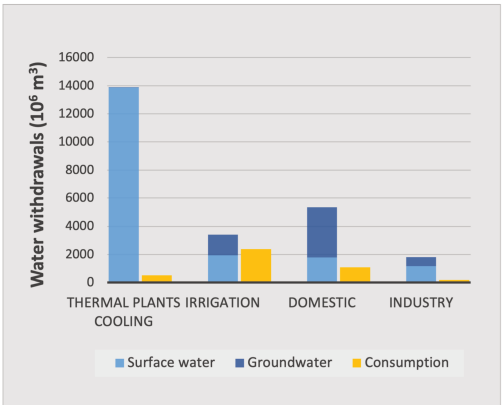

Figure 1.7: Water withdrawals and consumption in France in 2020 (million cubic meters). Source: Eurostat data

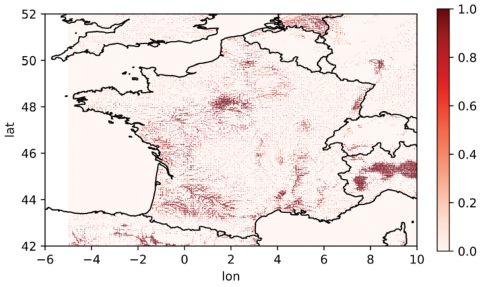

Figure 1.8: Fraction of 4km^2 pixels equipped for irrigation. Source: Lehner et al. (2011)

As indicated in Fig. 1.7, the majority of withdrawals are dedicated to the cooling of thermal power plants, mainly nuclear, for the production of electricity. Even if most of the withdrawn water is returned to the river, such use has a thermal effect as it warms the water. Following the usual convention, the volume of water that is turbined in order to produce hydroelectricity is not included in the calculation of water withdrawals and therefore does not appear in Fig. 1.7. The use of reservoirs may however modify river discharge patterns and increase the water evaporation. The French administration estimates that the excess evaporation from storage in artificial water bodies (of all types) in mainland France is 1 billion m^3 per year in the current climate, mainly due to reservoirs in lowland areas not dedicated to hydroelectricity (France Stratégie, 2024).

1.2.4 Climate change and the power sector

Many components of the energy system are affected by climate conditions (IPCC, 2022b). This raises the question of whether the energy system transformation needed to limit warming will be impacted by climate change.

1.2.4.1 Power demand

In France, electrical heating is particularly prevalent, with approximately one-third of households equipped with such a system. Power demand is therefore correlated with temperature. Below 15°C, the power demand decreases with temperature increase. Above 23°C, it increases with temperature due to increased air conditioning usage (Staffell et al., 2023). Independently from any other change, increasing temperatures will then lead to a decrease in power demand in winter and an increase in summer (Damm et al., 2017).

1.2.4.2 Electricity production

Several production technologies depend on climate variables to supply electricity and may therefore be affected by climate change. Cronin et al. (2018) and Yalew et al. (2020) built extensive reviews of studies projecting climate impacts on energy systems.

Hydropower

As discussed previously, climate change affects the various processes of the hydrological cycle, leading to changes in river discharges, which may impact hydropower production. Furthermore, climate change may alter the demands for water use by other sectors that often rely on the water stored in multipurpose reservoirs, potentially affecting the availability of water for hydropower generation. Finally, changes in the timing of river discharge peak may also modify the water availability for hydropower, requiring upgrading in storage capacity and adaptation of the hydropower plant management for fully exploiting the increase in water availability (IPCC, 2022a). Previous studies show that hydropower is particularly sensitive to climate change but projections are highly sensitive to the modeling uncertainties Cronin et al. (2018).

In Europe, most studies predict an increase in production by hydropower in the North and a decrease in the South (Gøtske et al., 2021; Lehner et al., 2005; van Vliet et al., 2016a). Reviewing 19 studies, Wasti et al. (2022) found the dominant effect of climate change on hydropower in the Alps to be the increased glacier melt. In Switzerland, it has increased hydropower generation by 3%-4% but a decrease by approximately 3% is projected by the end of the century as glacier volumes shrink (Schaefli et al., 2019).

Regarding France, projections are uncertain. The studies we identified that focus specifically on France have been carried out at the initiative of energy producers or by the French TSO. In particular, two local studies were conducted in the Pyrenees (Ariege and Aure basins), where the strongest decrease in precipitation is expected (Fig. 1.6) and where significant hydropower capacities are installed (Fig. 1.1).

First, IMAGINE30 project was funded by EDF (*Electricité de France*) to analyze the effect of climate change in the Ariege basin, (Hendrickx et al., 2013). Hydrological simulations indicate a reduction in annual inflows to dams, an earlier onset of snowmelt, and a greater frequency of low-water periods in response to climate change, resulting in a reduction in electricity production. Additionally, the simulations suggest that reservoirs should be filled earlier in the winter to anticipate a greater contribution from reservoirs to summer low-water support downstream. Secondly, the SHEM (*Société Hydro-Électrique du Midi*) has led a study focusing on the Aure Valley (Huang et al., 2022). The results show that annual hydropower production is mostly vulnerable to future drier conditions and that reservoir storage management is extremely sensitive to temperature increase that induces earlier snowmelt.

Finally, in the framework of their prospective study, RTE (2021) explore the impact of climate change on hydropower production based on the natural river discharges simulated by the SIM2 hydrological model. They found limited changes at the annual level but strongest changes in the seasonality of inflows which are projected to increase in Winter and early Spring and decrease in Summer and Autumn.

Nevertheless, despite the existence of several studies that have identified the anticipated changes in the seasonality of inflows, none of these studies have assessed the impact of these changes on the broader power system or considered them in relation to the anticipated changes in flexibility requirements. Such assessment would require comparing highlighted climate impacts at the catchment scale to power system needs at the scale of the power grid.

Thermal plants

Changes in ambient temperature have relatively small impacts on coal-fired and nuclear power plants, however, gas-fired power plants may have their thermal efficiency and power output significantly decreased. Furthermore, more frequent droughts decrease potential cooling water for thermal power plants and increase the probability of water outlet temperatures exceeding regulatory limits, leading to power production reduction or shutdown. The usable capacity of thermoelectric power plants using river water for cooling is expected to reduce in all European countries due to a combination of higher water temperatures and reduced summer river flows (van Vliet et al., 2016b). Robust and significant negative climate change effects are found, with a magnitude higher than for other power-generating technologies in Europe (Tobin et al., 2018). In France where 69% of the electricity production is provided by nuclear plants, this is a major concern.

Solar PV

Studies typically report unremarkable or small positive effects of climate change on regional solar power potentials as a net result of changes in irradiation driven by cloud, aerosol and water vapor trends and increasing surface temperature (Yalew et al., 2020).

Wind

The findings of climate impacts on wind power potential are mixed, with diverging results across regions as well as across studies. For Europe, for instance, both increases and decreases are reported. More specifically, wind power decreases are reported particularly for southern Europe, while slight increases in wind power are projected for central and northern Europe (Yalew et al., 2020).

1.3 Contributions and manuscript overview

1.3.1 Scientific questions

Two anticipated changes will impact French hydropower production. On the one hand, integrating more variable renewables into the grid may modify the need for production from dispatchable hydropower, which is required to mitigate the variability of renewable production and the uncertainties in its forecast. On the other hand, changes in climate and human water management are modifying river flows and reservoir operations, which may therefore impact hydropower production. Climate models project a general increase in river flows during winter and spring, and a decrease during summer and fall. Additionally, hydroelectric reservoirs are expected to be utilized more extensively during summer to supply irrigation and environmental requirements. The main question we address in this manuscript is therefore: ***Q1 - How will hydropower production evolve in the future French power system under climate change?***

In order to estimate the impacts of climate change on hydroelectric production, the modeling chain described in the section 1.2 is commonly used (Turner et al., 2022). Hydropower production can be computed at various junctures of this modeling apparatus, as illustrated in Fig. 1.9. Two methods can be used to compute the production as a function of water: (i) using a statistical model if data on the generation from existing plants under historical water conditions is available; (ii) in a physical-based approach, using Eq. 1.1.

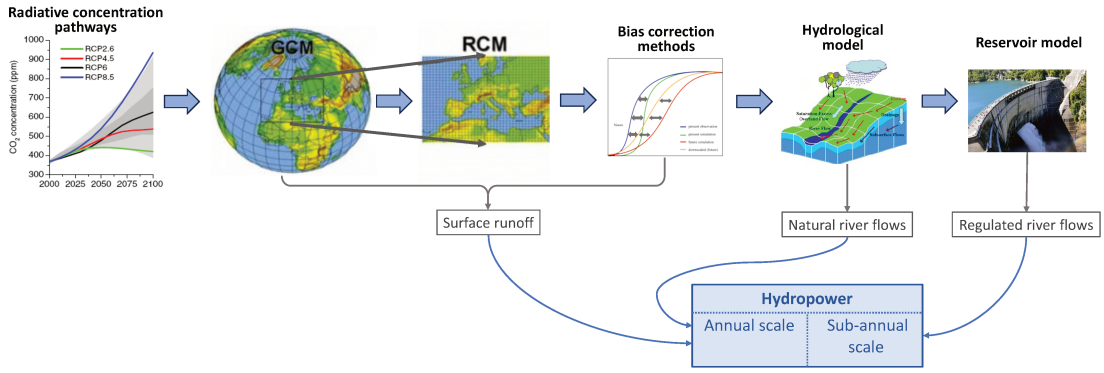

Figure 1.9: Methods used to derive hydropower from climate simulations

The first climate-driven hydropower studies have computed hydropower production based on simulated surface runoff (Hamududu et al., 2012; Lehner et al., 2005; Pokhrel et al., 2008) or natural river discharges (Lehner et al., 2005; Tobin et al., 2018; van Vliet et al., 2013). Consequently, they were unable to account for the capacity of reservoirs to delay power production and were only able to estimate the production at the annual timestep.

To estimate changes in hydropower production at smaller temporal scales, it is necessary to include a reservoir model in the modeling chain, in order to represent regulated river flows (Fig. 1.9). However, the reservoir models employed in previous studies (Chowdhury et al., 2021; Dang et al., 2020; Siala et al., 2021; van Vliet et al., 2016a; Voisin et al., 2020) are based on exogenous operating rules that do not account for power system dispatching decisions (see section 1.1.4). These decisions are however crucial for correctly determining the timing of the release from hydroelectric reservoirs. The existing reservoir models are therefore unable to: (i) accurately model the intra-annual flow variations for rivers equipped with hydroelectricity, and (ii) compute the hydropower production on a fine time resolution. The second research question addressed in the manuscript is: ***Q2: How to represent hydropower operation in a climate model taking into account power system balancing needs?***

Power system balancing needs may be estimated through the use of power system models. However, in order to provide an accurate estimation, it is important to accurately represent all flexibility options within power system models. In particular, the flexibility of hydropower plants is constrained by various factors, including the head-dependency of the production (see Eq. 1.1), the operation of reservoirs for other purposes, or the cascading effects if several reservoirs are located in the same river with upstream releases influencing downstream inflows. Most power system models poorly integrate these constraints and mainly rely on static operating guidelines for hydroelectric reservoirs. This prevents them from adapting to changes in hydrological conditions or power system needs by shifting their operations in the future. The third question addressed in the manuscript is therefore: ***Q3: How to represent dynamic hydropower constraints in power system models?***

1.3.2 Manuscript overview

Three questions are thus addressed in the manuscript. Q2 and Q3 focus on methodological contributions performed in order to answer the main question Q1.

1.3.2.1 Part I: How to represent hydropower operation in a climate model considering the needs for power system balancing?

The first part of the manuscript addresses the second question by proposing an innovative framework for representing hydropower based on a demand-driven approach.

Chapter 2 introduces this novel approach, aiming to enhance the modeling of release decisions from hydropower reservoirs in hydrological models. First, hydropower infrastructures are placed in coherence with the hydrological network and links are built between hydropower plants and their supplying reservoirs to explicitly represent water transfers built for hydropower generation. Then the multipurpose operation of these reservoirs is determined by considering the requirements for ecological flow, irrigation, tourism and power supply. For the latter, operations are driven by a target production time series (see Fig. 1.10). At each time step, an exogenous target of national hydropower production is used to determine the coordinated release of each hydroelectric reservoir. The target production is to be obtained from observations or simulations of a dispatching model, in order to reflect the power needs of the actual power system under study.

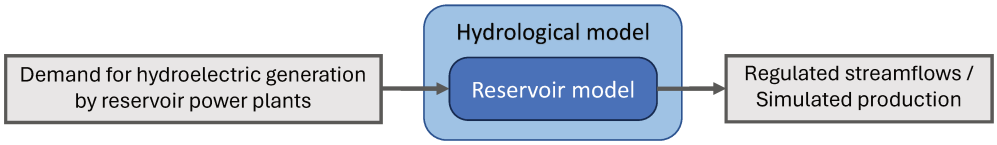

Figure 1.10: Schematic summary of the method outlined in Chapter 2.

Chapter 3 describes the implementation of this novel method within the ORCHIDEE land surface model. The method is assessed and validated through a case study of the French electrical system. We drive the model with a high-resolution atmospheric reanalysis and prescribe the observed national hydropower production as the total power demand to be met by hydropower infrastructures. By comparing the simulated evolution of the stock in reservoirs to the observations, we find that the model simulates realistic operations of reservoirs and successfully satisfies hydropower production demands over the entire period. We highlight the roles of uncertainties in estimated precipitation and of the limited knowledge of hydropower infrastructure on the estimation of production. Finally, we show that such an integration of hydropower operations in the model improves the simulations of river discharges in mountainous catchments affected by hydropower.

Finally, Chapter 4 extends the analysis of the new method's performance. First, it discusses the rule that distributes the national production demand among the individual plants. Comparing the model performance under three different rules, we find that the simplest one yields the most conclusive results. Furthermore, we show that the demand-based approach can also be employed to model the operation of PHS plants, which involves water transfers from one upstream reservoir to a downstream one.

1.3.2.2 Part II: How to represent dynamic hydropower constraints in power system models?

The second part of the manuscript addresses the third question. Chapter 5 demonstrates the value of coupling a power system model with a hydrological model to inform about time and climate-dependent hydropower constraints. The French power system is modeled with the optimization model EOLES-Dispatch. We show that the coupling of this model with the ORCHIDEE model allows to simulate a hydropower schedule closer to

the observed production. Considering a prospective 2050 power mix, we also find that the coupling leads to more frequent unsatisfied demand, which is underestimated by the usual representation of hydropower.

1.3.2.3 Part III: How will evolve hydropower production in the future French power system under climate change?

Finally, the last part of the manuscript provides some insights into the first question. Parts I and II lead to the creation of an integrated modeling framework, which is illustrated in Fig. 1.11. This original framework represents an innovative tool that allows for the joint consideration of scenarios of climate change and power mix. It ensures that the simulated production is consistent with water resource availability, reservoir operation rules, and the minimization of the total production cost of the power system. This allows for finer resolution than previous studies and the simultaneous consideration of seasonal changes in inflows, absolute changes in water resources, and changes in release decisions.

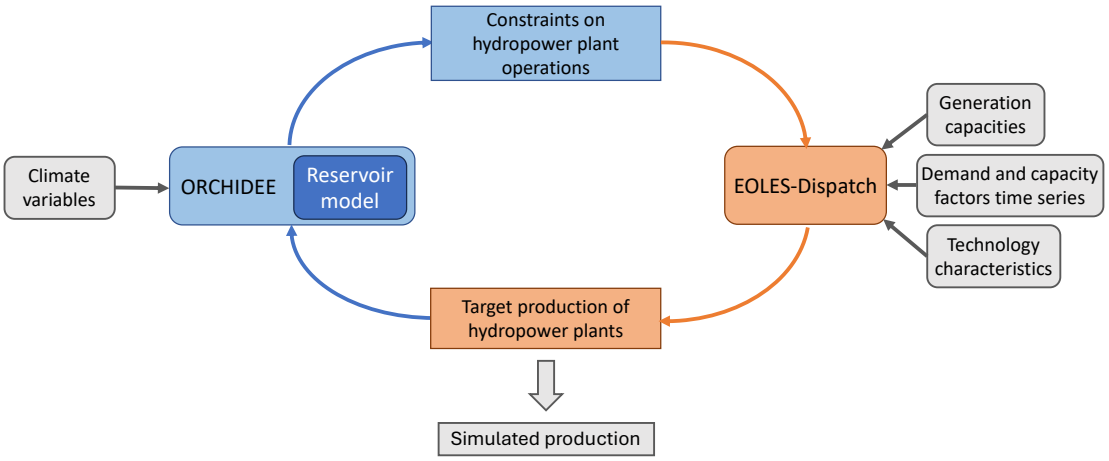

Figure 1.11: Schematic representation of the integrated modeling framework developed across Parts I and II.

Chapter 6 applies this novel modeling framework to the French study case, considering scenarios of future climate and power mix. Our findings indicate large uncertainties across climate models in the evolution of annual production, due to uncertainties in future precipitation, in particular over the Alps. However, consistent changes in the seasonality of production are found. Production is higher during winter due to higher liquid precipitations, at the expense of spring production due to lower snowmelt. When combined with changes in the power mix, we obtain an increase in the value of hydropower.

Chapter 7 analyzes in greater detail the sensitivity of our results to the uncertainties in climate change. While Chapter 6 addresses the uncertainties associated with the selection of climate models, Chapter 7 examines the uncertainties resulting from two additional links in the modeling chain presented in Fig. 1.9: the choice of radiative concentration pathway and the selection of bias correction methodology. We show that these two factors also introduce a considerable degree of uncertainty into the final results, which is of a similar magnitude to that of the inter-model uncertainty.

Finally, Chapter 8 examines the potential impact of anticipated changes in the power system on the operation of PHS plants and their business model. PHS plants represent the majority of storage options in France and are set for significant expansion in the coming years. Nevertheless, the profitability of these plants has been called into question,

prompting the French government to consider the creation of support mechanisms to encourage the development of new plants. This chapter examines the current business model of existing French PHS plants and explores how anticipated changes in the power system are expected to modify their revenues. In the scenario under study, we identified potential for increased revenues from PHS plants, driven by the increased variability of electricity prices due to increased penetration of renewable energies. Nevertheless, the uncertainty surrounding the evolution of thermal generation costs due to the use of decarbonized fuels makes it unclear whether these revenues will be sufficient to cover the investment costs of new projects.

Part I

Representing hydropower operations in hydrological models - A demand-based approach

CHAPTER 2

Presentation of the modeling framework

This chapter presents a novel demand-based approach for representing the complex operations of hydropower reservoirs in hydrological models. We first introduce the motivations for this new approach by outlining the limitations of existing methods. The new modeling framework that we propose is then carefully described.
This chapter corresponds to the first two sections of an article currently being revised for publication in the journal Hydrology and Earth System Sciences (Baratgin et al., 2024 (submitted)[b]).

Contents

2.1 Introduction 24
2.1.1 Background and motivation 24
2.1.2 Objectives 25
2.2 Presentation of the modeling approach 25
2.2.1 Definition of a routing network that includes hydropower connections 26
2.2.2 Dams and reservoir parametrization 28
2.2.3 Water demands 31
2.2.4 Validation diagnostics 33
2.2.5 Calibration 34
2.3 Summary 35

2.1 Introduction

2.1.1 Background and motivation

Hydroelectric power is set to play a pivotal role in numerous power grids in the coming decades, offering low-carbon and dispatchable generation capacity. However, power grids that rely on hydropower production are vulnerable to the unpredictability of weather and climate. Consequently, assessing the potential impact of drought events or climate change on hydropower production is a major concern for the development of resilient energy systems.

Numerous studies (Lehner et al., 2005; Turner et al., 2017; van Vliet et al., 2016b; Voisin et al., 2020; Zhou et al., 2018) have revealed significant impacts of climate change on hydropower production in certain regions, including southwestern Europe and France. These studies typically employ global hydrological models (GHMs) or land surface models (LSMs) driven by atmospheric projections generated by global climate models (GCMs) (Turner et al., 2022). These models simulate the regional-scale hydrological cycle, offering gridded assessments of surface runoff and streamflow, which are then used to derive hydropower production estimates.

However, the estimation process from streamflow to hydropower production is challenging for three reasons. Firstly, water can be stored in reservoirs for future use. The timing of reservoir releases is then the result of the management of the power grid and the coordinated operation of other plants across various water catchments. Secondly, reservoirs that feed hydropower plants are often multipurpose and operated to satisfy other water uses, namely irrigation or tourism. Thirdly, hydropower production can involve inter-catchment water transfers, particularly in mountainous regions where water is stored at higher elevations before being channeled to power plants located in the valleys.

Existing studies adopt diverse strategies to represent these complex operations of hydroelectric reservoirs, which are generally categorized into two main approaches (Nazemi et al., 2015c). On the one hand, simulation algorithms rely on predefined rules to compute reservoir releases. These rules are often a function of reservoir inflow and filling level, inspired by the pioneering work of Hanasaki et al. (2006) (e.g. in MOSART-WM a reservoir scheme used by Ralston Fonseca et al. (2021), Voisin et al. (2020), and Zhou et al. (2018)). They can also be defined based on target curves of water levels from which the release is determined (e.g. in VIC-RES (Dang et al., 2020) used by Chowdhury et al. (2021) and Siala et al. (2021)). Such methods account for the seasonal behavior of hydroelectric reservoirs, but they miss the representation of short-term operations, as no links with the power system needs are made. On the other hand, optimization algorithms based on the pioneering work of Haddeland et al. (2006) determine the optimal release for each dam. The objective function to optimize varies depending on the reservoir's primary purpose, aiming to maximize individual production for hydroelectric reservoirs. However, this method considers each reservoir independently and often employs large time steps (monthly) to reduce computational strain.

When the models differentiate the various uses of reservoirs, they categorize the reservoirs based solely on their primary purpose (Abeshu et al., 2023). This approach does not allow to capture the full range of constraints that apply to most hydroelectric reservoirs, which are often multipurpose. Moreover, none of these studies operate the dams as a network that takes advantage of the spatial complementarity of different climatic regions or the cascading effects within river systems.

Finally, none of these large-scale studies explicitly model the water transfers from reservoirs to power plants. In most cases, the flow rate within the grid cell where the

power plant is located is used to estimate its production, without considering the actual location of the reservoir (van Vliet et al., 2016b; Voisin et al., 2020; Zhou et al., 2018). This approach may lead to an overestimation of production, as the flow rate at the plant site is higher than at an upstream dam site, and inter-basin transfers may also occur.

2.1.2 Objectives

The objective of this study is to present the original methodology we developed to estimate hydropower production at the scale of a regional power grid. This approach is based on the simulations of a GHM or LSM and addresses the three challenges previously identified: (i) considering the coordinated management of the entire power system at the scale of the power grid; (ii) accounting for the multipurpose objectives of reservoirs that store water for hydropower production; (iii) representing the inter-catchment water transfers from reservoirs to power plants.

Our approach draws inspiration from the demand-based algorithms used for irrigation reservoir management, pioneered by Hanasaki et al. (2006). In these algorithms, a demand point (irrigated area) is connected to a supply point (river), with the water demand of the downstream irrigated area driving upstream reservoir releases (Nazemi et al., 2015c; Zhou et al., 2021).

In our methodology, hydropower plants are linked to reservoirs whose releases depend on the demand for hydropower production. At the geographical scale of the whole power grid, the primary concern is balancing total electricity demand with generation, regardless of the specific locations of consumption and generation. Consequently, we assume that all hydroelectric reservoirs within the power grid can contribute to satisfying the demand for dispatchable hydropower production, determined by grid-level power system dispatch decisions. Power dispatching involves deciding which types of power plants are activated to satisfy the total power demand, based on the cost and availability of generation resources. Our model does not explicitly represent this side of the power system decisions but uses the corresponding demand for dispatchable hydropower to drive the operation of the hydroelectric reservoirs.

We implement the proposed methodology in the ORCHIDEE LSM (Krinner et al., 2005), but it aims to be usable in any LSM or GHM. The first steps involve building a river network that represents inter-catchment hydropower transfers and defining rules for reservoir releases. These steps are generic and only require basic information on dam and plant characteristics. To validate the effectiveness of the approach, we apply it to the French power grid. A calibration step is added, which requires more information on individual plants. Finally, the simulated operations of hydroelectric reservoirs are compared with actual operations.

2.2 Presentation of the modeling approach

Our method relies on three main novelties: building a river network that includes hydropower-related infrastructures and represents inter-basin hydropower transfers (Sect. 2.2.1), implementing a reservoir scheme that accounts for multipurpose reservoirs (Sect. 2.2.2), and using hydropower demand to infer hydroelectric reservoir operations (Sect. 2.2.3).

2.2.1 Definition of a routing network that includes hydropower connections

The spatial resolution of GHMs or LSMs is typically constrained by the atmospheric grid of the forcing files, which is generally set at 0.5° (approximately 50 km) for large-scale implementations and 0.1° (approximately 10 km) for regional implementations. However, human activities, such as irrigation or urban areas, operate at much finer spatial resolutions, typically within a few kilometers. The concept of hydrological transfer units (HTUs) has been introduced in routing modules to bridge this resolution gap (Nguyen-Quang et al., 2018). HTUs correspond to sub-grid river basins, which allow runoff generated in one atmospheric grid cell to flow into multiple neighboring cells. The introduction of these smaller units allows for a more accurate representation of the river system and its interaction with human activities, including hydropower.

Three types of hydropower plants are distinguished, with different implications on locations:

- **Run-of-river plants** do not have any storage capacity and generate electricity according to the instantaneous river discharge at the plant location.
- **Reservoir plants** are fed by reservoirs that can store a specified water volume. These reservoirs often serve multiple purposes, which may constrain the operations of the plant. The electricity production does not necessarily take place at the location of water storage, therefore the plant and the reservoir need to be located separately on the model grid.
- **Poundage plants** are defined in some regions as a subcategory of reservoir plants whose upstream reservoir is relatively small and only allows to store water for a short period.

As an example of different locations of reservoir and power plant, the *La Bathie* power plant, the largest reservoir power plant in France, draws water from the Roselend reservoir, which is located about 20 km away (Fig. 2.1). At a kilometric resolution, this implies horizontal water transfers between these two locations (water withdrawal and restitution), which requires the reconstruction of the hydroelectric water supply network within the routing network of ORCHIDEE.

We proceed in three steps, as illustrated in Fig. 2.2. First (Fig. 2.2-b), we place dams and hydropower plants on a high-resolution river network (MERIT (Yamazaki et al., 2019) is used in this study), based on geo-referenced data and upstream area provided in infrastructure databases. The location procedure is detailed in Appendix A.1 and the infrastructure datasets used for our study of France are presented in Section 3.1.2. Then, we build the adduction network by identifying supposed connections between power plants and dams that feed them (see Appendix A.1 for more details on the procedure to build the adduction network). Finally (Fig. 2.2-c), we form HTUs by aggregating MERIT pixels in an atmospheric grid cell with the same general flow direction following the procedures described in Nguyen-Quang et al. (2018) and Polcher et al. (2023).

This procedure results in an HTU network representing natural and human-made water flows. This network can be seen as a directional graph (Fig. 2.2-d) where vertices correspond to HTUs and edges represent directional water flows, both natural and human-made flows for hydropower purposes. In this graph, hydropower plants are placed on the edges connecting the HTU of their withdrawal point and the HTU downstream

Figure 2.1: Schematic representation of the complex water adduction network feeding La Bathie power plant. Numerous water intakes can be identified. Among them, are the reservoirs of Roselend, Saint Guérin, and La Gittaz as well as other intakes directly connected to rivers or glaciers. Source:vpah-auvergne-rhone-alpes.fr

where they are located. Fig. 2.3 introduces the notation that will be used throughout the article to index HTUs and edges in such graphs. It shows that the water used to produce electricity can follow a different path from the natural flow out of the reservoir. This approach allows for the representation of this distinction independently of the atmospheric resolution.

The attributes and variables describing the reservoir and hydropower characteristics of each HTU i and vertex (i, j) are presented in Table 2.1.

vertex	$V_{tot,i}$	Total maximum storage capacity of the reservoir located in HTU i (m^3)
	$V_{elec,i}, V_{recr,i}, V_{irri,i}$	Maximum storage capacity dedicated to respective water uses (hydropower, recreation, and irrigation) (m^3)
	$H_{dam,i}$	Height of the dam (m)
	$\boldsymbol{V_i(t)}$	**Current total volume in the reservoir (m^3)**
	$V_{min,i}(t)$	Minimum water volume in the reservoir, it evolves with time to account for recreation uses (see Fig. 2.6) (m^3)
	$h_{res,i}(t)$	Water level in the reservoir (m)
	$A_{res,i}(t)$	Surface of the reservoir (m^2)
edge	$P_{(i,j)}$	Installed hydropower capacity of the plant located on the edge (i, j) (MW)
	$H_{(i,j)}$	Nominal hydraulic head of the plant, obtained with a full reservoir (m)
	$Typ_{(i,j)}$	Hydropower plant type (run-of-river, poundage, or reservoir)
	$\eta_{(i,j)}$	Production efficiency of the plant (conversion of potential energy to power)
	$E_{(i,j)}(t)$	Production of the plant (MWh)

Table 2.1: Model attributes and variables describing reservoirs and hydropower. The prognostic variable is distinguished in bold

During calibration (see Sect. 2.2.5), plants for which the identification of a single reservoir conducts to a significant misrepresentation of the plant's hydropower potential are identified, and a correction is made by moving the withdrawal point so that it gathers enough water to ensure the observed production is possible.

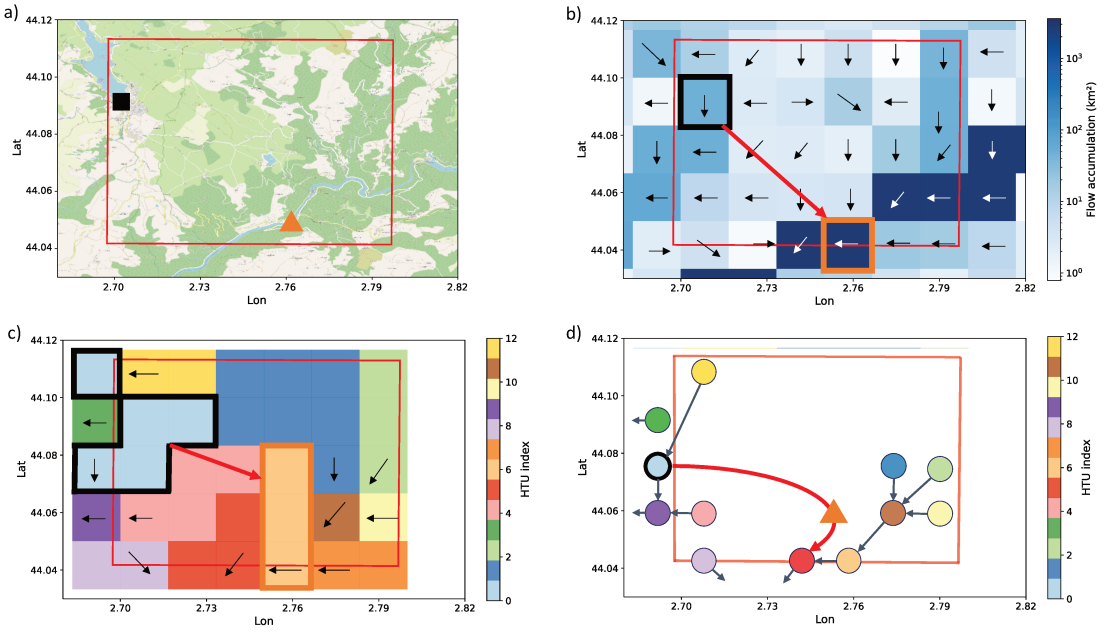

Figure 2.2: Illustration of the procedure to build the ORCHIDEE routing network using the Pouget hydropower plant in France as an example. (a) Geographic context of the Pouget power plant (orange triangle) and its feeding reservoir (black square indicating the location of the dam). The red grid indicates the atmospheric grid. (b) Flow directions and accumulation for the MERIT pixels overlapping the atmospheric grid. The MERIT pixels in which we located the power plant and the dam are respectively indicated in orange and black, while the red arrow represents the identified adduction network link. (c) Resulting HTU decomposition. The location of the infrastructures is reported in the corresponding HTUs. (d) Corresponding HTU graph. The HTU containing the dam is indicated with a bold black outline while the power plant (orange triangle) is placed on the edge between the reservoir HTU and the HTU downstream from the one where it has been located.

2.2.2 Dams and reservoir parametrization

In the initial version of ORCHIDEE (Polcher et al., 2023), each HTU i contains three natural water stores, characterized by their time constants (slow aquifer, fast aquifer, and stream storage). To represent water management we add a fourth store to the HTUs in which dams have been located to represent water storage in the reservoir (Fig. 2.4). This section presents the continuity equation for the water volume in this reservoir.

2.2.2.1 Prognostic equation for water in the reservoir

As represented in Fig. 2.4, the fast aquifer is filled by local runoff generated in the HTU, the slow aquifer by local drainage generated in the HTU, and the stream store by the discharge from upstream HTUs. The equations of these natural water stores are detailed in previous publications (Polcher et al., 2023; Zhou et al., 2021). They introduce the respective time constants of the natural stores g_{stream}, g_{fast} and g_{slow} (in unit $h.m^{-1}$) and the topographic index calculated for each HTU τ_i (in unit m^2).

The "natural discharge" $Dis_i(t)$ in the HTU i is generated by summing the outflows of the three natural water stores (Eq. (2.1)). This natural discharge is stored in the reservoir if there is one in the HTU, or routed towards the downstream HTU if there is

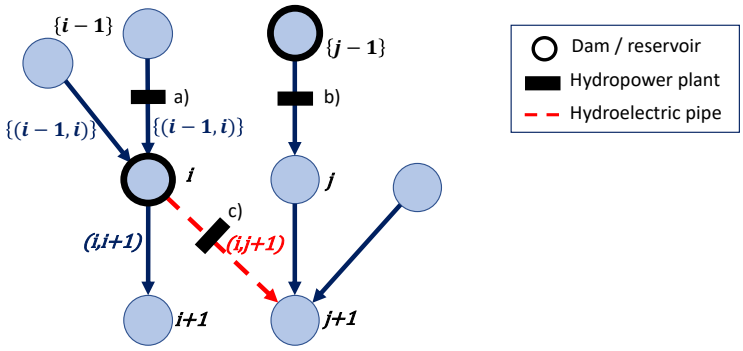

Figure 2.3: Graph representation of the river routing network built. Each vertex represents an HTU. HTUs containing a dam are represented by bold dark circles. Edges represent existing water flow directions (blue edges for natural water flows and dashed red ones for hydroelectric pipes). Power plants are placed on edges whose water flows they can use to produce power ((a): run-of-river plant, (b)-(c) reservoir or poundage plants)). The indexing convention is also presented on the graph, with integers used for vertices and couples of integers for edges. $i+1$ is the HTU directly downstream of i (natural flow) while $\{i-1\}$ denotes the ensemble of HTU flowing into HTU i. Similarly $(i, i+1)$ is the natural outflow edge from HTU i while $\{(i-1, i)\}$ represent the ensemble of inflow edges into HTU i, including basin transfers.

not.

$$Dis_i(t) = \frac{1}{\tau_i} * \left(\frac{W_{stream,i}(t)}{g_{stream}} + \frac{W_{fast,i}(t)}{g_{fast}} + \frac{W_{slow,i}(t)}{g_{slow}} \right) \tag{2.1}$$

The prognostic equation on reservoir volume is then given by:

$$\frac{dV_i}{dt}(t) = Dis_i(t) + p_{res,i}(t) - ev_{res,i}(t) - \sum_j F_{(i,j)}(t) \tag{2.2}$$

where $p_{res,i}(t)$ and $ev_{res,i}(t)$ are respectively the direct precipitation and evaporation over the reservoir, and $F_{(i,j)}(t)$ is the water released from the HTU i to the HTU j, which breakdowns as:

$$F_{(i,j)}(t) = \max\left(F^{ecol}_{(i,j)}(t), F^{irri}_{(i,j)}(t), F^{elec}_{(i,j)}(t)\right) + F^{spill}_{(i,j)}(t) \tag{2.3}$$

Reservoir releases aim at satisfying the different water demands addressed to the reservoir, which are described in Sect. 2.2.3.

Ecological and irrigation releases are limited by the demands addressed to the reservoir and the water available in the reservoir:

$$F^{ecol}_{(i,j)}(t) = \min\left(D^{ecol}_{(j,i)}(t), \frac{V^{\star}_i(t) - V_{min,i}(t)}{\tau_{res}}\right) \tag{2.4}$$

$$F^{irri}_{(i,j)}(t) = \min\left(D^{irri}_{(j,i)}(t), \frac{V^{\star}_i(t) - V_{min,i}(t)}{\tau_{res}}\right) \tag{2.5}$$

where $V^{\star}_i(t)$ is the theoretical volume to be obtained without any release (Eq. (2.6)) and τ_{res} is the time constant of the reservoir, which we assume to be of the order of magnitude of a few minutes.

$$\frac{dV^{\star}_i}{dt}(t) = Dis_i(t) + p_{res,i}(t) - ev_{res,i}(t) \tag{2.6}$$

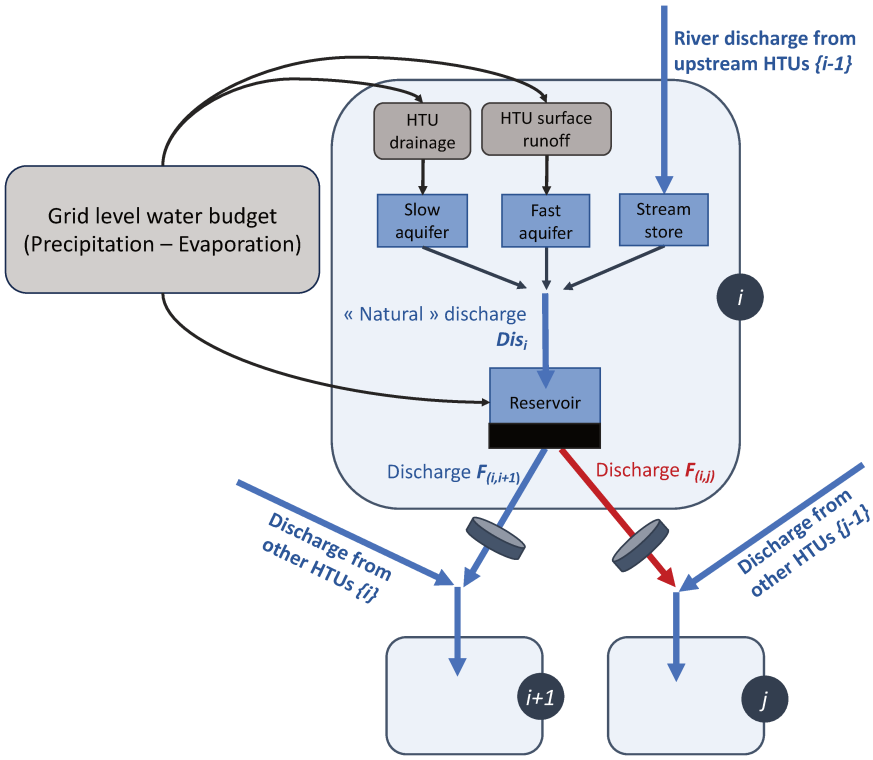

Figure 2.4: Schematic representation of water stores and flows in an HTU i

The water released for electricity generation is determined by the production of the plant, computed based on the distribution of the prescribed national demand (see Sect. 2.2.3).

$$F^{elec}_{(i,j)}(t) = \frac{E_{(i,j)}(t)}{\rho g \eta_{(i,j)} h_{(i,j)}(t)} \tag{2.7}$$

where ρ is the water density, g is the gravitational constant, $\eta_{(i,j)}$ is the efficiency of the plant (set at 0.9 by default), and $h_{(i,j)}(t)$ is the current hydraulic head, which varies with the water level of the reservoir (Eq. (2.8)).

$$h_{(i,j)}(t) = H_{(i,j)} - (H_{dam,i} - H_{res,i}(t)) \tag{2.8}$$

Finally, the spillage is defined as the water overflowing without being used for the different uses.

$$F^{spill}_{(i,j)}(t) = \begin{cases} \max\left(\frac{V^{\star}_i(t) - V_{tot,i}}{\tau_{res}} - \sum_k \max\left(F^{ecol}_{(i,k)}(t), F^{irri}_{(i,k)}(t), F^{elec}_{(i,k)}(t)\right),\ 0\right) & \text{, if } j = i+1 \\ 0 & \text{, else} \end{cases} \tag{2.9}$$

Ecological and irrigation flows $F^{ecol}_{(i,j)}(t)$ and $F^{irri}_{(i,j)}(t)$ are computed before the other flows, consistently with water management policy in most of the countries.

2.2.2.2 Diagnostic variables

As in previous studies (Fekete et al., 2010; Zhou et al., 2018), we represent each reservoir i in the form of a tetrahedron of height $H_{dam,i}$ and volume $V_{tot,i}$ (Fig. 2.5).

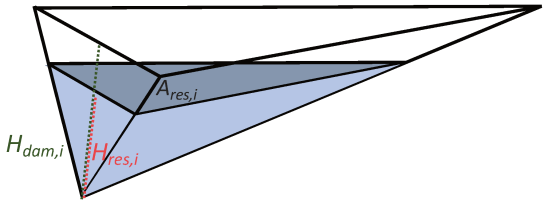

Figure 2.5: Geometry of the reservoir

Hence, the relations between the volume $V_i(t)$, the water level $H_{res,i}(t)$ and the area of the reservoir $A_{res,i}(t)$ are given by:

$$H_{res,i}(t) = H_{dam,i} * \left(\frac{V_i(t)}{V_{tot,i}}\right)^{\frac{1}{3}} \tag{2.10}$$

$$A_{res,i}(t) = \frac{3 * V_i(t)}{H_{res,i}(t)} \tag{2.11}$$

Direct precipitation and evaporation (m^3/s) over the reservoir are then given by $p_{res,i}(t) = P_i(t) * A_{res,i}(t)$ and $ev_{res,i}(t) = Ev_i(t) * A_{res,i}(t)$ where $P_i(t)$ and $Ev_i(t)$ are respectively the precipitation and evaporation over the HTU i (in m/s).

2.2.3 Water demands

Reservoirs are designed to store water for a variety of purposes, including energy production, irrigation, tourism, and domestic and industrial uses. As this study focuses on hydroelectric reservoirs, we adopt a simplistic representation of the other water uses and only consider those that can constrain hydropower operations: ecological flows, irrigation, and tourism.

2.2.3.1 Non-energy demands

In many countries, environmental laws require a minimum flow $F_{min,(i,i+1)}$ in the watercourse downstream of a dam in i, to guarantee the ecological quality of the river. These minimum flow requirements vary by region, and specific details for the French study case are presented in Sect. 3.1.3.1. Such an ecological demand $D^{ecol}_{(j,i)}(t)$ applies to all reservoirs, regardless of their intended use, and is defined as follows:

$$D^{ecol}_{(j,i)}(t) = \begin{cases} F_{min,(i,i+1)}, & \text{if } j = i+1 \\ 0, & \text{else} \end{cases} \tag{2.12}$$

In addition to ecological requirements, some reservoirs are used for irrigation purposes. Water withdrawals for irrigation can be made either directly from the reservoir or from the downstream river. Withdrawals from the river require corresponding releases from upstream reservoirs to maintain low flows. In this study, the water requirements for irrigation are represented in a highly simplified manner by assuming a need proportional to $F_{min,(i,i+1)}$ during the summer period. $D^{irri}_{(j,i)}(t)$ is then expressed as:

$$D^{irri}_{(j,i)}(t) = \begin{cases} \alpha_{irri} * F_{min,(i,i+1)}, & \text{if } j = i+1 \text{ and } V_{irri,i} > 0 \text{ and } t \in Summer \\ 0, & \text{else} \end{cases} \tag{2.13}$$

The proportional factor α_{irri} and the delimitation of the summer period may vary across regions. Details for the French case study are presented in Sect. 3.1.3.1.

Finally, during the summer months, some reservoirs also serve as tourist attractions, requiring the reservoir to be maintained at a high level to accommodate recreational activities. To ensure proper reservoir filling during the summer season, dam operators follow a filling guide curve. We define corresponding constraints on $V_{min,i}(t)$ based on previous research and available data for French reservoirs (e.g. François (2013) on the Serre Ponçon reservoir), as illustrated in Fig. 2.6. By default, the minimum volume is set at 10% of the total capacity of the reservoir and is increased to 90% during the tourist season for the reservoirs concerned.

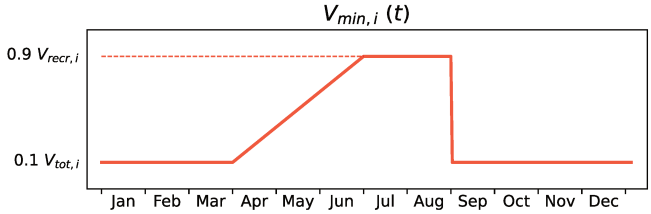

Figure 2.6: Minimum volume constraints throughout the year.

2.2.3.2 Hydroelectric demand

The production of hydropower plants is the result of the dispatch of the total power demand among the different power plants within the power grid (Stoft, 2002; Wood et al., 2013). To meet power demand at minimum cost, power generation units are called upon from least to most expensive. Run-of-river power plants, whose production is free and non-dispatchable, are called upon first, along with solar and wind power plants, to produce to their maximum potential (as long as it does not exceed total demand, otherwise there is a curtailment of their production). On the contrary, the call upon reservoir power plants is the result of a much more complex trade-off, aiming to minimize the total power system cost. From the perspective of a social planner, in charge of dispatch decisions and aware of the potentials and costs of all the units available within the power grid, as well as the electricity demand, a demand for dispatchable hydropower generation $D_{res}(t)$ can be defined at each time step. This demand (or production target) is defined for the whole grid and needs then to be allocated among the different plants to determine the energy generated at each location $E_{(i,j)}(t)$, which will then drive reservoir release decisions. Indeed, knowing $E_{(i,j)}(t)$, the model deduces the additional water release needed for the plant production (Eq. (2.7)) and can finally compute the reservoir release based on Eq. (2.3).

To distribute national demand $D_{res}(t)$ into individual plant production $E_{(i,j)}(t)$, the model proceeds in two steps.

1) Fatal production: The model starts by going through all the hydropower plants and calculates the energy they can produce or store without additional release, thanks to other releases (ecological or irrigation) or the water expected to overflow. Associated production $E_{fatal,(i,j)}(t)$ and $E_{spill,(i,j)}(t)$ are computed based on Eq. (2.14) and (2.15).

$$E_{fatal,(i,j)}(t) = \min\left(P_{(i,j)}\frac{h_{(i,j)}(t)}{H_{(i,j)}},\ \max\left(F_{ecol,(i,j)}(t), F_{irri,(i,j)}(t)\right) \times \rho g \eta_{(i,j)} h_{(i,j)}(t)\right) \tag{2.14}$$

$$E_{spill,(i,j)}(t) = \min\Bigg(P_{(i,j)}\frac{h_{(i,j)}(t)}{H_{(i,j)}} - E_{fatal,(i,j)}(t), \max\Bigg(\frac{V_i^{\star}(t) - V_{tot,i}}{\tau_{res}} - \max\left(F_{ecol,(i,i+1)}(t)\ ,\ F_{irri,(i,i+1)}(t)\right), 0\Bigg) \times \rho g \eta_{(i,j)} h_{(i,j)}(t)\Bigg) \tag{2.15}$$

The remaining production demand to dispatch is then $D_{res}(t) - \sum_{Typ(i,j)\in\{poundage,reservoir\}}(E_{fatal,(i,j)}(t) + E_{spill,(i,j)}(t))$.

2) Reservoirs withdrawals: If there is any national production demand left to dispatch ($D_{res}(t) > 0$), it should be met by withdrawing water from the reservoirs. In this study, we consider that the reservoirs are used in the decreasing order of their relative filling levels to produce power while respecting production constraints (installed capacity of the plant and the remaining volume of water in the reservoir). The remaining production is dispatched following this rule, until either all remaining production demand is fulfilled, or no more plants can produce. This rule leads to the equalization of relative filling levels at the end of each time step. This is equivalent to implementing a uniform rule curve for all reservoirs, as has been done in Dang et al. (2020). Another advantage of this rule is that hydropower production is distributed across the entire territory. All plants are required to produce a little power each day, close to the so-called stable productions modeled in other studies (Sterl et al., 2020).

2.2.4 Validation diagnostics

The performance of our model to estimate hydropower production will be assessed based on three main diagnostics: the annual hydropower potential (AHP) simulated at each individual plant, the hydraulic stock simulated at the national level, and the time series of simulated production by hydropower plant type.

We define $AHP_{(i,j)}(y)$ as the maximum energy that could be produced by the plant (i,j) over the year y in our simulation. To compute it, we run a simulation in which the demand for dispatchable hydropower $D_{res}(t)$ is fixed to infinite, leading all hydroelectric reservoirs to release water within the limits of water availability and the installed capacity of the plant. The simulated water flow $F_{i,j}(t)$ at the plant location is then used to compute $AHP_{(i,j)}(y)$ based on Eq. (2.16), considering the average head of each plant $\overline{h_{(i,j)}}$, which is determined based on Eq. (2.8), taking the average reservoir water level.

$$AHP_{(i,j)}(y) = \int_{t\ in\ y} \min\Big(\rho g \eta_{(i,j)} \overline{h_{(i,j)}} F_{(i,j)}(t)\ ,\ P_{(i,j)}\Big) dt \tag{2.16}$$

The hydraulic stock is the total energy that can be produced using energy stored in all the reservoirs of reservoir plants belonging to the power grid, it is defined by:

$$S(t) = \sum_{(i,j)s.a.Typ_{(i,j)}=reservoir} \int_{V_{min,i}(t)}^{V_i(t)} \rho g \eta_{(i,j)} h_{(i,j)}(V)\, dV \tag{2.17}$$

Finally, for a hydropower plant type k (run-of-river or reservoir), the simulated production $E_k(t)$ is given by:

$$E_k(t) = \sum_{(i,j)s.a.Typ_{(i,j)}=k} E_{(i,j)}(t). \tag{2.18}$$

2.2.5 Calibration

A calibration step is performed based on the comparison of simulated AHP and observed production at each individual plant, provided that such data are available. The objective of this step is to identify and correct errors from different sources, which are discussed in this section. The calibration procedure then varies according to the type of power plant.

2.2.5.1 Run-of-river plants

Discrepancies between the simulated AHP of a run-of-river plant $AHP_{(i,j)}(y)$ and its historical production $E_{(i,j)}(y)$ can arise from five factors:

1. Hydro-meteorological biases of the model may result in discrepancies in river discharges between the model and the actual river conditions;

2. An inexact location of the plant on the HTU graph may lead to inaccurate estimates of the available discharge at the plant's location;

3. The model assumes that the plant can harness the entire river volume. In reality, the river may split into several branches, with only one channeling water through the plant;

4. A uniform efficiency of 0.9 is assumed for all plants. However, actual efficiency varies depending on the type of hydroelectric turbine used (the choice is made based on the plant's rated head and flow) and flow conditions;

5. We assume that the plant produces at its maximum potential. In practice, it may be unavailable for maintenance and some of the plant's potential can be reserved for ancillary services to the grid or curtailed if non-dispatchable renewable generation potential exceeds the power demand. This can reduce the actual production compared to the potential.

As in previous studies (Wagner et al., 2017; Zhou et al., 2018), the unknown efficiency of the power plant $\eta_{(i,j)}$ is adjusted to calibrate the model against historical annual generation data, based on the previously estimated bias (Eq. (2.19)). Such calibration corrects the total error without differentiating its source.

$$\eta_{(i,j)} = \frac{1}{0.9} * \overline{\frac{E_{(i,j)}(y)}{AHP_{(i,j)}(y)}} \tag{2.19}$$

2.2.5.2 Poundage and reservoir power plants

Over a year, the water entering the reservoir i of a plant (i, j) can either contribute to the annual production of the plant $E_{(i,j)}(y)$, to the annual change in the hydraulic stock in the reservoir $\Delta S_i(y)$, or spill without generating power.

As for run-of-river plants, differences in simulated AHP and observed production can have different sources. In addition to the five errors listed above, a sixth possible error, related to the adduction network, should also be considered. Indeed, we assume in our model that each plant is only fed by one reservoir, which can lead to an underestimation of the plant production if some other water inputs are non-negligible. To account for these different error sources, we calibrate the model in two successive steps:

- Step 1: Dams with a large negative bias (inferior to -50 %) are shifted downstream from their original location to take into account the computed deviation. This adjustment can be seen as adding water intakes for the power plant based on the topography, such that the power plant receives enough water. Most concerned areas are located in mountains, where the water intakes are quite close geographically (on the same atmospheric grid) and therefore subject to the same precipitation, which allows us to assume that the water available per unit of area is similar.
- Step 2: For the other plants, the efficiencies are adjusted to match the observed production, as with run-of-river (Eq. (2.19)).

2.3 Summary

This chapter described the conceptual framework of a demand-based approach to simulate hydropower operations in land surface models. The method relies on three original features: (i) the reconstruction of the human-made hydropower network on the model grid to represent not only natural water flows but also those built for hydropower management; (ii) the implementation of reservoir operation rules that account for their multipurpose objectives; (iii) the prescription of an exogenous "hydropower demand" defined at the power grid level to drive the release of hydroelectric reservoirs, allowing coordinated management of all hydroelectric resources on the power grid and consistent with power system needs.

CHAPTER 3

Implementation in the ORCHIDEE model and validation with the French study case

This chapter aims at validating the modeling approach that has been described in the previous chapter. To this end, the framework is implemented in the ORCHIDEE LSM and the French power system is used as a study case.
Sect. 3.1 introduces the data and methods used for the case study of the French power grid. Sect 3.2 assesses the performance of ORCHIDEE in reproducing river discharges over this area. Sect. 3.3 details the modeling results and assesses the performance of the method to represent the historical operations of hydropower plants. Finally, Sect. 3.4 discusses these results and concludes by outlining future perspectives of research.
This chapter corresponds to the second part of the article submitted for publication in the journal Hydrology and Earth System Sciences (Baratgin et al., 2024 (submitted)[b]).

Contents

3.1 Data and methods for the study case over France 38
3.1.1 ORCHIDEE setup 38
3.1.2 Infrastructure datasets 39
3.1.3 Data for water demands and validation 41
3.2 Assessment of the performance of ORCHIDEE to simulate river discharges in France 43
3.2.1 Bias in average discharge 43
3.2.2 Discharge seasonality 46
3.3 Results 47
3.3.1 Calibration 47
3.3.2 Hydropower operations 50
3.3.3 Effects of hydropower operations on river discharges 53
3.4 Discussion and conclusion 54
3.4.1 Summary of the work 54
3.4.2 Limitations and opportunities for improvements 55
3.4.3 Sources of uncertainties 56
3.4.4 Perspectives 57

3.1 Data and methods for the study case over France

3.1.1 ORCHIDEE setup

In this study, ORCHIDEE is run in stand-alone mode, forced with the SAFRAN meteorological dataset (Quintana-Segui et al., 2008). SAFRAN (Système d'Analyse Fournissant des Renseignements Atmosphériques à la Neige) is a surface reanalysis resulting from the optimal interpolation between the vertical profiles of the atmosphere derived from ERA-40 atmospheric reanalysis and surface observations. It provides the required atmospheric variables - temperature, relative humidity at two meters, wind speed, downward radiation (shortwaves and longwaves), and precipitation (solid and liquid) - at an hourly time step over an 8 × 8 km grid that covers France and upstream part of its catchments beyond its borders.

To estimate the sensitivity of ORCHIDEE's simulations to the uncertainties of precipitation, we built two alternative atmospheric forcings by replacing precipitation data in SAFRAN with other precipitation datasets: COMEPHORE (Tabary et al., 2012) and SPAZM (Gottardi et al., 2008). These datasets are presented in detail in Appendix A.2.1 and their relative differences with SAFRAN are displayed in Fig. 3.1.

COMEPHORE dataset provides observations of surface precipitation accumulation over metropolitan France at an hourly and kilometric resolution based on a synthesis of radar and rain gauge data. We build a meteorologic dataset SAF_COM by replacing precipitation data in SAFRAN with data from COMEPHORE. As COMEPHORE does not distinguish solid and liquid precipitations, we keep SAFRAN's hourly ratio of solid/liquid precipitations when possible and discriminate based on the air temperature otherwise. The differences in annual mean precipitation between SAFRAN and COMEPHORE are generally small, with an average deviation inferior to 1.0% (Fig. 3.1). However, we find a small seasonal bias as this average deviation ranges from -2.0% in winter to +1.9% in summer. Moreover, discrepancies increase dramatically in mountainous regions, especially in the Alps and in the Pyrenees. For grid points with an average elevation above 1000m, the annual mean precipitation in COMEPHORE is, on average, 10.4% lower than in SAFRAN.

SPAZM is a daily reanalysis of precipitation at the kilometer scale, developed by EDF, France's main electricity producer. We interpolate the daily precipitation data from SPAZM to the hourly scale and merge it with SAFRAN data to create the alternative forcing dataset SAF_SPAZM. As for SAF_COM, we keep SAFRAN's hourly ratio of solid/liquid precipitations when possible. Compared to SAFRAN, SPAZM's precipitations are on average 2.7% higher, with a bias of +7.0% in summer and +2.1% in winter. The bias is heterogeneously spread over France (Fig. 3.1) with larger differences on the highest reliefs, without a clear sign. For grid points above 1000 meters, the average deviation is +3.9%.

The vegetation distribution map used in ORCHIDEE is derived from the ESA-CCI Land Cover dataset at 0.05° resolution for the year 2010. The soil background albedo map is derived from the MODIS albedo dataset aggregated at 0.5° resolution. Soil texture distribution maps are obtained from Reynolds map (Reynolds et al., 2000) at 5-arc-min resolution with 12 USDA soil texture classes (at 30 cm depth). In this study, ORCHIDEE performs the energy and water budgets at a 15-minute time step, and reservoir operations are performed at the same time step. Given that the time step is greater than the time constant of reservoirs, we consider that reservoir spillage always occurs within a single time step.

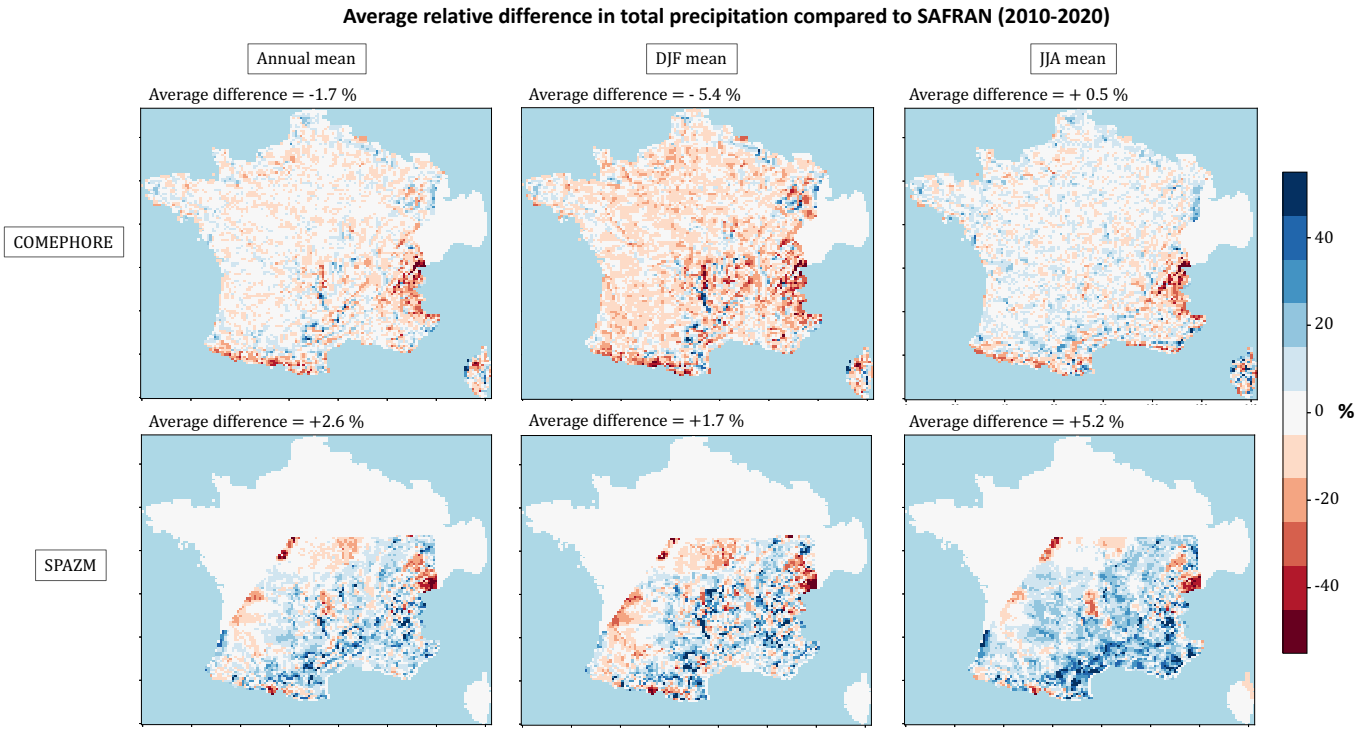

Figure 3.1: Relative differences in total precipitation across the datasets for the period 2010-2020. Left column: annual average difference; middle: average difference in winter (**D**ecember-**J**anuary-**F**ebruary); right: average difference in summer (**J**une-**J**uly-**A**ugust). Top: COMEPHORE dataset compared to SAFRAN; Bottom: SPAZM compared to SAFRAN

3.1.2 Infrastructure datasets

3.1.2.1 Dams and reservoirs

We use reservoir data from GRanD (Global Reservoirs and Dams) dataset (Lehner et al., 2011), which compiles data on large reservoirs and dams worldwide (volume $> 0.1km^3$, totaling 7320 dams). The database includes 137 dams in France, 63 of which are used for hydroelectricity. However, some important dams for French hydroelectricity are not documented in this database. Therefore, we completed the dataset with data from the CFBR (Comité Français des Barrages et des Réservoirs), responsible for the inventory of French dams higher than $15m$ for the ICOLD (International Commission on Large Dams). We extracted data from its website (CFBR, 2021) to complete the GRanD database. Our final dataset comprises 492 French dams. Their location, original data sources, and intended purposes are shown in Fig. 3.2.

3.1.2.2 Hydropower plants

The data used in this study are obtained from the European Commission et al. (2019) database. This database includes geographical coordinates, installed power capacity, plant type (run-of-river, reservoir, or pumped-hydro storage (PHS)), and hydraulic head information for 4186 European plants, totaling an installed capacity of 161 GW. Of these, 153 plants are located in France, representing 20.6 GW of capacity.

Other available datasets of French hydropower plants are the national registers of electricity generation and storage facilities published annually (ODRÉ, 2016, 2018). The

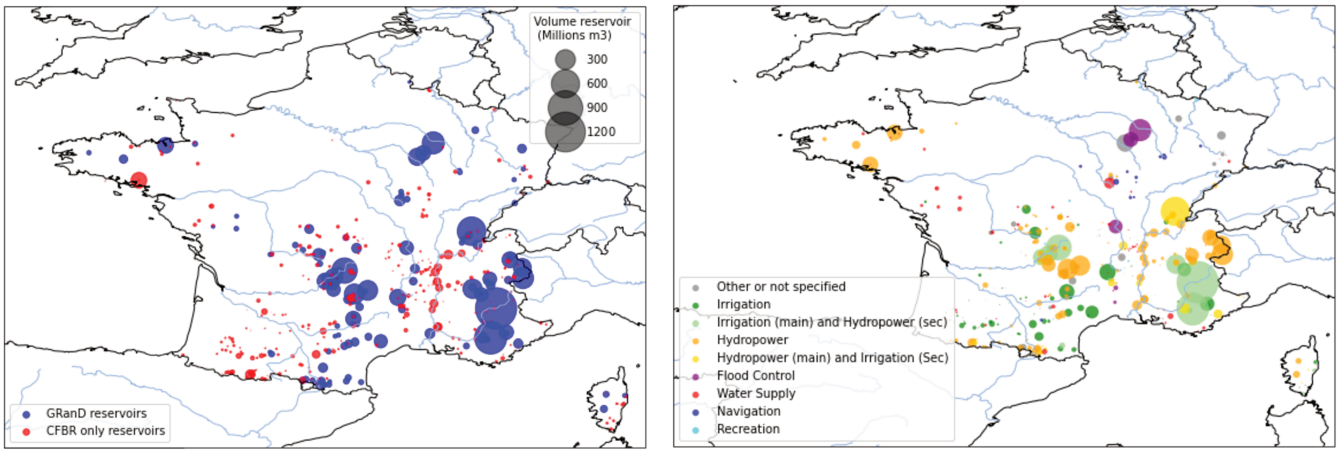

Figure 3.2: The reservoirs in the final database. Left: Source database; Right: Main uses of the reservoirs (*Sec* denotes secondary use.)

2016 register includes data on 414 hydropower plants, with a total installed capacity of 23.4 GW. However, as these registers do not provide the geographical coordinates of the plants, we chose to use the JRC database. Nevertheless, we use data from the 2016 national register to correct head information and categorize the plants according to the 4 categories used by the French operator: run-of-river, poundage, reservoir, and PHS. Figure 3.3 shows the locations of the plants included in our final database, while Table 3.1 summarizes the discrepancies between the databases in terms of installed capacities. Its last line details the main features of the final database we use for this study.

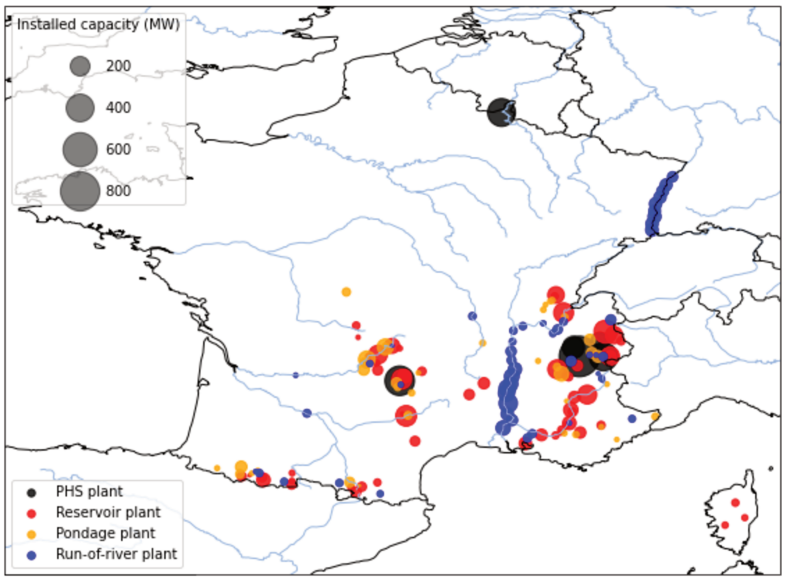

Figure 3.3: Typology of the plants in the database

3.1.2.3 Performance of location algorithm

Following the procedure outlined in Fig. 2.2, we locate the infrastructures on the MERIT river network and construct the HTU routing graph based on the simplification of this MERIT network (resolution of 2km) on the SAFRAN atmospheric grid (resolution of 8

	Total	Run-of-river	Poundage	Reservoir
National Register 2016 (ODRÉ, 2016)	23.426	5.943	3.715	8.748
JRC (initial categories)	19.695	5.87	-	8.76
Final database (plants from JRC database, classified following RTE categories which have been located on HTUs)	19.638	4.426	2.606	7.434
compared to ODRÉ (2016)	*84.6%*	*74.2%*	*71.7%*	*86.0%*

Table 3.1: Comparison of the different databases in terms of installed hydroelectric capacities (GW) in metropolitan France (without Corse et DOM-TOM)

km). HTU areas can thus theoretically vary from 0 to 64 km^2 and the average area of HTUs in our graph is 4.73 km^2. The upstream area of an HTU is defined recursively as the sum of the HTU area and the upstream area of all its tributaries. For each hydroelectric infrastructure, we compare in Fig. 3.4 its reference upstream area (from the database or MERIT network) to the upstream area of the HTU in which it is located. For most of the structures, the positioning error is lower than 20%. Some dams with a small upstream area are, however, located in HTUs with a higher upstream area, due to resolution constraints.

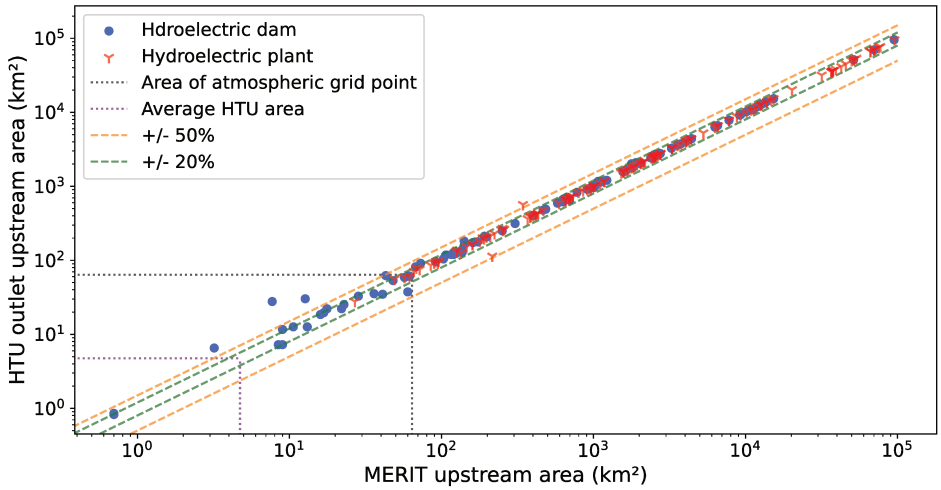

Figure 3.4: Comparison of the initial upstream area of the infrastructure (referenced in the database or upstream area of the MERIT pixel on which it is placed) with its final upstream area in the HTU graph. Blue dots represent hydroelectric reservoirs (reservoirs that have been associated with power plants during the adduction network building step) and red signs represent hydropower plants. Green and orange dashed lines delineate a respective error of +/- 20% and +/- 50%, while grey and purple dotted lines respectively refer to the area of an atmospheric grid point and the average area of an HTU.

3.1.3 Data for water demands and validation

3.1.3.1 Ecological and irrigation demands

In France, minimum flow requirements are defined relatively to the mean interannual flow downstream of the dam $\overline{Dis_i}$. They are summarized in Table 3.2. We ran a twenty-year

SAFRAN simulation without reservoir operations to calculate $\overline{Dis_i}$ at dam locations.

	$\overline{Dis_i} > 80m^3/s$	$\overline{Dis_i} < 80m^3/s$
Dam intended for hydropower purpose	$F_{min,(i,i+1)} = 0.05\overline{Dis_i}$ or flow immediately upstream of the dam if it is lower	$F_{min,(i,i+1)} = 0.05\overline{Dis_i}$ or flow immediately upstream of the dam if it is lower
Dam intended for other purpose	$F_{min,(i,i+1)} = 0.05\overline{Dis_i}$ or flow immediately upstream of the dam if it is lower	$F_{min,(i,i+1)} = 0.1\overline{Dis_i}$ or flow immediately upstream of the dam if it is lower

Table 3.2: French legal requirements for ecological flow, $\overline{Dis_i}$ is the mean interannual flow downstream of the dam

To account for the irrigation purposes of some reservoirs, we increase the minimum flow requirement downstream of reservoirs intended for irrigation during the summer period (June 1st to September 30th) by setting $\alpha_{irri} = 8$. This choice is based on information available from French reservoir concession contracts, which sometimes specify the volume of water reserved for irrigation. In the case of Serre-Ponçon, for example, the concession contract stipulates a reserve of 200 million m^3, to be used for irrigation, between July 1 and September 30. If we consider a constant withdrawal spanning three months, this corresponds to a $25m^3/s$ flow, which is 45% of the $55m^3/s$ mean interannual flow at this location, and thus 9 times larger than F_{min}, which is set to 5%, as explained above.

3.1.3.2 Hydropower production demand

As this study aims to validate our proposed reservoir operations model, we take the historical time series of production as the hydropower demand prescribed to the model. We can thus assess whether the model, when driven by the historical atmospheric dataset, can meet the observed production levels. Data on observed production for hydropower plants in the French power grid are available from 2015 onwards, published by RTE, the French TSO, at a 30-minute time step for 2 categories of plants (RTE, 2023b):

- **River production** $D_{river}(t)$ that gathers the production of pure run-of-river power plants and poundage power plants (reservoir plants with a storage below 400h)
- **Reservoir production** $D_{res}(t)$ that gathers the production of reservoir power plants with a greater storage capacity

In our model, $D_{river}(t)$ is then used to drive the production of run-of-river and poundage power plants, while $D_{res}(t)$ is used for the reservoir power plants with greater storage capacity, both using the method described in 2.2.3.2. We use the classification established by RTE and illustrated in Fig. 3.3.

3.1.3.3 Validation data

In France, hydropower reservoirs are managed by companies that do not share detailed data on their production or their filling level. Similarly, discharge data from gauging stations near hydroelectric power plants are often not publicly accessible. This limits the data available for validating our model.

However, as a delegate of public services, RTE provides some data, often aggregated at the national level, which allows us to calibrate and validate our model as shown in the following section. The available data are:

- National time series of production by hydroelectric sector (river and reservoir) at 30-minute time step from 2015 (RTE, 2023b) - which are the time series used for the hydropower production demand;
- Annual production of each hydroelectric power plant for the years 2015, 2016, and 2018 (ODRÉ, 2015, 2016, 2018);
- Weekly hydraulic stock (Eq. (2.17)) at national level from 2014 to 2020 (RTE, 2023d);

As mentioned in Section 3.1.2, our hydropower plant dataset does not cover all the installed plants in France. However, by using annual production data of each plant provided by (ODRÉ, 2015, 2016, 2018), we can estimate the share of the national production provided by the power plants in our database. This allows us to compute a factor for converting the production from national time series (RTE, 2023b) into representative production within our model, both for prescribing the production demand and comparing the results. The calculation of such conversion factors is presented in Table A.1.

We also compute the maximum hydraulic stock of the reservoirs associated with the power plants in our database using Eq. (2.17) and data from our plants and reservoirs databases. We obtain $S_{max} = 3.66\ TWh$, which is quite close to the 3.59 TWh value reported by RTE (RTE, 2023d). Therefore, we can consider that our database covers all the available storage and that missing hydropower capacity is linked to negligible reservoirs.

3.2 Assessment of the performance of ORCHIDEE to simulate river discharges in France

To evaluate the performance of the ORCHIDEE model in simulating river discharges in France, independent of reservoir operations, we compare the daily river discharges simulated by the model with observations from Schapi (2022) database. It is important to note that the observed discharge data represents actual discharge values, including water withdrawals, while, at this stage, ORCHIDEE generates natural discharges without accounting for such withdrawals and dam operations.

3.2.1 Bias in average discharge

Figure 3.5 displays the relative biases in the mean discharge simulated by ORCHIDEE forced by SAFRAN over the 2010-2020 period for a selection of gauging stations located on rivers with hydropower infrastructure (see Fig. 3.3 for the detailed locations of the power plants). We chose the bias metric because the annual mean discharge is the most relevant parameter for hydropower potential.

The overall performance of the model indicates a slight overestimation of flows, with an average bias of +2.4%.

The discharge bias increases with the upstream area of stations. For small catchments (less than 500 km^2), the average bias is -1.6%. In medium-sized catchments (between 500 and 5000 km^2), the bias is +1.1%. In large catchments (more than 5000 km^2), the bias becomes more pronounced, reaching +7.6%. It is, however, important to note that the smaller the upstream area, the greater the uncertainty in the location of the station. In Fig. 3.5, only the stations located with an error in the upstream area lower than 20% are displayed.

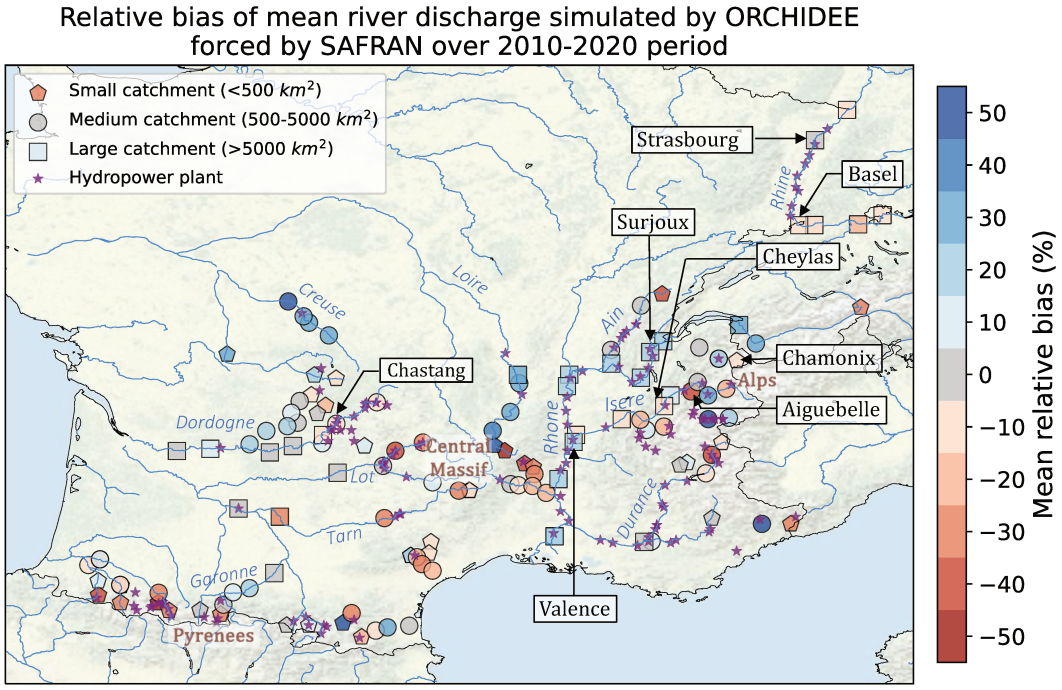

Figure 3.5: Relative bias in mean discharge for a selection of gauging stations located on French rivers equipped for hydropower, for the period 2010-2020. Each colored point represents a gauging station, with the shape indicating the size of its catchment, while the color indicates the discharge bias at this location. Purple stars indicate the locations of the hydropower plants located on the model grid.

On the largest rivers (Rhine and Rhone), where most run-of-river power plants are located, the bias shows little spatial variability, remaining around +20% for the Rhone and -10% for the Rhine. In contrast, in the Alps, where a significant share of dispatchable hydroelectric capacity is installed, the bias is highly variable, even within the same river. For instance, upstream of the Isere river, the bias varies from -19% to +26% between two stations located about twenty kilometers apart. The upstream reaches of the Durance also show negative biases. In the other massifs equipped for hydroelectricity, such as the Pyrenees and Massif Central, there are negative biases at higher altitudes, which gradually diminish downstream.

Assuming negligible observational errors, discharge bias can originate from several error sources:

- Errors in the atmospheric forcing applied to ORCHIDEE;
- Modeling errors in the representation of energy, water, and carbon cycles;
- Missing processes in ORCHIDEE, such as glacier melting, interactions with groundwater, and water withdrawals.

To explore the first hypothesis, Fig. 3.6 compares the discharges simulated by ORCHIDEE using the two alternative forcings (SAF_COM and SAF_SPAZM) with those from the reference SAFRAN simulation. The relative biases of these simulations compared to observations are presented in Fig. 3.7.

Under the SAF_COM forcing, simulated discharges show relatively small differences from those obtained with SAFRAN on an annual average, except in mountainous wa-

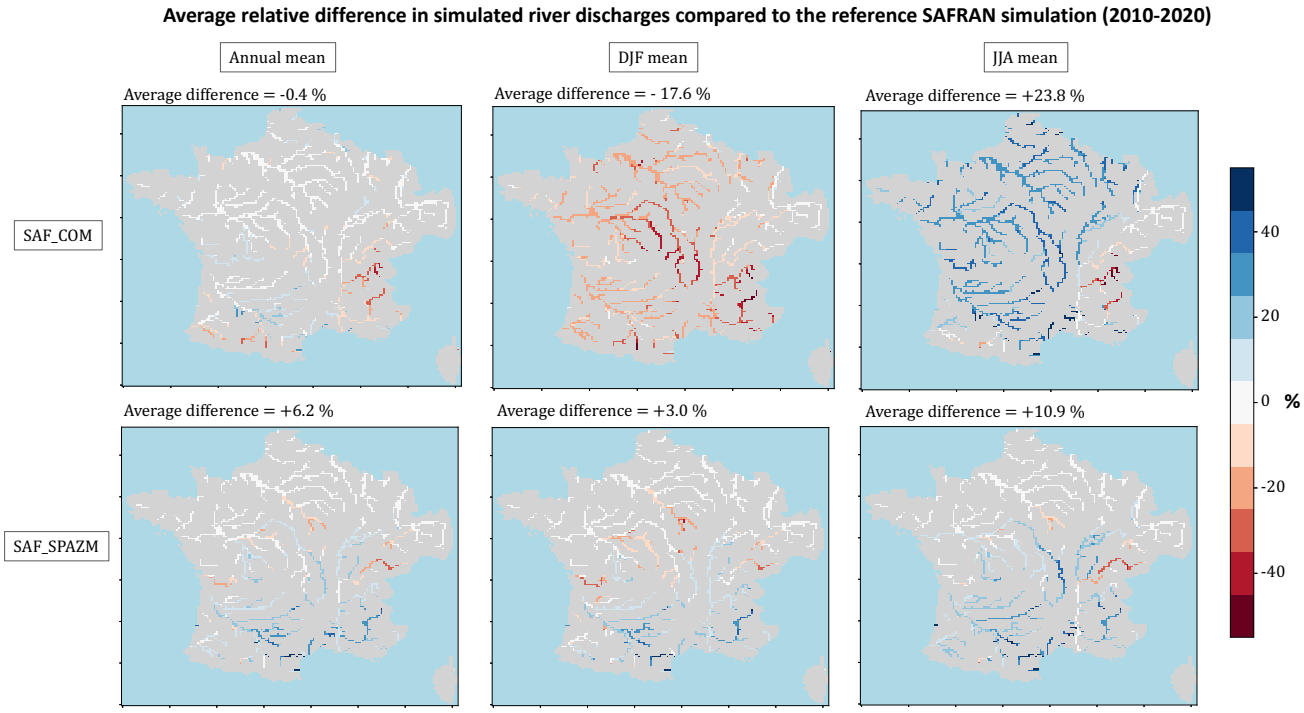

Figure 3.6: Relative difference in discharge simulated by ORCHIDEE under the alternative precipitation forcings. Results are expressed as average relative differences compared to the reference SAFRAN simulation for the period 2010-2020. Left: annual average difference; middle: average difference in winter (December-January-February); right: average difference in summer (June-July-August). The discharges are shown for all grid points with an upstream area greater than 1000 km^2.

tersheds (Alps and Pyrenees). In these regions, the lower precipitation in SAF_COM results in streamflows that are 30% to 40% lower when compared to the SAFRAN simulation. Besides, a pronounced seasonal pattern is observed. The simulated streamflows are lower in winter under SAF_COM across France (averaging -16% and up to -50% for the Loire and Durance rivers), while they are higher in summer (averaging +25% and up to +50% for the Loire River). Regarding the comparison with observed flows (Fig. 3.7), the negative biases observed with SAFRAN in the Alps and Pyrenees are accentuated under SAF_COM, particularly along the Durance and Isere rivers, where many hydroelectric power plants are located. However, for some Alpine stations and the Massif Central, where the flow is overestimated with SAFRAN, the flow is more accurately simulated under SAF_COM.

Under the SAF_SPAZM forcing, mean river discharges generally increase in most watersheds compared to the SAFRAN simulation, consistent with the higher precipitation in this dataset. However, the upper Rhone watershed stands out with a decrease in simulated discharge, reaching up to -40% during the summer, allowing for a reduction in the bias in simulated discharge in this area.

This analysis shows that variability in forcing data significantly influences simulated discharges, even if we limit our analysis to the precipitation variable without considering other forcing variables.

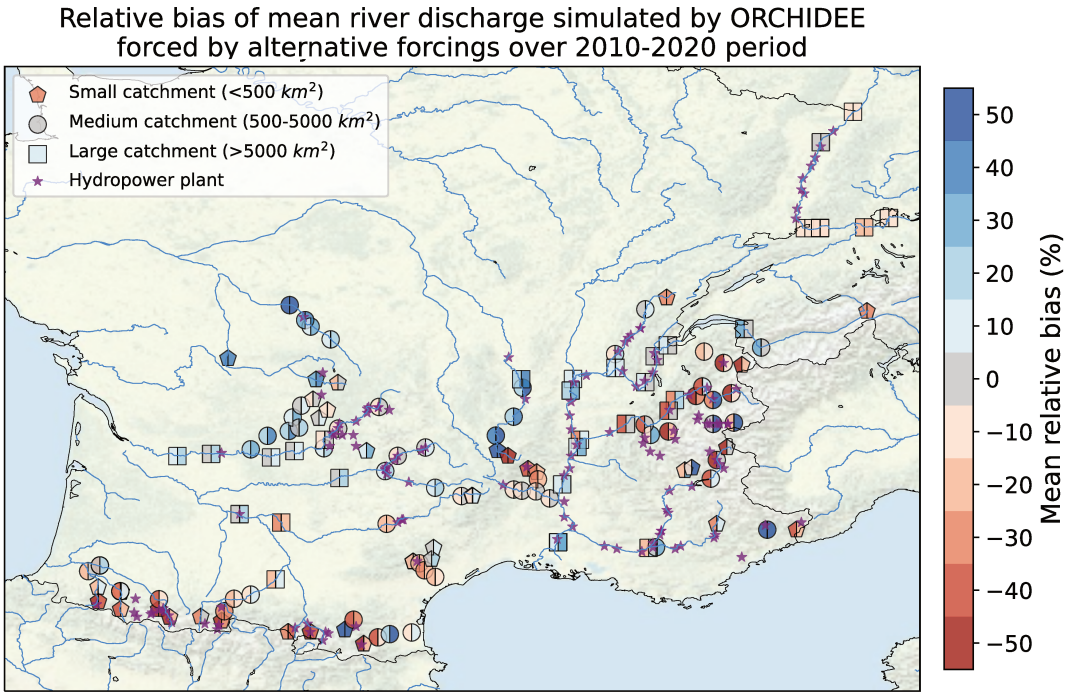

Figure 3.7: Relative bias in mean discharge simulated by ORCHIDEE under the alternative forcings for a selection of gauging stations located on French rivers equipped for hydropower, for the period 2010-2020. The left coloring indicates the discharge bias under SAF_COM while the right coloring indicates the discharge bias under SAF_SPAZM.

3.2.2 Discharge seasonality

Beyond the bias in mean values, the performance of ORCHIDEE in reproducing the seasonality of the discharge is key for the modeling of run-of-river production as well as that of poundage power plants, which have very limited storage capacity. Observations and simulations of daily discharges under the SAFRAN forcing are presented in Fig. 3.8 for selected gauging stations in catchments equipped with run-of-river or poundage power plants.

As depicted in Fig. 3.3, run-of-river plants are mostly located along the Rhone and Rhine rivers. In the upper Rhone (Surjoux station), there is a substantial overestimation of high flows and an underestimation of low flows. The error reduces progressively downstream: the Nash Sutcliffe efficiency (NSE) is better at the Valence station, despite a higher overall annual bias (likely due to the non-representation of water withdrawals). On the Rhine (Basel and Strasbourg stations), we see similar errors, with an underestimation of low flows during the Fall and an underestimation of the Spring maximum. The discrepancy in the Rhone's seasonality can be attributed to the non-representation of Leman reservoir management in our model, which is known to play a crucial role in shaping discharge seasonality in the upper Rhone (Habets et al., 1999).

Poundage plants are distributed across various catchments. Some of them are concentrated in the upper Dordogne river, notably the Chastang plant, the most powerful poundage facility, which benefits from a gauging station at its location. We find a positive NSE for this station, indicating that the seasonality is well captured by the model.

Finally, some run-of-river and poundage plants are also concentrated in the Alps, where we focus on two gauging stations: Chamonix, situated in a small upper catchment,

close to a run-of-river plant and Cheylas, positioned on a large river (l'Isère), downstream from several power plants. At Chamonix, we find a seasonal bias as the model simulates an earlier discharge peak compared to observations (around 2 months ahead). At Cheylas, the model overestimates the seasonal variability of the discharge, with higher flows during Spring and lower flows during Winter, which can be attributed - at least in part - to the non-representation of reservoir management at this stage of our study (see Sect. 3.3.3).

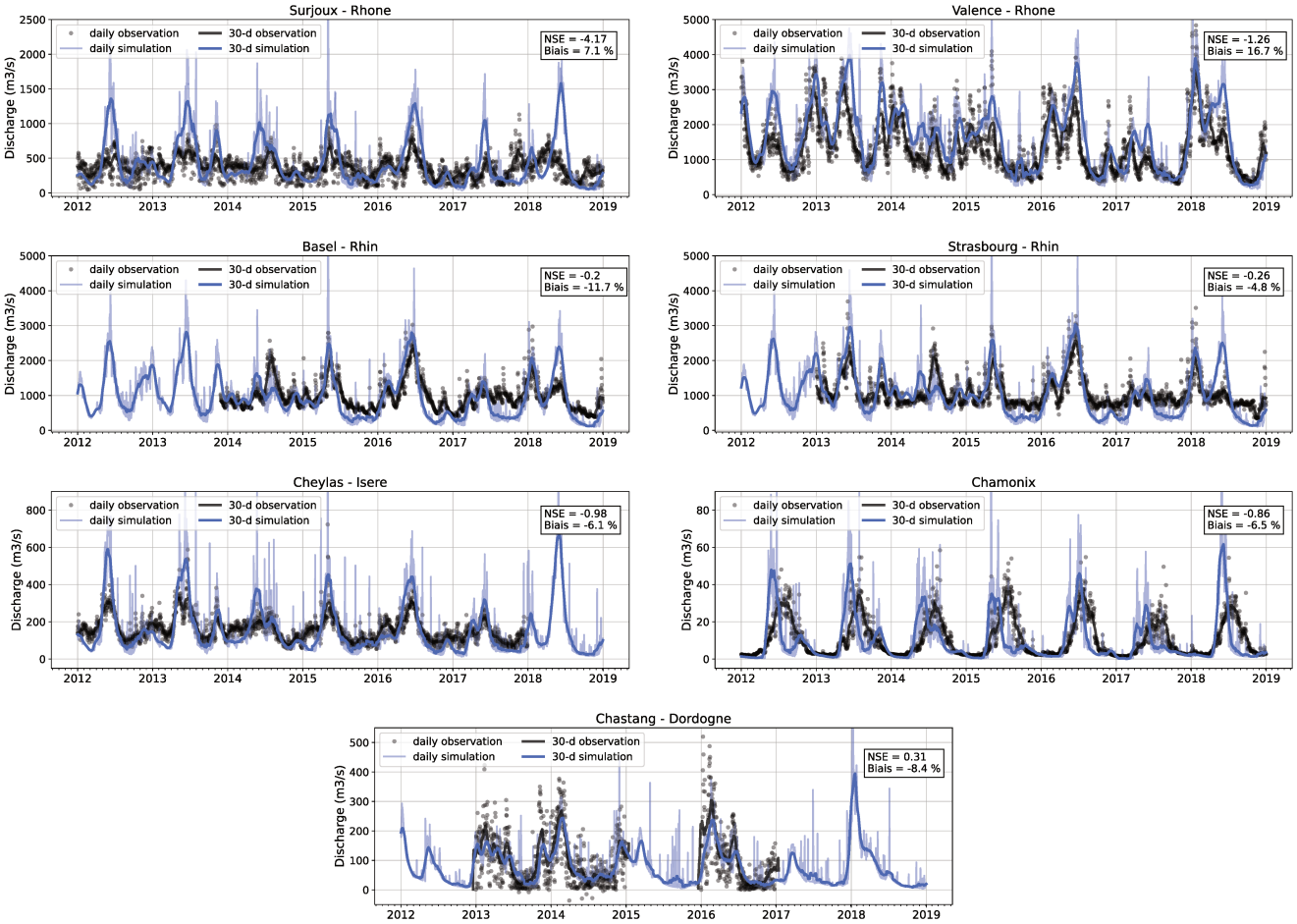

Figure 3.8: Comparison of simulated and observed river discharges for a selection of gauging stations. Locations of selected stations are indicated in Figure 3.5. Fine lines and dots are daily time series while ticker lines are 30-day sliding averages. NSE metrics are computed on a daily time series.

3.3 Results

3.3.1 Calibration

We present here the application of the calibration process to the French study case. First, we assess the discrepancies between the AHP simulated by the model (Eq. (2.16)) and the observed annual production at each power plant for the years with available data. We then discuss the likely origin of these discrepancies. Finally, the calibration process is validated by comparing annual potentials simulated in ORCHIDEE to the observed annual production at the national level for an extended period, using data from 2000 to

2020. We choose to use SAFRAN forcing as a reference for the calibration step, as this dataset is widely used in regional studies of France.

3.3.1.1 Discrepancies between AHP and the historical production

Figure 3.9 shows the average relative bias of simulated AHP compared to observed production for the three years with available data for the run-of-river plants in our database. For most plants, the bias in hydropower potential is comparable to the bias in river discharge computed at nearby stations, which is displayed in Fig. 3.5. This indicates that the bias mainly stems from hydro-meteorological errors (reason 1 of the list presented in Sect. 2.2.5). At the Caderousse and Gambsheim power plants, located in Fig. 3.9, a stronger positive bias is found. At these locations, only part of the river flows through the plant, which explains the computed bias (reason 3). The calibration leads to obtained efficiencies ranging from 0.43 to 1.31 with a median value of 0.88.

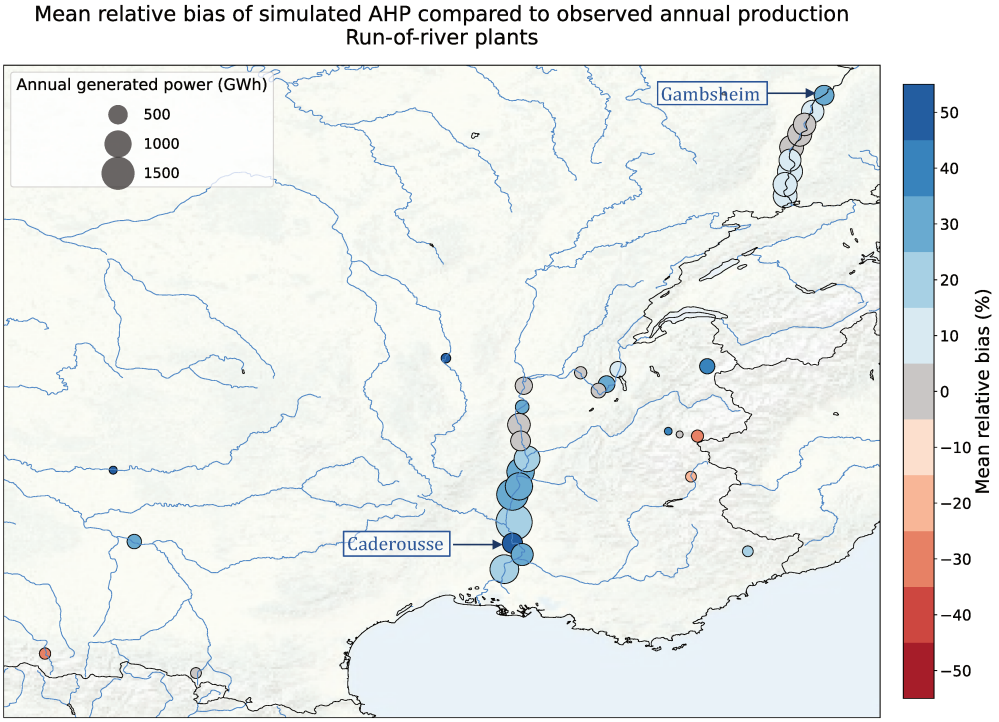

Figure 3.9: Average relative bias of simulated AHP compared to observed annual production for run-of-river power plants with available data. The point size corresponds to the average annual production.

Over a year, the water entering the reservoir of a reservoir or poundage power plant can either contribute to the annual production of the plant $E_{(i,j)}(y)$, to the annual change in the hydraulic stock within the reservoir $\Delta S_i(y)$, or spill without generating power. Observed production $E_{(i,j)}(y)$ is available for the three years mentioned earlier. However, observations of changes in the hydraulic stock are only available at the national level, for the national stock $\Delta S_{obs}(y) = \sum_{i \text{ in res}} \Delta S_i(y)$. To compare simulated AHPs with observations of production and stored energy, we make the two following assumptions: (i) spillages that do not produce power can be neglected, and (ii) the changes in the hydraulic stock are homogeneous across all reservoirs: $\forall i, \Delta S_i(y) = \Delta S_{obs}(y) \times \frac{S_{max}}{S_{i,max}}$. In Fig. 3.10, we plot the average bias of $AHP_{(i,j)}(y)$ relative to observed net production $E_{(i,j)}(y) + \Delta S_i(y)$ for the three years for which data are available. It enables us to

distinguish two types of bias in the simulated AHP, suggesting that two main error sources can be distinguished:

- Plants with an absolute bias inferior to 50% (represented by circles in Fig. 3.10). Their biases are generally similar to those of discharge for nearby stations, displayed in Fig. 3.5.
- Plants with a bias inferior to -50% (represented by pentagons in Fig. 3.10). These plants are mainly located in mountainous areas and have a negative bias stronger than that of the discharges in the area. Moreover, their biases have a small interannual variance, indicating that the error is stable over time (not shown).

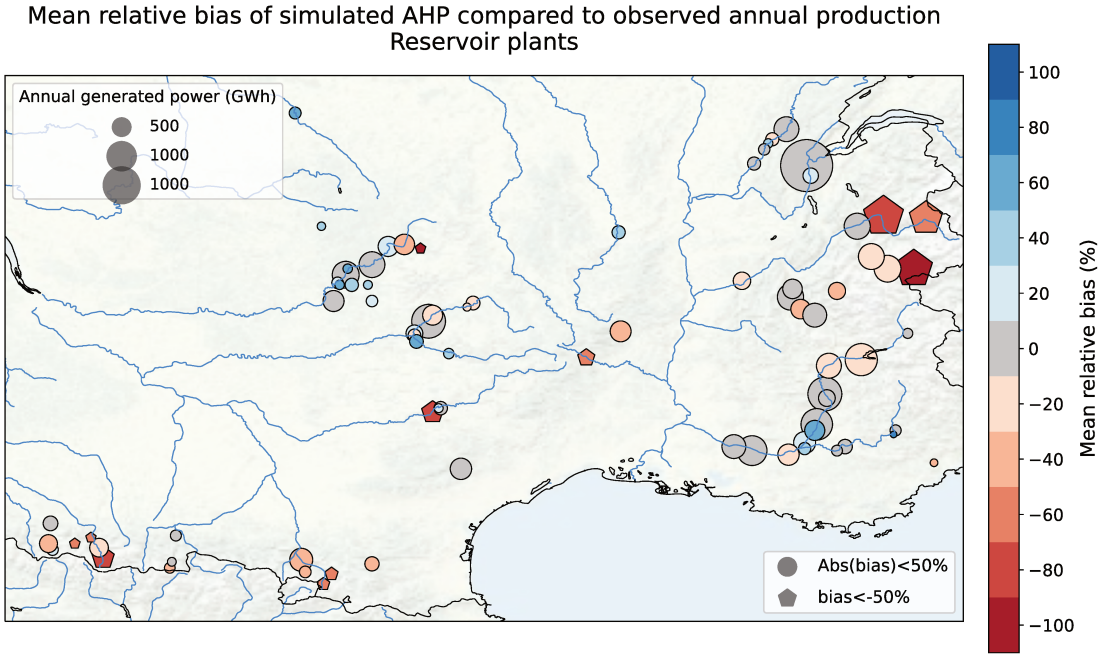

Figure 3.10: Average relative bias of simulated AHP compared to observed net annual production for reservoir and poundage power plants with available data. The point size corresponds to the average annual production.

3.3.1.2 Validation of the calibration

The performance of the calibrated model is assessed by comparing the potentials simulated by the calibrated model forced by SAFRAN with the historical annual production (RTE, 2023b) at the national scale over the whole period 2000-2020. For each plant category, the simulated annual potential is computed by summing the AHP of all plants within this category. For poundage and reservoir plants, we directly compare this aggregated potential to the historical production, as stock data (RTE, 2023d) are not available for the whole period. This relies on the assumption that the national stock returns to its initial value at the end of each year.

The calibration appears to be robust as very small biases (less than 3%) are obtained when comparing the simulated potentials to the observed production (Fig. 3.11). The relative differences in annual production are on average lower than 10%. This indicates that the model is able to capture the overall pattern of interannual variability of the observed production.

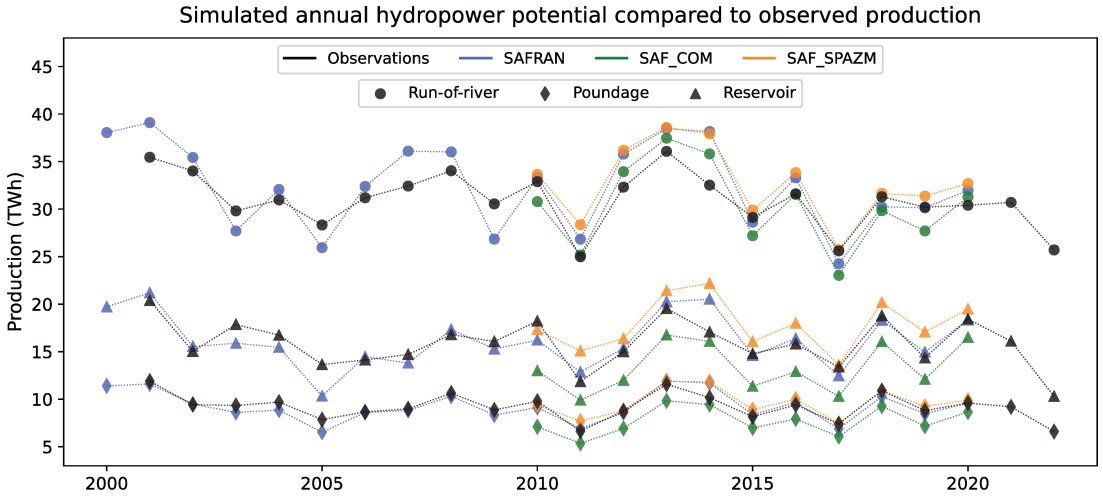

Figure 3.11: Comparison of estimated annual hydropower potential with observed annual production for the different categories of hydropower plants and for the different atmospheric forcings, after calibration based on SAFRAN.

We also explore the sensitivity of the model and calibration procedure to the uncertainties in precipitation forcings that are highlighted in Fig. 3.1 and 3.6. We compute AHPs under the two alternative forcings (Fig. 3.11) and compare the obtained inter-forcing variability with the inter-annual variability of observed production (Tab. 3.3). Run-of-river annual potentials exhibit little variation across the different forcings, as the simulated flows of major rivers hosting run-of-river power plants (primarily the Rhone and the Rhine) demonstrate a low sensitivity to precipitation uncertainty (see Fig. 3.7). Consequently, the inter-forcing variability of simulated potential is three times smaller than the interannual variability of run-of-river power production (see Table 3.3). It is also slightly smaller than the modeling error, indicating a low sensitivity of simulated run-of-river production to the precipitation uncertainty. Conversely, reservoir plant production shows a much higher sensitivity to precipitation disparities between forcings. Lower COMEPHORE precipitations in mountainous regions lead to an average decrease of 18.7% in the total simulated potential, compared to the SAFRAN simulation. As a result, the variability among forcings is of the same order of magnitude as the interannual variability of production and is higher than the modeling error. Finally, poundage power plants fall in an intermediate category, displaying an inter-forcing variability that is 41% lower than the interannual variability.

In conclusion, the uncertainties in precipitation forcing in mountainous regions prove to be critical in the estimation of realistic hydropower potentials for reservoir plants. The calibration carried out relative to SAFRAN is less effective for other forcings, SAF_COM for instance, as the differences in precipitation data appear as the main contributor to the differences in hydropower potentials.

3.3.2 Hydropower operations

In this section, we assess the model's ability to simulate reservoir management and hydropower production. Observed time series of river production (gathering run-of-river and poundage power plants) and reservoir production serve as demand inputs for the reservoir operations in the model. At each time step, the model aims to meet this target by operating the reservoirs according to the rules described in Sect. 2.2.3 and the

	Run-of-river		Poundage		Reservoir	
	Calibration Period	Validation Period	Calibration Period	Validation Period	Calibration Period	Validation Period
Mean relative error	-	+ 2.8 %	-	-2.6 %	-	-1.4 %
Mean absolute relative error	3.5 %	6.9 %	3.7 %	5.4 %	2.5 %	7.5 %
Interannual variability (TWh)[a]	3.71		1.71		2.61	
Inter-forcing variability (TWh)[b]	1.32		1.25		2.54	
Modeling error (TWh)[c]	2.64		0.67		1.33	

[a] We define the interannual variability daily as the standard deviation of observed annual productions.
[b] We define the inter-forcing variability as the mean standard deviation of annual potential across the forcings.
[c] We define the modeling error as the RMSE of SAFRAN simulated potentials compared to observations.

Table 3.3: Estimation of the errors in annual potentials prediction

simulated hydrological cycle. The objective is to verify if our model can simulate operations consistent with observed production. We present here the results obtained from a simulation spanning the period from 2015 to 2020.

3.3.2.1 River production

At each time step, the model first computes the available potential from fatal production (from run-of-river plants and spill or constrained releases from the reservoirs of poundage plants). If this potential falls short of fulfilling the production target, the model then operates the reservoirs connected with poundage plants to supplement the production.

Figure 3.12 details how the simulation compares to the prescribed production over the period when the model is forced by SAFRAN. The model successfully reproduces the overall seasonality of production, meeting the hourly production target 69.0% of the time. The failures (in red in Fig. 3.12) account for 6.9% of the total prescribed production across the six years. They mostly occur during summer and fall, indicating that the simulated hydrology is unable to produce what was actually produced during these periods. In winter and spring, on the contrary, there are instances when the potential of fatal production exceeds the target production (January and February 2018 for instance). This means that the model could have generated more power during these periods than was actually produced. These discrepancies are likely due to the seasonality bias in discharge within the Rhone and Rhine catchments, as highlighted in Fig. 3.8. Despite these discrepancies, the performance of the model remains satisfactory, as it captures the gross seasonality and magnitude of run-of-river production, in addition to the inter-annual variability (Fig. 3.11).

The run-of-river production simulated by the model when forced by the alternative forcings SAF_SPAZM and SAF_COM, are presented in Fig. A.1 and A.3. Using SAF_SPAZM, the failures in meeting the prescribed production are reduced (4.3% of production not satisfied compared to 6.9%) due to slightly higher annual potentials of run-of-river and poundage power plants (Fig. 3.11). On the other hand, higher failures are obtained with SAF_COM (15.4% of the total production), consistently with the lower potentials obtained in Fig. 3.11. However, the seasonality remains very similar in all three simulations, consistent with the similar seasonality of the simulated discharges for the Rhine and Rhone rivers (Fig. 3.6).

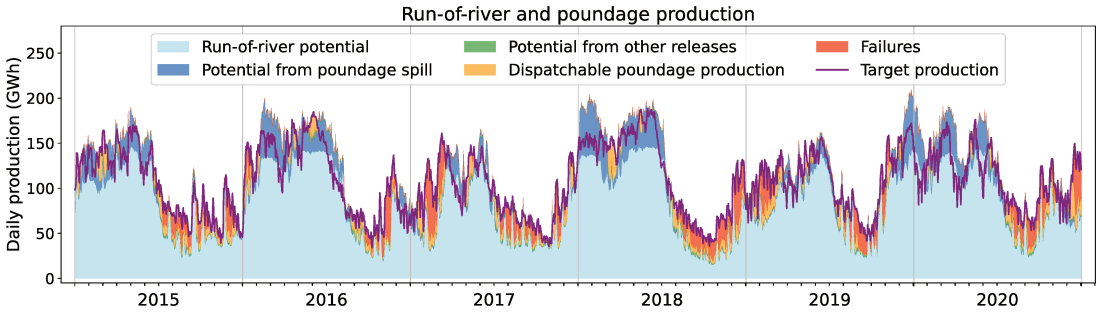

Figure 3.12: Daily production from run-of-river and poundage plants. The purple line indicates the production prescribed to the model and the red coloring shows the failures of the model to meet this target production, when the model is forced by SAFRAN. The other colors refer to the nature of the flow that contributes to the simulated production. Light blue represents the gross potential of run-of-river plants, dark blue represents the gross potential from spillage from poundage reservoir (water overflowing from the reservoir), green represents the potential from constrained releases from poundage reservoirs, and lastly orange represents the dispatchable production, generated by the water specifically released from the poundage reservoirs for power generation.

3.3.2.2 Reservoir production

Similarly, a 30-minute time series of observed production by reservoir power plants is prescribed to the model. To fulfill this demand, the model first computes the non-dispatchable production, available from reservoir spillage and constrained releases, by operating reservoirs according to the rules defined in Sect. 2.2.3. Figure 3.13 details how the simulation compares to the prescribed production throughout the period when forced by SAFRAN. Simulated production under the other forcings is presented in Fig. A.2 and A.4. Figure 3.14 displays the co-evolution of the observed national hydraulic stock (RTE, 2023d) and the one simulated by the model (Eq. (2.17)) with the three forcings under study.

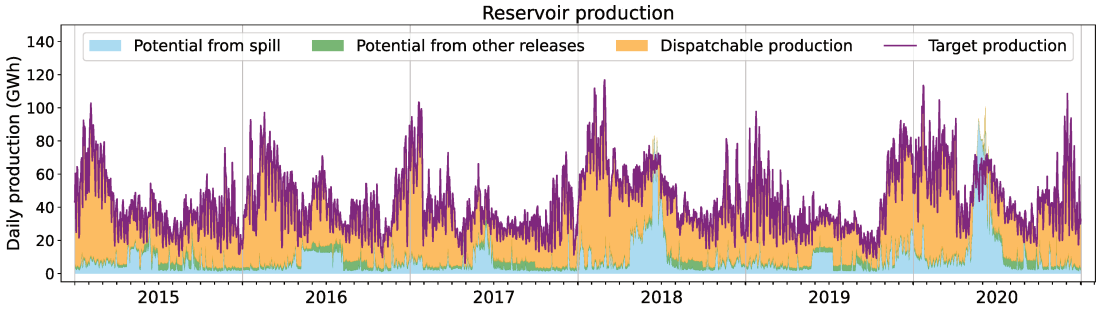

Figure 3.13: Daily production from reservoir plants. The purple line indicates the production prescribed to the model. The other colors refer to the nature of the flow that contributes to the simulated production. Blue represents the gross potential from reservoir spillage (water overflowing from the reservoir), green represents the potential from constrained releases from the reservoirs, and lastly orange represents the dispatchable production, generated by the water specifically released for power generation.

Under SAFRAN, the model successfully meets the production target while simulating hydraulic stock variations consistent with observations throughout the six-year period. Reservoirs are filled during the spring due to snowmelt and depleted during the winter

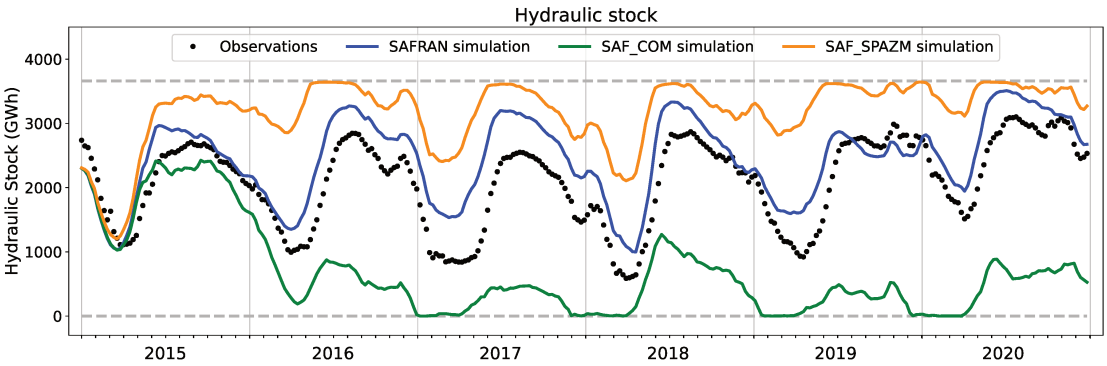

Figure 3.14: Comparison of simulated and observed national hydraulic stock evolution.

to meet the high electricity demand. Nevertheless, a slight temporal shift is observed, as the simulated stock starts to fill some weeks earlier compared to the observations. This temporal shift aligns with the seasonal biases in river discharges identified at the Chamonix Station (Fig. 3.8), indicating a consistent pattern.

Under SAF_SPAZM, the stock remains significantly higher than the observations. Indeed, the simulated annual potential of reservoir power plants exceeds their observed production (Fig. 3.11), resulting in reduced releases from the reservoirs to meet the prescribed demand. This leads to high levels of unused spillage, as shown in Fig. A.2.

Under SAF_COM, however, the stock is completely depleted after the two first years of simulation, and a significant portion of the demand cannot be satisfied (Fig. A.4). This is consistent with the huge difference in annual production estimates highlighted in Fig. 3.11. In addition to the substantial deficit in hydropower potential, a negative feedback loop comes into play. As the reservoir storage diminishes, the head of the power plants decreases, reducing the power generation for a given released volume. Consequently, more water is drawn to generate the same amount of energy, further exacerbating the decline in reservoir storage. The calibration carried out relative to SAFRAN is not effective in avoiding this outcome.

Figure 3.13 allows for the distinction of the different drivers of French hydropower production, depending on the season. In winter, hydropower production is substantial, driven primarily by high electricity demand. Most of the production stems from intentional reservoir operations, with a minimal portion attributed to fatal production. In spring, fatal production becomes more prominent, particularly due to snowmelt-induced spillage, resulting in a minimum hourly production, even during periods of low power demand, such as at night (only visible at the hourly resolution not displayed here). During summer, a significant portion of the hydropower potential comes from constrained ecological and agricultural water releases. When looking at the hourly production (not displayed here), we find a good agreement between the simulated minimum production and the observed troughs in RTE's production.

3.3.3 Effects of hydropower operations on river discharges

We explore in this section the extent to which the representation of hydropower operations can reduce the hydro-meteorological errors of the model discussed in Sect. 3.2, using the example of two gauging stations located in the Alps. Figure 3.15 details the location of these stations comparatively to the hydropower network. The Aiguebelle station is located on the Arc river, just upstream of its confluence with the Isère river, and

downstream from a series of hydropower plants, including one that generates electricity through the releases from a dam on the Isère river. The Cheylas station is located on the Isère river, downstream of its confluence with the Arc.

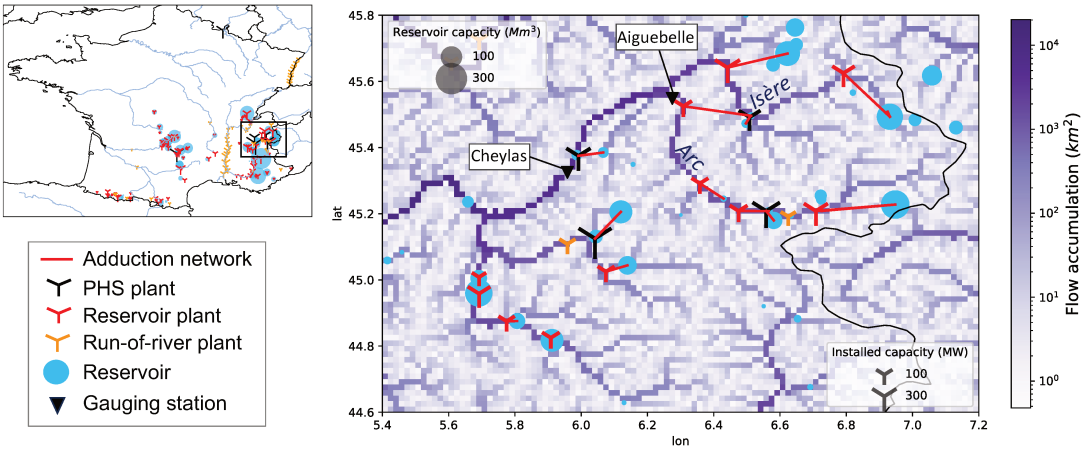

Figure 3.15: Location of Aiguebelle and Cheylas stations comparatively to hydropower infrastructures in Arc catchment (French Alps). PHS plants are pumped-hydro storage plants not considered in this study.

Figure 3.16 compares the seasonality of the discharges simulated at these two locations by ORCHIDEE forced by SAFRAN with and without activating the hydropower operations module.

At the Aigubelle station, implementing hydropower operations significantly reduces the annual bias from -31% to -4% (Fig. 3.16). Indeed, when hydropower operations are activated, a portion of the Isère's water is diverted from its natural outlet to supply a power plant on the Arc. At Cheylas, no change is observed in the bias of the simulated river discharge. Furthermore, the seasonality of discharge is improved at both stations, with higher flows in fall and winter due to releases for power generation. This results in a significant improvement in the NSE metric.

We found a similar effect for other French watersheds where flow observations near hydropower plants are available. However, as mentioned earlier, the confidentiality surrounding French hydroelectric production complicates a systematic and precise evaluation of this improvement in flow simulation.

3.4 Discussion and conclusion

3.4.1 Summary of the work

This study has assessed the performance of a demand-based approach to simulate hydropower production in a land surface model. The approach has been implemented on the ORCHIDEE model for the case study of the French power grid. The ORCHIDEE model was run driven by an atmospheric reanalysis dataset and national historic hydropower production time series were prescribed to the model as the hydropower demand to satisfy. First, we found that despite significant bias in the river discharges simulated by the model for the French rivers equipped with hydropower, the model is able to provide good estimates of past production, thanks to the calibration step. Second, the results indicate that, when the model is forced to reproduce the historic generation, the implemented

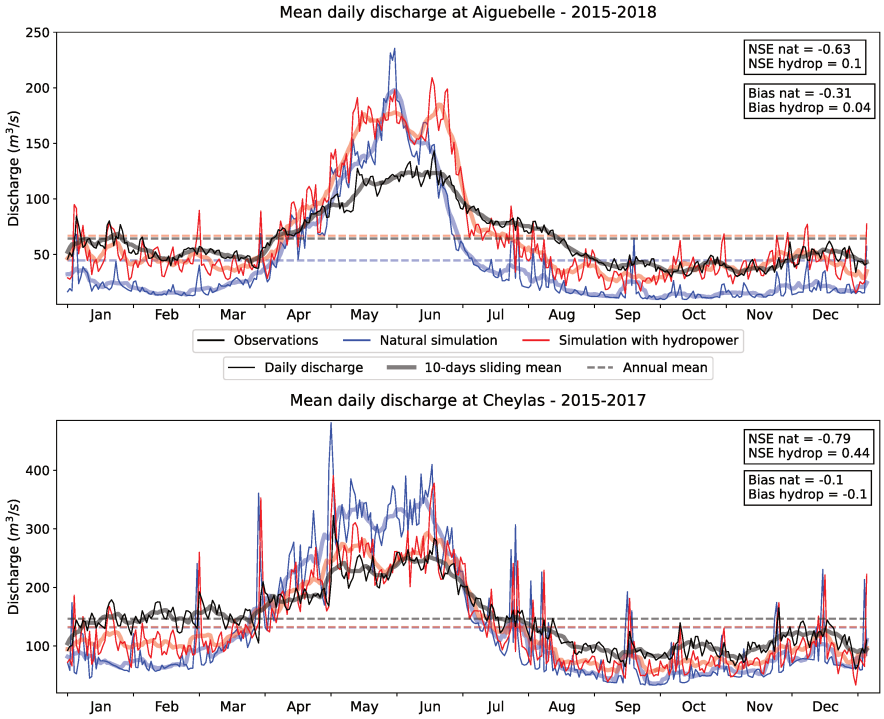

Figure 3.16: Comparison of daily (fine line) simulated river discharge with hydropower operations (red) and without (blue) and observed discharge (black) for two gauging stations in the French Alps. The thicker line is the 10-day average while the dashed line is the annual mean.

method simulates hydroelectric reservoir operations in line with observations of reservoir storage at the national level.

3.4.2 Limitations and opportunities for improvements

Beyond this satisfactory result, our method presents several limitations and opportunities for improvement.

First, the time series used to drive the reservoir releases in this study is the actual production of dispatchable hydropower plants, which may differ from the real demand for dispatchable hydropower production. Indeed, the actual production is the result of a trade-off between the demand and the prevailing hydrological conditions, particularly the storage level in reservoirs. If this storage is low, the demand might not be fully satisfied to preserve water for future needs. Besides, we consider an exogenous dispatch of the hydropower production across the different types of hydropower plants (namely run-of-river and reservoir) at each time step. This approach facilitates the identification of model deficiencies for each type of power plant. For instance, we found a seasonal bias in run-of-river hydropower production, that would have been overlooked if a single production target had been used for all power plants. The reservoir plants would have served as buffers, reducing their production during periods of excess run-of-river output and increasing it during periods of deficits, thereby resulting in discrepancies in the stock evolution. However, in reality, the dispatch of power demand across the different types of hydropower plants is not exogenous but also depends on the hydrological conditions, as the potential for run-of-river production is fully exploited before turning to dispatchable units. To capture these intricate interactions between hydrology and hydropower production decisions, a solution is to couple our model with an economic power system

dispatch model (Oikonomou et al., 2022). This coupling would ensure that the power demand dispatch used to drive reservoir operations in ORCHIDEE considers the hydrological conditions simulated within the model. This would result in a comprehensive modeling framework wherein simulated hydropower production simultaneously adheres to constraints related to water availability, non-power reservoir operations, and minimization of power system costs. In particular, hydropower demand would be endogenously adjusted to match the hydropower potentials of the simulated hydrology and could avoid entering the feedback loop where reservoirs are emptied, as in the SAF_COM simulation. This novel approach holds significant promises for enhancing the consistency and realism of hydropower production simulations, in particular to study the joint impacts of climate change and variable renewable energy integration.

Second, in this study, we opted for a simple rule to distribute national production among the power plants, and demonstrated that such a rule could simulate credible hydroelectric operations at the national level. Since no time series of production data is available for individual plants in France, the realism of the simulated operations at the granular level cannot be assessed. However, the choice of the distribution rule could be further investigated, in particular by testing alternative rules, such as those proposed by Lund et al., 1999. Additionally, the operations we simulate assume that a social planner controls the entire grid's power plants and reservoirs, optimizing the collective production. In reality, power plants may belong to different stakeholders, each seeking to maximize their profit. Ambec et al., 2003 have shown that such decentralized management can lead to suboptimal resource management, which could not be reproduced by the proposed model. However, in the case of France, our assumption is justified as the historical production company, EDF, owns nearly 85% of the hydroelectric production.

Third, as we focused primarily on hydroelectric usage, other water uses are simplified or even omitted in the current version of the model. Specifically, no water abstraction for domestic, industrial, or agricultural needs is included. Following Zhou et al., 2021, the irrigation demand could be explicitly calculated by the model based on the deficit between potential and actual evapotranspiration. In other studies, domestic and industrial water demands are estimated using socio-economic proxies such as population density or GDP (Neverre, 2015).

3.4.3 Sources of uncertainties

We have paid particular attention to identifying and discriminating among the various sources of uncertainty that may affect the estimation of hydroelectric production using such a method. Our findings indicate that while errors in simulated discharge are prevalent in most watersheds in our case study, the limited knowledge of the hydroelectric adduction network is the main source of uncertainty for hydropower infrastructures in mountainous basins. To our knowledge, no dataset comprehensively documents these complex "hydroelectric links", which operate on a small scale. Therefore, an in-depth analysis of the gray literature released by the various stakeholders is necessary to reconstruct this network in detail. Furthermore, we proposed a calibration method to overcome this limitation and validated it against observations for the case study of France. This method can therefore be extended to countries with limited information available on the hydroelectric network.

Regarding hydro-meteorological errors, the use of three different precipitation datasets allows us to understand their more precise origin. In several watersheds crucial for hydroelectricity (such as Durance or Lot), and especially in the upstream parts, uncertainties in observed precipitation appear to be the primary contributor to the error in simulated

discharge. On the Rhone or the Rhine rivers, on the contrary, errors in the simulated discharges seem to stem more from processes not represented in the model, such as water withdrawals for human uses. Though incomplete, this work contributes to the current effort to integrate human water management into hydrological models, in order to simulate a more realistic water cycle (Nazemi et al., 2015b). We show that our method can improve river flow simulations in some mountain catchments where hydropower cannot be neglected.

Finally, our study shows that comparing hydropower estimates with observed production offers an indirect means of assessing the quality of meteorological data. In our study case, we demonstrated the lower quality of the COMEPHORE dataset in mountainous regions compared to SAFRAN or SPAZM, something already identified by Birman et al., 2017; Magand et al., 2018.

3.4.4 Perspectives

In conclusion, the demand-based operations proposed in this study hold promising prospects for enhancing our understanding of the resilience of different power mix scenarios to changes in climate, water management, or land use. The next steps in this trajectory involve (i) integrating our climate-based hydropower model with a power system model to get a comprehensive framework that captures all relevant constraints on hydropower production, (ii) applying this integrated framework to climate change scenarios and power system scenarios to evaluate the adaptive capacity of the power grids, and (iii) refining the description of other water uses to more completely describe the competition for water resources.

Such a detailed model could also be instrumental in planning future hydropower expansion more sustainably. It would help assess the demand satisfied by new hydropower plants at the grid scale, considering both existing and planned hydropower plants. Besides, the model could evaluate the potential impacts of new projects on river discharges and ecosystems.

CHAPTER 4

Supplementary analysis and extended results

This chapter extends the analysis of the new method's performance. First, Section 4.1 discusses the choice of the rule used to distribute the national production demand among the individual plants. Then, Section 4.2 examines the applicability of the demand-based approach to model the management of the French pumped hydro storage plants.

Contents

4.1 Which rule to model the coordinated operation of a hydropower network? - Comparison of different rules 60

4.1.1 Introduction 60

4.1.2 Methods 61

4.1.3 Results 63

4.1.4 Conclusion 67

4.2 Representing the management of pumped hydro storage (PHS) plants 67

4.2.1 Presentation of French PHS plants 67

4.2.2 PHS modeling 68

4.2.3 Results 70

4.2.4 Discussion - Competition with reservoir production 71

4.1 Which rule to model the coordinated operation of a hydropower network? - Comparison of different rules

4.1.1 Introduction

The actual operation of hydropower reservoirs is the result of a complex set of tradeoffs, involving power sector dispatch, competing water uses and the spatial allocation of power generation within the grid. Defining rules for a coordinated and efficient operation of hydropower reservoirs is therefore a challenging task. In their study, Macian-Sorribes et al. (2020) examine the advantages and drawbacks of the various existing approaches for deriving and representing optimal operating rules. They distinguish three main approaches: (i) direct optimization of operation, (ii) a priori rule forms and (iii) rule inference from optimization results. In the first category (i), the operating rules are a direct output of the optimization of a benefit function defined based on the reservoir purpose (Haddeland et al., 2006). In the second category (ii), the mathematical expression of the operating rule is decided prior to the execution of the optimization algorithm, which aims to calibrate the parameters of the a priori rule form to achieve the best performance. Finally, in the last category (iii), optimal operating rules are inferred from the analysis of the results from optimization algorithms.

We focus here on the last category of approaches, which are better suited for use in complex models like ORCHIDEE. Lund et al. (1999) provide the foundational article for this approach, by defining theoretical rules for the operation of reservoirs based on their usage and the parallel or structure of the reservoir network, whether in series or parallel. Specifically, concerning hydroelectric reservoirs, Lund et al. (1999) recommend the following:

- For reservoirs in series, they advise distinguishing between drawdown and refill seasons.
  - During the *refill* season, the objective is to maximize the storage at the end of the season. Their rule is **to fill the highest reservoirs first**. This rule is naturally followed by hydrological models equipped with a river routing module such as ORCHIDEE.
  - During the drawdown season, the objective is to maximize hydroelectric production given the available storage. This involves **allocating water preferentially to the reservoirs that lose the most head with declining storage levels, and emptying the reservoirs that lose the least head**. The loss of head with storage level is quantified using the storage effective index (SEI).
- For parallel reservoirs, different rules are proposed:
  - The **space rule** aims to leave more space in reservoirs where larger inflows are expected in order to minimize the total volume of spills.
  - The **storage effective index (SEI) rule** is similar to that used in the case of reservoirs in series. It involves emptying parallel reservoirs sequentially, beginning with those with the smallest SEI.

In this study, we evaluate how the empirical rules proposed by Lund et al. (1999) perform in comparison with the simple rule previously used, in the context of the operation of hydroelectric reservoirs in France over the 2015-2020 period.

4.1.2 Methods

4.1.2.1 Description of the different rules

As presented in the previous chapter, our modeling approach relies on specifying an exogenous production target $D_{res}(t)$ that must be met by the aggregate production from all reservoir plants. The potential energy production from minimum releases and spillage is first computed. If this potential is insufficient to meet the prescribed target, additional releases from the reservoirs need to be determined.

To determine the additional release required at the individual plant level, several rules can be used. The rules under consideration here are all based on the definition of an α function, which ranks the reservoir plants by their priority. At time t, the power plant (i,j) with the smallest $\alpha\left((i,j),t\right)$ is used first. We consider three different rules, each defining the α function differently.

Rule 1: Uniform filling of reservoirs This rule is the default rule used in the previous chapters. Plants are used in the decsending order of the of their reservoirs' filling level, from the most to the least filled. The α function is then defined as the inverse of the filling level of the plant's reservoir: $\alpha_1\left((i,j),t\right) = \frac{V_{tot,i}}{V_i(t)}$.

Rule 2: Storage effectiveness index (SEI) (Lund et al., 1999) The SEI provides a method to rank reservoirs based on their potential loss of energy from releasing water. Releasing a water volume δV from a reservoir i decreases its water level and then the energy head $h_{(i,j)}(V_i(t))$ of its plant and thus the energy likely to be generated from future releases. Considering a quasi-stationary state, Lund et al. (1999) express this energy loss $\Delta E_{(i,j)}(t)$ as:

$$\Delta E_{(i,j)}(t) = \rho g \eta_{(i,j)} \left(h_{(i,j)}(V_i(t)) - h_{(i,j)}(V_i(t) - \delta V)\right) \mathcal{I}_i(t) \tag{4.1}$$

$$\Delta E_{(i,j)}(t) = \rho g \eta_{(i,j)} \delta V \frac{\partial h_{(i,j)}}{\partial V}(V_i(t)) \mathcal{I}_i(t) \tag{4.2}$$

where $\mathcal{I}_i(t)$ is the total inflow expected to enter the reservoir until the end of the drawdown period. Based on stock data from RTE (2023d), we consider that the drawdown period extends from April 1st to August 1st for all reservoirs.

Lund et al. (1999) propose then to empty the reservoirs in the ascending order of their energy loss. In our model, we assume all reservoirs to have a tetrahedral geometry presented in Fig. 2.5, characterized by the dam height $H_{dam,i}$ and the total volume capacity of the reservoir $V_{tot,i}$. The water head $H_{res,i}(t)$ in the reservoir evolves then with the filling level following Eq. 4.3 and the actual head of the power plant is defined by Eq. 4.4.

$$H_{res,i}(t) = H_{dam,i} * \left(\frac{V_i(t)}{V_{tot,i}}\right)^{\frac{1}{3}} \tag{4.3}$$

$$h_{(i,j)}(t) = H_{(i,j)} - \left(H_{dam,i} - H_{res,i}(t)\right) = H_{(i,j)} - H_{dam,i}\left(1 - \left(\frac{V_i(t)}{V_{tot,i}}\right)^{\frac{1}{3}}\right) \tag{4.4}$$

We have thus $\frac{\partial h_{(i,j)}}{\partial V_i}(V_i(t)) = \frac{H_{dam,i}}{3V_{tot,i}^{\frac{1}{3}} V_i(t)^{\frac{2}{3}}} = \frac{H_{dam,i}}{3V_{tot,i}(\frac{V_i(t)}{V_{tot,i}})^{\frac{2}{3}}}$

In this rule, the α function is then defined by Eq. 4.5, which is the so-called SEI by Lund et al. (1999).

$$\alpha_2((i,j),t) = \eta_{(i,j)} \frac{H_{dam,i}}{V_{tot,i}(\frac{V_i(t)}{V_{tot,i}})^{\frac{2}{3}}} \mathcal{I}_i(t) \tag{4.5}$$

Figure 4.1,(a) shows the α_2 values on January 1st, assuming all reservoirs are 60% filled. These values spread across very different orders of magnitude due to the spread of the two components: the geometric ratio $\frac{H_{dam,i}}{V_{tot,i}}$ (Fig. 4.1,(b)) and the expected future inflow $\mathcal{I}_i(t)$ (Figure 4.1,(c)). The plants with the lowest α_2 values are mostly located in the Alps and Pyrenees, while those on large rivers show the highest values. The differences are mostly coming from the discrepancies in expected inflow.

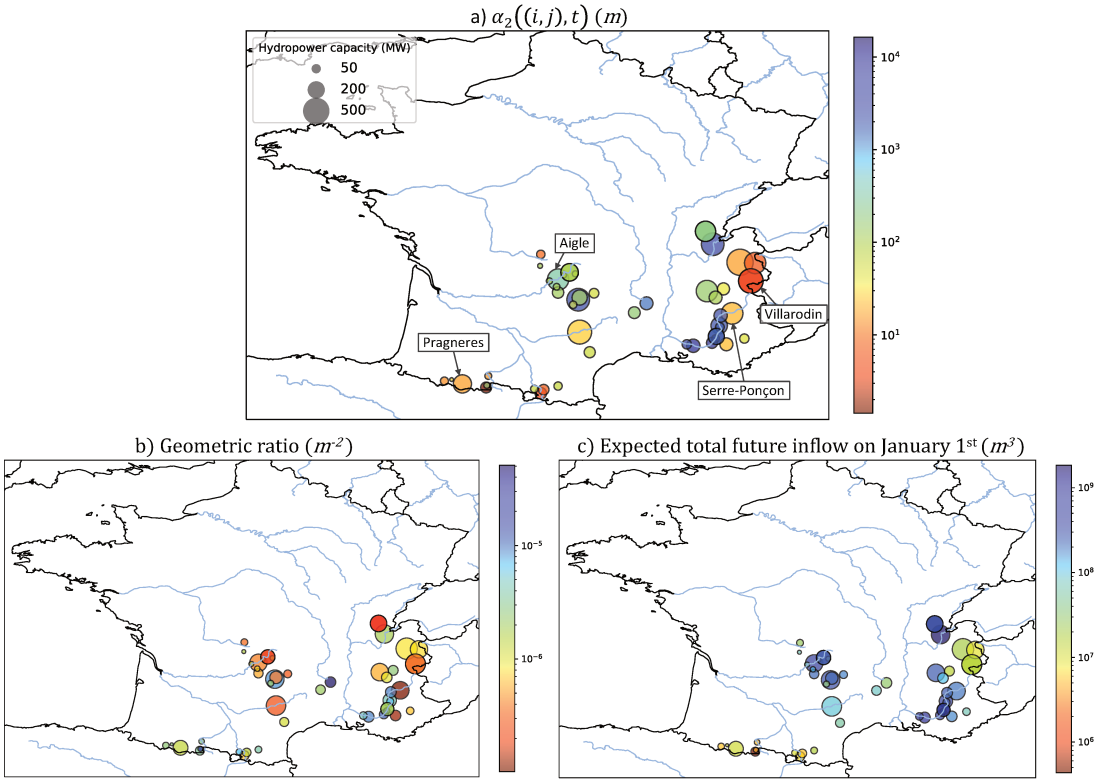

Figure 4.1: Top: a) Obtained values for $\alpha_2((i,j),t)$ on January 1st, assuming all reservoirs are equally filled at 60%. Bottom: The two components involved in the computation of $\alpha_2((i,j),t)$. b) Geometric ratio of reservoirs, defined by $\frac{H_{dam,i}}{V_{tot,i}}$; c) Total expected inflows between January 1st and April 1st, computed based on average river discharges simulated without accounting for reservoir operations. It corresponds to values taken for $\mathcal{I}_i$ on January 1st.

Rule 3: Hydropower space rule In the case of reservoirs in parallel, an approach suggested by Lund et al. (1999) is the space rule. This rule aims to prevent spillage by prioritizing withdrawals from reservoirs that are more likely to overflow in the near future. In this rule, the α_3 function is defined by the ratio of the available space in the reservoir to the expected inflow, expressed in terms of stored energy:

$$\alpha_3((i,j),t) = \frac{H_{(i,j)}V_{tot,i} - h_{(i,j)}(t)V_i(t)}{h_{(i,j)}(t)I_i(t)} \tag{4.6}$$

where $I_i(t)$ is the expected future inflow to the reservoir. In this study, we use the interannual mean inflow over the 30 following days.

Using Eq. 4.4 and given that $V_{min,i}(t) \geq 0.1V_{tot,i},\ \forall t$, we have
$h_{(i,j)}(t) \leq H_{(i,j)} \left(1 - \frac{H_{dam,i}}{H_{(i,j)}} \left(1 - 0.1^{\frac{1}{3}}\right)\right) \leq H_{(i,j)} \left(1 - 0.1^{\frac{1}{3}}\right),\ \forall t.$
Hence, $\alpha_3((i,j),t) \leq \frac{V_{tot,i}}{\left(1-0.1^{\frac{1}{3}}\right) * I_i(t)},\ \forall t$

Fig. 4.2 displays the average filling time of hydroelectric reservoirs in our study, defined by the ratio $\frac{V_{tot,i}}{\overline{I_i}}$, and shows that it spreads over different time scales. Reservoirs with the longest filling time are typically located in mountainous areas, while those on larger rivers, such as the Rhone or the Lot, have shorter filling times and are prioritized for withdrawals under this rule.

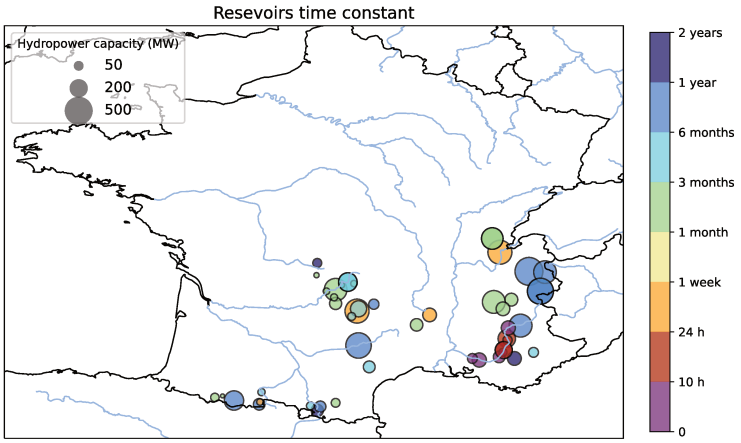

Figure 4.2: Average filling time of hydroelectric reservoirs in our study

4.1.2.2 Hydrological simulations

The ORCHIDEE model is run on the 2015-2020 period for each of these three rules, driven by SAFRAN atmospheric reanalysis and with the observed production as the target production that drives reservoir releases.

4.1.3 Results

We begin by assessing the performance of the different simulations in meeting the prescribed demand and in simulating a stock evolution that aligns with the observations.

Fig. 4.3 displays the co-evolution of the simulated production and the aggregated hydraulic stock for the three rules. The results show that rules 2 and 3 underperform compared to rule 1, particularly during the winters. The hourly reservoir production demand is unmet during 3.0% of the time with rule 2 and 12.1% of the time with rule 3, whereas it is fully satisfied with rule 1. Additionally, the hydraulic stock depletes more rapidly under rules 2 and 3. These findings indicate that rules 2 and 3 withdraw a greater volume of water to generate the same amount of energy. This suggests that the order in which power plants are operated under these rules does not sufficiently optimize water management. The suboptimal prioritization of power plants under rules 2 and 3 leads to a less efficient use of water resources, resulting in a faster depletion of the hydraulic stock.

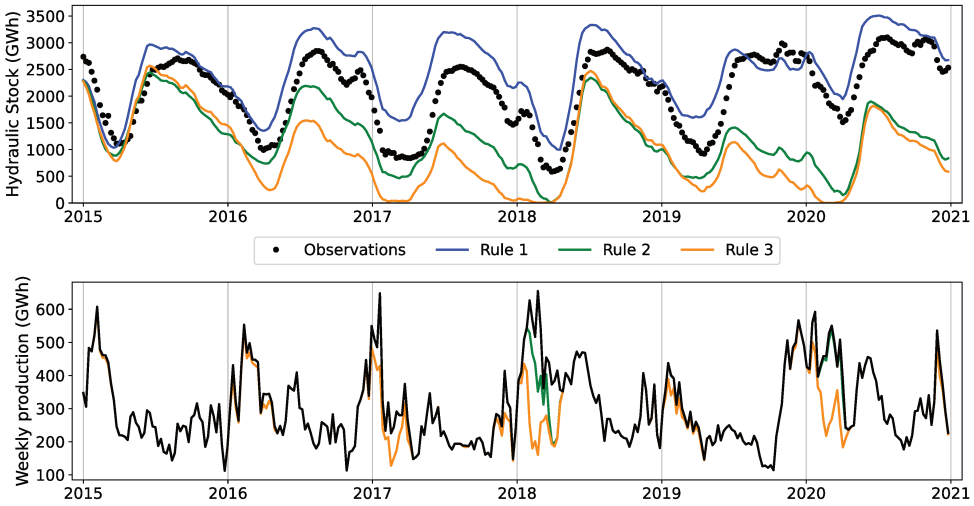

Figure 4.3: Comparison of the weekly national hydraulic stock (top panel) and weekly reservoir production (bottom panel) simulated under the three withdrawal rules. In the bottom panel, the blue line is overlapped by the black line.

To understand the differences in the utilization order of power plants based on the three rules, we analyze the behavior of four individual reservoir power plants under each rule. We specifically select four plants with contrasting characteristics as presented in Table 4.1. Their respective locations are shown in Fig. 4.1,a).

Reservoir plant name	Aigle	Pragneres	Villarodin	Serre-Ponçon
Dam Altitude (m)	382	2161	1930	757
Reservoir volume ($10^6 m^3$)	225	332	63	1270
Mean inflow (m^3)	48.2	12.1	2.0	45.1
Time constant (days)	54	316	359	325
Nominal head (m)	80	855	1255	129
Dam height (m)	92	120	85	129
Geometric ratio ($10^6 m^{-2}$)	0.41	0.36	1.34	0.10

Table 4.1: Characteristics of the reservoir of the four plants considered

The reservoir filling dynamics and power production of each of the four plants under the three operating rules under study are presented in Fig. 4.4. In the simulation with rule 1, reservoirs are operated to equalize their filling levels. The evolution of the filling level is therefore similar for all reservoirs, resulting in individual power production driven by national demand (especially in winter) and the respective inflow peaks (winter for the Aigle power plant, spring and summer for the other plants). As illustrated in Fig. 4.1, rule 2 prioritizes the use of mountainous reservoirs with low expected inflow. This strategy leads to the complete depletion of the Pragneres reservoir, followed by the Villarodin reservoir, while no withdrawal is made from the Aigle reservoir. This approach results consequently to spillage in reservoirs with larger inflows such as Aigle. Rule 3 prioritizes the depletion of reservoirs most likely to overflow in the coming days. Consequently, it gives priority to emptying the Aigle reservoir, which has a shorter response time compared

to other reservoirs (see Fig. 4.2). This leads to production from a poorly filled Aigle reservoir, which does not benefit from a significant head and results in water wastage. Hence, only 520 GWh are produced by the Aigle power plant when using rule 3 compared to 714 GWh with rule 1, whereas more water is withdrawn from the reservoir. Once the Aigle reservoir is completely emptied, the Pragneres reservoir is withdrawn, as it has the second smallest time constant.

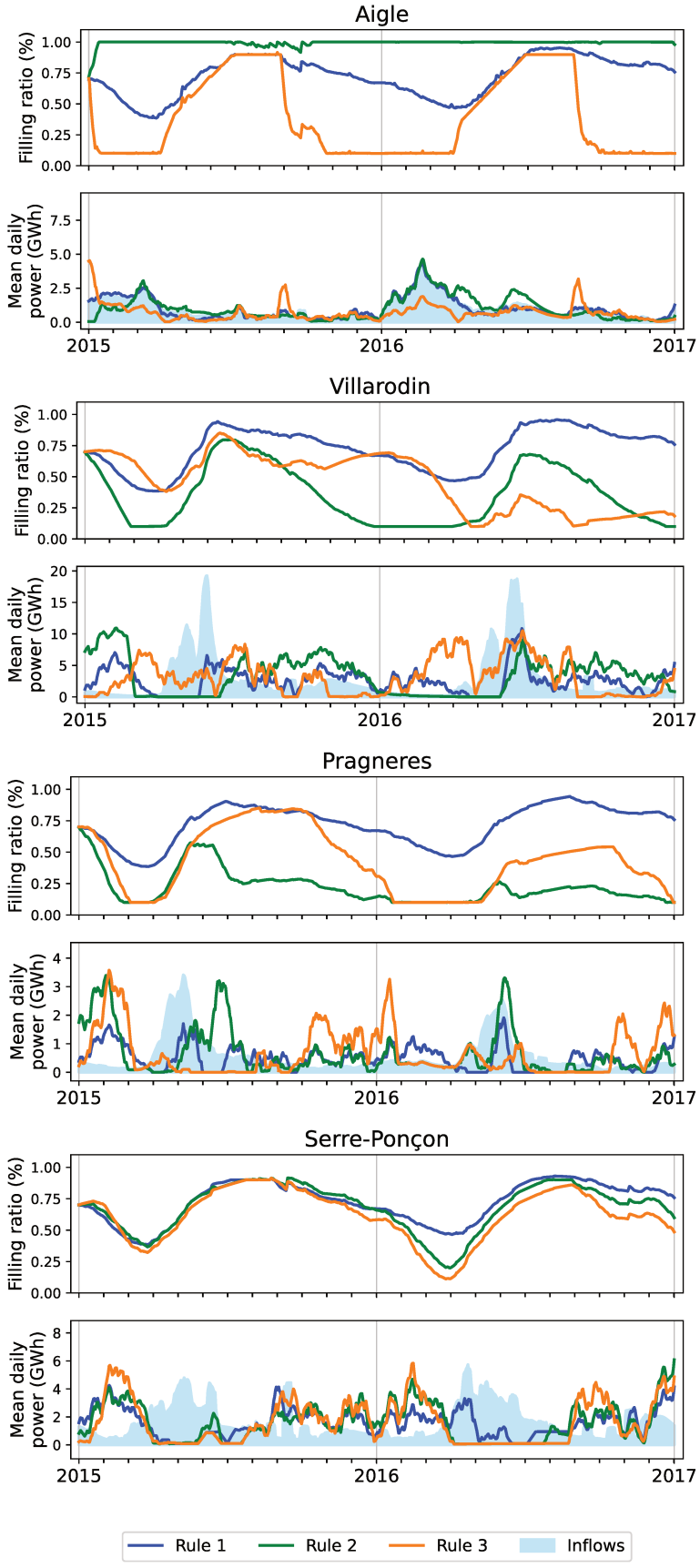

Figure 4.4: Simulated filling level, inflows and production for four power plants representative of different French hydropower catchments.

The water wastages caused by rules 2 and 3 explain the increased depletion of the hydraulic stock in these rules to produce a given amount of energy and justify the observed superior performance of rule 1.

4.1.4 Conclusion

The comparison of these three rules allows us to identify two key factors that must be considered in order to define an efficient operating rule for hydropower reservoirs:

- the variation of the head with the water filling of the reservoir, which reduces the generating efficiency of a power plant as the water in the reservoir is withdrawn;
- the spillage from some reservoirs that can result in wasted energy potential if the operating rule does not allow to use it effectively.

As demonstrated in Chapter 3, the first rule allows for the successful operation of hydropower reservoirs in comparison to historical production. It will therefore be used throughout the remaining chapters.

4.2 Representing the management of pumped hydro storage (PHS) plants

In Chapter 3, we applied the demand-based approach to operate reservoirs from French poundage and reservoir power plants. This section explores the potential for extending this methodology to the operation of PHS plants. We begin by detailing the modeling of reservoir and power plants. We then assess the performance of this methodology in representing historical PHS management. Finally, we discuss the choice of appropriate operating rules for these plants.

4.2.1 Presentation of French PHS plants

France has six main PHS plants, with differentiated characteristics, as indicated in Table 4.2. The Revin and La Coche plants have fully artificial upstream reservoirs, which are filled exclusively by pumping, with no natural inflow. In contrast, the other four plants have both their upstream and downstream reservoirs connected to the natural hydrological system, with natural inflows.

	Grand Maison	Montezic	Bissorte	Revin	Cheylas	La Coche
Production capacity (MW)	1690	910	825	808	500	320
Pumping capacity (MW)	1200	840	600	800	500	340
Upstream reservoir capacity (10^6 m^3)	137	67.2	39.5	8.3	4.8	2.1
Upstream mean inflow (m^3/s)	2.9	0.49	0.45	0.02	0.15	0.03
Downstream reservoir capacity (10^6 m^3)	15.6	56.1	1.3	9.0	5.0	0.7
Downstream mean inflow (m^3/s)	4.3	38.1	18.0	2.33	154.8	47.0

Table 4.2: Characteristics of the individual reservoirs considered

4.2.2 PHS modeling

As described in section 2.2, our method relies on three main novelties: (i) locating PHS plants on the river network, (ii) representing the water transfers between reservoirs resulting from PHS operation, and (iii) determining the releases from each reservoir.

4.2.2.1 Locating PHS plant on the river network

Similarly to other power plants, PHS plants are initially located on the high-resolution MERIT river network using the georeferenced data provided in the European Commission et al. (2019) database. The adduction links are then built between each PHS plant and two reservoirs, an upper one and a lower one. These reservoirs are selected based on an algorithm (Neverre, 2015; Zhou et al., 2021).

In addition to the attributes and variables described in Table 2.1, each edge (i, j) containing a PHS plant is also characterized by the installed pumping capacity of the plant located on the edge $P'_{(i,j)}$, the pumping efficiency of the plant $\eta'_{(i,j)}$ and the power consumed at each time step by the plant to pump water $E'_{(i,j)}(t)$.

4.2.2.2 Water continuity equations

In addition to the reservoir scheme presented in Fig. 2.4, PHS management induces water transfers from the downstream reservoir to the upstream reservoir through pumping. We introduce therefore additional water fluxes $\phi_{(i,j)(t)}$ defined as the water transferred from a reservoir located in the HTU i to the reservoir located in the HTU j. These different water fluxes are represented in Fig. 4.5.

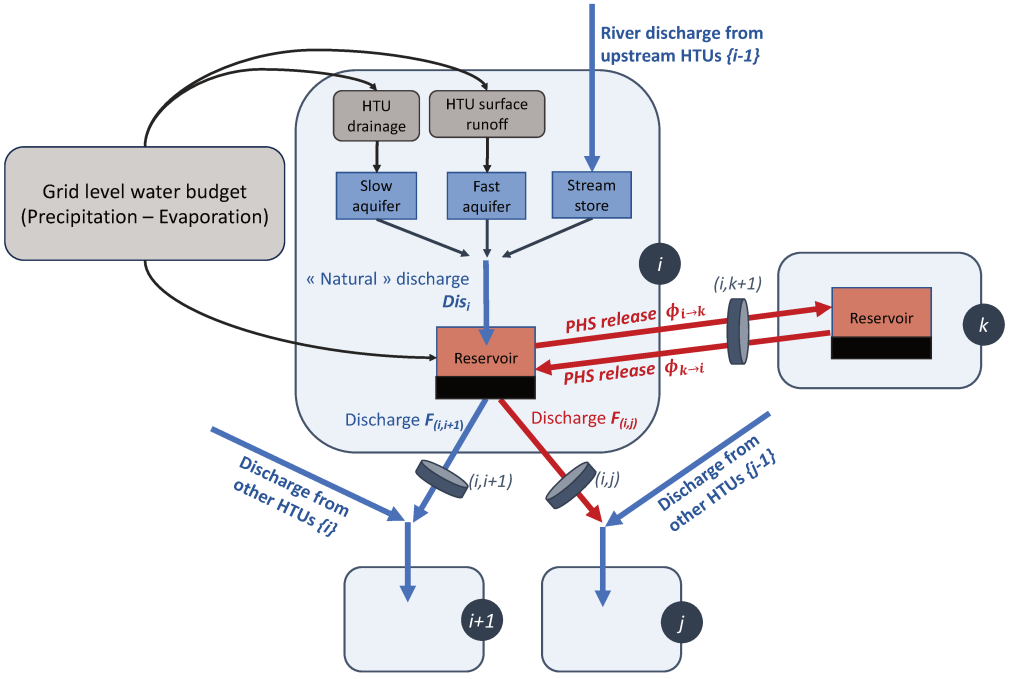

Figure 4.5: Schematic representation of water stores and flows in an HTU i

The new prognostic equation of the water volume in a reservoir i is then given by:

$$\frac{dV_i}{dt}(t) = Dis_i(t) + p_{res,i}(t) - ev_{res,i}(t) + \sum_k \phi_{k\to i}(t) - \sum_k F_{(i,k)}(t) - \sum_k \phi_{i\to k}(t) \quad (4.7)$$

The reservoir is filled by incoming inflow $Dis_i(t)$, direct precipitation $p_{res,i}(t)$ and water pumped from other reservoirs by PHS $\sum_k \phi_{k\to i}(t)$ (defined in Eq. 4.9). Outputs from the reservoirs are the water released towards downstream HTUs $\sum_k F_{(i,k)}(t)$, downstream reservoir of the PHS plant $\sum_k \phi_{k\to i}(t)$ (4.8) and direct evaporation $ev_{res,i}$.

PHS plant's releases from and to the reservoir i are respectively determined by the power produced by the plant $E_{(i,j)}(t)$, and the power consumed for pumping $E'_{(i,j)}(t)$:

$$\phi_{i\to j}(t) = \frac{E_{(i,j)}(t)}{\rho g \eta_{(i,j)} h_{(i,j)}(t)} \quad (4.8)$$

$$\phi_{j\to i}(t) = \frac{E'_{(i,j)}(t)\eta'_{(i,j)}}{\rho g h_{(i,j)}(t)} \quad (4.9)$$

4.2.2.3 Energy production and storage

Similarly to the previous chapter, national time series of power generated $D_{phs}(t)$ and consumed for pumping $D'_{phs}(t)$ by PHS plants are prescribed to the model. Local demands at each plant level are then determined by the following algorithm.

1) Fatal production and pumping from spillage The model starts by going through all PHS plants and computes the energy they can generate $E_{spill,(i,j)}$ or store $E'_{spill,(i,j)}$ without additional releases, thanks to spillage.

$$E_{spill,(i,j)}(t) = \min\Bigg[P_{(i,j)}\frac{h_{(i,j)}(t)}{H_{(i,j)}}, \min\left(\frac{V_i^\star(t) - V_{tot,i}}{g_{res}\tau_i} - \max\left(F_{ecol,(i,i+1)}(t), F_{irri,(i,i+1)}(t)\right), 0\right) \times \rho g \eta_{(i,j)} h_{(i,j)}(t)\Bigg] \quad (4.10)$$

$$E'_{fatal,(i,j)}(t) = \min\Bigg[P'_{(i,j)}\frac{h_{(i,j)}(t)}{H_{(i,j)}}, \min\left(\frac{V_j^\star(t) - V_{tot,j}}{g_{res}\tau_i} - \max\left(F_{ecol,(j+1,j)}(t), F_{irri,(j+1,j)}(t)\right), 0\right) \times \frac{\rho g h_{(i,j)}(t)}{\eta'_{(i,j)}}\Bigg] \quad (4.11)$$

The remaining production (respectively consumption for pumping) demand to dispatch is then $D_{phs}(t) - \sum_{Typ(i,j)=phs} E_{fatal,(i,j)}(t)$ (respectively $D'_{phs}(t) - \sum_{Typ(i,j)=phs} E'_{fatal,(i,j)}(t)$).

2) Reservoir withdrawals If there is any national production (or pumping) demand left to dispatch, it should be satisfied by withdrawing water from the reservoirs. We consider a function $\alpha((i,j),t)$ (resp. $\alpha'((i,j),t)$) which ranks the PHS plants in ascending order of use for production (resp. pumping). Withdrawals are done in this order until the corresponding generation (resp. pumping) satisfies the national demand or all the plants have been used to their maximum potential.

Defining a ranking rule for the operation of PHS plants is challenging because the production of a plant affects the filling of two separate reservoirs.

We test here two different rules for operating the PHS reservoirs. In a first simulation (*rule 1*), PHS plants are operated based solely on the filling level of their upstream reservoirs. Production is prioritized at plants whose upstream reservoirs are the most filled while pumping is prioritized at those with the least filled upstream reservoirs. In a second simulation (*rule 2*), the alternative rule considers the filling levels of both the upstream and downstream reservoirs. For production, the model continues to prioritize power plants with the most filled upstream reservoir. However, for pumping, the model prioritizes power plants with the most filled downstream reservoirs, regardless of the filling level of the upstream reservoir.

4.2.2.4 PHS plants efficiencies

Following the literature (Blakers et al., 2021), we consider a generation efficiency η equal to 0.9 for all plants. We use observations of production by the Revin plant to estimate the pumping efficiency. Indeed, as this plant does not have any natural inflow, all the production comes from water that first has to be pumped. Over the 2015-2020, the Revin plant has an overall efficiency $\eta \times \eta' = 0.75$ (production corresponds to 75% of the energy consumed by the plant), consistent with the literature (Blakers et al., 2021; Wessel et al., 2020). This leads to a pumping efficiency of 0.83.

4.2.3 Results

The ORCHIDEE model is run on the 2015-2020 period for each of these two rules, driven by SAFRAN atmospheric reanalysis and with the observed production and consumption (RTE, 2023b) as the target time series that drives reservoir releases.

Throughout the entire period, the model successfully meets both production and pumping targets the large majority of the time for both rules. Rule 1 slightly outperforms rule 2 in terms of production satisfaction, with the hourly production target being met 98.4% of the time, compared to 96.8% of the time with rule 2. In contrast, Rule 2 performs marginally better in meeting the pumping target, achieving it 98.4% of the time, against 98.0% for rule 1.

Fig. 4.6 shows the occurrences of failures and the evolution of the cumulative stock in both upstream and downstream reservoirs (aggregated for the 6 PHS plants). Rule 2 leads to more frequent shortages of the upstream reservoir, since the pumping is not prioritized based on the upstream reservoir's filling level. However, this rule allows for more pumping, as it aims at avoiding spills from the downstream reservoir.

Since observed production time series are available at the unit level for most French PHS plants (RTE, 2023c), we can directly compare the dispatch of the national production simulated by the model with actual operations. Figure 4.7 shows this comparison for rule 1. The simulated operations align globally well with observed data for all major

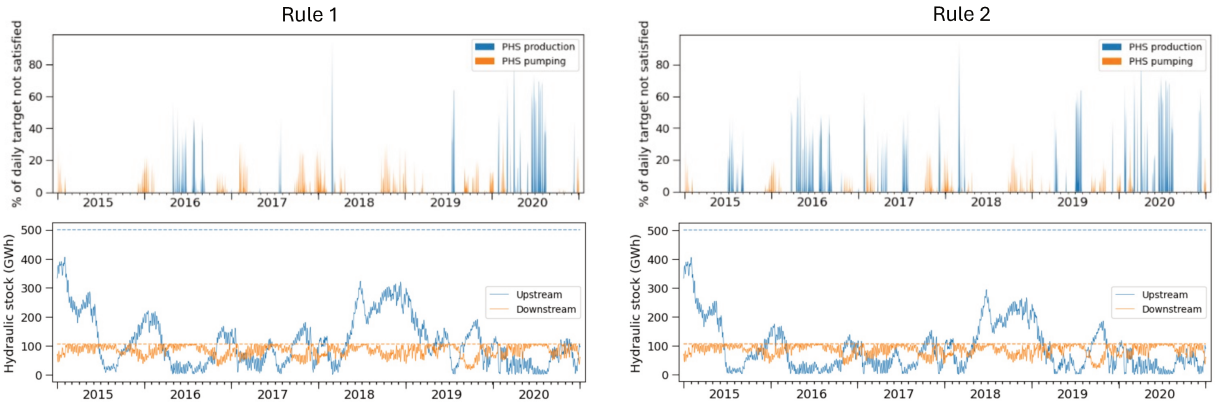

Figure 4.6: Occurrences of failures to meet production or pumping demand time series and evolution of aggregated stock in downstream and upstream reservoirs in the 6 French PHS plants.

French PHS plants. This good agreement indicates that the dispatch rule we implemented, despite its simplicity, is effective in simulating realistic operations.

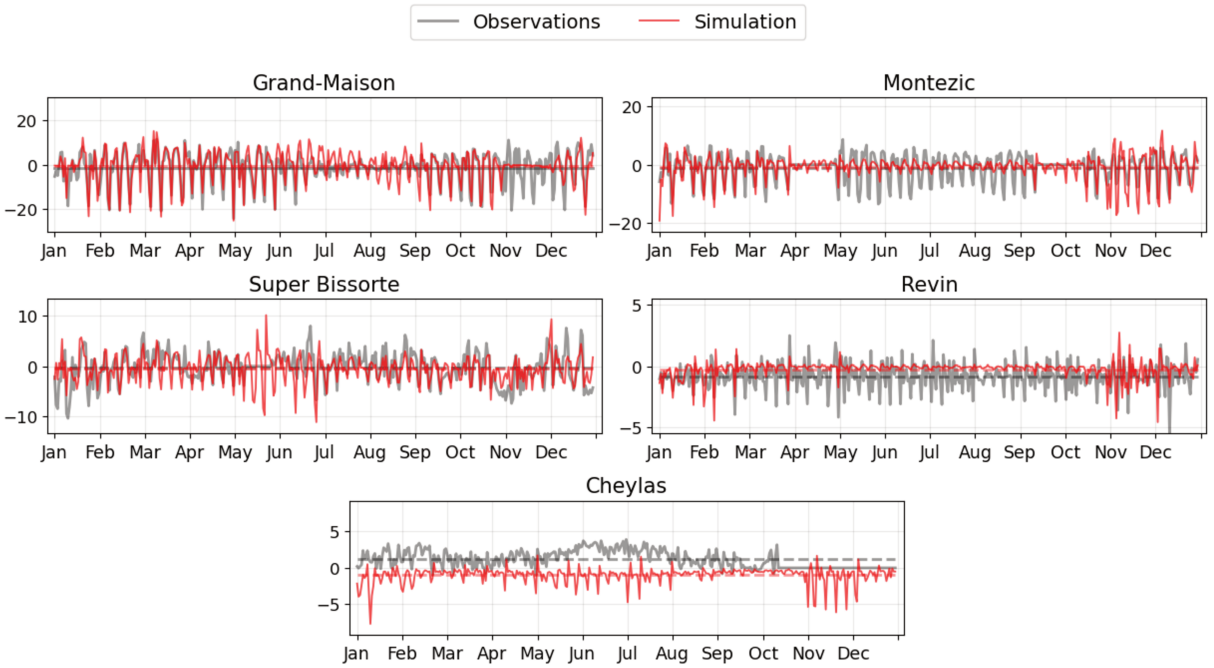

Figure 4.7: Comparison of observed and simulated daily net production (power production minus power consumption, in GWh) for the five largest French PHS plants in 2016. The dashed lines represent the annual mean net production. PHS plants are presented in decreasing order of installed capacity. No data is available for the last PHS plant (La Coche).

4.2.4 Discussion - Competition with reservoir production

Three out of the six PHS have their downstream reservoir also serving as upstream reservoir for a poundage power plant. Consequently, water can be withdrawn from these reservoirs either to generate electricity through the associated poundage power plant or to store energy by pumping water through the PHS plant. When both poundage and PHS demand time series are provided to the model, competition may arise regarding

the use of these shared reservoirs. The rule for distributing national poundage demand prioritizes the production from poundage plants with the most filled upstream reservoirs. However, the reservoirs supplying poundage plants undergo annual cycles, with at least one period of complete shortage (Fig. 4.8). As a result, jointly simulating the operation of poundage and PHS plants can reduce the satisfaction of PHS demands. When poundage demand is accounted for, the national demand for PHS generation is not met 5.6% of the time, compared to only 1.5% when poundage demand is not considered. Similarly, the pumping demand is unmet 4.2% of the time when poundage demand is included, versus only 2.0% when it is not.

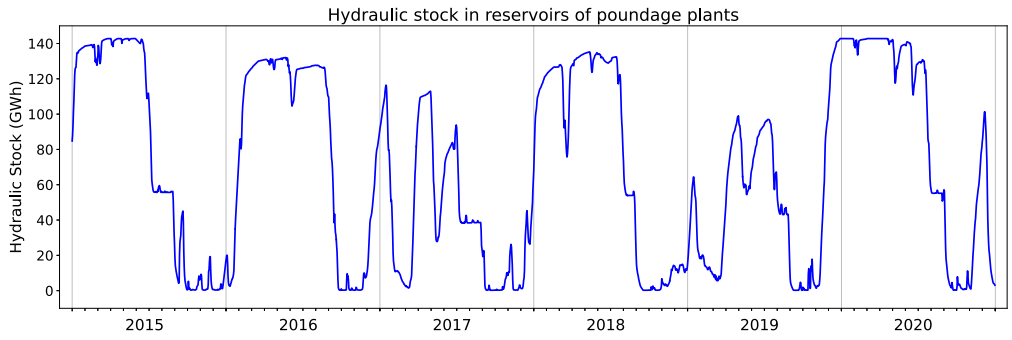

Figure 4.8: Simulated stock of poundage plants when their operations are simulated by the model

Part II

Representing dynamic hydropower constraints in power system models

CHAPTER 5

Coupling a power system model with a hydrological model improves the representation of hydropower flexibility

This chapter focuses on the modeling of hydropower production from the perspective of Power System Models (PSMs) that aim at optimizing the dispatch of the electrical demand among the various power supply technologies. Sections 5.1 to 5.6 investigate the extent to which the coupling with a hydrological model can contribute to improving the simulation of hydropower production by a PSM. This work has been submitted as a research paper to the Applied Energy Journal (Baratgin et al., 2024 (submitted)[a]). Finally, 5.7 provides supplementary analysis of two other parameters found to affect the modeling of hydropower in PSMs.

Contents

5.1 Introduction . . . 76
5.2 Model presentation . . . 78
5.2.1 ORCHIDEE land surface model . . . 79
5.2.2 EOLES-Dispatch power system model . . . 80
5.2.3 Coupling approach . . . 81
5.3 Simulation framework . . . 83
5.3.1 ORCH_EOLES - Procedure for coupling the two models . . . 84
5.3.2 Data inputs . . . 84
5.4 Results . . . 86
5.4.1 Improvements in simulated hydropower production . . . 86
5.4.2 Impacts of a change in the power mix on the hydropower generation . . . 89
5.4.3 Impacts on the European power system . . . 91
5.4.4 Identifing the main drivers of the change . . . 92
5.5 Discussion . . . 93
5.5.1 Increasing the complexity while maintaining a simple linear model with a representative reservoir plant . . . 93
5.5.2 Discrepancy between simulated production and historical data 95
5.5.3 Improving reservoir operations in the hydrological model . . . 96
5.6 Conclusion . . . 97

5.7 Supplementary material: Further insights on hydropower modeling in EOLES-Dispatch 97
5.7.1 Simulation area 97
5.7.2 Distinguishing poundage and run-of-river power plants 99

5.1 Introduction

The increasing use of renewable energy sources is one of the least costly options to mitigate greenhouse gas emissions (IPCC, 2022b). In developed countries, such as France, substantial development of new hydro potential is not foreseen. Achieving high shares of renewable energy in the electricity sector requires, however, a massive deployment of variable wind and solar power generators. Flexible installations that can fill the gap between consumption and variable generation will become crucial for providing electricity supply security. Among these flexible options, existing reservoir hydropower infrastructure is particularly valuable, due to its low carbon emissions and generation costs compared to gas (Gaudard, 2014).

The flexibility of reservoir power plants stems from their capacity to store water for later electricity generation. Their power generation has therefore an opportunity cost, as the amount of water available is limited by both inflows and storage capacity. Moreover, several limitations can impede the dispatchability of hydropower reservoir plants. Firstly, the water stored in the reservoirs often serves multiple purposes beyond hydropower, including domestic use, irrigation, flood control, and recreation. In France, 43% of the 13 billion cubic meters of reservoir capacity allocated for hydropower also serve irrigation or recreational purposes (Lehner et al., 2011). Secondly, regulatory constraints, such as minimum ecological flow rates, apply to outflows from the reservoirs and may constrain the reservoir releases. Thirdly, water inflows to the reservoir may depend on the operation of upstream assets. Finally, the production of a reservoir plant is determined by the efficiency of the plant, the volumetric flow rate of the water released from the reservoir, and the hydraulic head, which is the height difference between the water surface in the reservoir and the plant's turbine. A decrease in the reservoir's water level reduces then the maximum electricity output available from the plant.

To make informed energy policy decisions in the context of energy transition and climate change, these constraints (multipurpose reservoir operations, regulatory requirements, accurate water availability, and head dependence) need to be accounted for to thoroughly assess hydropower flexibility potentials. However, most commercial and academic power system models (PSMs) used to simulate the power grid and study its reliability poorly integrate these constraints (Rheinheimer et al., 2023). Recent reviews on hydropower modeling in PSMs (Oikonomou et al., 2022; Turner et al., 2022) indicate that in most PSMs, hydropower production is represented simplistically, only constrained by installed power capacities and exogenous inputs of monthly hydropower potential. Within each month, these models then simulate the hourly schedule of hydropower to minimize the system cost, assuming no other constraints on the intra-month operation of reservoirs than the plant's installed capacity. These monthly estimates are typically based on historical data, such as in PROMOD (Kintner-Meyer et al., 2012), PLEXOS (Ibanez et al., 2014), or EOLES (Shirizadeh et al., 2021). They can also be derived from hydrological model simulations to account for inter-annual variations in hydrological inflows. For instance, O'Connell et al., 2019; Voisin et al., 2016, 2018 use the VIC hydrological model to assess mean annual deviations in river flows from a reference year at hydropower

facilities. They then apply this deviation to the monthly production of the reference year to obtain monthly production targets. This monthly target approach assumes a fixed distribution of production across months. However, this may not hold in the future, as anticipated shifts in the power sector are likely to modify the annual hydroelectric generation pattern Dimanchev et al., 2021; Gøtske et al., 2021. These shifts include the growing integration of variable power sources, and the effects of climate change on water resources, that may modify dam operations.

To address these issues, various methods have been used in previous studies, as illustrated in Fig. 5.1. One approach involves representing operation constraints of reservoirs within PSMs based on historical operation data (De Felice, 2021; Huertas-Hernando et al., 2017; Marshall et al., 2022; Turner et al., 2019) (arrow (a'') in Fig. 5.1). This method incorporates non-power constraints into the PSM but it requires a significant amount of data, which is often unavailable at the plant level in many regions of the world, including France, where hydropower operations are considered trade secrets.

Another strategy is to combine the PSM with a reservoir model. In some studies (Su et al., 2020; Tarroja et al., 2019), reservoir models are used to estimate daily hydropower plant production, which is then optimized at the hourly scale by the PSMs (arrows (b) in Fig. 5.1). This approach enables the consideration of dependencies between assets on the same river. However, the operating rules used in the hydrological models do not reflect the actual power needs, especially when considering future energy scenarios.

Ibanez et al. (2014) goes further, by exploring the value of coupling the PLEXOS PSM with the detailed hydropower model RiverWare, in the context of the Western interconnection in the United States. In this approach, the prices output from an initial PLEXOS simulation are taken as inputs in RiverWare to optimize the operations of the 10 main reservoirs of the interconnection. Optimized hydropower profiles are then given back to PLEXOS (arrows (c) in Fig. 5.1). This study shows a significant effect of this detailed hydropower modeling on the PSM outputs. However, the results require further exploration, as the simulation was performed for only one week and involved only one iteration of the coupled model. Moreover, the approach relies on a highly detailed hydropower model, adjusted to a specific river catchment, which demands substantial information about the infrastructures.

Furthermore, most PSMs assume a constant hydraulic head to keep a linear optimization problem and therefore do not represent the head-dependency constraint.

This chapter aims to explore the value of an integrated framework, that combines a PSM with a large-scale hydrological model to simulate hydropower production at the national power grid level. Specifically, we link the EOLES-Dispatch PSM with the ORCHIDEE land surface model, which represents the operation of hydroelectric reservoirs.

Using the 2019 French power system over five weather years as a case study, we first present the coupling procedure and validate this new approach. We find that such a coupling improves the realism of the simulated production, with a reduction of 29% of the RMSE when compared to the non-coupled version. We then examine the impact of this coupling in a hypothetical 2050 power mix scenario, which highlights the importance of considering additional constraints on hydropower production to avoid overestimating the reliability of future power mixes.

The remainder of the chapter is structured as follows: Section 5.2 describes the two models utilized in this study (ORCHIDEE and EOLES-Dispatch), and our proposed approach to couple them to model hydropower production. Section 5.3 introduces the simulation framework and the power scenarios under examination. Section 5.4 presents

the results, which are then discussed in section 5.5. Finally, section 5.6 concludes by outlining future research perspectives.

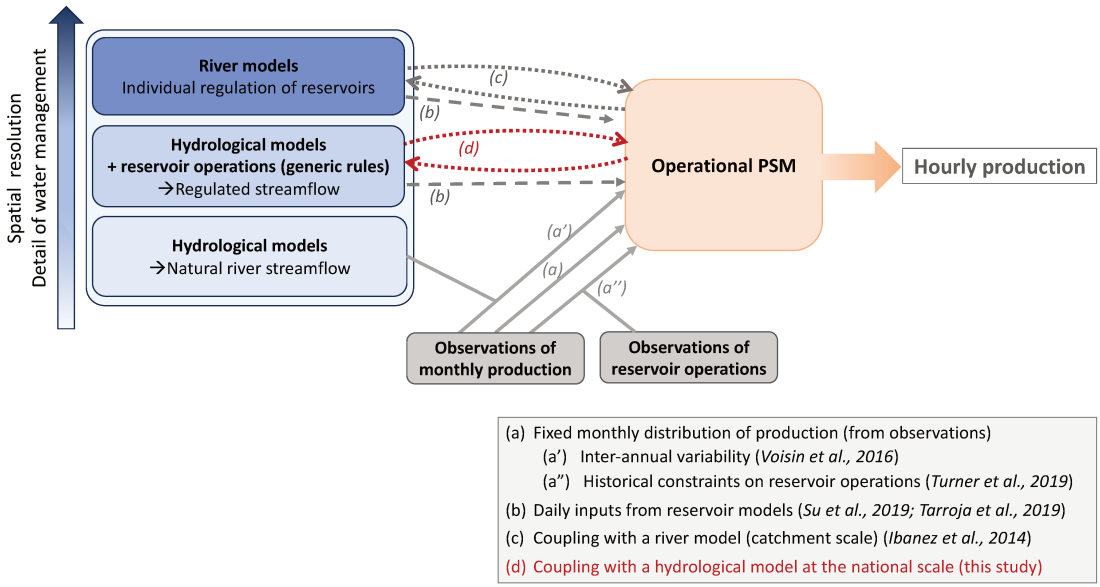

Figure 5.1: Schematic review of the different modeling options to inform constraints on production by reservoir plants in a PSM.

5.2 Model presentation

We adopt a whole-system approach by coupling a land surface model, ORCHIDEE, with a PSM, EOLES-Dispatch, both focusing on France.

ORCHIDEE is a land surface model (Krinner et al., 2005) which represents the continental hydrological cycle. It includes a module representing reservoir operations, which has been validated over France in Chapter 3. In the model, the operation of hydroelectric reservoirs is decided based on an exogenous target time series for national production by reservoir power plants, that ORCHIDEE seeks to satisfy by dispatching the national production across each reservoir plant.

EOLES-Dispatch (Leblanc, 2023) is a linear optimization model derived from the EOLES model developed by Shirizadeh et al. (2022). It focuses on the optimization of the French electric dispatch. The model minimizes the total dispatch cost of the electric system while covering electricity demand at an hourly time-step, assuming perfect foresight.

The coupling relies on an exchange of information between the two models, aiming to obtain a hydropower production schedule simulated by EOLES-Dispatch that aligns with the operating rules represented in ORCHIDEE. Since EOLES-Dispatch performs the dispatch optimization over the whole period, we adopt an iterative process, as represented in Fig 5.2. At each iteration, variables related to water availability and multipurpose reservoir management are derived from ORCHIDEE to constrain the hydropower production in EOLES-Dispatch. The resulting time series of national production by reservoir power plants simulated by EOLES-Dispatch is then prescribed to ORCHIDEE as the target production to be met.

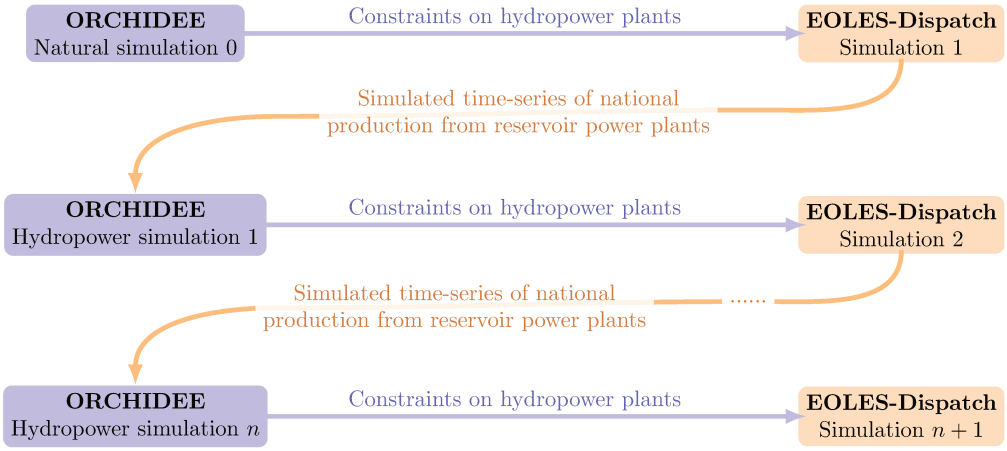

Figure 5.2: Iterative process for coupling ORCHIDEE and EOLES-Dispatch.

5.2.1 ORCHIDEE land surface model

In the ORCHIDEE model, hydrological simulations are performed over a grid on which French reservoirs and hydropower plants have been located, consistently with the river network. Two types of plants are distinguished:

- **Run-of-river plants** do not have any storage capacity and generate electricity according to the instantaneous river discharge at the plant location;
- **Reservoir plants** are fed by reservoirs that can store a specific water volume and are often also used for other purposes that may constrain their operations. For those plants, electricity production does not necessarily take place at the location of water storage, therefore both the plant and the reservoir need to be located and connected;

A demand-based approach is adopted to simulate the release of the reservoirs linked to the power plants. An exogenous time series of national production by reservoir power plants is taken as input by ORCHIDEE. The model then operates all the reservoirs connected to power plants in order to meet the production target as closely as possible while following the operational limitations of each reservoir. The reservoirs are operated in a coordinated manner, by releasing water from the most filled reservoir first, in order to equalize the filling level of all reservoirs at each time step.

For each reservoir plant i of installed capacity P_i and efficiency η_i, multiple operating constraints are represented, depending on the intended functions of its supplying reservoir (indicated in the database used to locate the infrastructures). These constraints include *(i)* time-dependent requirements for irrigation and ecological flows, denoted as $Rc_i(t)$; *(ii)* a time-dependent minimum volume of water in the reservoir (to account for the touristic use of some reservoirs during the summer), denoted as $V_{min,i}(t)$; *(iii)* a maximum volume of water in the reservoir, denoted as $V_{max,i}$; *(iv)* the variation in hydraulic head with changing water level $h_i(V_i(t))$; and *(v)* a maximum outflow limit for energy production, denoted as $R_{max,i}$ and defined as the water discharge needed to generate at full capacity when the reservoir is full (Eq. 5.1).

$$R_{max,i} = \frac{P_i}{\rho g h_i(V_{max,i})} \tag{5.1}$$

where ρ is the water density and g the gravitational acceleration. For further information on the representation of these constraints, see Chapters 2 and 3.

In this study, we focus on the French power grid. Data for hydropower plants are taken from European Commission et al. (2019) and the national register of electricity generation and storage facilities (ODRÉ, 2016). Dams and reservoirs data are taken from GRanD (Lehner et al., 2011) and the CFBR (CFBR, 2021) databases. The location of these different infrastructures is presented in Fig. 5.3.

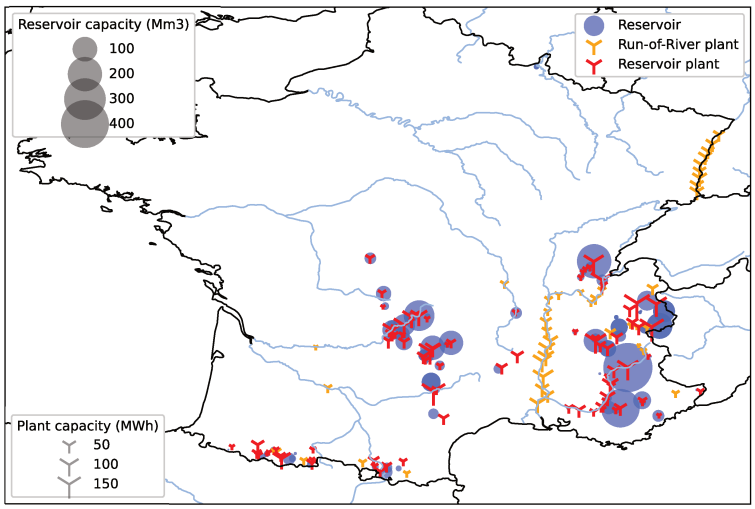

Figure 5.3: Location of the French hydropower plants modeled in ORCHIDEE and their associated supplying reservoirs.

5.2.2 EOLES-Dispatch power system model

5.2.2.1 General equations of the model

The model represents France and all the power systems that share a direct interconnection with it, namely Belgium, Germany (including Luxembourg), Switzerland, Italy, Spain, and Great Britain. In each region a, each generation or storage technology k is represented by one representative plant. In the versions used here, we do not consider the provision of ancillary services, though it is an option that can be activated in the model. The model is described in detail by Leblanc (2023). We present below only the equations required for understanding this study.

The model's objective is to minimize the total cost of the electric dispatch across the entire time-span T, the set of areas A, and the set of technologies K, over the whole set of endogenous variables (identified in the following by bold notations):

$$\min \left(\sum_{a \in A} \sum_{t \in T} \sum_{k \in K} \left(cg_k \mathbf{G}_{a,k,t} + cg'_k \mathbf{G'}_{a,k,t} + csu_k \mathbf{SU}_{a,k,t} + cr_k \mathbf{R}_{a,k,t} \right) + voll \mathbf{LL}_{a,t} \right) \tag{5.2}$$

where $\mathbf{G}_{a,k,t}$, $\mathbf{G'}_{a,k,t}$, $\mathbf{SU}_{a,k,t}$ and $\mathbf{R}_{a,k,t}$ are respectively the electricity generated, the electricity consumed for storage, the capacity started up and the increase in production for the technology k in area a at time t; cg_k, cg'_k, csu_k and cr_k are the associate costs; $\mathbf{LL}$ is the unsatisfied demand that is not met by supply ($\mathbf{LL}$ standing for lost load), as imposed by the adequacy constraint (Eq. 5.3) and $voll$ is the value applicable to one unit of unsatisfied demand (value of lost load).

The key constraint imposed on this minimization problem is the adequacy constraint (Eq. 5.3) which ensures that the whole demand is met by the power supply at each

period t in each area a. The supply side (left) includes the total amount of electricity generated by the capacities within the area and the imports of electricity from neighboring countries $\sum_{a' \in A} \mathbf{IM}_{a,a',t}$. The demand side (right) includes the local demand for final consumption $d_{a,t}$, the total exports to neighboring countries $\sum_{a' \in A} \mathbf{EX}_{a,a',t}$ and the electricity consumed by storage technologies. The difference between supply and demand is the lost load $\mathbf{LL}_{a,t}$. We set *voll* to 15,000 €/MWh, so that, as generation costs are much cheaper, the model always meets the power demand if possible.

$$\sum_{k \in K} \mathbf{G}_{a,k,t} + \sum_{a' \in A} \mathbf{IM}_{a,a',t} + \mathbf{LL}_{a,t} = d_{a,t} + \sum_{a' \in A} \mathbf{EX}_{a,a',t} + \sum_{k \in K} \mathbf{G'}_{a,k,t} \tag{5.3}$$

Various generation technologies are available in the model to meet electricity demand, subject to specific constraints.

5.2.2.2 Constraints on hydropower production in EOLES-Dispatch's preexisting version

In the preexisting version of the model, the run-of-river plant *ror* is modeled as any other variable renewable technology through an exogenous hourly capacity factor $CF_{a,ror,t}$, that accounts for the potential production at the national level. Its production $\mathbf{G}_{a,ror,t}$ is then constrained by:

$$\mathbf{G}_{a,ror,t} \leq CF_{a,ror,t} * capa_{a,ror} \tag{5.4}$$

where $capa_{a,ror}$ is the installed capacity of run-of-river in the area a. This capacity factor is based on observations of actual production for a reference year.

The production by reservoir plants $\mathbf{G}_{a,res,t}$ is constrained by monthly observed production $lake_{a,month}$ of a reference year and the installed capacity of the plant $capa_{a,res}$:

$$\sum_{t \in month} \mathbf{G}_{a,res,t} \leq lake_{a,month} \ ; \ \mathbf{G}_{a,res,t} \leq capa_{a,res} \tag{5.5}$$

5.2.3 Coupling approach

5.2.3.1 From ORCHIDEE to EOLES-Dispatch

ORCHIDEE simulates the river discharge $Q_i(t)$ at each run-of-river plant location in France, which allows to compute the corresponding capacity factor:

$$CF_{FR,ror,t} = \frac{\sum_{i \in \text{ror}} \min(P_i, \rho g \eta_i H_i Q_i(t))}{P_{FR,ror}} \tag{5.6}$$

Such capacity factor can then capture the cascading effect of the hydropower network.

For plants associated with reservoirs, the model simulates the inflow $Q_i(t)$ and release $R_i(t)$ at each reservoir location, from which we can derive the time series of the water volume in the reservoir $V_i(t)$ and the actual head $h_i(V_i(t))$ that depends on the filling level of the reservoir. Moreover, the model also informs on the non-power constraints applying to the reservoir: the constrained reservoir release $Rc_i(t)$ for environmental and irrigation uses and the minimum volume to be maintained in the reservoir $V_{min,i}(t)$, which increases during the summer for touristic reservoirs. We can then follow the stock $S_i(t)$ available for each reservoir plant, defined as the energy that can be generated by the plant given the current water volume in the reservoir:

$$S_i(t) = \int_{V=0}^{V_i(t)} \rho g \eta_i h_i(V) dV \tag{5.7}$$

The maximum and minimum stocks in the reservoir are then respectively referred to as $Smax_i$ and $Smin_i(t)$.

Based on ORCHIDEE's simulations, we define 5 energy variables at the reservoir plant level that we will use in this study to allow the coupling with EOLES-Dispatch (Eq. 5.8 to 5.12). These 5 variables are illustrated in Fig. 5.4 for a schematic reservoir-plant pair.

- **Net inflow** $\mathcal{I}_i(t)$: the equivalent in energy terms of the water volume entering the reservoir during the current time-step Δt.

$$\mathcal{I}_i(t) = \min\left(Q_i(t)\Delta t, V_{tot,i} - V_i(t)\right) * \rho g \eta_i h_i(t) \tag{5.8}$$

- **Constrained release** $\mathcal{R}_i(t)$: the equivalent in energy terms of the constrained releases from the reservoir during the current time-step

$$\mathcal{R}_i(t) = Rc_i(t)\Delta t * \rho g \eta_i h_i(t) \tag{5.9}$$

- **Maximum potential of constrained release** $\mathcal{R}'_i(t)$: the maximum energy that can be produced from the constrained reservoir releases during the current time-step

$$\mathcal{R}'_i(t) = min\left(P_i \frac{h_i(t)}{H_i}\Delta t \ , \mathcal{R}_i(t)\right) \tag{5.10}$$

- **Maximum potential of spillage** $\mathcal{Y}_i(t)$: the maximum energy that can be produced from the water that spills in any case from the reservoir during the current time-step

$$\mathcal{Y}_i(t) = \min\left(P_i \frac{h_i(t)}{H_i}\Delta t - \mathcal{R}'_i(t) \ , \ \max\left(V_i(t) + Q_i(t)\Delta t - V_{tot,i} - \mathcal{R}_i(t), 0\right) * \rho g \eta_i h_i(t)\right) \tag{5.11}$$

- **Maximum capacity** $\mathcal{P}max_i(t)$: maximum capacity of the plant constrained by the water level in the reservoir

$$\mathcal{P}max_i(t) = min\left(P_i \frac{h_i(t)}{H_i} \ , \ \left(Q_i(t) + \frac{V_i(t) - V_{min,i}(t)}{\Delta t}\right) * \rho g \eta_i h_i(t)\right) \tag{5.12}$$

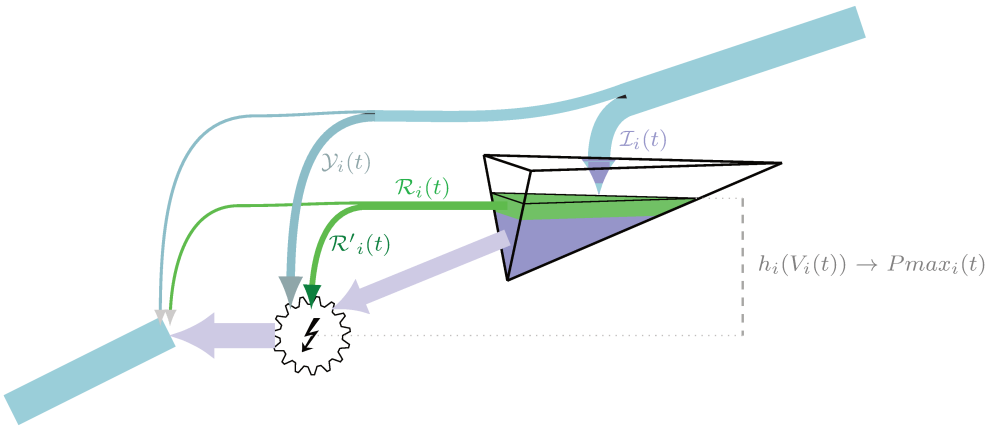

Figure 5.4: Schematic representation of the time series of ORCHIDEE outputs that will serve for the coupling with EOLES, represented here for an individual reservoir.

The 5 variables are computed at 15-minute intervals, which is the resolution of the ORCHIDEE model. They are then aggregated to an hourly resolution, to match the time resolution of EOLES-Dispatch.

The information extracted from ORCHIDEE allows us to inform new constraints on the hydropower generation of the French representative reservoir plant in EOLES-Dispatch. This new set of constraints (Eq. 5.13 to 5.16), is illustrated in Fig. 5.5. Two new positive state variables are introduced in EOLES-Dispatch: the total amount of energy stored in reservoirs $\mathbf{S}_{res,t}$ and the additional release to be made from reservoirs $\mathbf{Re}_{res,t}$.

$$\sum_{i \in res} Smin_{i,t} \leq \mathbf{S}_{res,t} \leq \sum_{i \in res} Smax_i \tag{5.13}$$

$$\mathbf{S}_{res,t+1} = \mathbf{S}_{res,t} + \sum_{i \in res} \mathcal{I}_i(t) - \sum_{i \in res} \mathcal{R}_i(t) - \mathbf{Re}_{res,t} \ , \mathbf{S}_{end} = \mathbf{S}_0 \tag{5.14}$$

$$\mathbf{G}_{FR,res,t} \leq \mathbf{Re}_{res,t} + \sum_{i \in res} \mathcal{Y}_i(t) + \sum_{i \in res} \mathcal{R}'_i(t) \tag{5.15}$$

$$\mathbf{G}_{FR,res,t} \leq \sum_{i \in res} \mathcal{P}max_i(t) \tag{5.16}$$

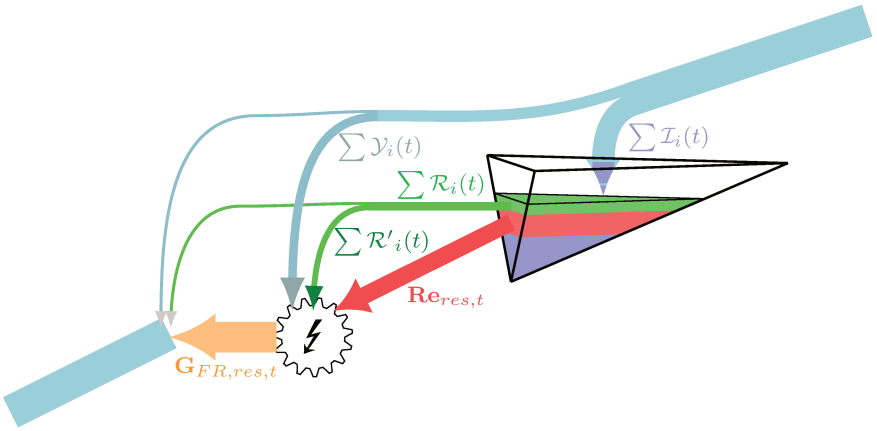

Figure 5.5: Variables constraining the production of the representative reservoir plant in the new version of EOLES-Dispatch we propose.

5.2.3.2 From EOLES-Dispatch to ORCHIDEE

The hourly hydropower dispatch obtained at the end of the EOLES-Dispatch's simulation is then prescribed as the hydropower production target to be met in ORCHIDEE.

Initial stock $\mathbf{S}_{res,0}$ obtained in the EOLES-Dispatch simulation is used to initialize the filling level of individual reservoirs in ORCHIDEE at the beginning of the simulation, assuming a homogeneous filling level across all reservoirs.

5.3 Simulation framework

The analysis is based on the comparison of 5-year simulations using different versions of EOLES-Dispatch, with or without coupling the model with ORCHIDEE, as presented in Table 5.1:

- The preexisting version, referred to as **EOLES**, in which constraints on hydroelectric power plants are defined based on observations of a reference year.
- A partly coupled simulation, labeled **ORCH_EOLES_res**, in which the outputs of the ORCHIDEE model are used to constrain the production of the French reservoir power plant, while a capacity factor based on observations is still used for run-of-river production.
- A fully coupled version, referred to as **ORCH_EOLES_full**, in which ORCHIDEE's simulations are used to define the capacity factor of the French run-of-river plant.

Technology	**EOLES**	**ORCH_EOLES_res**	**ORCH_EOLES_full**
Run-of-river	Capacity factor taken from observed production		Capacity factor computed based on ORCHIDEE's simulations
Reservoirs	Monthly constraints	Flexibility constraints from ORCHIDEE's simulations	

Table 5.1: Description of the simulations conducted in this study.

5.3.1 ORCH_EOLES - Procedure for coupling the two models

In ORCH_EOLES_res and ORCH_EOLES_full versions, we iterate several consecutive runs of the two models, using outputs from one model to inform the other. This procedure is inspired by Ibanez et al. (2014) and is described in Fig. 5.2.

Initial run A "natural" run of ORCHIDEE is first performed, without any hydropower demand prescribed to the model. The reservoirs are then only operated for other water uses (tourism, irrigation, and ecological flow), and the simulated water volume in each hydroelectric reservoir $V_i(t)$ remains near its maximum as no water is used for hydropower. Some adjustments to the previous equations (Eqs. 5.8 to 5.12) are made to obtain the first constraints to inform EOLES-Dispatch. First, the inflow $\mathcal{I}_i(t)$ is computed by replacing $V_i(t)$ with the minimum volume $V_{min,i}(t)$ in Eq. 5.8, which corresponds to the absolute maximum hourly inflow likely to enter the reservoir. Similarly, by replacing $V_i(t)$ by $V_{min,i}(t)$ in Eq. 5.11, we obtain the absolute minimum of hydropower potential of the water that is sure to spill.

Following iterations Hourly hydropower schedule simulated by EOLES-Dispatch is then used to prescribe hydropower production in ORCHIDEE, which leads to a new hourly time series of constraints that can once again inform a new EOLES-Dispatch run.

We iterate over this procedure until the mean absolute difference in schedule simulated by EOLES-Dispatch for two consecutive iterations is below 10% of the mean hourly production. An example of these iterations and their convergence assessment are displayed in Appendix B.1.

5.3.2 Data inputs

The ORCHIDEE model is driven by the SAFRAN climate reanalysis dataset (Quintana-Segui et al., 2008). This dataset provides the required atmospheric variables - temperature, relative humidity, wind speed, downward radiation (shortwaves and longwaves), and precipitation (solid and liquid) - at an hourly time step over 8x8 km grid cells that cover France and the upstream part of the international catchments beyond its borders.

Following the procedure described in Section 2.2.5, efficiencies of individual power plants have been calibrated based on available data of annual production.

Exogenous inputs to the EOLES-Dispatch model include the generation portfolio, hourly power demand time series, hourly capacity factors of variable renewable technologies, variable generation costs, start-up costs, ramping costs, minimum off-times, and minimum and maximum load levels of thermal power plants. The simulations are conducted for two scenarios that only differ in terms of generation portfolio and hourly power demands. Hourly capacity factors of solar, wind, and run-of-river are derived from observations for the 2015-2019 period (ENTSO-E, 2023) while cost assumptions follow the calibration made by Leblanc (2023) and are detailed in Appendix B.2.

5.3.2.1 2019 power mix

In the first step, simulations of the different model versions are conducted in the context of the 2019 European power system (detailed in Fig. 5.6).

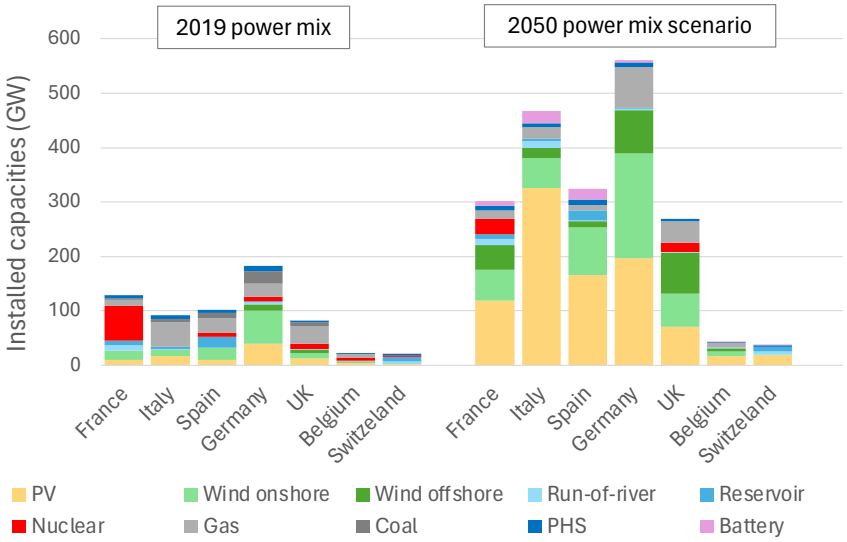

Figure 5.6: Installed capacities in the two power scenarios (adapted from RTE (2021)).

5.3.2.2 2050 power mix scenario

In the second step, we analyze the effect of the coupling in the case of a possible future power mix. The scenario we consider is briefly described here, for more details see Appendix B.3.

In France, a detailed prospective study by RTE (2021) has proposed various trajectories for the power system in order to achieve carbon neutrality in 2050. Among these, the scenario referred to as *N1* appears as the most plausible given current national policies. This scenario is based on the massive integration of renewables and the replacement of a portion of the aging nuclear power plants. The nuclear capacity is more than halved compared to 2019 (Fig. 5.6). For neighboring countries, we use the central projection of RTE (2021) when available and the TYNDP projection otherwise (ENTSO-E, 2011). They both project a massive integration of renewables in all countries and the phase-out of coal power plants. By 2050, gas plants are expected to be fully decarbonized, either by using hydrogen or synthesis methane as fuel or by being equipped with carbon capture and storage (CCS) technologies (see Appendix B.2 for the assumptions on costs).

The power-to-gas chain is modeled through an exogenous total demand for hydrogen production. This demand is assumed to be completely flexible and more details are provided in Appendix B.3. The interconnections capacities and hourly power demands are increased following assumptions of RTE (2021) and ENTSO-E (2011) (see Appendix B.3 for details).

We do not attempt to provide a full assessment of future power systems, as important items are missing such as demand flexibility. Instead, the primary objective of this prospective scenario is to investigate the effect of the coupling methodology within a different power mix than the one for which the preexisting version of EOLES-Dispatch was calibrated.

5.4 Results

5.4.1 Improvements in simulated hydropower production

We simulate the historical power dispatch for the 2015-2019 period using the three model versions presented above. In this subsection, we explore how the coupling affects the simulated French hydroelectric production and how it compares with the observed one (RTE, 2023b).

5.4.1.1 Reservoir plant production

First, we focus only on the effect of changing the definition of the constraints on reservoir production. To achieve this, we compare simulations of EOLES and ORCH_EOLES_res model versions. In ORCH_EOLES_res, iterative simulations of ORCHIDEE and EOLES-Dispatch are conducted, following the procedure described in Fig. 5.2. The convergence of this iterative process is described in Appendix B.1 and requires six iterations.

As shown in Chapter 3, the hydropower module of ORCHIDEE can reproduce realistic hydropower potentials. In the ORCH_EOLES_res version, the production by the reservoir plant is simulated to be 72.1 TWh over the entire period, compared to the observed production of 74.8 TWh during the same period (3.6% less). The coupling with ORCHIDEE introduces new constraints on the upper and lower production limits for the representative reservoir hydropower plant, which yield the simulated hourly production to align more closely with observed data compared to the simulation relying on the preexisting version (Fig. 5.7).

During winter, the production capacity of the reservoir plant $\sum_i Pmax_{i,t}$ is reduced due to the limited stock in the reservoirs. This reduces the production by the reservoir plant during demand peaks, as shown in Fig. 5.7,a) for the week of January 18th, 2016, bringing it closer to observed production compared to the EOLES version. In summer, the main constraint is the fatal production from minimum releases for ecological and irrigation needs $\sum_i \mathcal{R}'_i(t)$, which leads to a minimum production that matches the observations. Examining the average hourly production throughout a week (Fig. 5.7,b) shows significant impacts. In the EOLES version, the model is under-constrained and produces more output during peak demand periods (early mornings and evenings on working days) and less during off-peak periods (nights and weekends) compared to observed data. The ORCH_EOLES_res version yields results that align better with observed data, thanks to the new constraints. The differences are particularly marked during the spring and summer seasons. As a consequence of these improvements, the Root Mean Square Error (RMSE) of simulated reservoir production is improved from 2.39 GWh in the EOLES version to 1.73 GWh in the ORCH_EOLES_res version. Significant differences remain

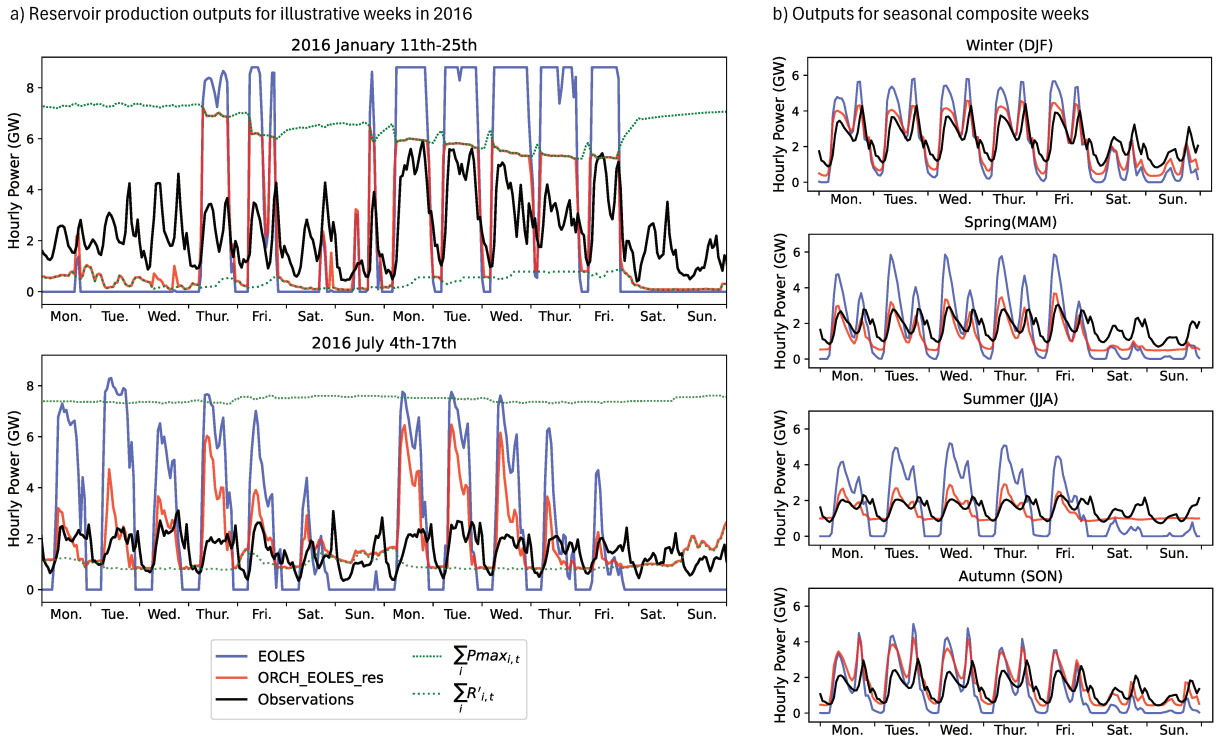

Figure 5.7: Comparison of hourly production obtained for the French reservoir plant by EOLES-Dispatch in the EOLES and ORCH_EOLES_res versions and the observed production. a) Simulated and observed production by the French reservoir plant during illustrative weeks in winter and summer. Green dotted lines indicate the additional constraints implemented in the ORCH_EOLES_res version (maximum capacity and minimum production due to minimum releases). b) Mean simulated and observed production for seasonal composite weeks.

between the production simulated by the model and the observed one, which will be further discussed in Section 5.5.2.

The monthly distribution of simulated production is however closer to the observations in the EOLES version than in the ORCH_EOLES_res version (Fig. 5.8). This is because the EOLES version includes a monthly constraint calibrated on the observed production. In the ORCH_EOLES_res version, optimizing monthly production results in overestimating the production in early winter (November and December) and underestimating it during the spring and summer (March to September).

Moreover, the equations in ORCH_EOLES_res allow for the simulation of the evolution of the energy stored in the reservoirs ($\mathbf{S}_{res,t}$), which is not possible with the EOLES version. Comparing the simulated hydraulic stock with the observed one (RTE, 2023d) (Fig 5.9) shows a good agreement in the timing of inflows to the reservoirs. However, there are some discrepancies in the timing of release, due to the discrepancies in production previously highlighted. The release starts later in the simulation than in the observations consistently with less production in September and is larger in the model in early winter (November and December) due to more production simulated by the model than observed during these months. Furthermore, the simulated stock exhibits higher maximum and lower minimum yearly values than the observed stock, suggesting that the constraints imposed on minimum and maximum stock limits in the model may be too lenient compared to those considered by reservoir managers. This issue is discussed further in Section 5.5.2.

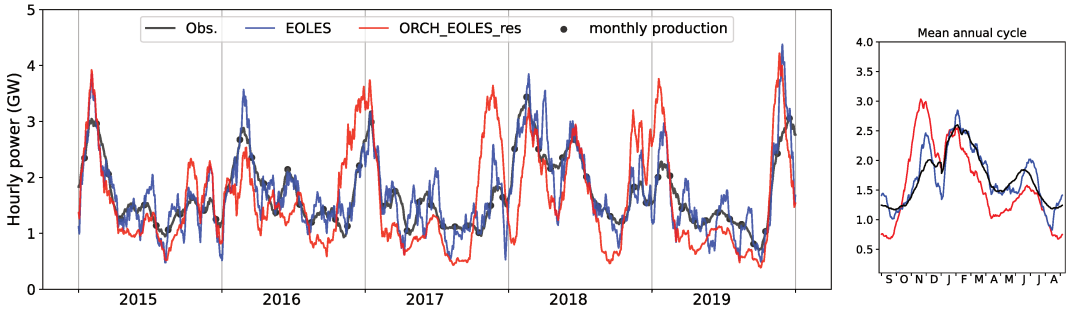

Figure 5.8: Comparison of 30-day average production obtained for the French reservoir plant by EOLES-Dispatch in the EOLES and ORCH_EOLES_res versions with the observed one. The right panel is the mean annual cycle of 30-day average simulated and observed production.

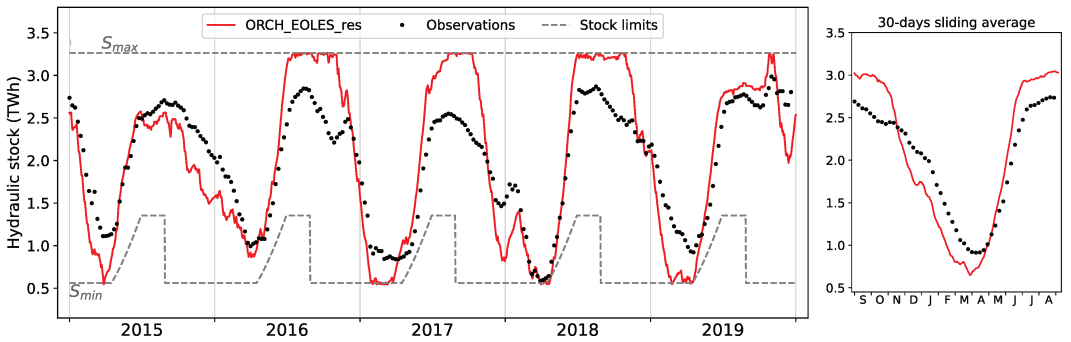

Figure 5.9: Simulated hourly stock in ORCH_EOLES_res compared to weekly observations over the 5-year simulation. In ORCHIDEE, the maximum volume of each reservoir $V_{max,i}(t)$ is set to 90% of the total reservoir capacity. The minimum volume $V_{min,i}(t)$ is set to 15% of the total reservoir capacity by default and is increased for touristic reservoirs during the Summer. The right panel is the mean annual cycle of simulated and observed stock.

5.4.1.2 Run-of-river production

In ORCH_EOLES_full, the capacity factor of the French run-of-river plant is computed in ORCHIDEE instead of being based on observations. The calibration performed in ORCHIDEE allows the model to simulate the total production very closely to the observations (RTE, 2023b) (less than 1% difference). The seasonality of the capacity factor simulated in ORCHIDEE is also in good agreement with the observed data (Fig. 5.10). A small seasonal bias is nevertheless observed, due to the hydrological errors of the model, leading to a small underestimation of production in January and February, and an overestimation in May and June. This seasonal shift in run-of-river production leads to a negligible increase in the dispatch cost as additional thermal capacities are required during Winter in ORCH_EOLES_full (less than 0.1%) compared toORCH_EOLES_res . The impacts on the simulated reservoir production are also negligible.

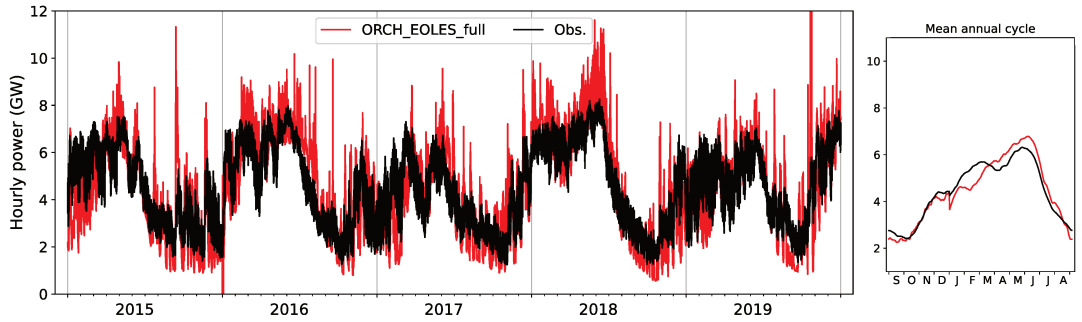

Figure 5.10: Comparison of hourly simulated and observed production by run-of-river hydropower plants. The right panel is the mean annual cycle of 30-day average simulated and observed production.

5.4.2 Impacts of a change in the power mix on the hydropower generation

We now analyze the effect of a change in the power mix. The outputs obtained using the ORCH_EOLES_full version for each power mix are presented in Fig. 5.11. Despite the same water resources being available in both simulations, the annual production by the reservoir power plant is slightly increased (+1.4%) in the 2050 energy scenario compared to the 2019 power mix. This change is attributed to the influence of the height on the production. In the 2050 power mix scenario, hydropower is produced on average with reservoirs filled to 55.5% (production-weighted average filling level), against 54.0% in the 2019 power mix. We also observe negligible differences (-0.3%) in the production by the run-of-river plant, which can be attributed to differences in the operation of upstream reservoir plants.

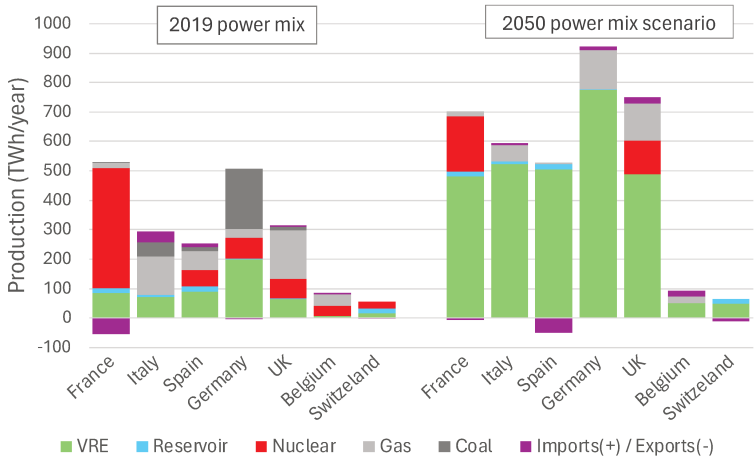

Figure 5.11: Average annual electricity supply by technology simulated by EOLES-Dispatch in the EOLES version. Imports and exports are included in the generation column with exports contributing negatively and imports contributing positively. Storage technologies are not shown here. Solar PV, onshore and offshore wind, and run-of-river are grouped in VRE technology, which stands for Variable Renewable Energy.

Figure 5.12 displays the 5-year average of 30-day sliding average production by reservoir plants obtained in each energy scenario with the two model versions. In the EOLES

version, the monthly production is set, which prevents large changes in the production seasonality. In the coupled version, however, the model optimizes the production of the reservoir power plant throughout the year, as long as all constraints are met. The production obtained in the 2050 energy scenario exhibits less intra-annual variability compared to that of the 2019 mix. This change is attributed to the significant integration of variable renewable energy sources in the 2050 mix, resulting in greater intra-monthly and intra-weekly variability of variable production. In the 2019 mix, the net load (demand minus variable production) follows a distinct seasonal pattern, with high peaks in winter due to high power demand and troughs during summer. In the 2050 scenario, there are local peaks of net load throughout the year due to the increased use of wind and PV technologies.

These changes in production result in small changes in the storage evolution. In the 2019 mix, water depletion starts in late October and is important during winter months to match the pronounced generation winter peak. In the 2050 mix, however, water releases begin earlier, generating more power in September-October, and are smaller during the winter.

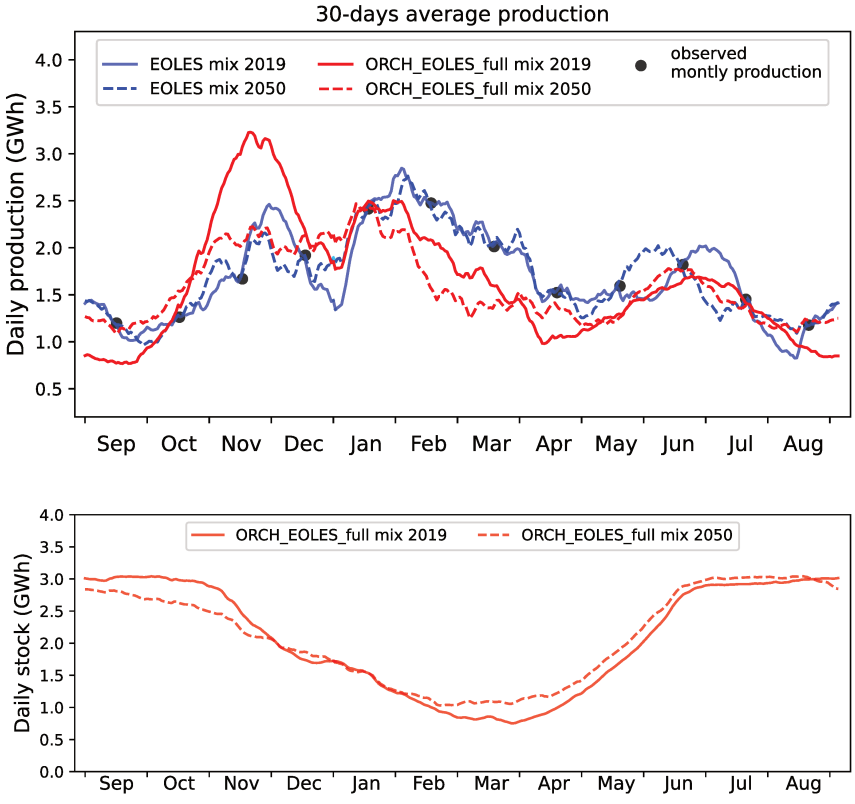

Figure 5.12: Top: Inter-annual average of 30-days sliding average production by the reservoir plant for the two power mix scenarios and the two EOLES-Dispatch versions. By definition, the monthly simulated production is set to the observed one in the EOLES version. Bottom: Comparison of stock simulated by EOLES-Dispatch (ORCH_EOLES_full version) for the two power mix scenarios.

5.4.3 Impacts on the European power system

This section explores the broader impacts of the new constraints on hydropower production on the whole power system. The differences in outputs obtained with each version are compared in Fig. 5.13 for each power scenario. Table 5.2 details the differences in terms of unsatisfied demand (Eq. 5.3), production by technology, and dispatch cost (Eq. 5.2).

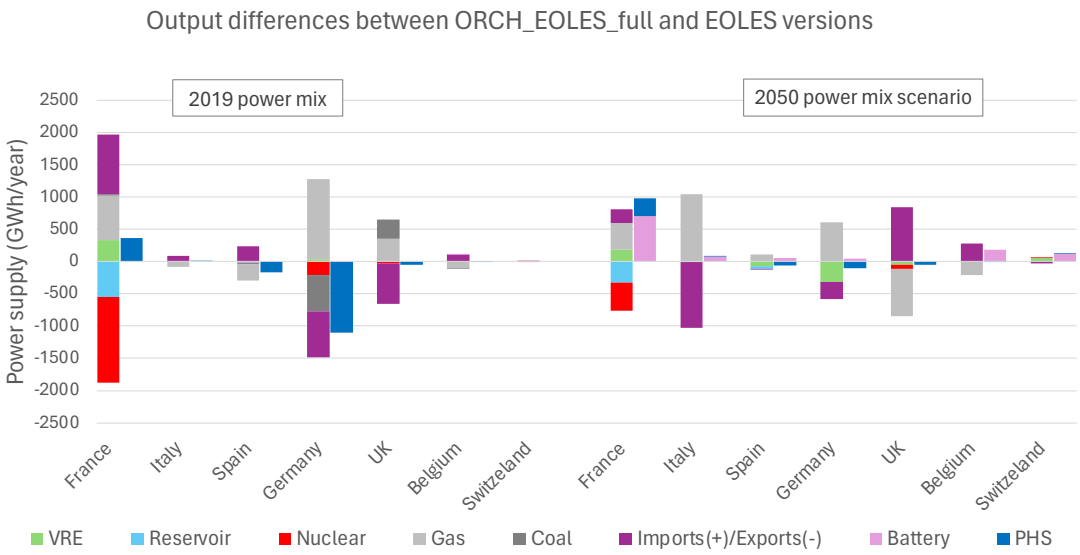

Figure 5.13: Differences in average annual electricity supply of each technology when moving from the EOLES version to the ORCH_EOLES_full version. For each country, the left column shows the difference in annual production by technology, while the right column shows the change in electricity supply for storage technologies.

In the 2019 mix, both model versions meet the power demand in all countries throughout the entire period. The simulated dispatch cost is slightly higher in the coupled version (+0.2% at the aggregate level), as a consequence of the small changes in the power dispatch noticeable in Fig. 5.13. In France, as previously mentioned, the coupled version results in a slight decrease in the simulated production by the reservoir plant (-3.7%) compared to the preexisting version. This decrease in electricity supply is offset in France by increased production of gas power plants, greater use of PHS plants, and decreased exports to neighboring countries. Electricity imports decrease in Germany, Spain, and the UK, resulting in additional thermal production in these countries. Additionally, due to the new constraint on minimum water releases for irrigation and environmental purposes ($\sum_{i \in res} \mathcal{R}'_i(t)$), a portion of the output from reservoir plants is no longer dispatchable and replaces baseload nuclear generation. An increase in gas generation compensates for this loss of flexibility from hydropower.

In the 2050 power mix scenario, some demand is unsatisfied in both model versions, essentially in France and the UK. The unsatisfied demand increases significantly in the coupled version (+575%) compared to the preexisting one. When analyzing events of unsatisfied demand simulated in the ORCH_EOLES_full version (see Fig. 5.14 for an example), we see that they correspond to times when the reservoir plant production is significantly lower in the ORCH_EOLES_full version than in the EOLES one, because of the additional constraints on maximum capacity ($\sum_{i \in res} \mathcal{P}max_i(t)$), which reduces the available power output of the reservoir plant. This also reduces possible exports

Power mix scenario	2019		2050	
Model version	EOLES	ORCH_EOLES_full	EOLES	ORCH_EOLES_full
Total unsatisfied demand (GWh/year)	0	0	5.59	37.8
Electricity supply by technology (TWh/year)				
VRE	533.11	533.42	2828.5	2828.3
Reservoir	61.02	60.48	60.96	60.59
Nuclear	647.96	645.83	329.6	329.1
Gas	469.95	472.40	311.7	312.9
Coal	279.20	279.17	0	0
Storage (PHS and batteries)	50.23	49.06	134.44	135.70
Total dispatch cost (billion €/year)	**43.1**	**43.2**	**66.6**	**67.5**
Cost of thermal generation	42.7	42.8	65.5	66.0
Cost of thermal startups	0.34	0.37	1.04	1.05
Cost of thermal ramping	0.02	0.02	0.008	0.008
Cost of unsatisfied demand	0	0	0.08	0.57

Table 5.2: Comparison of unsatisfied demand, electricity supply by technology, and dispatch cost obtained in the different simulations.

from France to neighboring countries at these time steps (or requires additional imports to France), which explains why we also find an increase in the unsatisfied demand in other areas in the coupled version. This increase in unsatisfied demand explains 45% of the increase in dispatch cost observed in Table 5.2. The second driver of the cost increase is the higher power supply by gas power plants (41% increase in generation costs).

5.4.4 Identifing the main drivers of the change

Previous results indicate that shifting from the EOLES version to the ORCH_EOLES_full version slightly increases the dispatch cost. These changes are the result of four interacting effects: (i) the removal of the monthly power production limit for reservoir plants, which reduces the dispatch cost; (ii) the modification of the annual production potential of the reservoir plant from an estimation based on observed production to one based on ORCHIDEE's simulation. In our case study, the production predicted by ORCHIDEE is slightly lower than the observed production (Section 5.4.1.1), which increases the dispatch cost; (iii) the introduction of new constraints on hourly production by the reservoir plant (Eq. 5.13 to 5.16), which increases the dispatch cost; and finally (iv) the change in the computation of the run-of-river capacity factor (Eq. 5.6). In our case study, this change increases the annual potential of production by run-of-river plants but slightly modifies its seasonality (Section 5.4.1.2), hence an uncertain effect on the dispatch cost.

An evaluation of additional model runs allows for the decomposition of these different effects to isolate their relative contribution to the observed change when shifting from one version to the other. We start with the EOLES baseline version and first remove the monthly limit on reservoir production by replacing it with a yearly limit (still based on observations). This annual production limit is then modified to account for the actual reservoir potential simulated in ORCHIDEE. Finally, comparing ORCH_EOLES_res and ORCH_EOLES_full version allow us to distinguish the effect of the change in run-of-river capacity factor.

In both power mixes, introducing new hourly constraints on reservoir production

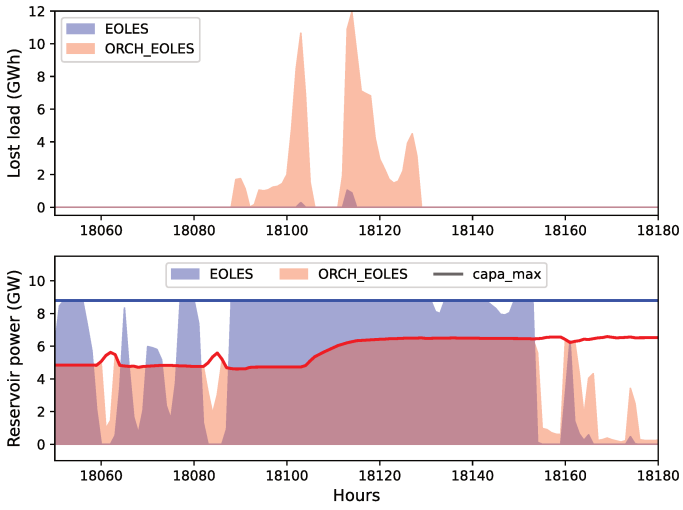

Figure 5.14: Top: Comparison of the unsatisfied demand (also called lost load) simulated in the two versions of EOLES-Dispatch. Bottom: Comparison of reservoir production during the same period. The solid lines indicate the constraint on maximum production present in each version. In the EOLES version, this constraint is set to the total installed capacity of reservoir plants (8.8GW), whereas it varies according to reservoirs' filling levels in the ORCH_EOLES_full version.

emerges as the primary driver, contributing to respectively 100% and 84% of the change in dispatch cost in the 2019 and 2050 scenarios. In comparison, removing the monthly limits has only a very limited effect, as it represents respectively 18% and 6% of the previous changes. Changing the run-of-river capacity factor increases the dispatch cost in both cases, indicating a stronger effect of the seasonal than annual change. The overall capacity factor effect is however very small compared to the introduction of the new hourly constraints on reservoir production.

5.5 Discussion

Previous research has emphasized the need for introducing additional constraints into PSMs to better represent the real flexibility of hydropower plants. In this section, we discuss how our approach compares to these previous findings.

5.5.1 Increasing the complexity while maintaining a simple linear model with a representative reservoir plant

Several studies have pointed out the limitations of using a single equivalent reservoir instead of individual reservoirs in PSMs (Brandão, 2010; Ek Fälth et al., 2022). According to these studies, using a single reservoir often leads to overestimating hydropower flexibility due to various factors.

(i) When dealing with reservoirs in series, it is important to consider that the inflow to the downstream reservoir may depend on the production of the upstream reservoirs. A model with a single reservoir cannot account for these temporal dependencies (cascading effect). This effect also impacts downstream run-of-river generation.

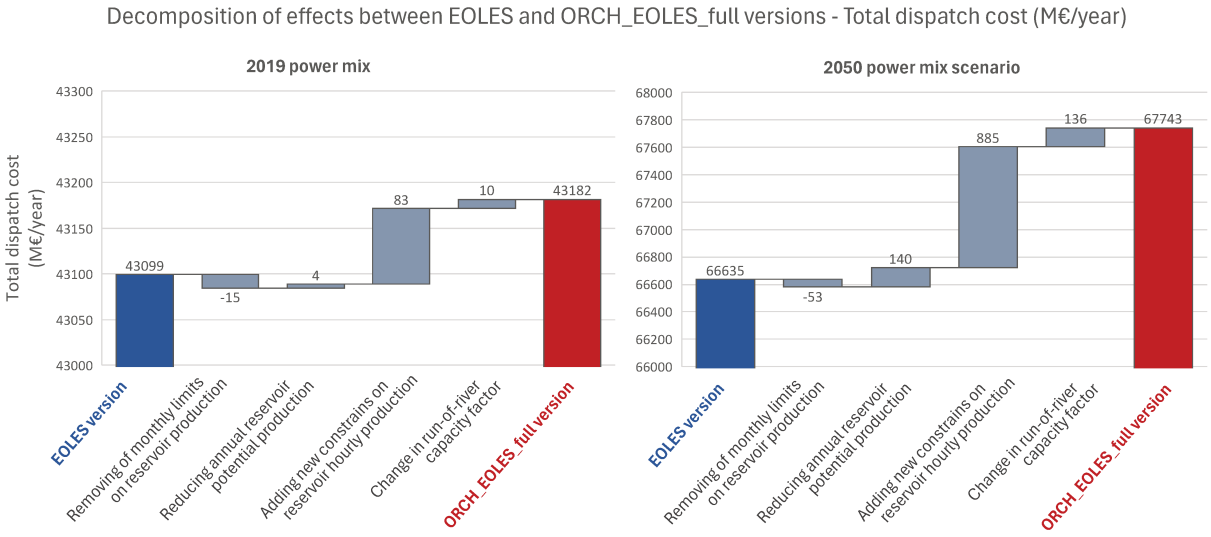

Figure 5.15: Decomposition of effects explaining the observed change in dispatch cost between EOLES and ORCH_EOLES_full version. Left: Results for the 2019 power mix. Right: Results for the 2050 power mix scenario.

(ii) Most models that use a representative reservoir consider the sum of individual reservoir inflows as the overall inflow. This may result in an overestimation of the reservoir's storage capacity since the model cannot ensure that each individual reservoir has enough free capacity to accommodate its specific inflow.

(iii) Additionally, linear optimization models struggle to incorporate the effect of variable head on production due to the introduction of non-linearities. Each reservoir is assumed to have a constant average water head. This difficulty is even more pronounced in models that only have one representative reservoir.

(iv) The hourly production of an individual reservoir power plant is limited both by the reservoir stock $S_i(t)$ and the installed capacity P_i. Noting $G_i(t)$ the production of this individual plant, we have then $G_i(t) \leq \min(S_i(t), P_i)$. When utilizing a representative reservoir, only the total stock $\sum_i S_i(t)$ and the total installed capacity $\sum_i P_i$ across all reservoirs and plants are taken into account. We have then $\sum_i G_i(t) \leq \min(\sum_i S_i(t), \sum_i P_i)$, which is less constraining than the previous equation as $\min(\sum_i S_i(t), \sum_i P_i) \geq \sum_i \min(S_i(t), P_i)$. This allows a plant with a higher capacity to leverage the storage of a less powerful one, which can be misleading.

Despite still relying on a single reservoir representation, the coupled version proposed here overcomes these four simplifications.

(i) In ORCHIDEE, the river routing is explicitly represented. The time travel of water from one reservoir or plant to another is therefore computed with greater detail than is usually done in PSMs when it is done (Liu (2019) for example), as ORCHIDEE uses the topography and river steepness to determine the water velocity at each grid point. While EOLES-Dispatch does not explicitly model the links between reservoirs and plants, the iterative process allows for accounting for the cascading effect. Indeed, inputs for a given iteration of EOLES-Dispatch are derived from an ORCHIDEE simulation that sought to satisfy the production simulated by EOLES-Dispatch in the previous iteration. These updated time series therefore reflect the dependencies between infrastructures under the conditions close to those simulated by EOLES-Dispatch in the prior iteration. The coupling of the PSM with a grid-based hydrological model like ORCHIDEE enables

therefore the integration of cascading effects without an explicit representation of the hydropower network in the PSM, which would be cumbersome to implement and run.

(ii) Net inflows are explicitly distinguished from spillage at the plant level before being aggregated at the national level to inform EOLES-Dispatch. This overcomes the issue previously highlighted.

(iii) In the coupled version, all hydropower inputs (inflows, spillage, minimum releases, and maximum capacity) are computed by taking the actual head simulated by ORCHIDEE at each time step. This allows us to account for the effect of the variable head on production while keeping a linear problem.

(iv) The proposed iterative process aims to obtain a reservoir management setup in ORCHIDEE that meets the national production simulated by EOLES-Dispatch. Therefore, the final iteration is supposed to propose a way to operate each individual reservoir to achieve the national production, while satisfying the individual constraints of each plant. This enables to overcome the non-linearities highlighted in the previous equations.

Despite these improvements in modeling, it is important to note that this new method requires multiple iterations of both models, resulting in a substantial increase in computational time. For instance, Appendix B.1 shows that six iterations are necessary, in the case of the 2019 electricity system, resulting in a total of twelve model runs instead of only one in the preexisting version.

5.5.2 Discrepancy between simulated production and historical data

As shown in Fig. 5.7, introducing additional constraints on hydropower generation through the coupling with ORCHIDEE makes the optimal production profile more realistic. However, notable discrepancies remain between the simulated production and the historical data. Specifically, the simulated production varies over a wider range than the observed data, and the monthly distribution is not well reproduced. As discussed by Ek Fälth et al. (2022), several factors can explain these differences.

First, EOLES-Dispatch optimizes the dispatch by assuming perfect foresight of future power demand, capacity factors, and hydropower inputs. Energy planners and dam operators do not have access to this information and therefore may tend to be more cautious in their water management. Some PSMs assume perfect foresight for a few days and manage long-term storage using a linear decreasing relation between power price and storage level (Tour, 2023).

Second, some constraints highlighted in previous studies are not considered in this work. In particular, we assume a constant efficiency of each plant, whereas, in reality, it varies with the water outflow (Ek Fälth et al., 2022). This variable efficiency discourages both very low and very high power production, hence taking it into account would reduce the excessively high hourly variability we obtain. Moreover, our model is based on a simplistic modeling of irrigation demand, which may underestimate the constraints on summer production and could partly explain the seasonal difference with observed data shown in Fig. 5.8. There are also additional ecological constraints that are not considered in this work. Ramp rates may be reduced to limit the ecological impact of hydropeaking, which risks flooding or stranding of aquatic organisms (Richter et al., 2007). The frequency of hydropower generation reversals, or the number of changes between rising and falling generation per day, may also be ecologically impactful and therefore limited (McManamay et al., 2016).

Finally, our model conveys a simplified vision of the power market, in which only the day-ahead market is represented, excluding both balancing and capacity markets.

However, these other markets may also provide incentives for electricity producers and planners (Perez-Diaz et al., 2020; Scharff et al., 2014).

5.5.3 Improving reservoir operations in the hydrological model

A previous work implementing the demand-based approach in the uncoupled ORCHIDEE model identified a limitation of this approach with biased precipitation data (see the results presented in Section 3.3.2 for the SAF_COM climate product, Fig. 3.14). Specifically, when the prescribed production exceeded the annual inflows simulated by the model, reservoirs were systematically emptied and the model failed to represent realistic operations. The root of this failure was the fixed nature of the production target, which did not adapt to the availability simulated in the model. The coupling method presented in this study, also based on a demand-based approach to pass information from EOLES-Dispatch to ORCHIDEE, addresses this issue by ensuring that the prescribed production is consistent with the hydrological conditions simulated in the model, thus closing the feedback loop.

To illustrate this improvement, we conducted a simulation of the integrated modeling framework ORCH_EOLES_full driven by SAF_COM climate data, which underestimates mountain precipitations compared to SAFRAN. In this simulation, the production prescribed to ORCHIDEE has been simulated by EOLES-Dispatch based on ORCHIDEE's outputs and is therefore consistent with the hydrological conditions simulated in ORCHIDEE. Figure 5.16 compares the simulated stock obtained in this new simulation to the one obtained in section 3.3.2 and shows that the coupling allows indeed for a more realistic representation of stock dynamics.

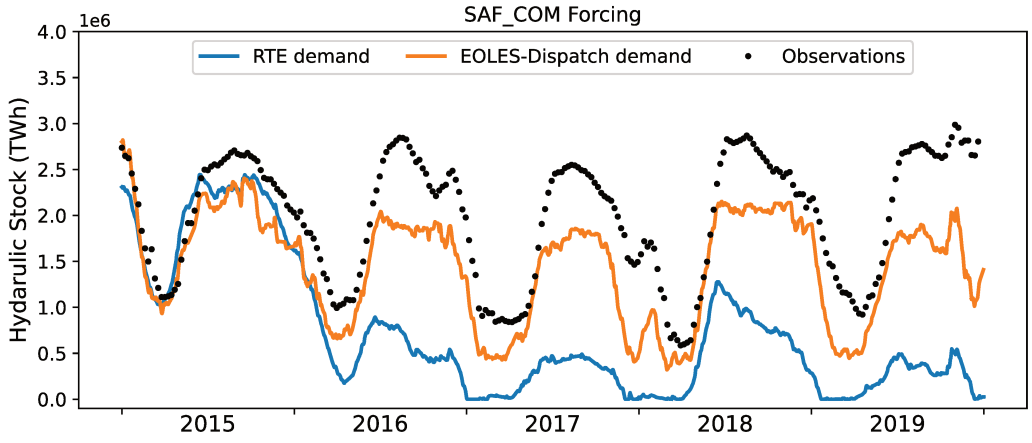

Figure 5.16: Comparison of the hydraulic stock simulated by ORCHIDEE depending on the target production prescribed to the model is derived from the observations (RTE demand) or the EOLES-Dispatch model.

Though this study focuses on the value of the coupling from the perspective of PSMs, this also shows its value for the representation of realistic reservoir operations in hydrological models. Such coupling can help improve the integration of anthropogenic processes in the water cycle.

5.6 Conclusion

In most PSMs, production by hydropower reservoir plants is constrained by monthly production limits. This method introduces two opposing biases in the representation of hydropower flexibility. On the one hand, assuming a fixed monthly distribution of production underestimates flexibility. On the other hand, the models do not represent any constraints within one month, while the operation of an actual hydropower plant may be constrained by water availability, the multipurpose reservoir operation, regulatory requirements, and the water level in the reservoir. This leads to an overestimation of the flexibility within a month.

This study introduces a new method to inform constraints on hydropower generation within a PSM (EOLES-Dispatch) through an iterative coupling with a grid-based hydrological model (ORCHIDEE). This comprehensive modeling framework ensures that the hourly simulated hydropower schedule simultaneously adheres to constraints related to water availability, non-power reservoir operations, and the minimization of power system cost.

The study shows that the revised method provides a more accurate representation of hydropower flexibility throughout the day and week than the original method. Moreover, it allows for the quantification and comparison of the two opposing simplifications present in traditional PSMs. We find that the inclusion of monthly production limits has minimal impact when compared to the implementation of new constraints that reflect the actual maximum capacity and fatal production of the plant.

Accounting for these additional constraints appears insightful when examining the reliability of future power mixes with higher integration of variable renewable power.

The coupled approach presented here allows us to investigate a wide range of scenarios in terms of power mixes and climate change, while the classic modeling approach relies on the assumption of a fixed frame for reservoir operations. It holds promising prospects for exploring the joint impacts of changes in climate, water management, and power mixes.

5.7 Supplementary material: Further insights on hydropower modeling in EOLES-Dispatch

This section examines the impact of two parameters on the modeling of hydropower in EOLES-Dispatch. The analysis is based on a comparison of simulations performed with different versions of the EOLES-Dispatch model.

5.7.1 Simulation area

The first parameter to evaluate is the spatial scale of the simulation. Two simulations are conducted using the initial version of EOLES-Dispatch (EOLES version). The first simulation, referred to as *France only*, models solely the French power system, with the objective of minimizing its cost. The second simulation, referred to as *France + neighbors*, represents the power system of France and its neighboring countries, minimizing their total cost.

Changing the spatial scale mainly results in differences in simulated prices (Fig. 5.17). In the *France only* simulation, no power trade is represented, meaning that French power plants are dispatched from the least to the most expensive to meet the national power demand at each time step. As a result, nuclear plants are often the marginal technology, particularly from March to October, when power demand is sufficiently small, resulting in

a relatively constant price at 14.3 €/MWh during this period. In contrast, when neighboring countries are included in the simulation, French power plants can also contribute to meeting power demand in other countries, provided their generation cost is lower than the marginal technology in those countries and within the limits of the interconnections capacities. Consequently, in the *France + neighbors* simulation, French nuclear plants operate almost always at maximum capacity (adjusted for their weekly availability factor) to export electricity to countries where more expensive thermal plants are in use. As a result, gas power plants become the marginal technology more frequently in France, setting higher power prices that are much more closely aligned with the observed prices.

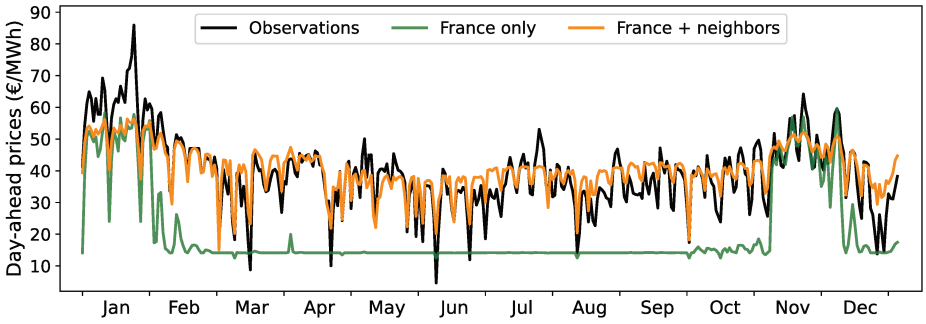

Figure 5.17: Day-average of simulated power prices compared to day-average of observed day-ahead prices in the French market for the year 2019 (ENTSO-E, 2023)
As usually done, the Lagrange multiplier associated with the adequacy constrain in period t and in market area a can be interpreted as a proxy of the electricity price in market a at time t (Leblanc et al., 2022).

This change in power prices has a direct impact on the simulated production of dispatchable hydropower plants in France, as illustrated in Fig. 5.18 and Table 5.3.

	Observations	France only	France + neighbors
Annual reservoir production (TWh)	14.35	14.35	14.35
Pearson correlation coefficient of hourly reservoir production	-	0.52	0.51
Annual PHS production (TWh)	5.46	2.69	6.19
Pearson correlation coefficient of hourly PHS production	-	0.31	0.35
Annual energy consumption for PHS pumping (TWh)	6.43	3.32	7.64
Pearson correlation coefficient of hourly PHS pumping	-	0.38	0.50

Table 5.3: Comparison statistics computed from hourly time series.

When only France is modeled, the relatively constant prices result in very low activity of the PHS plant for the most of the year, except during the winter months, when prices are higher. In contrast, when neighboring countries are included in the model, the increased price variability leads to more frequent PHS production and pumping, with the timing of simulated peaks aligning with the observations. Regarding the reservoir plant, the annual production is identical in both simulations, as it is determined by the hydrological conditions. However, the daily production is more variable when

neighboring countries are modeled, in response to the larger price fluctuations. In both cases, the model largely overestimates the variability of reservoir production compared to observations.

Table 5.3 indicates that accounting for neighboring countries improves the Pearson correlation coefficient compared to observations for the PHS plant, but slightly worsens it for the reservoir plant.

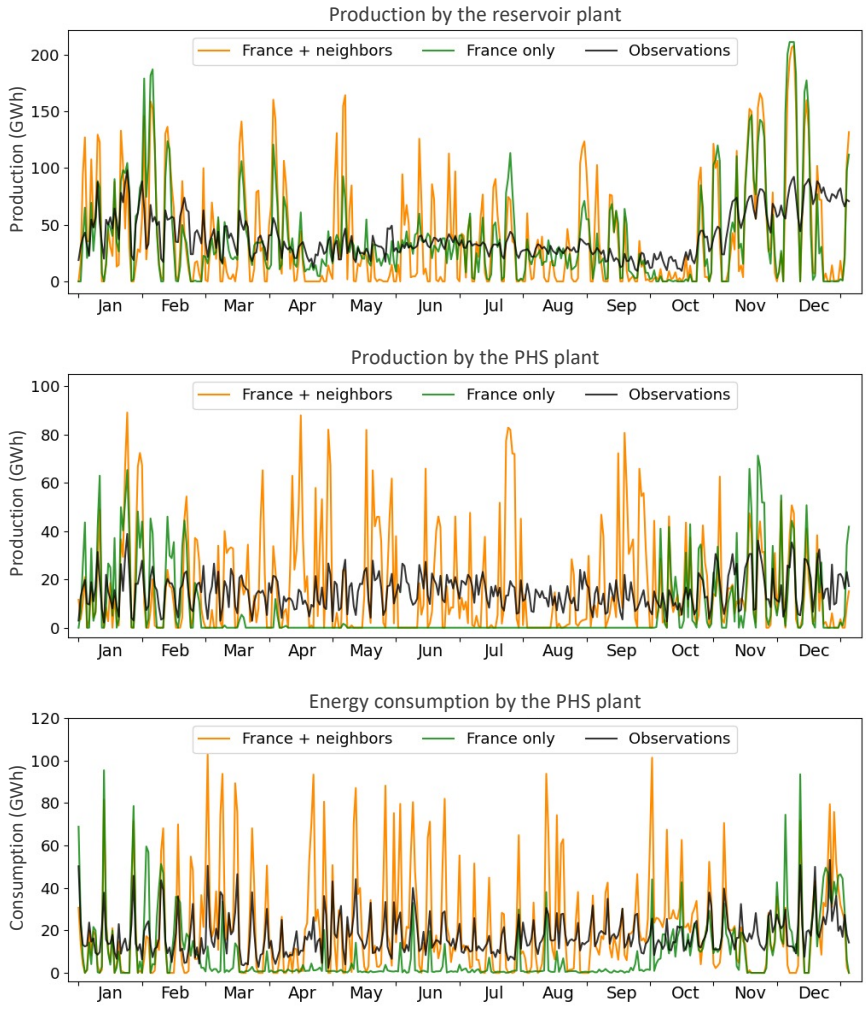

Figure 5.18: Comparison of daily simulated and observed hydropower outputs for the year 2019.

5.7.2 Distinguishing poundage and run-of-river power plants

As presented in section 1.1.1, four types of hydropower power plants can be distinguished: run-of-river, poundage, reservoir and PHS.

In the previous sections, poundage plants were modeled as run-of-river plants and included within the representative run-of-river plant in the EOLES-Dispatch model. The production of this representative plant was then entirely determined by a prescribed capacity factor, which was either based on historical production data (in the EOLES and ORCH_EOLES_res versions) or on ORCHIDEE simulations (in the ORCH_EOLES_full version). We explore here the value of considering the flexibility provided by poundage plants in the model. To this end, we introduce a fourth version of the EOLES-Dispatch

model, referred to as *ORCH_EOLES_poundage*. In this version, poundage plants are represented as a distinct technology in addition to the representative run-of-river and reservoir plant. The production of the representative poundage plant is constrained by a set of equations similar to those used to constrain the production of the reservoir plant, drawing on the operation of individual poundage plant reservoirs simulated by ORCHIDEE.

Figure 5.19 compares the outputs from the simulations conducted over the year 2019 in the 2019 power mix with the *ORCH_EOLES_full* and *ORCH_EOLES_poundage* model versions.

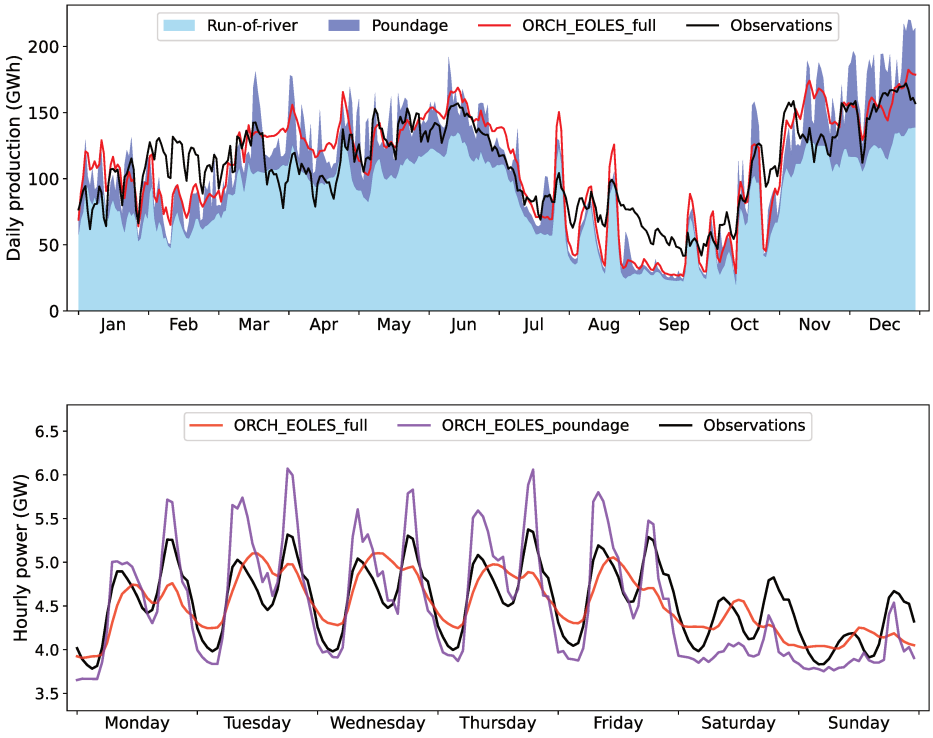

Figure 5.19: Comparison of simulated and observed production by run-of-river and poundage plants in 2019. Top: Daily production. The color filled areas represent the respective production by run-of-river and poundage in the *ORCH_EOLES_poundage* simulation. The black and red lines represent, respectively, the observed and simulated (*ORCH_EOLES_full* version) cumulative production by run-of-river and poundage plants. Indeed, no sub-annual observations distinguishing between run-of-river and poundage plants are available. Bottom: Mean hourly production across a week for aggregated run-of-river and poundage plants.

At the yearly scale, the difference in simulated poundage production is very small, particularly when compared to the existing discrepancies between simulations and observations. Differences are larger when examining the intra-day flexibility, with poundage production responding more effectively to power price variations in *ORCH_EOLES_poundage*. The impact on the total system cost is however negligible, shifting from 5.1403 to 5.1386 billion euros. Besides, it is worth noting that in the EOLES version, some demand-response is already observable, due to the cascading effect of reservoir releases that influence the production of downstream run-of-river plants.

Part III

The future of hydropower in the French power system under climate change

CHAPTER 6

Exploring the joint impacts of climate change and renewables penetration on French hydropower generation

This chapter applies the modeling framework developed in the first two parts of the manuscript to investigate the joint impacts of climate change and renewables penetration on French hydropower generation. The assessment relies on the reference scenarios developed by French public actors, respectively based on the Explore2 project (Marson et al., 2024) for climate change projections and RTE (2021) assumptions for the change in the power system.
This chapter is scheduled for adaptation into a draft article for submission to the Climatic Change journal in the forthcoming months.

Contents

6.1 Introduction . . . 104
6.2 Methods and data . . . 105
6.2.1 Modeling framework . . . 105
6.2.2 Climate scenarios . . . 108
6.2.3 Power system scenarios . . . 108
6.3 Results . . . 110
6.3.1 Stand-alone ORCHIDEE simulations . . . 110
6.3.2 Coupled simulations - Impacts of climate change on reservoir operations in the 2019 power scenario . . . 113
6.3.3 Coupled simulations - Economic consequences of the hydrological changes in the 2019 power scenario . . . 114
6.3.4 Coupled simulations - Joint impacts of renewable energy integration and climate change . . . 116
6.3.5 Coupled simulations - Impact on the overall power system . . . 121
6.4 Discussion . . . 121
6.4.1 Limitations of the study . . . 121
6.4.2 Climate change uncertainties . . . 122
6.4.3 Uncertainties of future power systems . . . 123
6.5 Conclusion . . . 123

6.1 Introduction

European countries are embracing extensive electrification and decarbonization of power generation in order to fulfill their climate commitments. This transition involves integrating solar and wind power plants, which strengthens the need for balancing technologies such as hydroelectric reservoirs.

Climate change is, however, affecting water resources and may impact hydropower production. Large-scale climate studies (Turner et al., 2017; van Vliet et al., 2016b) project a north-south division of Europe with the Nordic countries expected to see an increase in annual hydropower production, while the Mediterranean countries are projected to suffer a decline. Regarding France, studies have found a slight decrease in annual production under a 3°C rise in global temperature (Tobin et al., 2018; van Vliet et al., 2016b), but they also highlight large climate model uncertainties (Cronin et al., 2018; Gøtske et al., 2021). Furthermore, the seasonality of inflows to reservoirs is changing, with higher inflows during the winter and lower inflows during the summer (Gøtske et al., 2021). However, no previous study has analyzed this change in seasonality in regard to the power system needs, and assessed its impacts on power system cost and operation.

Production by hydroelectric reservoirs may also be impacted by changes on the power grid side, such as the increasing integration of variable solar and wind power plants. Gøtske et al. (2021) found that in European countries, an increased seasonality of hydropower operation would generally be required to balance higher renewable generation, with higher production from hydroelectric reservoirs during the winter. In contrast, Dimanchev et al. (2021) found that in Quebec, high renewable power scenarios could lead to decreased production by hydropower in winter and increased production in summer, to balance solar variability between day and night. Power demand patterns are also expected to change, as a result of the electrification of new final uses and the integration of new flexibility options such as power-to-gas-to-power storage (Boßmann et al., 2015). Finally, a seasonal shift in the power demand is also expected as a consequence of global warming, with a decrease in the demand for heating in winter and an increase in cooling demand in summer (Perera et al., 2020). These changes affect the net load, which governs the dispatch decisions of hydropower plants.

We may then wonder how these various effects on hydropower production interact and what the resulting impact on the power system might be. However, comprehensive studies examining the joint impacts of changes in climate and energy systems are scarce. Addressing this knowledge gap requires understanding the interplay between water availability and power grid dynamics, which necessitates the coupling of hydrological models with power system models (Chowdhury et al., 2021). Su et al. (2020) developed such a framework within the CAPOW model, which was later used by Hill et al. (2021) to examine the impacts of climate change on interconnected hydropower-dependent markets on the US West Coast. However, such a model relies on static operating guidelines for hydroelectric reservoirs and therefore does not take into account that dam operators may shift seasonal operations in the future to accommodate changes in hydrology or power grid needs.

This chapter examines the intertwined effects of climate change and the integration of renewable energy on French hydropower production. We leverage a dispatch optimization model that incorporates constraints on hydropower production from a hydrological model to analyze the resulting changes in production under different climate and power scenarios. We first assess the effect of projected hydrological changes on the current

power system. In the second step, we explore how these changes affect a prospective future power mix that includes a substantially larger proportion of renewable energies.

The remainder of this paper is structured as follows: Section 6.2 outlines the modeling framework used in this study and introduces the climate and power scenarios under study. Section 6.3 presents the results, which are then discussed in Section 6.4. Finally, 6.5 summarizes the main findings and draws future research perspectives.

6.2 Methods and data

6.2.1 Modeling framework

We take a whole system approach coupling a hydrological model, ORCHIDEE, with a power system model, EOLES-Dispatch. The framework is presented in detail in Chapter 5 and summarized in Fig. 6.1.

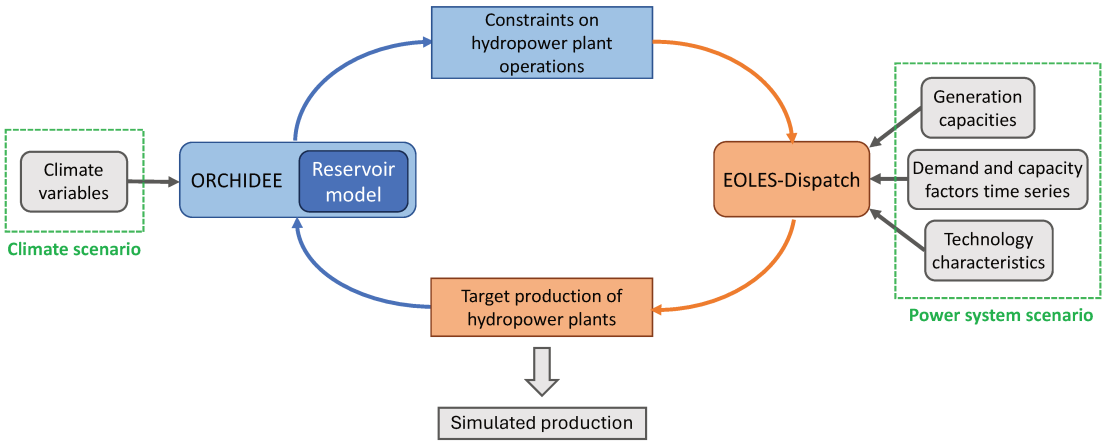

Figure 6.1: Modeling framework used in the study.

6.2.1.1 Hydrological model: ORCHIDEE

ORCHIDEE is a gridded land surface model (Krinner et al., 2005) that represents the continental hydrological cycle. It includes a module for reservoir operations, specifically for hydropower production (described in Chapters 2 and 3). The operation of hydroelectric reservoirs is driven by an exogenous target time series of aggregated production by reservoir power plants. The module aims to satisfy this target as closely as possible by dispatching the total production on each reservoir plant in the power grid.

Hydroelectric infrastructures (reservoirs and power plants) have been located on the model grid based on available datasets (GRanD (Lehner et al., 2011) for reservoirs and JRC hydropower database (European Commission et al., 2019) for hydropower plants). Their locations are shown in Fig. 6.2.

Two types of power plants are distinguished in the model:

- **Run-of-river plants**, which have no storage capacity and generate electricity according to the instantaneous river discharge at the plant location. They are primarily located on large rivers (Rhine and Rhone) to take advantage of their large water flows;

- **Reservoir plants**, whose production is dispatchable. They are fed by reservoirs that can store a specific volume of water and are often also used for other purposes that may constrain their operations. These plants are typically located in mountainous areas to benefit from high elevation differences between the reservoir where the water is stored and the plant where the water is used to generate electricity.

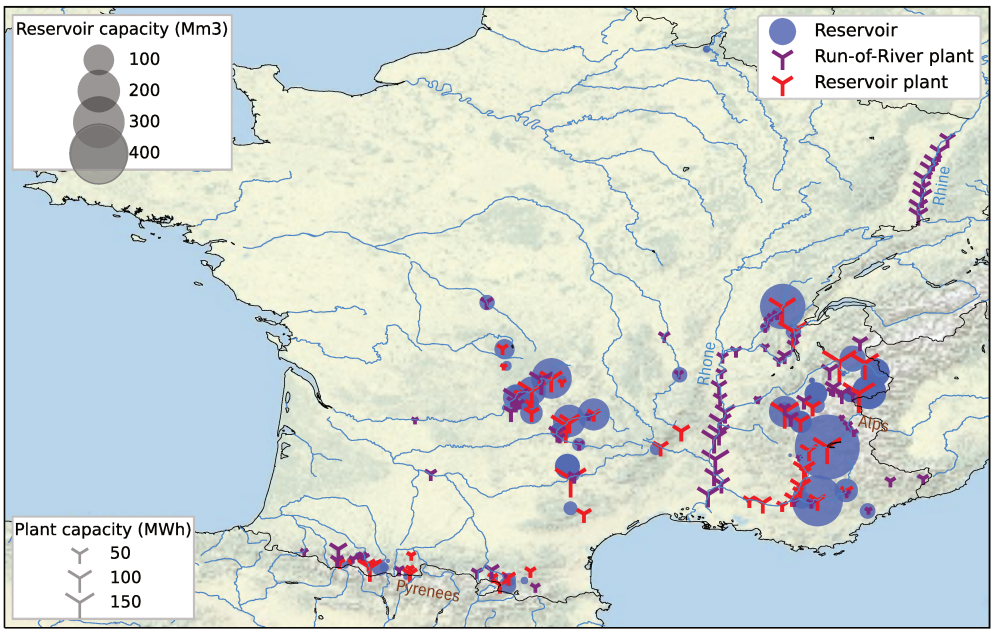

Figure 6.2: Location of the French hydropower plants modeled in ORCHIDEE and their associated supplying reservoirs.

6.2.1.2 Power system optimization model: EOLES-Dispatch

EOLES-Dispatch is a linear optimization model (Leblanc, 2023) that focuses on the optimization of the French electric dispatch. The model minimizes the total dispatch cost of the electric system while covering electricity demand at an hourly time-step, assuming perfect foresight of future demand, capacity factors, costs, and technology availability. Each generation or storage technology is represented by one representative plant k whose hourly production $\mathbf{G}_{k,t}$ is subject to various constraints.

The production from variable renewable technologies (solar PV, onshore and offshore wind, and run-of-river) is free but strictly limited by exogenous capacity factor inputs. In contrast, the production from thermal plants (coal, gas, and nuclear) is costly and must adhere to start-up and ramping constraints. Storage technologies (reservoir plants, batteries, and PHS) must comply with constraints relative to their storage and discharge characteristics.

In the model version used here, additional constraints apply to the representative reservoir hydropower plant res. These constraints are detailed below, with model decision variables indicated in bold.

- The energy stored in the representative reservoir, $\mathbf{S}_{res,t}$, is limited by lower and upper limits.

- At the end of the period, the energy stock should return to its initial value.

- $\mathbf{S}_{res,t}$ evolves with the net inflow to the reservoir $\mathcal{I}_t$, the minimum release requirement $\mathcal{R}_t$, and the additional release decided by the model to generate electricity $\mathbf{Re}_t$:

$$\mathbf{S}_{res,t+1} = \mathbf{S}_{res,t} + \mathcal{I}_t - \mathcal{R}_t - \mathbf{Re}_t \tag{6.1}$$

- The production by the reservoir plant $\mathbf{G}_{res,t}$ should not exceed the sum of the potential production from spillage $\mathcal{Y}_t$, from the minimum release $\mathcal{R}'_t$, and from the additional release $\mathbf{Re}_t$:

$$\mathbf{G}_{res,t} \leq \mathcal{Y}_t + \mathcal{R}'_t + \mathbf{Re}_t \tag{6.2}$$

- The production by the reservoir plant is limited by its maximum capacity $\mathcal{P}max_t$, which evolves with the water level of the reservoir.

$\mathcal{I}_t$, $\mathcal{R}_t$, $\mathcal{R}'_t$, $\mathcal{Y}_t$, and $\mathcal{P}max_t$ are exogenous hourly time series computed based on the individual reservoir operations simulated by ORCHIDEE. The hourly capacity factor of run-of-river plants is also computed from the ORCHIDEE's simulation and prescribed as an exogenous input to EOLES-Dispatch.

Other exogenous inputs to the EOLES-Dispatch model include the generation portfolio, hourly power demand, hourly capacity factors of solar and wind power plants, variable generation costs, start-up costs, ramping costs, minimum off-times, and minimum and maximum load levels of thermal power plants. The simulations are run for two scenarios: the 2019 power mix and a prospective 2050 power scenario further described in section 6.2.3.

As generally done in power system model studies, the Lagrange multiplier of the adequacy constraint - reflecting the balance between power demand and supply in period t - is interpreted as a proxy for the wholesale electricity price at time t. In this chapter, the model does not include the cross-border exchanges between France and its neighboring countries due to the high computational requirements of multi-year simulations.

6.2.1.3 Simulations

Two types of simulations are performed in this study:

- **"Stand-alone ORCHIDEE simulation"**: ORCHIDEE is run with a target production set to infinite at each timestep, leading all hydroelectric reservoirs to release water within the limit of the installed capacity of the plant. This allows us to compute the annual hydropower potential of each plant, defined as the maximum energy the plant could produce over one year. This simulation is run for each scenario over the entire period 1975-2099, in order to quantify the effect of climate change independently of the power system.

- **"Coupled simulations"**: In this case, the target production prescribed to ORCHIDEE is derived from the optimal dispatch obtained in EOLES-Dispatch ($\mathbf{G}_{res,t}$). Several iterations are performed until reaching a convergence between the two models (as detailed in Chapter 5). Such simulations allow accounting for power system needs, in order to accurately predict the timing of hydroelectric releases. For each climate and power scenario, coupled simulations are run over three different 20-year windows: 2010-2029, 2040-2059, and 2070-2089, representing climate conditions for approximately 2020, 2050 and 2080.

6.2.2 Climate scenarios

In this study, we use climate projections based on the RCP8.5, in order to highlight the most pronounced trends.

The atmospheric datasets used to drive ORCHIDEE are acquired from the Explore2 project, which aims to update knowledge on the impact of climate change on French rivers. For this project, 17 pairs of global climate models (GCM) and regional climate models (RCM) were selected from the EURO-CORDEX set (Marson et al., 2024). The initial daily projections were bias-corrected and desegregated to hourly time steps using the ADAMONT method (Verfaillie et al., 2017), which involves quantile mapping by weather type. A hierarchical classification of these 17 pairs for RCP 8.5 identified three clusters (Corre et al., 2023), which served as a basis for defining three storylines illustrating the most contrasting possible futures. In this study, we select four model pairs to explore these different storylines:

- CNRM-CM5-LR_ALADIN63, representative for the storyline *Weak changes*, further noted CNRM
- MPI-ESM-LR_REMO2009, representative for the storyline *Weak changes*, further noted MPI
- HadGEM2_CCLM4, representative for the storyline *Seasonally contrasted (wetter in winter and drier in summer)*, further noted HadGEM2
- EC-EARTH_RCA4, representative for the storyline *Drier*, further noted EC-EARTH

Two models were selected for the storyline *Weak changes* in order to assess the uncertainties within that storyline.

Fig. 6.3 illustrates the projected changes in precipitation for the period 2070-2099 compared to the historical period 1975-2004, across the four model pairs under consideration. The annual changes vary among the different simulations. HadGEM2 and EC-EARTH anticipate a significant decrease in annual precipitation over all mountainous regions where hydroelectric reservoirs are situated (Fig. 6.2), while CNRM and MPI simulate an increase or non-significant changes over the Northern Alps.

All four model pairs concur on stronger seasonal effects compared to annual changes, with a significant increase in precipitation over most areas during winter and a significant decrease during summer, especially in the South. However, they differ in terms of spatial distribution and magnitude. HadGEM2 and MPI anticipate highly contrasted seasonal patterns, with reductions exceeding 50% in the South during summer. In contrast, CNRM shows lower seasonal changes (less than 40% for all areas). Finally, EC-EARTH predicts a drier climate with no winter increase exceeding 35% and a significant decrease in precipitation over the southern Alps and Pyrenees in winter.

An important consensus among all models is the significant decrease in snowfall, with reductions exceeding 50% in all projections (see Table 6.1). In mountainous areas, there is a notable shift from snowfall to rainfall during winter months.

6.2.3 Power system scenarios

Our assumptions for the 2050 power scenario are based on RTE (2021), a detailed prospective analysis conducted by the French Transmission System Operator (TSO). The study outlines different national power mix trajectories to achieve carbon neutrality in 2050. We select the scenario labeled *N1*, as it appears the most credible given

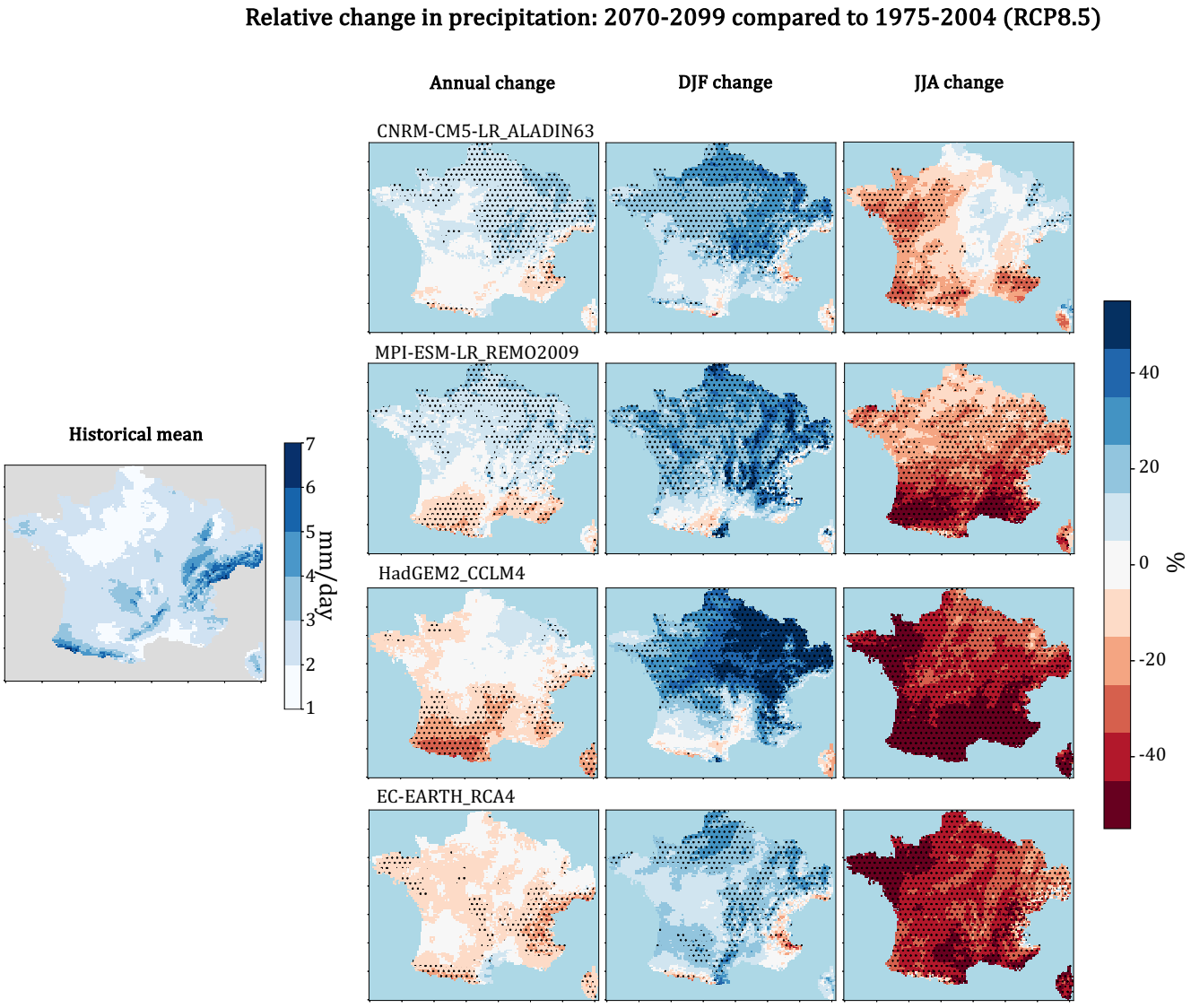

Figure 6.3: Relative change in precipitation: 2070-2099 compared to 1975-2004 (RCP8.5). Black dots indicate areas where changes are statistically significant, which is assessed through a Student test (p-value of 0.05).

current national policies. This scenario is based on the substantial integration of renewable energy sources and the replacement of a portion of existing nuclear power plants that are nearing the end of their operational lifespan. By 2050, the nuclear capacity is reduced by more than half compared to 2019 (see Table 6.2). Gas plants are fully decarbonized through the use of hydrogen or synthetic methane as fuel, which substantially increases their generation costs compared to the 2019 power mix (see Appendix B.2 for the assumed costs).

The RTE scenario indicates a 30% increase in annual power demand, which we assume is split into a 15% increase that follows the historical demand profile, and a 15% increase that is fully flexible. The latter represents water electrolysis and flexible consumption, with an assumed hourly maximum capacity of 30GW.

This study does not aim to provide a full assessment of the future power system, as it does not include important factors such as interconnections with neighboring countries

		CNRM	MPI	HadGEM	EC_EARTH
Historical period 1975-2004	Mean annual rainfall (mm)	850	860	838	845
	Mean annual snowfall (mm)	89	91	86	88
Future period 2070-2099	Mean annual rainfall (mm)	922	899	855	859
	Mean annual snowfall (mm)	60	68	56	52

Table 6.1: Annual rainfall and snowfall means

		2019 power mix	2050 scenario
Variable renewable energy	Solar PV	9.2	120
	Onshore wind	16.5	60
	Offshore wind	0	48
	Run-of-river	10.6	10.6
Thermal plants	Nuclear	63.13	29
	Gas CCGT	9	12
	Gas OCGT	3	3
	Coal	3	0
Storage	PHS	5	8
	Batteries	0	9
	Reservoir	8.8	8.8

Table 6.2: Installed capacities (GW) of each technology in the two power scenarios under consideration.

or the impact of climate change on the power demand pattern. The objective is to investigate the impacts of climate change on hydropower production and how they interact with changes in the power mix.

For each 20-year coupled simulation, hourly capacity factors of solar and wind plants are derived from observed production data covering the 2000-2019 period. A 20-year hourly power demand time series is built using the observed power demand over the 2015-2021 period (annual time series are repeated in order to obtain a 20-year time series). Finally, we define a weekly profile of the availability of nuclear plants over one year based on the average weekly production of nuclear power plants from 2015 to 2019. Our analysis does not consider the temporal correlation between renewable energy availability profiles, hydrological inputs, and demand, nor the impact of climate change on other technologies than hydropower. However, it is adequate for examining the impact of climate or mix changes on reservoir plant output.

6.3 Results

6.3.1 Stand-alone ORCHIDEE simulations

6.3.1.1 Uncertain changes in annual hydropower potentials

The projected changes in mean river discharge simulated by ORCHIDEE in "stand-alone" mode under the four climate scenarios are presented in Fig. 6.4. They are the results of the changes in precipitation (Fig. 6.3) and evapotranspiration (ET) (Fig. C.2). Accordingly, the projected changes in river discharge also vary between the scenarios. A decrease is projected over the Pyrenees in all scenarios, while the changes over the

Northern Alps and the Rhone are more uncertain.

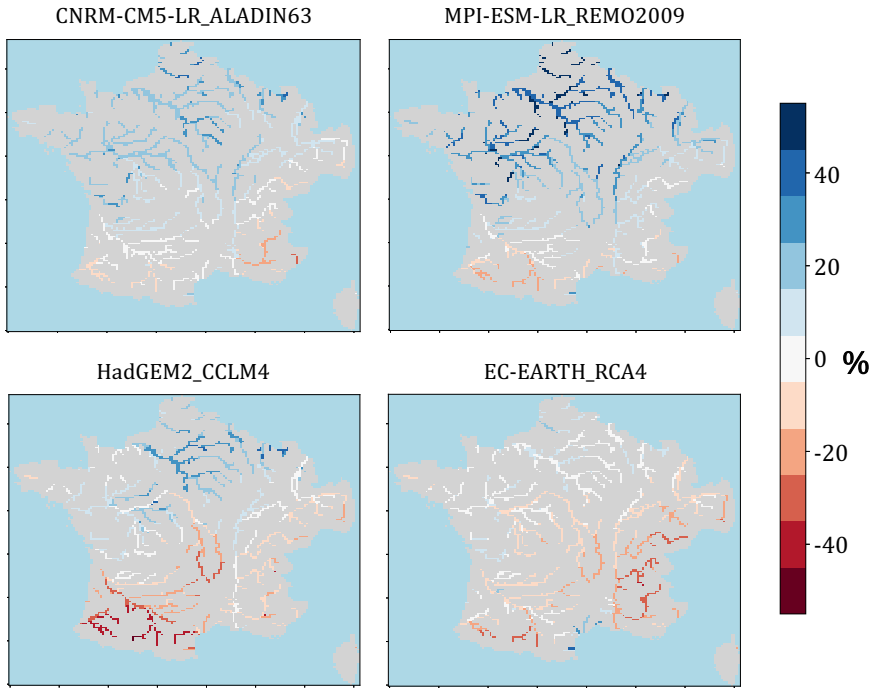

Figure 6.4: Relative change in mean river discharge: 2070-2099 compared to 1975-2004 (RCP8.5). The discharges are shown for all grid points with an upstream area greater than 1000 km^2.

These differences in simulated river discharges lead to varying results regarding hydropower generation potentials (Fig. 6.5). On the one hand, the HadGEM2 and EC-EARTH scenarios project a significant decrease in the annual national hydropower potential throughout the 21st century, with a more pronounced decline for reservoir plants (respectively -18.4% and -20.8% in each scenario) than for run-of-river plants (respectively -15.6% and -14.6%). On the other hand, the MPI and CNRM scenarios project non-significant changes for both technologies.

Besides, the annual hydropower potentials show substantial interannual variability in the four climate scenarios. The coefficient of variation[1] in the reference period ranges from 16.2% to 18.7% for reservoir plants and 12.3% to 14.7% for run-of-river plants. We find that this interannual variability increases with climate change in the MPI, HadGEM2, and EC-EARTH scenarios, but without statistical significance (Fig. 6.5).

Regarding the changes at the level of individual plants (Fig. 6.6), they evolve with climate change according to the regional patterns of change in annual river flows shown in Fig. 6.4. In most areas, the outcome varies depending on the climate scenario. In the Pyrenees, however, all scenarios project a significant decline in the production of all hydropower plants.

6.3.1.2 Energy losses through reservoir evaporation increase but remain negligible

In order to accurately quantify the annual hydropower potentials, direct precipitation and evaporation on the reservoir should also be considered, as these factors modify the volume of water available for hydropower production. In particular, reservoir evaporation

[1]Ratio of standard deviation to the mean

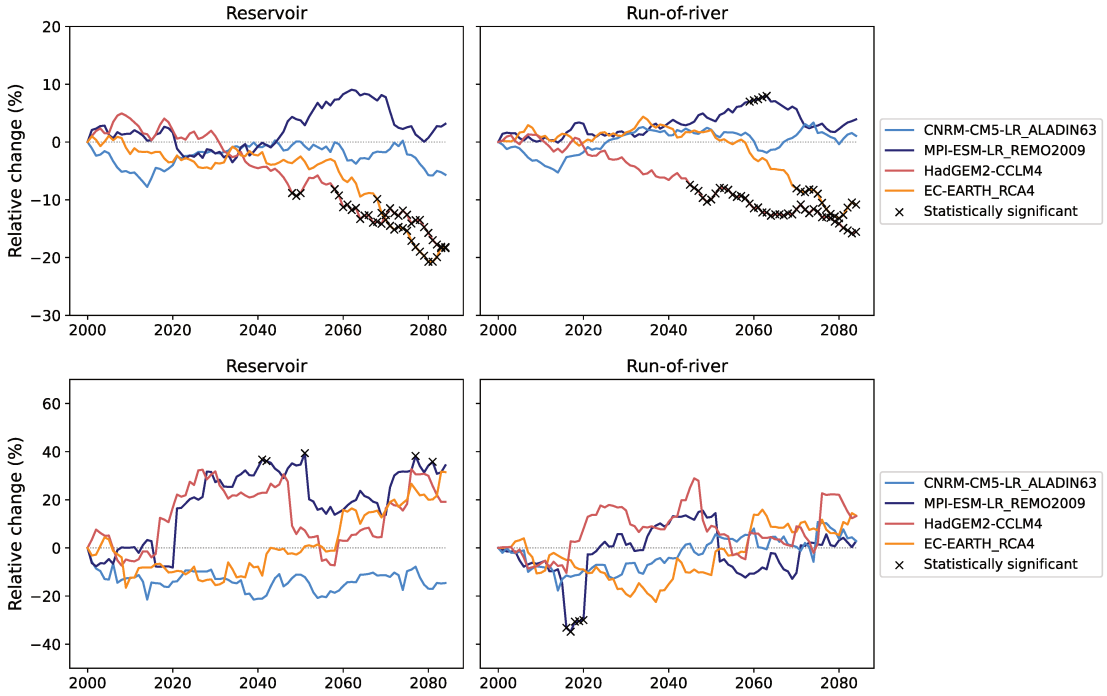

Figure 6.5: Top: Relative changes in the 30-year average of annual hydropower potentials. The statistical significance is assessed through a Student test (p-value of 0.05). Bottom: Relative change in the standard deviation of annual hydropower potentials over 30-year sliding periods. The statistical significance is assessed through a Fisher test (p-value of 0.05).

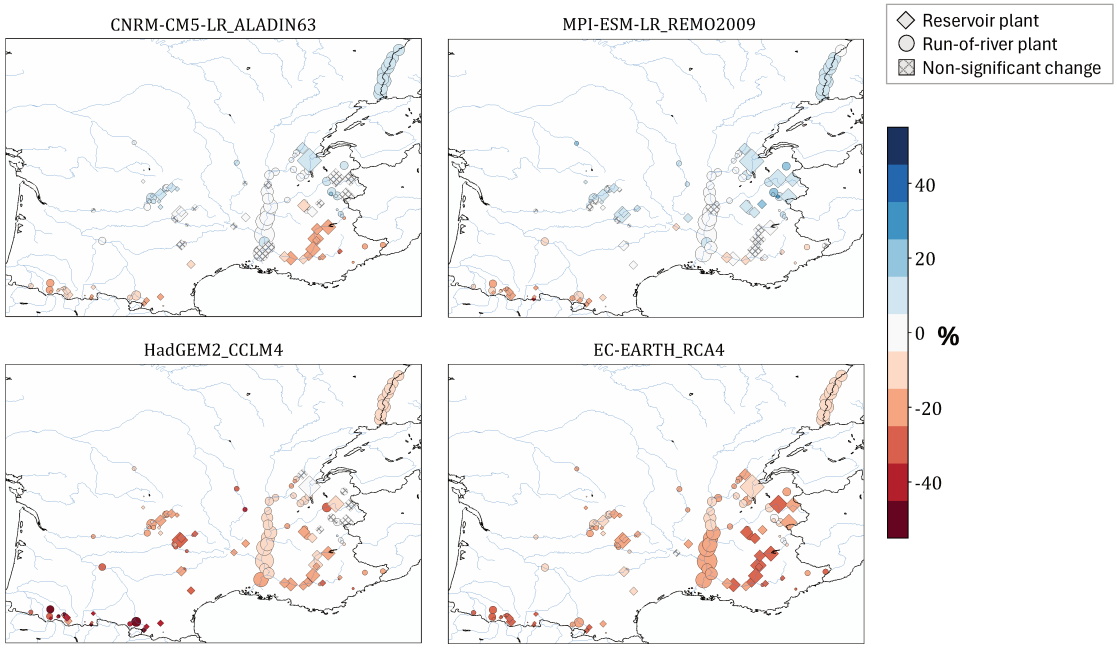

Figure 6.6: Relative changes in annual hydropower potential: 2070-2099 compared to 1975-2004 (RCP8.5). The statistical significance is assessed through a Student test (p-value of 0.05).

is found to increase significantly as a consequence of the significant increase in PET which is projected in all scenarios (see Fig. C.1).

Figure 6.7 illustrates the evolution of these net direct inputs (direct precipitation

minus evaporation) over the 21st century. Despite a significant decline in all scenarios, this factor remains insignificant in comparison to the annual production potential (30 GWh of annual energy losses versus an annual production of 15 TWh on average).

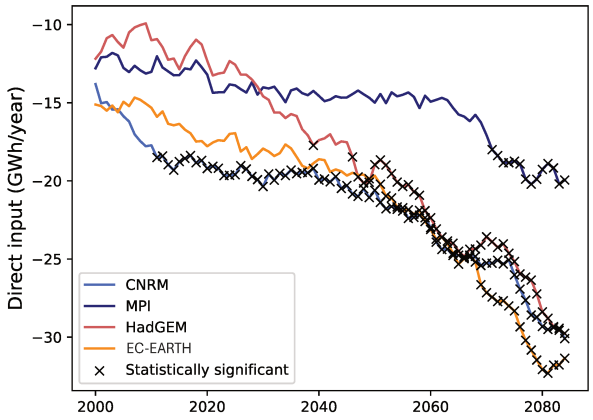

Figure 6.7: 30-year sliding average of annual direct input to the reservoir (GWh/year) at the national scale. This factor is defined by the difference between direct precipitation and direct evaporation on the reservoir.

6.3.1.3 Robust seasonal changes in reservoir inflows and run-of-river production

While large uncertainties are found in the evolution of mean annual river discharge, a higher consensus emerges among climate scenarios regarding the seasonal changes in river discharges, especially over the Alps in winter and summer (see Fig. C.3). In this area, all scenarios project a significant increase in river discharge by more than 50% in winter and a strong decrease by more than 50% in summer, as a result of the shift from snowfall to rainfall in winter.

Figure 6.8 presents the results of a Mann-Kendall test[2] applied to analyze potential trends in monthly reservoir inflow and run-of-river production under the four climate scenarios, at the national scale. All scenarios project an increase in inflows during the winter (January to March) and a decrease between May and August, consistently with the seasonal variations of river flows in the regions where reservoirs are located. Similarly, run-of-river production significantly increases with climate change in winter (January to April) and decreases in the spring and summer. The Mann-Kendall test reveals nevertheless that these changes are not consistently significant, due to the substantial interannual variability in river discharges.

6.3.2 Coupled simulations - Impacts of climate change on reservoir operations in the 2019 power scenario

To accurately assess the impact of the seasonal changes in inflow on final production by reservoir plants, we now consider the series of 20-year "coupled simulations", in which

[2]The Mann-Kendall test is a non-parametric statistical test used to identify significant trends in time series data. It evaluates whether there is a consistent increase or decrease in the sequence of data points, which indicates a monotonic trend.

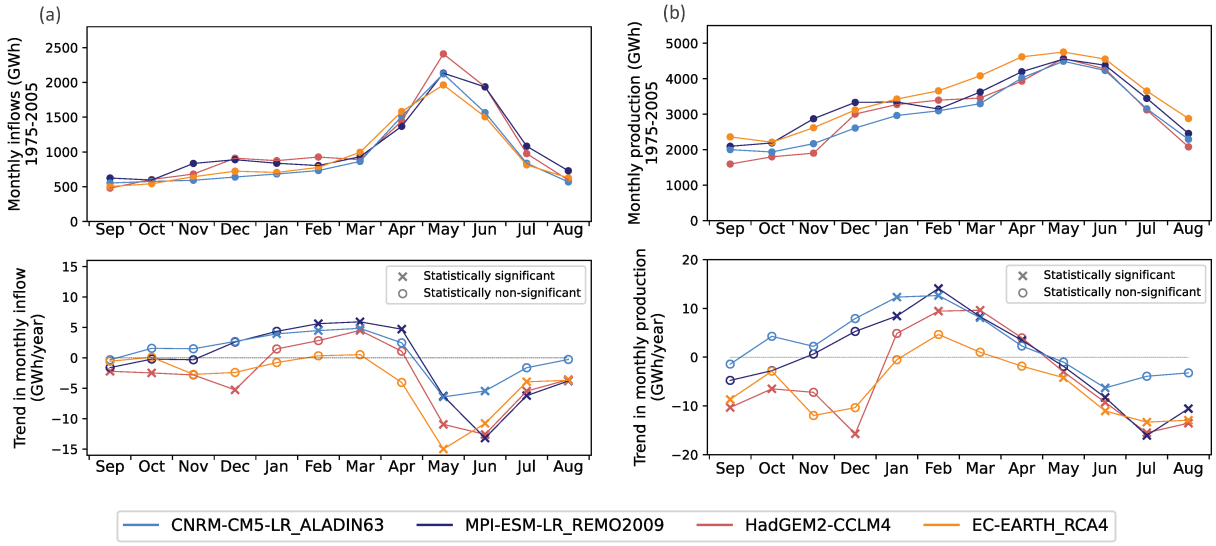

Figure 6.8: Top: Interannual average of total monthly inflow to the reservoirs (a) and total production by the run-of-river plants (b) in the 2010-2029 period. Bottom: Trend in monthly inflow (a) and run-of-river production (b) obtained using a Mann-Kendall test (p-value of 0.05).

several iterations of the coupled framework presented in Fig. 6.1 are run to obtain hourly production time series. In this section, we focus on the simulations carried out with the 2019 power scenario to explore the effect of climate change within this scenario.

Figure 6.9,a) shows the monthly production by reservoir plants simulated for each climate scenario in the 2010-2029 period. As previously, we perform a Mann-Kendall test to evaluate the presence and significance of a trend due to climate change. In the two climate scenarios projecting non-significant changes in annual potentials (CNRM and MPI), we find small seasonal changes in production, with an increase in winter (November to April) and a decrease in spring and summer (May to September). In the two other climate scenarios (HadGEM and EC-EARTH), the production declines throughout the year, although the relative changes in spring and summer are far greater than in winter. The majority of these changes are however non-significant, due to the large interannual variability. Only the reduction of production in summer is significant in most scenarios.

Similarly, Fig. 6.9,b) presents the average monthly hydraulic stock simulated for the 2010-2029 period. We find a high degree of concordance in the annual stock variation pattern across the four scenarios. Moreover, there is robust consensus regarding the impact of climate change on the reservoir stock level. In all scenarios, reservoirs are projected to fill earlier due to increased inflows during the winter months. Consequently, the average minimum stock level is expected to increase with climate change, by approximately 600GWh between 2020 and 2080. This would increase the resulting $Pmax_t$, allowing for more flexibility from the reservoir power plants during the spring.

6.3.3 Coupled simulations - Economic consequences of the hydrological changes in the 2019 power scenario

6.3.3.1 Change in electricity prices

The electricity price simulated by EOLES-Dispatch for the reference 2010-2029 period exhibits a seasonal pattern (Fig. 6.10). From April to October, the price remains relatively constant, primarily determined by the generation costs of nuclear power plants. It

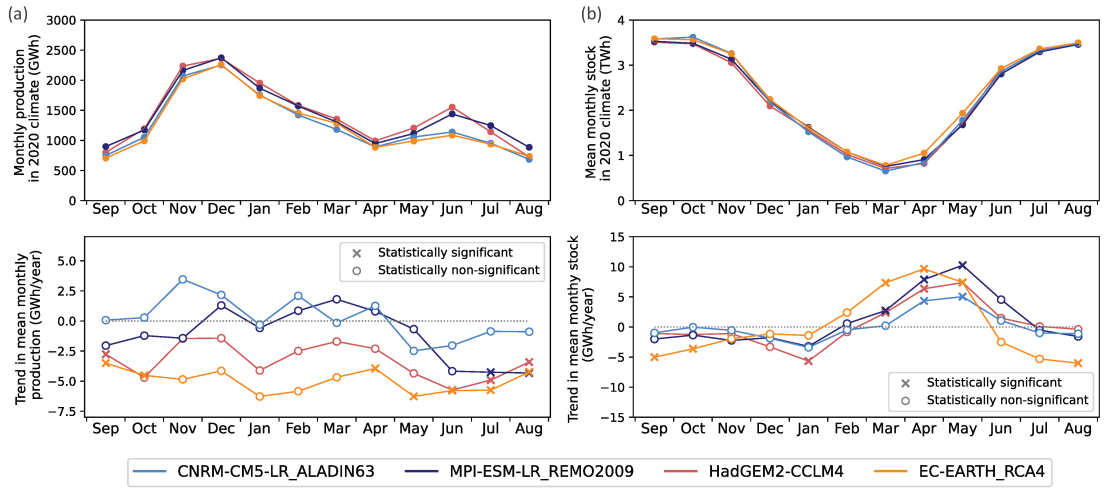

Figure 6.9: a) Top: Interannual average of monthly production by the representative reservoir plant under 2020 climate (2010-2029 climate years) in the 2019 power scenario. Bottom: Trend in monthly production obtained using a Mann-Kendall test (p-value of 0.05). b) Top: Interannual average of monthly total stock in the reservoirs under 2020 climate (2010-2029 climate years) in the 2019 power scenario. Bottom: Trend in monthly total stock obtained using a Mann-Kendall test (p-value of 0.05).

then rises during winter, as the more expensive gas and coal-fired power plants are called upon to meet the higher net load, which increases due to heating needs. See Appendix C.2 for more details on the price simulation.

In the climate scenarios that project higher generation from reservoir plants in winter (CNRM and MPI), we find a decrease in the electricity price in winter (Fig. 6.10). This price drop occurs because the additional hydropower generation can replace the generation by thermal plants, allowing therefore a cheaper technology, such as nuclear, to set the price instead. In contrast, in the climate scenarios that project a decline in winter generation by reservoir plants (HadGEM2 and EC-EARTH), we find an increase in electricity prices in winter. Across all scenarios, the changes in spring and summer prices are minimal, as the change in hydropower generation is not sufficient to fully replace the electricity generation from nuclear plants that set the price during these seasons. Nevertheless, the changes in electricity prices induced by climate change in winter are found to be non-significant due to the non-significance of changes in monthly production in winter.

6.3.3.2 Change in annual revenues of individual plants with climate change

Finally, we assess the impact of climate change on the annual revenues of individual plants between the periods 2010-2029 and 2070-2089. The change in revenues is composed of two effects: the change in annual production, and the change in the average price of electricity at the times when the power plant is producing (thereafter referred to as the average selling price). Understanding these two effects is crucial, as they determine not only how much electricity is generated but also how valuable that electricity is in the market. Their quantification is shown in Fig. 6.11 for the different climate scenarios.

On the one hand, the annual production of each plant evolves with climate change according to the change in hydropower potential presented in Fig. 6.6. On the other hand, the change in the average selling price depends on the climate scenario. In the

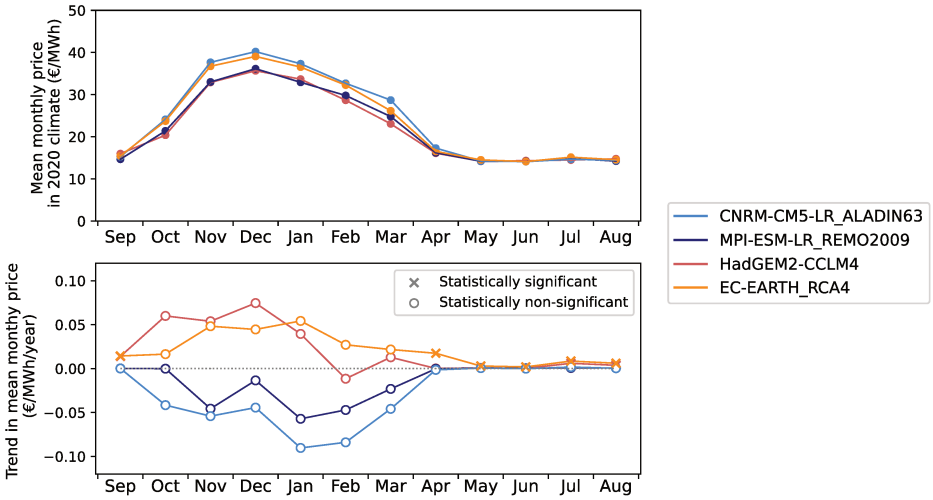

Figure 6.10: Top: Interannual average of monthly mean power price simulated by EOLES-Dispatch for the 2010-2029 period in the 2019 power scenario. Bottom: Trend in mean monthly power price obtained using a Mann-Kendall test (p-value of 0.05).

scenarios that simulate non-significant changes in annual production (CNRM and MPI), it decreases for all hydropower plants, in line with the general trends in power prices presented in Fig. 6.10. The decrease is more pronounced for reservoir plants than for run-of-river plants, as their production is dispatchable and concentrated in winter, when the decrease in electricity prices occurs. Conversely, in the two other scenarios, the average selling price increases with climate change, in line with the general increase in electricity prices. This increase is greater for reservoir plants than for run-of-river plants.

The result of these two effects varies depending on the climate scenario, the geographical location, and the type of power plant. A general decline in revenues is projected for most plants, with the most pronounced decline observed for the power plants in the Pyrenees (more than 20% in all scenarios) and in the Southern Alps. The only exception is the run-of-river plants along the Rhine, which do not experience a decrease in revenues in any of the climate scenarios.

6.3.4 Coupled simulations - Joint impacts of renewable energy integration and climate change

In this section, we analyze how climate change interacts with the change in the power system. Due to computational requirements, we limit our analysis to two climate scenarios, CNRM, which projects no significant change in annual production, and EC-EARTH which projects a significant decline in hydropower production.

6.3.4.1 Changes in annual production due to the integration of renewable energies

For a given climate scenario, the annual potentials of hydropower generation are identical across different power scenarios, as the hydrological conditions are identical and the stock in reservoirs is constrained to return to its initial value at the end of each 20-year simulation. However, the actual production may vary due to two factors. Some non-dispatchable hydropower production (from run-of-river plants or minimum release from reservoir plants) may be curtailed when the potential of renewable energies exceeds

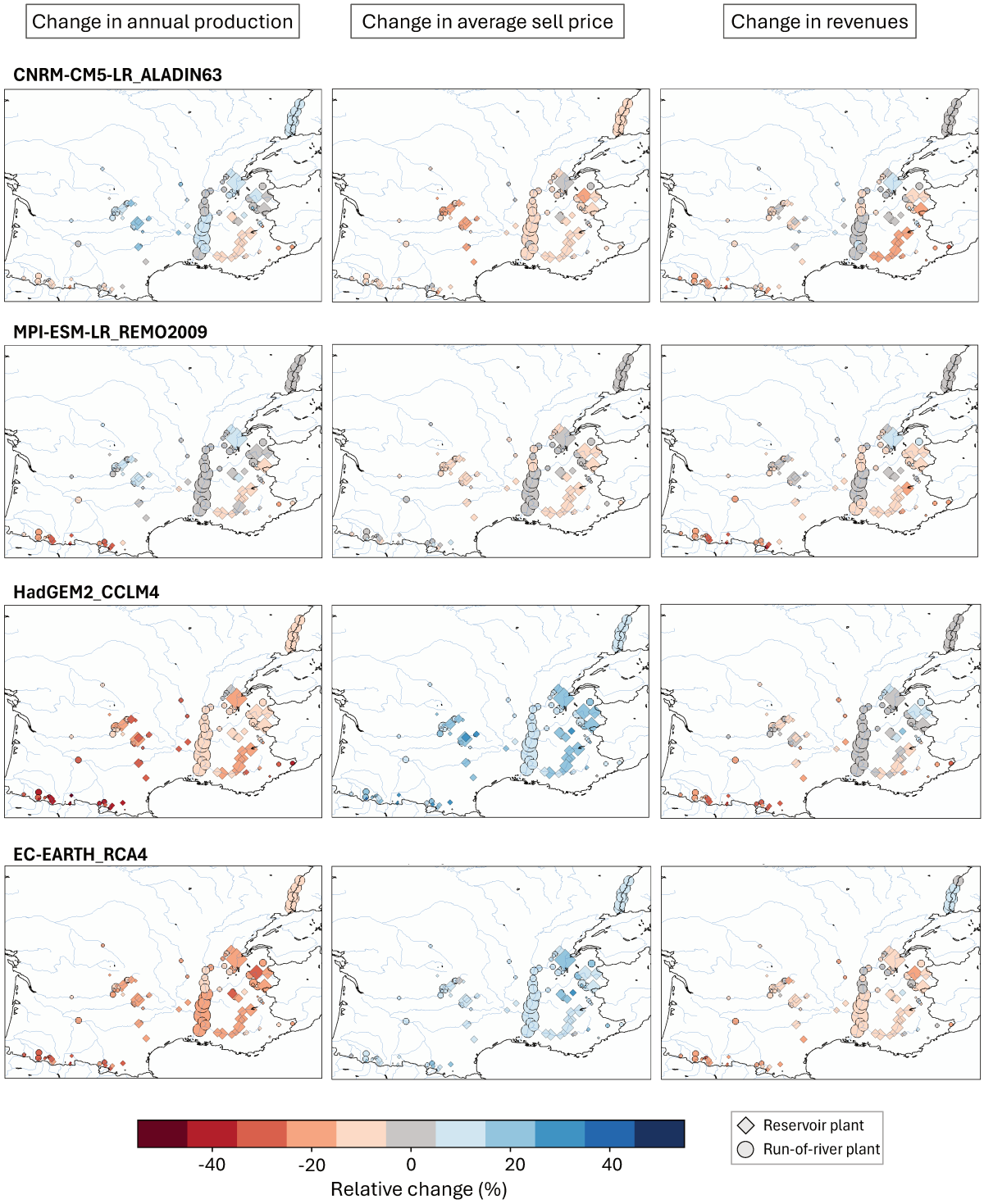

Figure 6.11: Relative changes between the 2010-2029 and 2070-2089 period in annual production (left column), average selling price (middle column), and revenues (right column) in the 2019 power scenario.

electricity demand. Additionally, differences in the mean water level of the reservoirs can affect the actual production due to its dependence on the head and consequently on the reservoir water level.

Therefore, we obtain small differences in the annual production simulated in the two power scenarios under the same climate scenario (Table 6.3), with slightly lower hydropower production in the 2050 scenario compared to the 2019 scenario, both for run-of-river and reservoir plants. This is due to higher renewable production in the 2050 power scenario, leading to some curtailment of non-dispatchable production.

Climatic Period	Plant type	CNRM-CM5-LR_ALADIN63	EC-EARTH_RCA4
2010-2029	Run-of-river	-1.85 (-11%)	-1.75 (-12%)
	Reservoir	-0.85 (-5.3%)	-0.62 (-4.3%)
2040-2059	Run-of-river	-1.78 (-10%)	-1.64 (-11%)
	Reservoir	-0.60 (-3.5%)	-0.50 (-3%)
2070-2089	Run-of-river	-1.68 (-10%)	-1.42 (-12%)
	Reservoir	-0.71 (-4.4%)	-0.49 (-4.1%)

Table 6.3: Differences in mean annual hydropower production (TWh) in the 2050 power scenario compared to the 2019 power scenario

Nevertheless, the curtailment of hydropower production may not be very meaningful, as the model does not prioritize which type of plant - whether wind, solar or hydropower - is curtailed.

6.3.4.2 Seasonal changes

The change in the power system leads to changes in the net load pattern, which affects the timing of production by reservoir plants in a given climatic period. Figure 6.12 provides a detailed comparison of the hourly power dispatch simulated in both power scenarios within the EC-EARTH climate scenario for three illustrative weeks in February, July, and November. Significant differences appear across the power scenarios. In the 2019 power mix, the reservoir plant operates at maximum capacity on all working days in the weeks of November and February, while its output is minimal in the entire week of July. In contrast, in the 2050 power scenario, reservoir production mainly takes place at night, regardless of the time of year, and only when the net load is high. For example, there is almost no production by the reservoir plant on the Tuesday of the illustrated week in February and on the Thursday of the week in November, while the reservoir plant operates at maximum capacity on the night from Friday to Saturday in the week in July.

Figure 6.13 illustrates the effect of the change in power scenario on the seasonality of reservoir plant production. Transitioning from the 2019 power mix to the 2050 scenario substantially reduces the production peak in November, while slightly increasing the peak in January, Regardless of the climatic period and climate scenario (Fig. 6.13). This change is driven by the change in the net load pattern (see Appendix. C.3 for more details). In contrast, spring production remains unchanged, as it is primarily driven by non-dispatchable production from reservoir spillage. Furthermore, the production variability increases, reflecting the heightened variability in net load shown in Fig. C.5.

For a given climate scenario, we find a similar effect of climate change across power scenarios. In the CNRM scenario, the production increases in the winter and decreases in the summer. In the EC-EARTH scenario, it decreases throughout the year, with the strongest relative decrease in summer.

The changes in the seasonality of reservoir plant production have a visible impact on reservoir operations. With the change in the power system, reservoir withdrawals decrease during winter, and reservoirs are filled up more slowly in spring. These effects

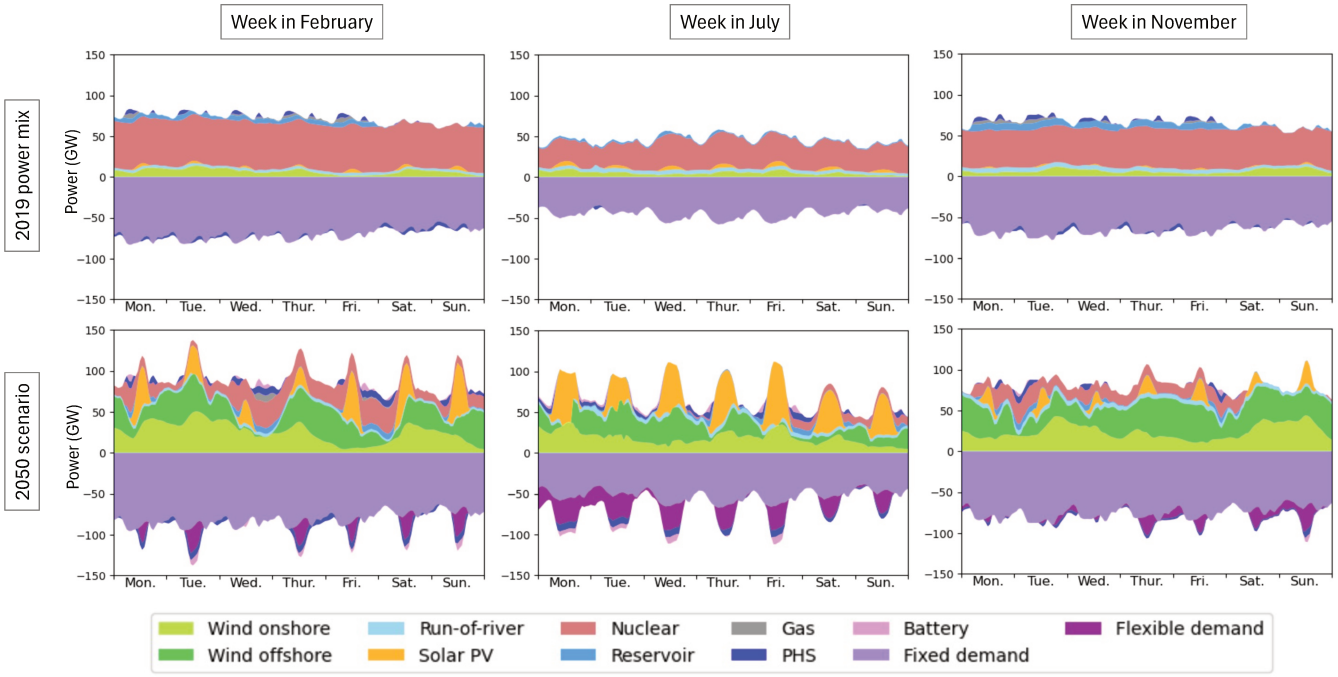

Figure 6.12: Comparison of the hourly power system dispatch simulated by EOLES-Dispatch in the EC-EARTH scenario for three illustrative weeks of the 2010-2029 climatic period. The illustrative weeks respectively correspond to the following dates: February 9th to 15th, July 13th to 19th, and November 23rd to 29th, 2015, for power demand, and February 8th to 14th, July 12th to 18th, and November 22nd to 28th, 2010, for climate variables.

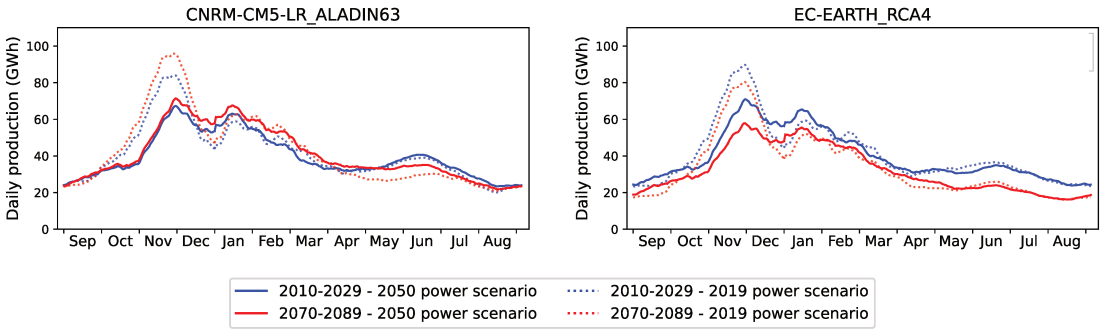

Figure 6.13: Interannual average of 30-day sliding average of the daily production by the reservoir plant, simulated in CNRM and EC-EARTH climate scenarios, for the two power scenarios, in the climate periods 2010-2029 and 2070-2089.

are similar to the impacts of climate change presented in Fig. 6.9,b). Both changes in climate and the power system contribute to reducing the amplitude of stock variation, with reservoirs being filled more in winter and less in summer (Fig. 6.14).

6.3.4.3 Economic consequences

The assumption about the evolution of gas-fired plant generation costs (see Appendix B.2) has a critical impact on the power prices simulated in the 2050 power scenario. The average price increases substantially in winter compared to those obtained in the 2019 power mix (Fig. 6.15). The changes in power prices due to the power system are therefore much higher than those resulting from the hydrological changes.

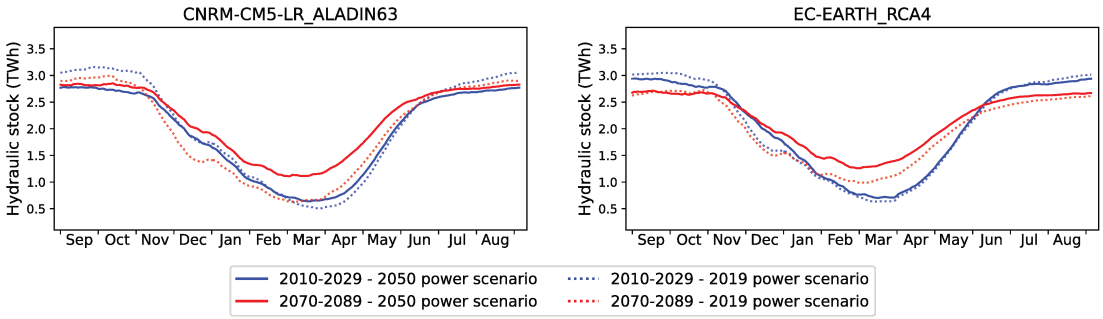

Figure 6.14: Interannual average of daily stock in reservoirs simulated in the CNRM and EC-EARTH climate scenarios, for the two power scenarios, in the climate periods 2010-2029 and 2070-2089.

To isolate the contribution of this strong assumption on the resulting prices, we consider an additional power scenario, referred to as *"2050 unchanged cost"*, which mirrors the 2050 power scenario but retains the 2019 generation costs of thermal plants. Figure 6.15 shows that the average prices simulated in this scenario are lower than those obtained in the 2019 scenario, except during the winter months. Besides, price variability is significantly increased in both 2050 scenarios compared to the 2019 power mix (not shown in the figures).

Furthermore, we find a consistent effect of climate change across all power scenarios, with an increase (respectively decrease) in the winter price in the scenarios forecasting a decrease (respectively increase) in hydroelectric production in winter and no change in spring and summer.

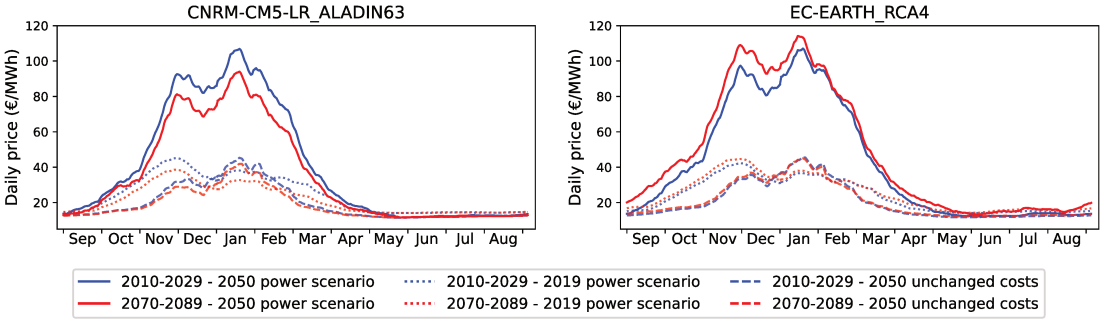

Figure 6.15: Interannual average of 30-day sliding average of daily power price simulated with the CNRM and EC-EARTH climate scenarios, in the two power scenarios, for the climate periods 2010-2029 and 2070-2089.

The significant increase in winter power prices in the 2050 power scenario leads to a significant rise in the average selling price of hydropower plants, particularly for reservoir plants which generate most of their production during winter. This effect is illustrated in Fig. 6.16,a) for the case of the EC-EARTH climate scenario and the 2010-2029 period.

The "2050 unchanged costs" scenario allows us to isolate the contribution of the changes in the power mix from the assumption about the increased generation cost of gas-fired plants (Fig. 6.16,b)). In this scenario, we find a decrease in the average selling price for run-of-river plants and an increase for reservoir plants. This highlights the differentiated value of hydropower plants in future power mixes, depending on the dispatchability of their production. This higher value of reservoir plants stems from the higher variability of power prices.

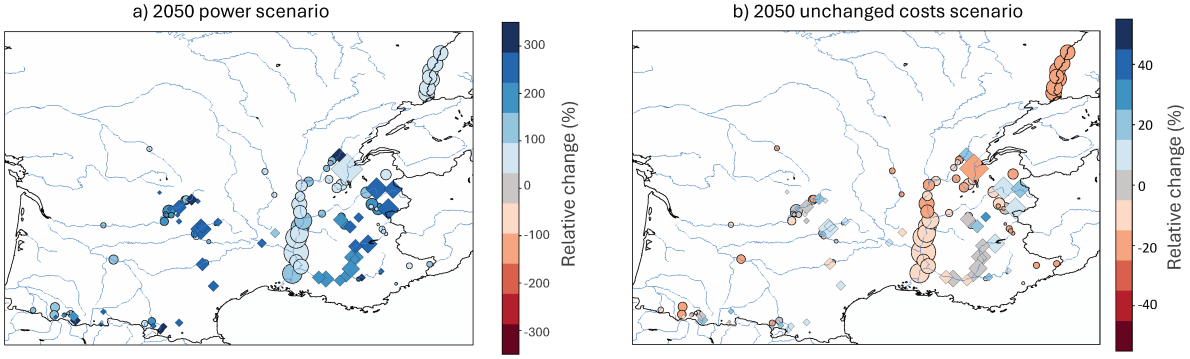

Figure 6.16: Relative change in the average selling price of hydropower plants in EC-EARTH_RCA4 climate scenario for the period 2010-2029 when transitioning from the 2019 scenario to the 2050 scenario (a) and 2050 unchanged costs scenario (b).

6.3.5 Coupled simulations - Impact on the overall power system

In both power scenarios, the impact of the modified hydropower production due to climate change on the overall power system cost is non-significant. In the 2019 scenario, the total cost variation between the 2010-2029 and 2070-2089 periods ranges from -3% and +2% depending on the climate scenario. In the 2050 scenario, the variation extends from -5% to +5%. This low impact, even in scenarios projecting a decrease in hydropower production, is due to the seasonal asymmetry of variation, with most of the decline occurring during summer, a period that is not critical for the system's reliability. Figure 6.17 presents the evolution of production by each technology across the different power and climate scenarios. It shows that the reduction in hydropower is primarily offset by an increase in nuclear power production and increased use of storage options, while the power supply by gas power plants is less affected and even (non-significantly) decreases in some cases. Non-significant changes in renewables curtailment and unsatisfied demand are found.

6.4 Discussion

This section outlines the main limitations of the methodology employed throughout this study and discusses the sources of the uncertainties in the different scenarios.

6.4.1 Limitations of the study

This study does not address the impact of climate change on the seasonality of power demand. Previous research indicates that global warming will decrease heating demand during the winter and increase cooling demand during summer in France (Larsen et al., 2020). Nevertheless, by assuming that half of the additional demand in 2050 will be flexible, we indirectly account for some changes in the power demand seasonality. Indeed, this flexible increase in power demand is simulated to occur primarily during the daytime in summer, to align with periods of high solar PV production, which also coincide with peak cooling demand.

Furthermore, this study does not consider the effects of global warming on the production of other technologies. In particular, higher water temperatures and reduced

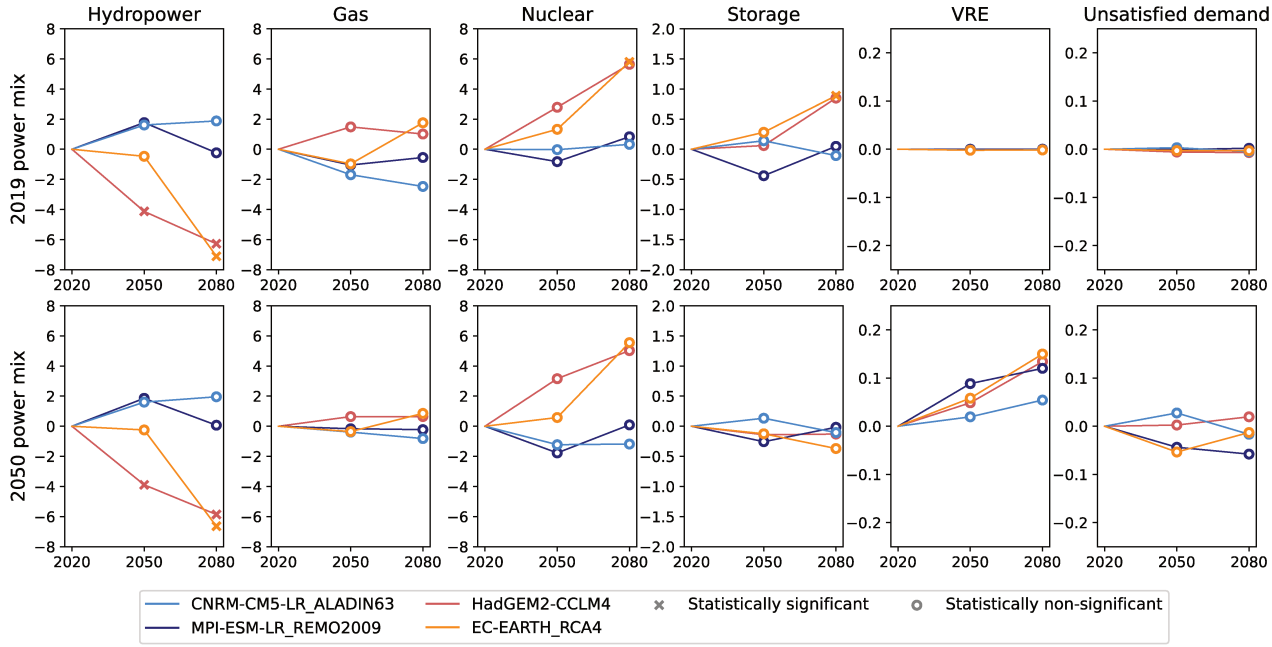

Figure 6.17: Evolution of the mean annual power supply by technology and unsatisfied demand across scenarios (GWh). *Storage* includes the production by PHS and batteries. *VRE* refers to Variable Renewable Energy and encompasses the production by solar and wind power plants. VRE production changes only due to curtailment, as capacity factors are consistent across climate scenarios and periods. The statistical significance of each 20-year future period is assessed relatively to the 2010-2029 period using a Student test (p-value of 0.05).

summer river flows pose a threat to summer production by thermal plants that rely on river water for cooling. In France, a significant share of existing nuclear power plants are concerned by this issue, which could increase the impact of climate change on the power system cost. Nevertheless, new nuclear plants are planned to use seawater or closed-loop cooling systems, which mitigates their vulnerability to climate change.

Finally, although the initial version of the EOLES-Dispatch model accounts for cross-border exchanges between France and its neighboring countries (see Chapter 5), this functionality is not activated in this study due to its high computational demands. Simultaneously optimizing power dispatch in seven countries on an hourly basis over a 20-year period significantly increases computational time and memory requirements. However, in Chapter 5, we tested the effect of the change in the power mix over a shorter period (five years) including additional countries and found similar effects, suggesting that the findings are robust to this simplification.

6.4.2 Climate change uncertainties

Previous studies have identified variation between climate projections as a large source of uncertainty when assessing the impacts of climate change on hydropower (Cronin et al., 2018; Gøtske et al., 2021). The four climate projections utilized in this study also exhibit a substantial divergence in projected precipitation changes, particularly over mountainous regions. This led to considerable discrepancies in the projected annual hydropower potential, with two climate models projecting a significant decline, while the two others project no significant change.

Regional climate projections are affected by three main sources of uncertainty: emis-

sion scenario, model diversity, and natural climate variability (Lehner et al., 2020). In this study, only one emission scenario is considered (RCP8.5), so uncertainties related to the emission scenario are not captured. Analyzing a large ensemble of 87 EURO-CORDEX climate projections, Evin et al. (2021) found that model uncertainties are the most significant contributors to the total variance in precipitation projections. These uncertainties stem from the complexity of the processes involved and the small scale at which they occur, which current-generation climate models cannot fully capture. Inherent model limitations have been identified in three specific areas: atmospheric convection, cloud-aerosol interactions, and land surface processes (IPCC, 2021a).

6.4.3 Uncertainties of future power systems

While climate projections present notable uncertainties, the future evolution of the French power system also introduces its own set of uncertainties, that may impact the evolution of hydropower production. In particular, the production by reservoir plants is highly determined by the pattern of net load, making changes in the power demand pattern and the relatives share of solar PV and wind technologies crucial for predicting its evolution.

Furthermore, all the prospective scenarios proposed for achieving a net-zero power mix in France by 2050 rely on some thermal plants running on decarbonized fuel to provide flexibility (IEA, 2021; RTE, 2021). These thermal plants are likely to be the most expensive generation units on the grid, making their generation costs a key determinant for future peaks in power prices and resulting economic revenues for hydropower plants. However, there are large uncertainties regarding the type of fuel these thermal plants will use and its corresponding cost. Hydrogen is the most likely option, though other fuels such as ammonia or biogas are also being considered. The cost of hydrogen generation, however, remains highly uncertain, as RTE (2021), for instance, estimates it to range from 70 to 160€/MWhPCI.

6.5 Conclusion

This study implemented an interdisciplinary modeling framework to investigate the future of French hydropower production, accounting for changes in both the hydrological cycle and the national power system.

We first analyzed the hydrological changes projected by the ORCHIDEE model using four climate projections derived from EURO-CORDEX simulations and found large uncertainties in projected precipitation and river flow changes, especially in the Alps. The four climate models yield therefore disparate results regarding the evolution of annual national hydropower production. At the regional scale, however, some robust changes could be identified, especially in the Pyrenees where all climate simulations project a significant decrease in production. Additionally, more consistent changes were found in the seasonality of river discharges, with earlier inflows to the reservoirs driven by increased winter rainfall and earlier snowmelt. There is also a consensus on a seasonal shift in run-of-river production, with higher output in winter and reduced output in spring and summer.

The coupling of the ORCHIDEE model with the EOLES-Dispatch model allowed us to investigate the impact of these hydrological changes on current and future power systems. We found that the seasonal changes in reservoir inflows help to mitigate the impact of a potential reduction in annual hydropower production. Most of this reduction

is expected to occur in summer, a period when the power system is less critically dependent on hydropower. Consequently, no significant change in power system adequacy was found, regardless of the power scenario.

Furthermore, the effect of a change in the power system could also be assessed through this integrated framework. We found that integrating more variable renewable energy sources into the power system dampens the seasonality of the production by reservoir plants, in response to the increased variability of net load throughout the year. Additionally, this increased variability was also found to enhance the differentiated value of dispatchable reservoir plants relative to run-of-river plants in future power mixes.

Though climate warming and increased renewable energy penetration affect the seasonality of reservoir production differently, both contribute to reducing the annual variation in reservoir stock. On the one hand, climate warming leads to earlier inflows to reservoirs at the beginning of winter. On the other hand, the reduced seasonality in net load lessens the need for winter reservoir withdrawals for hydropower production, while slightly increasing the demand during summer. Such an evolution would reduce water stocks in reservoirs during summer, potentially leading to conflicts with other water needs, such as irrigation or ecological requirements, which are expected to rise in summer with climate change.

Future research could aim to improve the representation of non-energy water use in the ORCHIDEE model to better capture the potential competition between the different water needs during summer. The integrated framework used in this study offers a promising tool for exploring this issue, as it allows the consistent management of individual reservoirs in conjunction with the operation of the national power grid. The methodology developed here could therefore provide valuable insights to inform water management policies at both local and national levels. Additionally, incorporating factors such as seasonal variations in power demand due to climate change and the effects of climate change on other technologies would provide a more comprehensive assessment of its impact on future power systems.

CHAPTER 7

Uncertainties of climate projections

This chapter examines the sensitivity of the findings of the previous chapter to the uncertainties in climate change projections. While the previous chapter addresses some of these uncertainties through the comparison of different climate models, this chapter focuses on the uncertainties associated with the choice of the RCP scenario and the selection of the bias-correction method.

Contents

7.1 Sensitivity to radiative concentration scenarios 126
7.1.1 Introduction 126
7.1.2 Results 126
7.2 Role of the bias-correction method 130
7.2.1 Introduction 130
7.2.2 Description of the ADAMONT bias correction method 130
7.2.3 Results 131
7.2.4 Conclusion 135

Uncertainties in climate projections arise from three main sources (Hawkins et al., 2009). The first is the internal variability of the climate system, which refers to the natural climate fluctuations that occur in the absence of any radiative forcing. The second is model sensitivity to climate change, as different climate models simulate varying changes in response to the same radiative forcing. The third is scenario uncertainty, which stems from uncertainties in future greenhouse gas emissions that lead to uncertainties in future radiative forcing, and hence climate. The relative importance of each uncertainty source varies with the timescale of interest (Hawkins et al., 2009). For time horizons of many decades or longer, the model and scenario uncertainties become the dominant sources. The previous chapter addresses model uncertainty. In the current chapter, section 7.1 examines scenario uncertainty.

Furthermore, raw outputs from climate models suffer from biases compared to observations due to the imperfect representation of physical processes within climate models. To make these outputs usable for impact models such as GHMs, they are commonly bias-corrected in a post-processing step. However, performing such bias correction can modify the simulated climate signal (Maurer et al., 2014). Therefore, this post-processing introduces an additional source of uncertainty in the final climate projections, as different

bias-correction methods may yield different projections for the same climate model and emission scenario. Section 7.2 examines how the climate change signal is altered by the bias-correction method applied to the climate projections used in the previous chapter.

7.1 Sensitivity to radiative concentration scenarios

7.1.1 Introduction

In the previous chapter, we limited our analysis to climate projections based on RCP8.5, which represents the very high-end of future emissions pathways in the literature. The plausibility of this scenario has been debated, in light of the global decline in coal use over the past decade and the falling prices of clean energy technologies (IPCC, 2021a). In particular, the International Energy Agency World Energy Outlook aligns more closely with weak or moderate emission scenarios like RCP4.5 or RCP6.0 (Hausfather et al., 2020). IPCC (2021a) claims nevertheless that climate projections from RCP8.5 remain valuable, as such concentration levels could still be reached under nominally lower emission trajectories due to the uncertainties in carbon cycle feedbacks and climate sensitivity.

This section examines the uncertainties associated with the choice of RCP by comparing the outputs of stand-alone ORCHIDEE simulations based on two emission scenarios (RCP4.5 and RCP8.5) and two GCM-RCM couples (CNRM-CM5-LR_ALADIN63 and EC-EARTH_RCA4).

7.1.2 Results

Figure 7.1 displays the evolution of the annual hydropower potential simulated at the national scale for each of the scenarios. We find large discrepancies between the two RCP scenarios for the EC-EARTH_RCA4 climate model. A significant decrease in annual hydropower potential is projected under RCP8.5 throughout the 21st century, while no significant change is obtained under RCP4.5. Such differences, resulting from both emission uncertainty and climate variability, are comparable in magnitude to those discussed in the previous chapter, which captured both model uncertainty and climate variability (Fig. 6.5). For CNRM-CM5-LR_ALADIN63, we obtain closer results between the two RCPs.

The differences in simulated potentials found with the EC-EARTH_RCA4 model are a direct consequence of the varying changes in river discharge projected across the two simulations (Fig. 7.2). Significantly lower streamflows are projected in almost all French regions under the RCP8.5 scenario compared to the RCP4.5 scenario. This difference is mainly driven by the changes simulated during the summer, with summer flows projected to decrease substantially more under RCP8.5. In contrast, winter streamflow changes are more consistent between the two scenarios.

To identify the primary drivers of these discrepancies in river flows, Fig. 7.3 shows the absolute changes in precipitation, potential evapotranspiration (PET), and evapotranspiration (ET) projected in each scenario. The differences are more pronounced for precipitation than for ET. A significant decrease in precipitation over the mountainous regions is projected under the RCP8.5 scenario, while under the RCP4.5 scenario changes projected in this area are not significant. This difference in precipitation is therefore identified as the main factor responsible for the observed change in streamflow.

Figure 7.4 depicts the seasonal variations in precipitation and ET. While the winter precipitation patterns are similar across both scenarios, the summer precipitation de-

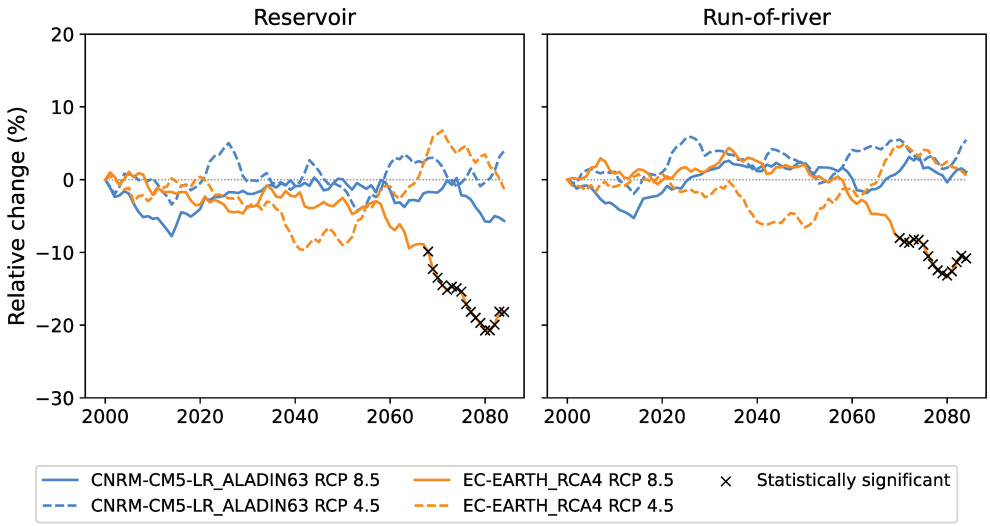

Figure 7.1: Relative change in the 30-year average of annual hydropower potentials obtained for different climate scenarios.

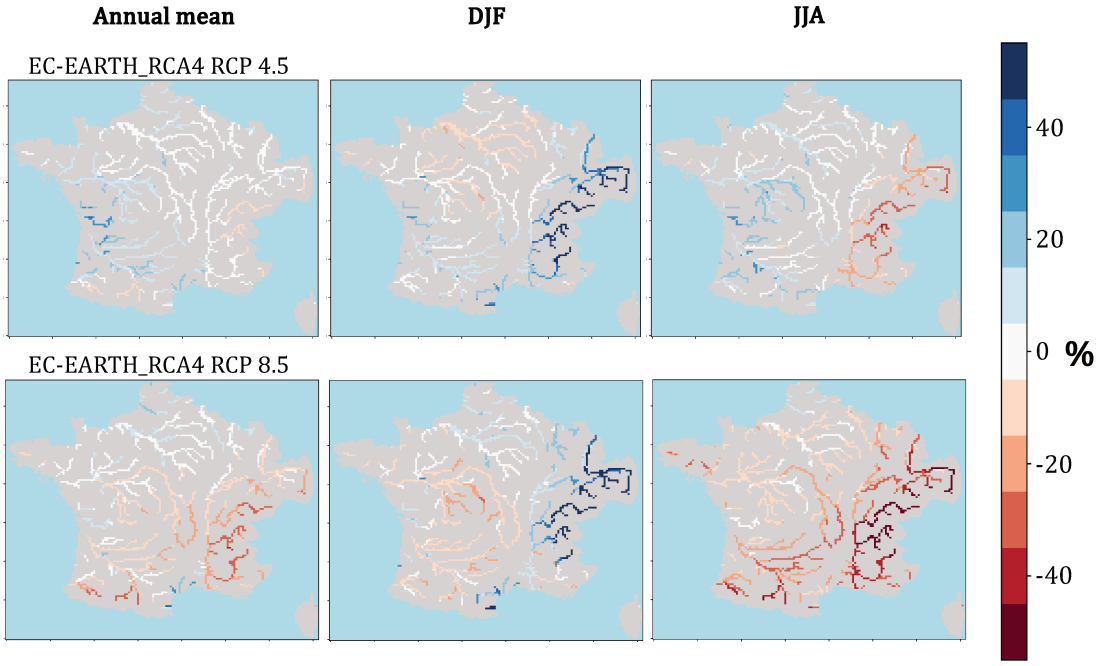

Figure 7.2: Relative change in mean river discharge simulated by ORCHIDEE under EC-EARTH_RCA4 climate forcing for the two different RCPs. 2070-2099 period compared to 1975-2004.

creases more significantly under the RCP8.5, especially over the mountainous regions, accounting for the observed change in summer and annual streamflow.

PET significantly increases under both scenarios due to rising temperatures (Fig. 7.3). The increase is notably higher under RCP8.5 because of the greater temperature rise (+1.01mm/d on average in RCP8.5 compared to +0.45mm in RCP4.5, at the end of the century). However, the change in ET shows the opposite trend. Mean ET decreases under both scenarios, especially during the summer, with a more pronounced decrease under the RCP8.5 scenario than the RCP4.5 scenario. This stronger decrease in ET in

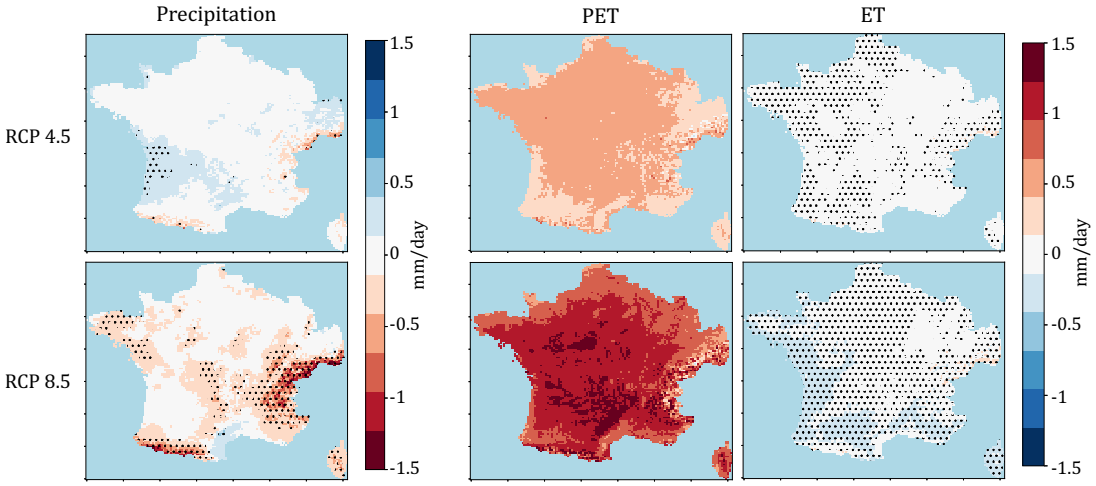

Figure 7.3: Left: Change in mean daily precipitation simulated by EC-EARTH_RCA4 under the two RCPs, 2070-2099 compared to 1975-2005. Right: Change in mean daily PET and ET simulated by ORCHIDEE driven by EC-EARTH_RCA4 forcing for the two RCPs, 2070-2099 compared to 1975-2005.
For precipitation and ET, black dots indicate the area where the changes are statistically significant, which is assessed using a Student test (p-value of 0.05). For PET changes are statistically significant everywhere.

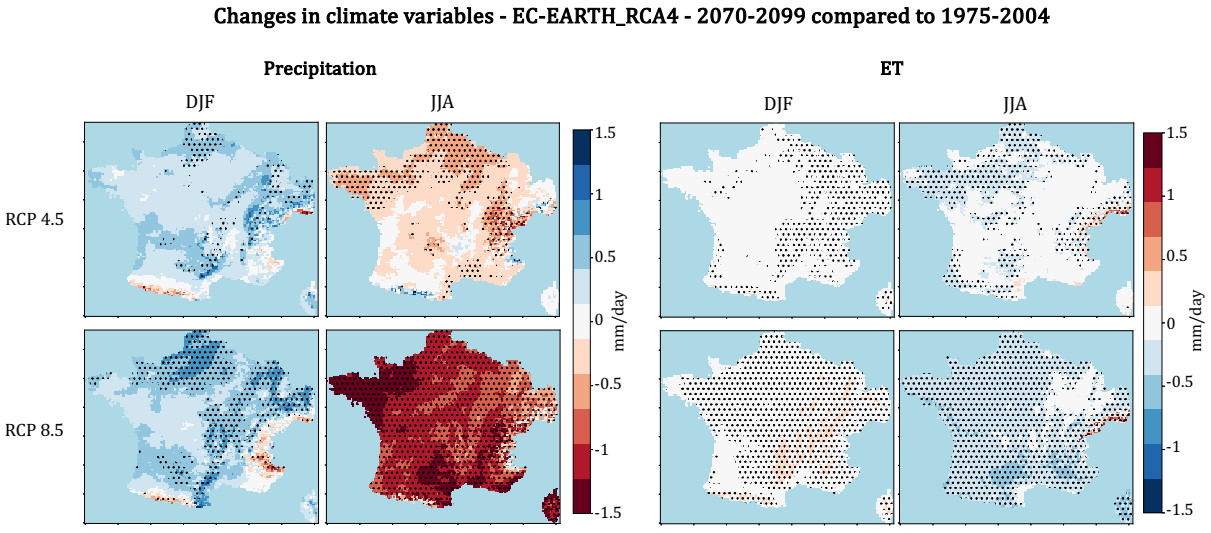

Figure 7.4: Left: Change in winter and summer mean daily precipitation simulated by EC-EARTH_RCA4 under the two RCPs, 2070-2099 compared to 1975-2005. Right: Change in winter and summer mean daily ET simulated by ORCHIDEE driven by EC-EARTH_RCA4 forcing for the two RCPs, 2070-2099 compared to 1975-2005.
Black dots indicate the area where the changes are statistically significant, which is assessed using a Student test (p-value of 0.05).

the RCP8.5 scenario could be attributed to two factors: reduced water resources due to the lower precipitation or the effect of increased CO2 concentration on plant physiology, which may affect plant transpiration. Indeed, previous studies have shown that elevated CO2 concentration causes stomatal closure, thus reducing water loss through evaporation while maintaining efficient photosynthesis (Allen Jr, 1990).

Using a counterfactual simulation driven by RCP4.5 atmospheric variables but with CO2 atmospheric concentration set to RCP8.5 levels, we can separate these two effects (Fig. 7.5). We find that the ET simulated in the counterfactual scenario aligns much more closely with the ET simulated under RCP8.5 than under RCP4.5. This indicates that ET simulated by ORCHIDEE is more sensitive to the change in CO2 atmospheric concentration than to the change in climate variables.

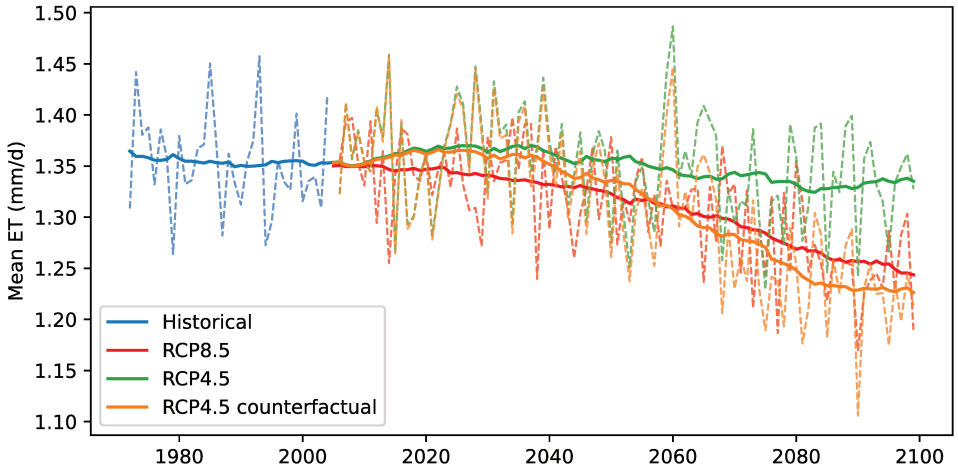

Figure 7.5: Evolution of daily ET (mm/d) throughout the 21st century under the different scenarios. Dashed lines represent annual means, while solid lines indicate 30-year sliding averages.

The simulated change in ET due to the difference in CO2 concentration between RCP8.5 and RCP4.5 is found to be approximately 0.1mm/d at the end of the century, representing a 7.5% change. These figures are consistent with the higher range of estimates suggested by other studies (Lemaitre-Basset et al., 2022; Zhou et al., 2022). However, IPCC (2022a) highlights that *"the relative importance of the physiological and radiative effects of CO2 on future ET is a crucial knowledge gap, partly because many ESM land surface schemes still use representations of this process based on older experimental studies"*. Further research should therefore be carried out to enhance our knowledge and better estimate future changes in ET.

7.1.2.1 Conclusion

This section extends the uncertainty analysis of the previous chapter by considering emission scenario uncertainty, in addition to model uncertainty.

The uncertainty range due to the emission scenario is found to be equivalent to that driven by model variety: ranging from no significant change in national annual hydropower production to a significant reduction of about 17%. This uncertainty range is consistent with the findings of previous studies regarding the evolution of hydropower production in France (Tobin et al., 2018). As with model uncertainty, precipitations over the mountainous regions, especially the Alps, appear to be the main driver of this variability.

Nevertheless, the analysis conducted in this section and the previous chapter does not allow us to further distinguish scenario uncertainty (or model uncertainty in the previous chapter) from natural climate variability. Further analysis relying on several members of

the same simulation (for a given model and scenario) would be needed to determine this.

Finally, regarding the evolution of ET, we show that within the ORCHIDEE model, the physiological effect of CO2 on transpiration is a dominant factor. Further research is required to assess the validity of this modeling, as it has implications for the simulated change in hydropower production. Overestimating the physiological effect of CO2 would underestimate ET, and therefore overestimate resulting river discharges and hydropower potentials.

7.2 Role of the bias-correction method

7.2.1 Introduction

As presented in Chapter 1, GCMs and RCMs outputs suffer from biases compared to the observations. The main reasons for these biased model outputs are imperfect model representations of atmospheric physics, incorrect initialization of the model, or errors in the parameterization chain (Ehret et al., 2012). In particular, RCM resolutions are not sufficient to capture the fine-scale processes in mountainous regions. However, impact models are commonly very sensitive, often non-linearly, to the input climatic variables and their biases (IPCC, 2021a). Therefore, the correction of model output in a post-processing step is usually done to allow the further use of climate outputs by impact models. The process of bias correction involves adjusting model outputs to align with observed data, typically by applying scaling factors or statistical adjustments. Despite their widespread use, several studies have highlighted the limitations of these bias correction methods, which introduce additional uncertainty into climate models (Ehret et al., 2012). Particularly, concerns have been raised regarding the stationarity of correction methods and the preservation of spatiotemporal and inter-variable coherence. Furthermore, bias adjustment methods like quantile mapping can modify simulated climate trends (Maurer et al., 2014).

In this section, we examine the role of the bias correction performed on the climate forcings used in Chapter 6. Specifically, we investigate its impact on the hydrological changes simulated by the model. To this end, we compare climate variables from a raw EURO-Cordex simulation with those from the same simulation corrected with the ADAMONT method, as well as the outputs from the ORCHIDEE model driven by each set of climate variables. We chose to focus on the CNRM-ALADIN63 projection, as it is used in several studies. The ALADIN RCM is namely used by Verfaillie et al. (2017) to introduce the ADAMONT method and assess its performance over the French Alps.

7.2.2 Description of the ADAMONT bias correction method

The ADAMONT method aims at adjusting and disaggregating daily climate projections from an RCM against an observational dataset at an hourly time resolution (Verfaillie et al., 2017). The method produces ultimately adjusted hourly time series of temperature, precipitation, wind speed, humidity, and short- and long-wave radiation, which can be used to force any energy balance land surface model, such as ORCHIDEE. It relies on a refined quantile mapping approach for statistical adjustment and an analogous method for sub-daily disaggregation.

Quantile mapping is considered to be an efficient and easy-to-implement adjustment method. It is an empirical statistical technique that matches the quantile of a simulated climate value to the observed value at the same quantile. The quantiles are determined by sorting climate model output and observations for the same historical period and

constructing cumulative distribution functions (CDFs) for each (Maurer et al., 2014). The main limits of quantile mapping methods are the assumption of time-invariant model deviation to observations on which it is based, and the fact that the temporal properties of the model are not adjusted. If the model has a chronological behavior that differs from the observations (too chaotic or too persistent), this will not be adjusted (Verfaillie et al., 2017). Moreover, quantile mapping does not guarantee spatial and inter-variable consistency.

The ADAMONT method consists of the following steps:

1. **Grid point selection** For each observation point, an RCM grid point is selected by minimizing a distance function.

2. **Weather regime computation** Each day of the RCM and observational records are clustered into four different weather regimes based on the geopotential height at 500 hPa.

3. **Aggregation from hourly to daily observations**

4. **CDF computation** Computation of quantile distribution of each observational dataset and corresponding RCM grid point distribution for each variable, each season, and each weather regime.

5. **Quantile mapping** Quantile mapping is applied to each RCM point for the application time period, taking into account the season and weather regime.

6. **Selection of analog day for sub-daily disaggregation** For each day in the RCM dataset, an analogous day is chosen in the observational dataset following specific criteria.

7. **Sub-daily disaggregation** The adjusted RCM dataset is disaggregated from a daily into an hourly time step by using the hourly observational data from the analogous date chosen in the previous step to reconstruct the daily cycle of the data.

8. **Snow/rain partitioning** Total precipitation is separated into rainfall and snowfall based on hourly adjusted temperature (a threshold of 1°C is used). An additional quantile mapping against the observational dataset is then applied for daily cumulated adjusted RCM rainfall and snowfall separately.

7.2.3 Results

7.2.3.1 Correction of model biases in the historical period

First, we examine the existing biases in the raw EURO-CORDEX simulation over the historical period compared to the observations (SAFRAN reanalysis data in our case study) and verify the performance of the ADAMONT method to manage them.

Precipitation, both liquid and solid, is strongly overestimated in the raw climate simulation, with an average bias of 62% for total precipitation compared to SAFRAN (Fig. 7.6). The bias is especially pronounced over mountainous areas, where it exceeds 100%. The overestimated snowfall leads to a simulated snow cover that persists year-round when the ORCHIDEE is forced by the raw projection, whereas it melts during the summer in the simulation forced by SAFRAN (not shown in the figure). This persistent snow cover results in an underestimation of PET in mountainous areas in the simulation

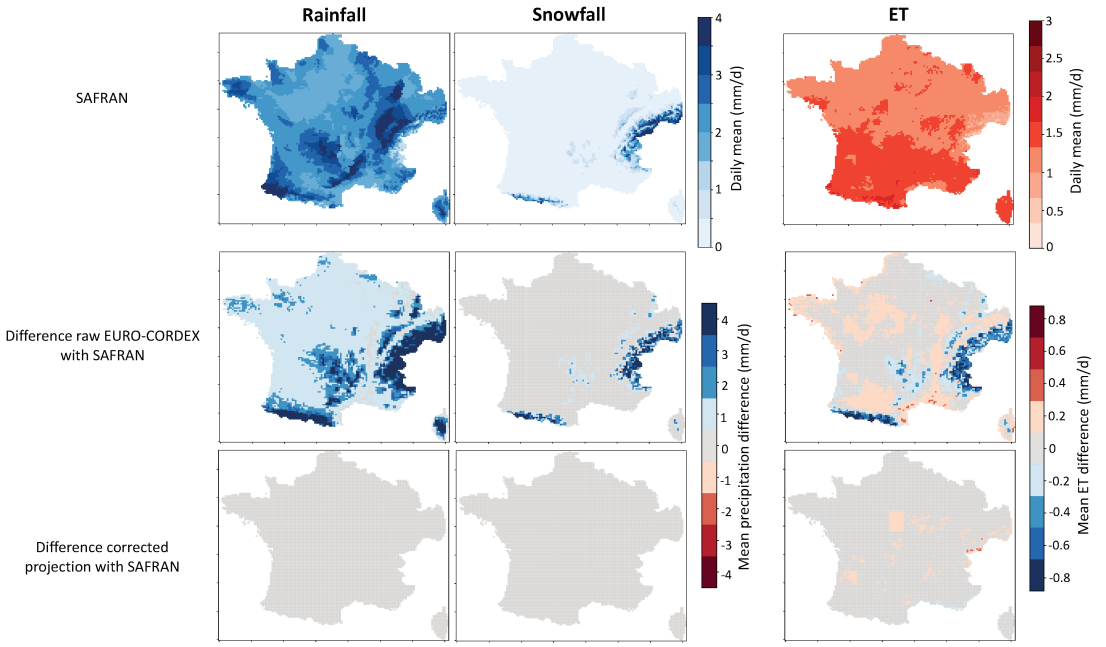

Figure 7.6: Comparison of daily average climate variables for the period 1975-2004. Precipitation data are directly taken from the climate datasets (SAFRAN, raw EURO-CORDEX, bias-corrected EURO-CORDEX), while ET is derived from simulations run with the ORCHIDEE model, forced with each of the climate datasets. Top: Daily means of SAFRAN precipitation and ET simulated by ORCHIDEE under the SAFRAN forcing. Bottom: Differences in mean daily precipitation and ET. The raw EURO-CORDEX simulated precipitation is interpolated toward the SAFRAN grid.

driven by the raw projection, which explains the negative bias in ET found in these regions (Fig. 7.6).

The ADAMONT method proves effective in correcting precipitation biases, as residual biases after correction are very low, +2.5% on average. The persistence of small residual biases is the result of the conditioning by weather regime (step 2 of the method). Indeed, the frequencies of weather regimes may differ between the model and the observations.

The correction performed for the historical period is then applied to the future projection. In the following, we will examine the impact of this correction on the hydrological changes simulated by ORCHIDEE.

7.2.3.2 Simulated changes in river discharge

Figure 7.7 presents the changes in river discharge simulated by ORCHIDEE driven by the raw and bias-corrected climate projections. The simulated impact of climate change varies considerably between the two simulations. Overall, the changes are more positive with the bias-corrected projection, leading to opposite effects of climate change for some rivers. For instance, river flows in the upper Loire are projected to decrease by more than 5% when ORCHIDEE is driven by the raw EURO-CORDEX projection, while they increase by more than 5% in the simulation driven by the bias-corrected projection.

These discrepancies warrant further investigation, as the difference in trend due to bias correction is of the same magnitude as the projected impact of climate change.

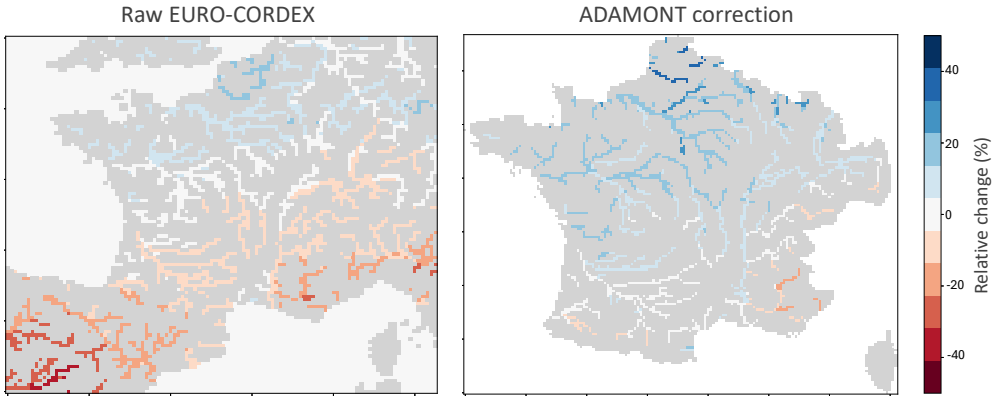

Figure 7.7: Relative changes in streamflow projected by ORCHIDEE when driven by the raw CNRM-ALADIN63 EURO-CORDEX projection and its ADAMONT bias-corrected version, 2070-2099 compared to 1975-2004

7.2.3.3 Investigating the reasons for these differences

The changes in streamflow are the result of the simulated changes in precipitation (both rain and snowfall) and ET. Figure 7.8 illustrates the relative changes in these atmospheric climate variables simulated for the two climate inputs. The changes in ET are relatively similar in the two simulations, except over the Alps and Pyrenees, where higher changes are projected with the raw EURO-CORDEX projection. This discrepancy is due to the bias in ET in the historical period discussed above. Conversely, the changes in total precipitation differ significantly between the two simulations, with the bias-corrected simulation projecting a wetter climate. In particular, the raw EURO-CORDEX simulation projects a decrease in total precipitation over the entire Alps massif, whereas the bias-corrected version projects an increase in the Northwestern part of the massif. For example at Bourg Saint Maurice (black point in Fig. 7.8), the raw EURO-CORDEX simulation projects a decrease of 6% in total precipitation, whereas the bias-corrected version projects an increase of 9%.

Figure 7.9 presents the absolute changes in ET, rainfall, and snowfall. Despite the large relative changes in some areas, the changes in ET are negligible compared to the changes in precipitation, particularly in snowfall over the Alps and Pyrenees. Consequently, the primary drivers of the differences in river discharge changes highlighted in Fig. 7.7 appear to be the differences in precipitation changes over the mountains.

Figure 7.10 depicts the CDF of the raw and bias-corrected precipitation for Bourg Saint Maurice (location indicated in Fig. 7.8), during the winter (DJF) and summer (JJA) seasons, for both the historical (1975-2004) and future (2070-2099) periods (without accounting for the decomposition in weather regimes). In the raw future simulation, a decrease in total precipitation is projected across the entire PDF in winter, primarily driven by a decrease in snowfall. However, the bias correction leads to an increase in the highest quantiles of total precipitation (from Q_{70} to Q_{100}). This discrepancy may stem from the decomposition in weather regimes performed before the quantile mapping in the ADAMONT method (step 2). Indeed, the frequency of weather patterns is likely to change in the future. Previous studies have shown that most GCMs used in EURO-CORDEX simulations predict an increase in the frequency of the NAO- regime by 2100 and a slight decrease in the Atlantic Ridge regime (Cattiaux et al., 2013). Furthermore, the final step of the ADAMONT method, which involves an additional quantile mapping

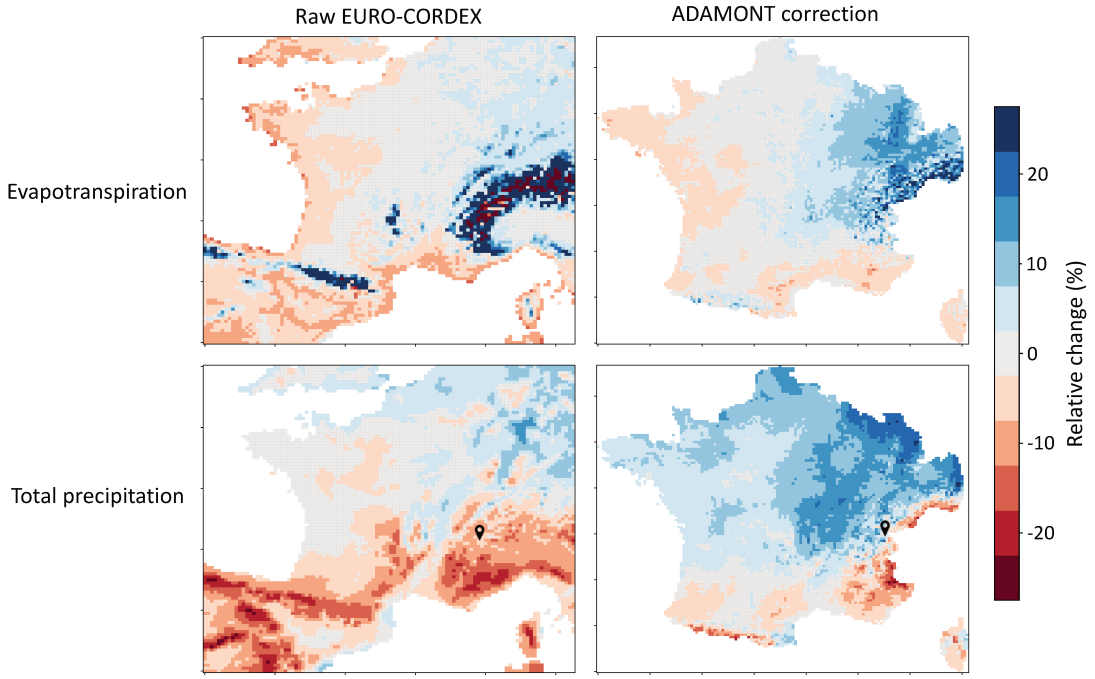

Figure 7.8: Relative changes in ET and precipitation projected with the raw CNRM-ALADIN63 EURO-CORDEX projection and its ADAMONT bias-corrected version, 2070-2099 compared to 1975-2004.

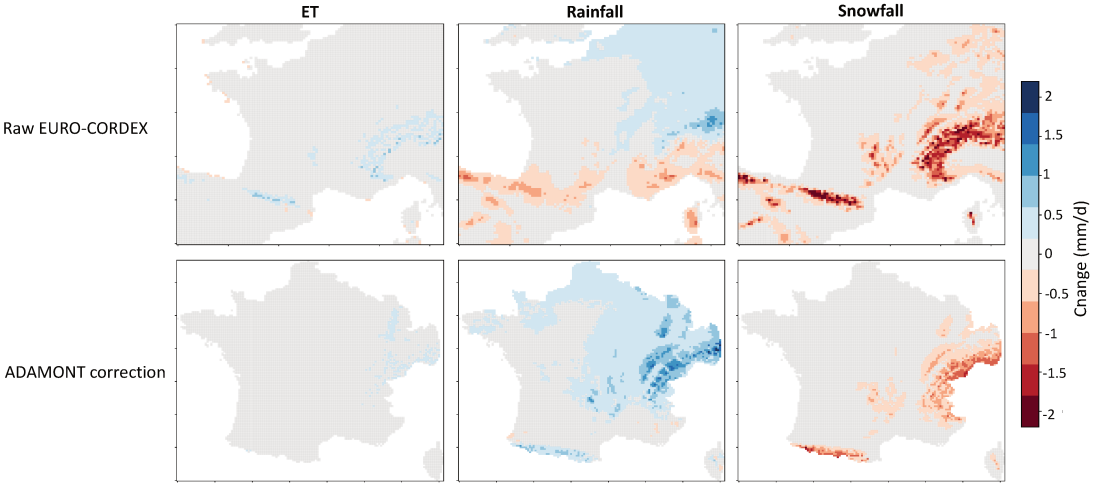

Figure 7.9: Absolute changes in mean daily ET and precipitation projected with the raw CNRM-ALADIN63 EURO-CORDEX climate scenario and its ADAMONT bias-corrected version, in 2070-2099 compared to 1975-2004

of rainfall and snowfall separately may also explain some of the observed differences.

More generally, quantile mapping inevitably alters the climate change signal (Hagemann et al., 2011; Maurer et al., 2014). Based on synthetic precipitation data, Maurer et al. (2014) shows for instance that underestimating the variance for a bounded positively skewed distribution, common for daily precipitation, tends to amplify projected trends during quantile mapping. Conversely, overestimating the variance will tend to dampen projected trends. They also highlight higher changes due to the bias-correction process for winter precipitation than summer.

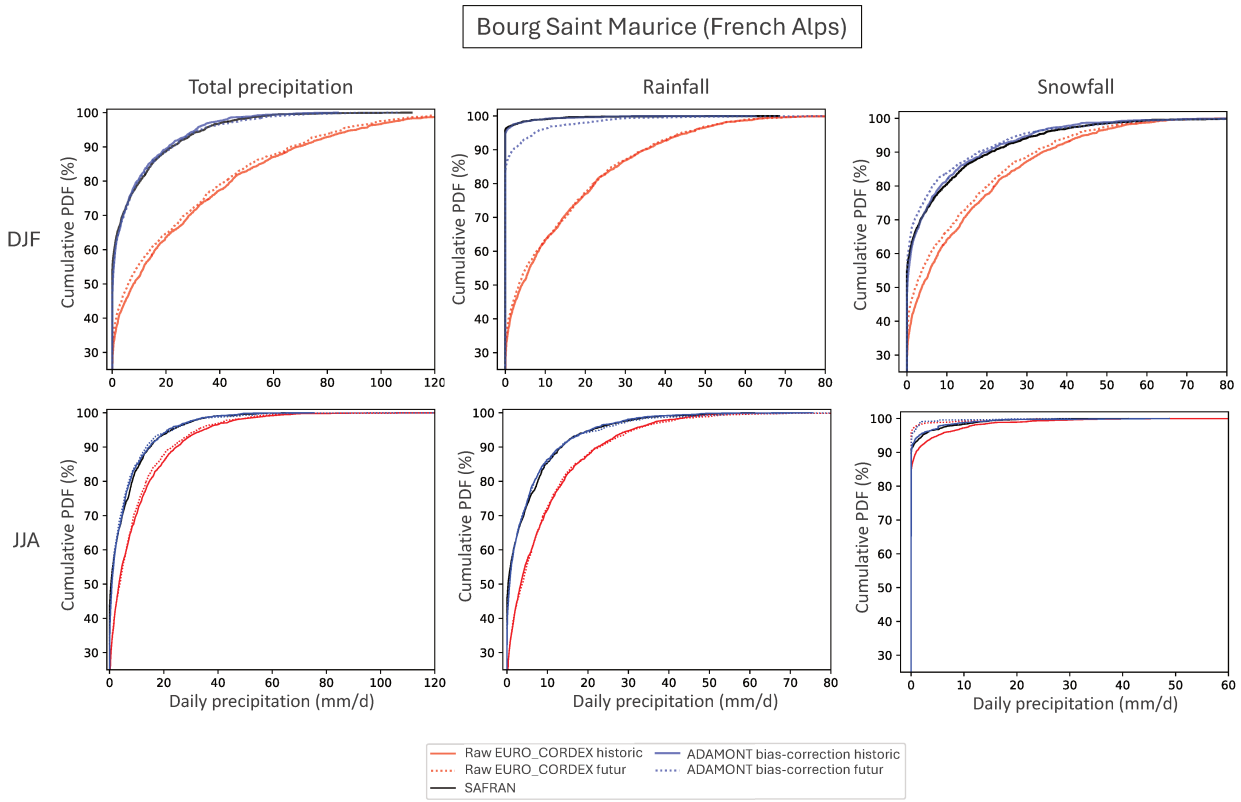

Figure 7.10: CDF of raw and bias-corrected precipitations in the historical period (1975-2004) and future period (2070-2099) at Bourg Saint Maurice.

7.2.4 Conclusion

Comparing a raw EURO-CORDEX simulation with its bias-corrected version, we show that the ADAMONT method significantly alters the simulated climate change signal on precipitation. This was already found by Robin et al. (2023). The changes in precipitation patterns are particularly modified in the mountainous regions, which are critical for water resources studies and especially hydropower. Moreover, the seasonal changes are also likely to be altered.

An important question then is whether it is more legitimate to preserve the raw simulated precipitation trend during bias correction or to allow it to be modified by the process. In their study, Maurer et al. (2014) found that quantile mapping bias correction improves the correspondence with observed changes in some locations and degrades it in others. Similar to the suggestions of Cloke et al. (2013), they encourage practitioners to examine the projected trends in both raw and bias-corrected climate output to be fully transparent about the effects of bias correction on trends. Indeed, bias correction processes add significantly to the uncertainties in modeling climate change impacts, but this step may be hidden from end users and decision-makers.

Applying this recommendation to the analysis carried out in chapter 6 involves considering the hydrological changes simulated in the raw simulation (Fig. 7.7, left) to estimate the change in hydropower production. In this case, the greater decrease in river discharges simulated in the Southern part of France would result in a greater decrease in hydropower potential compared to the results derived from bias-corrected climate projection.

CHAPTER 8

The evolution of pumped hydro storage profitability with the integration of renewable energies

Pumped Hydro Storage (PHS) plants represent the majority of current energy storage options in France and are set for significant expansion in the coming years, based on the national energy policy plans. Nevertheless, the profitability of these plants has been questioned, prompting the French government to consider creating support mechanisms to encourage the development of new plants. This chapter examines the current business model of existing French PHS plants and explores how anticipated changes in the national power system are expected to modify their revenues.

Contents

8.1 Introduction . . . 138
8.2 The business model of PHS plants . . . 138
8.2.1 Investment costs . . . 138
8.2.2 Various sources of revenue and estimates for 2019 . . . 139
8.2.3 Balance . . . 140
8.3 Modeling reserves in power system models . . . 141
8.3.1 Implementation of the reserves mechanism in EOLES-Dispatch model . . . 141
8.3.2 Validation . . . 143
8.4 Evolution of the revenues from PHS plants in 2050 . . . 145
8.4.1 Revenues from reserves . . . 145
8.4.2 Energy market . . . 147
8.4.3 Conclusion . . . 148

8.1 Introduction

Energy storage assets provide a flexible option for mitigating the variability and uncertainty of solar and wind production (IEA, 2021). In France, energy storage is currently provided by PHS plants, which were developed between 1970 and 1990 to support the expansion of the nuclear fleet, which increased the price gap between off-peak and peak hours. The existing French PHS plants represent an installed capacity of 5 GW for power production and 184 GWh for energy storage. To accommodate the anticipated increase in the variability of power supply and demand, the French energy policies plan for the installation of new PHS plants, with a target of 1.5 GW additional capacity being commissioned between 2030 and 2035. Energy scenarios proposed by RTE (2021) rely on the addition of 3 GW by 2050.

However, despite the encouraging long-term signals sent by the government and the TSO, new projects are struggling to emerge due to the significant investment required and the lack of visibility on future revenues (Loisel et al., 2021). In 2023, the French government initiated a public consultation on the creation of a public support mechanism to encourage the development of new PHS plants.

The objective of this chapter is to analyze how the revenues of the French PHS plants could evolve in response to the anticipated changes in the power mix and how these changes might impact their profitability.

8.2 The business model of PHS plants

8.2.1 Investment costs

Zakeri et al. (2015) reviewed the existing literature on the life cycle costs of utility-scale electricity storage systems, providing an updated database for the cost elements. According to this study, the investment cost of a PHS plant is composed of:

- The cost of power conversion systems C_{PCS}, which mainly includes the turbines, pumps, and power interconnections, estimated at 513€/kW by Zakeri et al. (2015).
- The cost of the storage part C_{Stor} (reservoirs), estimated at 68€/kWh by Zakeri et al. (2015).
- The cost of balance of plant C_{BOP}, which includes all the supporting components and auxiliary systems needed to deliver the energy, other than the generating unit itself (Boroomandnia et al., 2024). Zakeri et al. (2015) estimate it at 15€/kW.

Assuming that all investments are done in the first year of the project, the annualized total cost Ca of a PHS plant of power capacity P, energy capacity S, and annual production E is given by Eq. 8.1.

$$Ca = ((C_{PCS} + C_{BOP}) * P + C_{stor} * S) \times \frac{i(i+1)^T}{(i+1)^T - 1} + C_{fOM} * P + C_{vOM} * E \quad (8.1)$$

where C_{fOM} and C_{vOM} are respectively the fixed and variable costs of operation and maintenance (OM), and i is the interest rate during the lifetime T. Zakeri et al. (2015) estimate 4.6€/kW for C_{fOM} and 0.22€/MWh for C_{vOM} for PHS plants. The annualized costs obtained for the French PHS plants assuming the above-mentioned values, and an interest rate of 4% and a lifetime of 70 years are presented in Table 8.1.

When considering new projects to be developed, a smaller cost of storage should be accounted as the new projects could be developed on existing reservoirs.

	Grand Maison	Montezic	Bissorte	Revin	Cheylas	La Coche	**Total**
Production capacity (MW)	1690	910	825	808	500	320	**5053**
Storage capacity (GWh)	50.7	36.4	4.13	4.04	3.0	0.96	**99.3**
Electricity generated in 2019 (GWh)	2003	1087	719	563	594	565	**5531**
Annualized cost (Million €)	194	131	34	34	20	12	**426**
Annualized cost (€/kW)	114.5	143.6	41.8	41.8	44.7	36.1	**84.4**

Table 8.1: Characteristics of the biggest French PHS plants and their estimated costs.

8.2.2 Various sources of revenue and estimates for 2019

PHS facilities generate revenue through multiple streams, derived from their unique operational capabilities within the electricity grid.

8.2.2.1 Price arbitrage

Firstly, PHS can generate revenue from the difference in electricity prices between periods of low prices, during which they purchase electricity to store water, and periods of high prices, during which they produce electricity by releasing water. Based on the 2019 observations of PHS operations at 30-minute resolution (RTE, 2023b) and wholesale power prices (ENTSO-E, 2023), we find a total revenue of 73.4M€ for all PHS together.

8.2.2.2 Ancillary services

Ancillary services encompass various functions contracted by TSOs to ensure system security. PHS facilities can participate in several ancillary services markets, in particular in the reserves required by the TSOs to prevent any outage in power generation. In France, there are three types of reserves that are successively applied in the case of an outage (Fig. 8.1):

- **Frequency containment reserve (FCR)**, also known as *"Primary reserve"*, is automatically activated within 30 seconds in response to a sudden change in frequency. In Europe, this reserve is shared among 11 TSOs, including RTE, as part of the ENTSO-E. The European reserve must be capable of compensating for the loss of the two largest capacity units, totaling 3 GW, with a contribution of 540 MW from France. Since 2017, the market has operated through tenders selected based on the merit order principle. Initially held daily, tenders are now selected for 4 hours.

- **Automatic frequency restoration reserve (aFRR)**, also referred to as *"Secondary reserve"*, is automatically activated by RTE within 400 seconds. In France, this reserve ranges from 500 MW to 1180 MW, depending on demand and renewable energy production. Initially, all producers operating generating units exceeding 120 MW were required to participate, with remuneration provided at a fixed price (19.36/MW/h in 2019). In 2021, the market was briefly opened to competition before reverting to its initial form due to market failures. It was then reopened in June 2024.

- **Tertiary reserve**, which gathers manual Frequency Restoration Reserves (mFRR), also known as *"Fast reserve"* for activation within 13 minutes, and Replacement

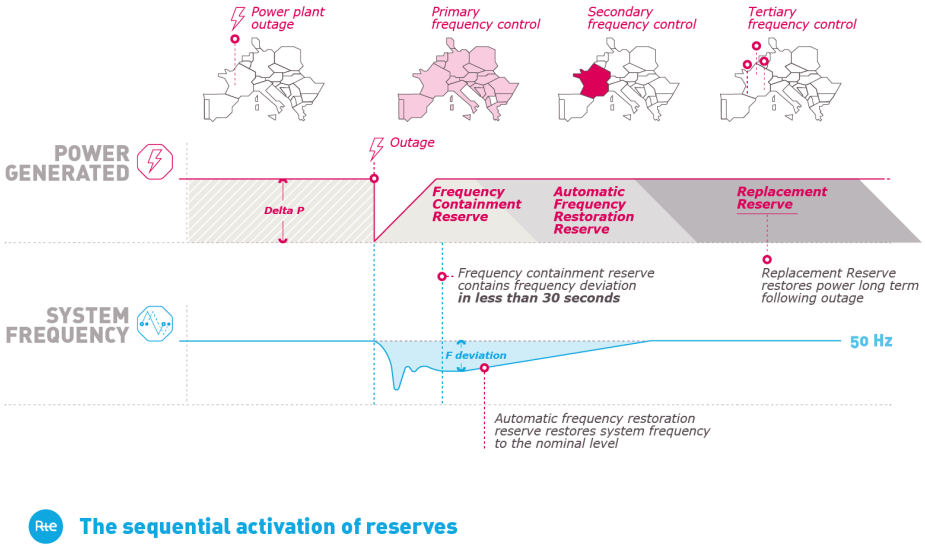

Figure 8.1: The sequential activation of reserves. Source: RTE

Reserves (RR). The required capacities are 1000 MW for mFRR and 500 MW for RR. All dispatchable generation facilities connected to the grid are required to offer their available power for the tertiary reserve. Other resources, such as non-dispatchable generation, demand-side management, and storage, may participate voluntarily. The majority of this capacity is contracted through an annual tender, with prices for mFRR and RR amounting to 8.3 k€/MW/year and 7.3 k€/MW/year, respectively, in 2019.

Crampes (2014) indicates that the participation of a PHS plant in the reserve mechanism is limited to 7% of the plant's total capacity, with 2.5% allocated to FCR and 4.5% to aFRR. If we assume that PHS plants are always participating in reserves at their maximum capacity and consider the historical reserve prices from 2019, the resulting annual revenues would be 8.3 million euros for FCR and 38 million euros for aFRR. No data is available on the participation of PHS plants in the tertiary reserve.

8.2.2.3 Capacity market

Finally, PHS facilities can also generate revenues through the capacity market, where they are remunerated for their ability to deliver reliable and flexible electricity generation. In 2019, the capacity price was set to 18k€/MW, hence an annual revenue of approximately 90.23 million euros for all PHS plants.

8.2.3 Balance

The estimated annualized costs and revenues estimated for the French PHS plants in 2019 are presented in Fig. 8.2. The revenue breakdown is consistent with the figures provided by EDF (2017). Regarding other countries, Chyong et al. (2022) estimated that 84% of the revenues earned by PHS in the UK has been from ancillary services, with fast reserve service accounting for 81% of this amount. Similarly, in the Ontario region in Canada, Bassett et al. (2018) found that 87% of PHS revenues in 2015 were derived

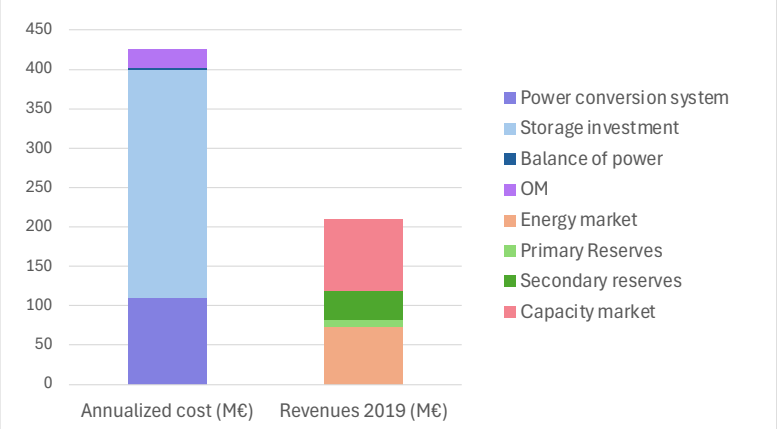

Figure 8.2: Estimated costs and revenues of French PHS plants.

from ancillary services. Our estimation may underestimate the revenues from ancillary services due to the lack of data on the participation of PHS plants in the tertiary reserve.

Although our estimation is simplified due to the lack of detailed data on PHS plants' participation in ancillary services and to the use of simplified cost assumptions, it underlines that, in the current energy mix, revenues from the energy market alone are insufficient to ensure the profitability of PHS plants. This finding is supported by previous studies (Bassett et al., 2018; Chyong et al., 2022; Loisel et al., 2021; Staffell et al., 2016), both in France and other countries. Focusing on the French PHS plants, Loisel et al. (2021) showed in particular that they behave non-strategically on the market, as the full potential for price-arbitrage is not exploited. This suggests that the owner and operator EDF is not using PHS storage strategically in the day-ahead market, instead relying on other services to secure revenues.

Nevertheless, it is important to note that for existing French PHS, the majority of costs are attributed to the investment in storage infrastructure. If future projects can leverage existing reservoirs, this substantial cost component may be significantly reduced, thereby making new projects more financially viable.

The objective of the remainder of this chapter is to explore how the revenues of PHS plants are expected to evolve in a different power mix. The first step involves modeling reserves within the EOLES-Dispatch framework, as they represent an important source of revenue.

8.3 Modeling reserves in power system models

8.3.1 Implementation of the reserves mechanism in EOLES-Dispatch model

Several studies have described and analyzed the implementation of reserve requirements in power system models (Chyong et al., 2022; Zerrahn et al., 2017). We build on these studies to integrate reserve operations into the EOLES-Dispatch model. We model only upward reserves, as it is anticipated that renewable curtailment would largely provide downward reserves in the future. This implementation involves several steps.

The first step is to delineate the set of technologies that are authorized to participate in reserve services. Based on the existing regulatory framework, we assume that only thermal plants (coal, gas and nuclear), reservoir power plants and storage units (batteries

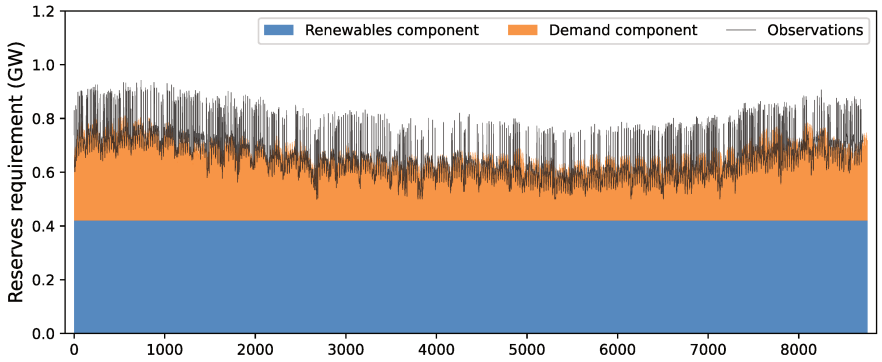

Figure 8.3: Estimated aFRR requirements compared to observed aFRR volumes in 2019 (RTE, 2024a). aFRR requirements are estimated based on Eq. 8.2 using 2019 historical data for power demand and renewable energy share.

and PHS) are eligible.

The second step consists in defining the reserve requirement. FCR requirement, $D_{a,h}^{FCR}$, is currently fixed in each country (540 MW in France). The quantity of aFRR required to meet ENTSO-E's guidelines, $D_{a,h}^{aFRR}$, is given by Eq. 8.2. It varies with the share of renewable energy production in the mix, the variability of demand and forecast errors.

$$D_{a,h}^{aFRR} = D_{a,h} * loadUnc * (1 + loadVar) + \sum_{tec \in vre} capa_{a,vre} * vreReq_{vre} \tag{8.2}$$

where $loadUnc$ denotes the uncertainty on power demand due to forecast errors, $loadVar$ is the load variation factor and $vreReq$ is the additional reserve requirement for VRE technologies due to forecast errors. The method for calculating these various coefficients according to ENSTO-E guidelines is detailed by Van Stiphout et al. (2017) and we present in Table 8.2 the values taken in this study for each of the parameters. Fig. 8.3 shows the good fit between the estimated and observed demand for secondary reserve in 2019.

Parameter	Value
$loadUnc$	0.0045
$loadVar$	0.01
$vreReq_{pv}$	0.01
$vreReq_{wind}$	0.02

Table 8.2: Assumed values for the parameters defining secondary reserve requirements in Eq. 8.2. They are defined following guidelines from Van Stiphout et al. (2017) and adjusted so that simulated requirements match the observed ones in Fig. 8.3.

The third step is to define the portion of the contracted reserves that is activated, denoted as $\phi_{a,tec,h}$. Since FCR operates on very short timescales compared to the hourly resolution of the EOLES-Dispatch model, we only model aFRR activation. Based on historical observations of reserve activation (RTE, 2024b), we assume that at each timestep 9% of the reserve provided by each technology is activated.

These three steps lead to new equations in EOLES-Dispatch. The hourly capacity of each technology participating in FCR, respectively aFRR, are noted $\mathbf{FCR}_{a,tec,h}$, resp. $\mathbf{aFRR}_{a,tec,h}$. They are subject to the series of following equations:

1. Reserve requirements have to be satisfied by eligible technologies *tec*.

$$\sum_{tec} \mathbf{FCR}_{a,tec,h} = D_{a,h}^{FCR} \ \forall a, \forall h \tag{8.3}$$

$$\sum_{tec} \mathbf{aFRR}_{a,tec,h} = D_{a,h}^{aFRR} \ \forall a, \forall h \tag{8.4}$$

2. The participation of each technology is limited by its power modulation rate ρ_{tec} and the reserve activation time τ_{rsv}.

$$\mathbf{rsv}_{a,tec,h} \leq \rho_{tec} * \tau_{rsv} * capa_{a,tec} \ \forall rsv \in \{FCR, aFRR\}, \forall a, \forall h, \forall tec \tag{8.5}$$

   The activation time are respectively 30 seconds and 5 minutes for FCR and aFRR. Following Chyong et al. (2022), we take $\rho_{CCGT} = 3.44h^{-1}$, $\rho_{OCGT} = 8.18h^{-1}$ and $\rho_{coal} = 1.84h^{-1}$ and assume. For nuclear plants, we take $\rho_{nuc} = 0.5h^{-1}$. Hydropower plants are known to have very high technical ramping rates, ranging from 6 to $18h^{-1}$. However, these rates can be limited in practice to avoid negative ecological effects downstream of the dams. The numbers indicated by Crampes (2014) suggest rather an effective ramping rate of $3h^{-1}$. In the following, we consider two cases linked to this uncertainty, a first one called *Hydroflex* $\rho_{reservoir} = \rho_{PHS} = 10h^{-1}$ and a second one called *Hydrolimited* in which $\rho_{reservoir} = \rho_{PHS} = 3h^{-1}$. Finally, we consider than batteries can fully modulate their power output within one hour.

3. The participation of thermal plants *thr* requires them to be switched on:

$$\mathbf{G}_{a,thr,h} + \mathbf{FCR}_{a,thr,h} + \mathbf{aFRR}_{a,thr,h} \leq \mathbf{ON}_{a,thr,h} \ \forall a, \forall h, \forall thr \tag{8.6}$$

4. The energy produced through reserve activation should be discounted from the energy stock of storage technologies *sto*. The evolution of the energy stored by storage technologies is then given by

$$\mathbf{S}_{a,sto,h+1} \leq \mathbf{S}_{a,sto,h} + \underline{\mathbf{G}}_{a,sto,h} r_{sto} - \mathbf{G}_{a,sto,h} - \phi_{a,sto,h} \mathbf{aFRR}_{a,sto,h} \ \forall a, \forall h, \forall sto \tag{8.7}$$

5. Similarly, the activated reserve should be discounted from the ramping constraint of thermal power plants.

$$\mathbf{R}_{a,thr,h+1} \leq \mathbf{G}_{a,thr,h+1} + \phi_{a,thr,h+1} \mathbf{aFRR}_{a,thr,h+1} - \mathbf{G}_{a,thr,h} - \phi_{a,thr,h} \mathbf{aFRR}_{a,thr,h} \ \forall a, \forall h, \forall thr \tag{8.8}$$

6. Finally, the reserve activation is counted in the cost function that the model seeks to minimize:

$$Cost = \sum_{a} \sum_{h} \sum_{k} \left((\mathbf{G}_{a,k,h} + \phi_{a,k,h} \mathbf{aFRR}_{a,k,h}) cg_k + csu_k \mathbf{SU}_{a,k,h} + cr_k \mathbf{R}_{a,k,h} + \underline{\mathbf{G}}_{a,k,h} \underline{cg}_k \right) \tag{8.9}$$

8.3.2 Validation

To validate this modeling approach, we compare the outputs from the EOLES-Dispatch simulation of the year 2019 to observed data. Figure 8.4 compares the simulated reserve prices, derived from the dual of the Equations (8.3) and (8.4), with the observed prices (RTE, 2024a) for the *Hydrolim* and *Hydroflex* scenarios. We find a good fit between

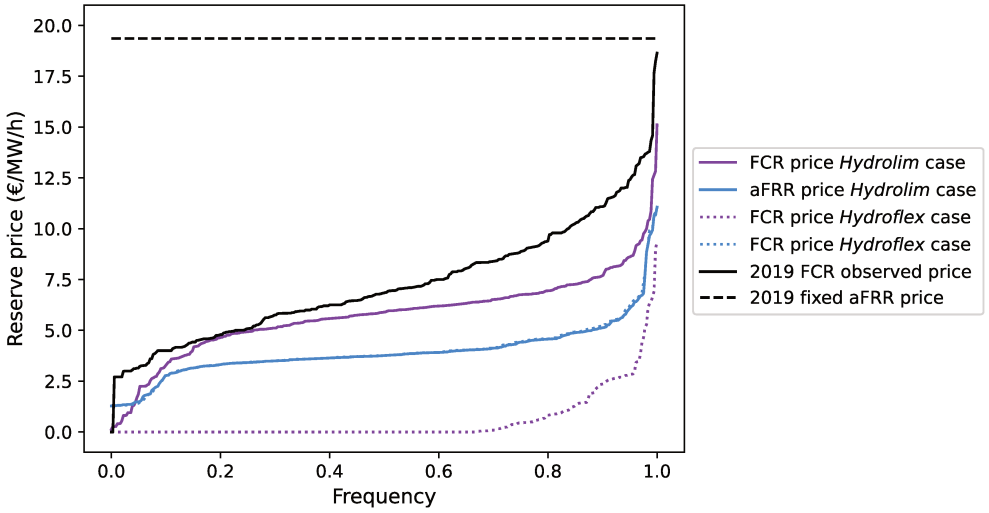

Figure 8.4: Cumulative density function (CDF) of daily simulated and observed reserve prices in France for 2019. Observed prices are taken from RTE (2024a).

the simulated and observed FCR prices in the *Hydrolim* scenario. In contrast, in the *Hydroflex* scenario, the prices are largely underestimated. Regarding aFRR prices, the differences between the two scenarios are negligible, as the modulation rate assumed for hydropower plants in the *Hydrolim* scenario does not substantially limit their participation in the aFRR reserve.

Figure 8.5 shows the relative participation of each technology to the two reserve services for both scenarios. Since no observational data is available for comparison, we cannot validate our outputs. As expected, the participation of hydropower plants in the FCR reserve is higher in the *Hydroflex* scenario due to the increased power modulation rate assumed in this case. Consequently, in the *Hydrolim* scenario, a greater share of thermal plants, particularly gas-fired ones, contributes to the FCR reserve. For the aFRR reserve, there is no significant difference between the two scenarios.

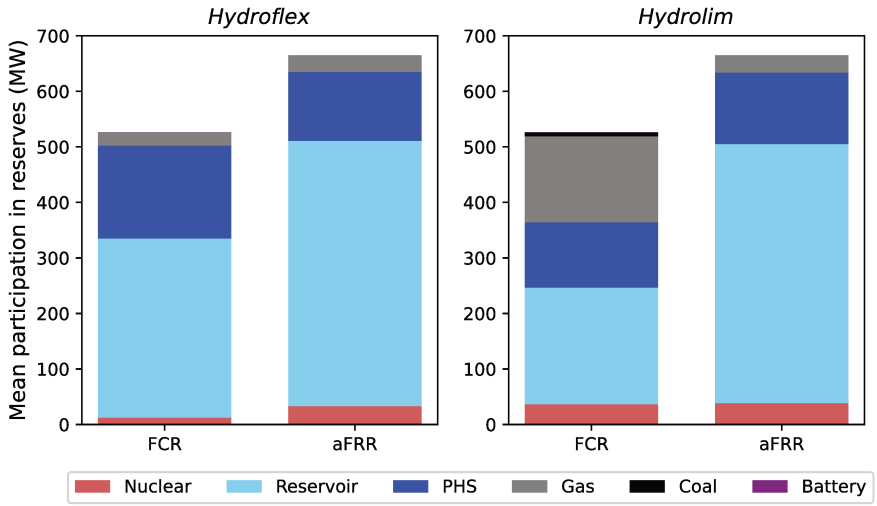

Figure 8.5: Mean contribution of each technology to the reserve requirements for the year 2019.

8.4 Evolution of the revenues from PHS plants in 2050

As in Chapter 5, two energy scenarios for France and its neighboring countries are considered: the *2019 scenario*, based on the 2019 historical power mix, and the *2050 scenario*, based on the central assumptions from RTE (2021). For further details, see Section 5.3.2. The two energy scenarios differ in terms of the installed capacities of each technology, the demand time series, and the assumptions made regarding the generation cost of gas-fired power plants. Specifically for PHS plants, the installed capacity is 8GW in the *2050 scenario*, compared to only 5GW in the *2019 scenario*.

Chapter 6 shows that the assumption made about the evolution of the generation cost of gas-fired plants in the *2050 scenario*, though uncertain, may have a significant impact on the simulated power prices. To account for this uncertainty, we consider a third energy scenario referred to as *2050 unchanged cost*, in which generation capacities and demand time series are those from the *2050 scenario* (further denoted *2050 ref scenario*) while cost assumptions are those from the *2019 scenario*. As in Chapter 5, a five-year simulation of the power dispatch is conducted for each of the three scenarios, relying on historical time series data from 2015 to 2019.

In the following, we only consider the *Hydrolim* case, as it yields reserve prices that are more closely aligned with the observed data (Fig. 8.4).

8.4.1 Revenues from reserves

We assume that the current regulatory framework will remain in place in the future, such that Eq. (8.4) remains legitimate to define the requirement for secondary reserve in the 2050 power mix. In light of the considerable expansion in solar and wind plants, the requirement for the secondary reserve is dramatically increased, as represented in Fig. 8.6 for France (to be compared to Fig. 8.3).

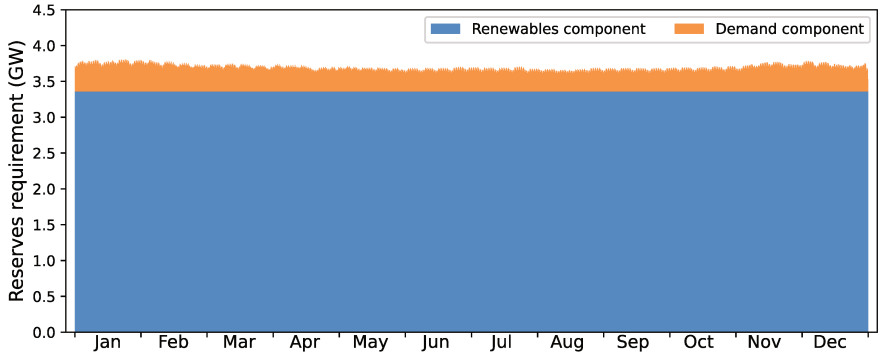

Figure 8.6: Simulated requirements for the secondary reserve in the 2050 energy scenario, based on Eq. 8.2, for the 2019 weather year.

Figure 8.7 presents the relative contribution of each technology to the reserve requirements in the two 2050 scenarios. The results are very similar across the two scenarios. In both cases, batteries supply 60% of FCR requirements, while gas-fired plants contribute very little to the total reserve requirement. Regarding the aFRR, hydroelectric units provide 60% of the requirements, with PHS plants contributing 15%.

The significant participation of batteries in the FCR market results in a significant decrease in FCR prices between the *2019* scenario and the *2050* scenarios (Fig. 8.8), with hourly prices being zero 95% of the time in the latter scenarios. The evolution of

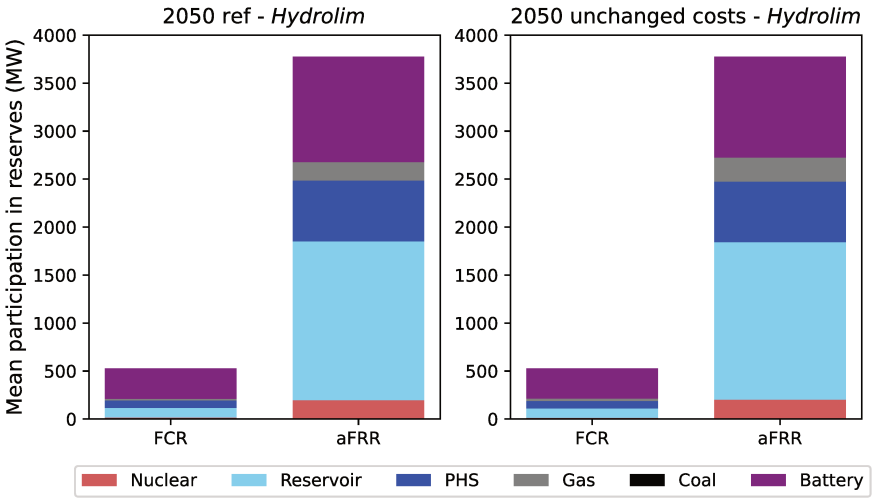

Figure 8.7: Mean contribution of each technology to the reserve requirements in the 2050 energy scenarios.

aFRR prices depends on the assumption made about the cost of gas-fired plants. In the *2050 unchanged cost* scenario, hourly aFRR prices are lower 90% of the time compared to the 2019 scenario. On the contrary, in the *2050 ref scenario*, prices significantly increase when gas plants participate in supplying power demand or reserves, resulting in higher prices than in the 2019 scenario 55% of the time.

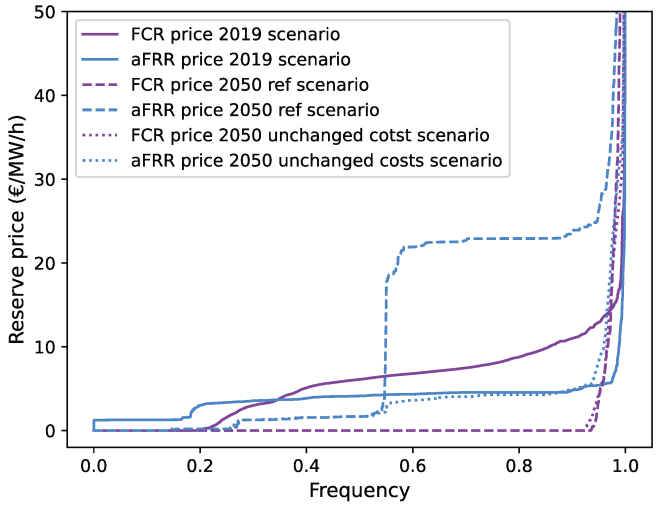

Figure 8.8: CDF of hourly reserve prices simulated in the three energy scenarios (for the *Hydrolim* case).

The resulting revenues of PHS from reserves provision are presented in Table 8.3. A reduction in revenues from FCR is observed in the two 2050 scenarios as a consequence of the decreased participation of thermal plants, which are replaced by batteries that have a null generation cost. Regarding the revenues from aFRR provision, they are significantly increased in the *2050 ref scenario* and decreased by 62% in the *2050 unchanged costs scenario*, compared to the *2019 scenario*.

2019 scenario	
FCR	1.24 €/kW
aFRR	1.24 €/kW
2050 ref scenario	
FCR	0.109 €/kW
aFRR	5.98 €/kW
2050 unchanged costs scenario	
FCR	0.08 €/kW
aFRR	1.68 €/kW

Table 8.3: Simulated mean annual revenues of PHS plants from FCR and aFRR mechanisms, for the *Hydrolim* case.

8.4.2 Energy market

The CDF of hourly power prices simulated in France in each of the three energy scenarios are presented in Fig. 8.9. In both 2050 scenarios, the integration of renewable energies leads to more hours during which the power price is set by nuclear (+117%), despite lower total production of nuclear (-63%). In the *2050 unchanged costs scenario*, simulated prices are consistently lower than in the 2019 scenario, except when some unsatisfied demand occurs. Conversely, driven by the increased generation cost of gas-fired thermal plants, the hourly prices are higher 50% of the time in the *2050 ref scenario*.

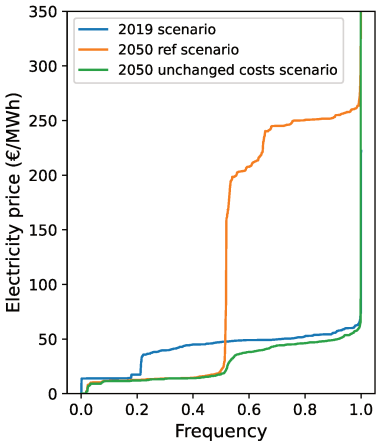

Figure 8.9: CDF of hourly power prices simulated in France over the 5-year period in each energy scenario.

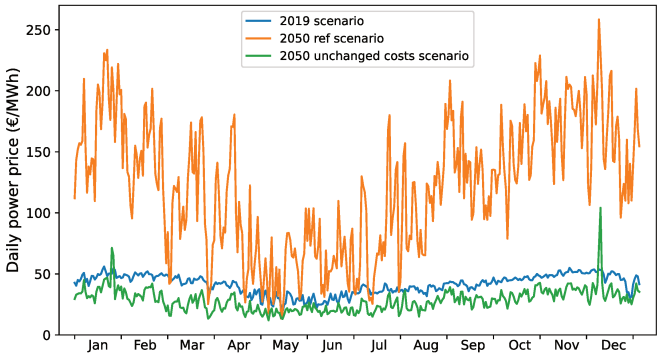

Figure 8.10: Interannual average of mean daily price simulated in each energy scenario.

Mean daily prices are simulated in Fig. 8.10. In both 2050 scenarios, the hourly and daily variability of power prices is significantly increased (see Table 8.4). The increase in variability is more pronounced in the *2050 ref scenario*, reflecting the larger gap between off-peak and peak prices.

This higher variability in power prices leads to PHS plants being utilized more frequently in the scenarios with a higher share of renewable energies (see Fig. 8.11).

Such an increase in the use rate of PHS plants, coupled with the higher variability in power prices, results in a notable increase in the annual revenues generated by PHS plants on the energy market in the 2050 energy scenarios, especially in the *2050 ref*

	2019 scenario	2050 ref scenario	2050 unchanged costs
Mean standard deviation of hourly prices within a day	8.45	50.3	9.19
Standard deviation of daily prices	7.90	53.8	9.36

Table 8.4: Mean daily and hourly variability of power prices simulated in each energy scenario (€/MWh).

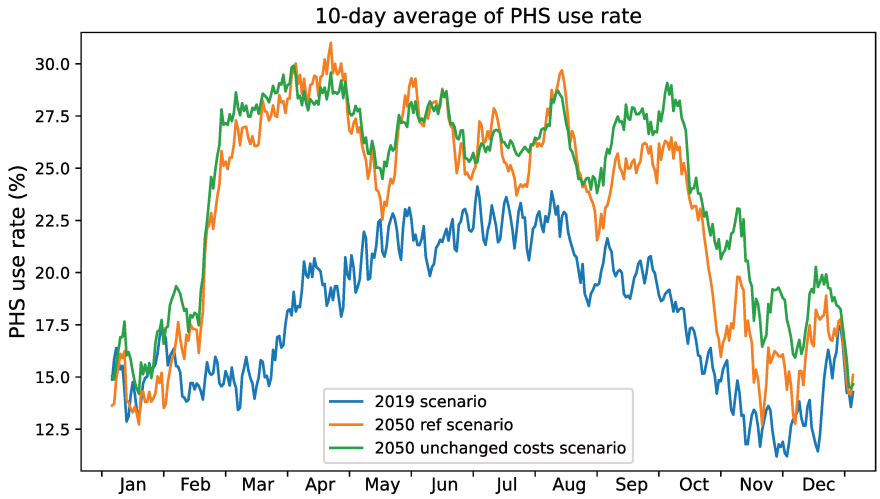

Figure 8.11: Interannual average of PHS use rate simulated over the 5-year period (10-day sliding average).

scenario where an increased generation cost of gas-fired power plants is assumed. The mean annual revenue then increases from 26.7€/kW in the *2019 scenario* to 332€/kW in the *2050 ref scenario* and 37.9€/kW in the *2050 unchanged costs scenario*.

Besides, it can be noted that, as highlighted by Loisel et al. (2021), the revenues found with the optimization model over the historical period are higher than those observed (an overall average annual revenue of 132.6M€ is found in the simulation against an observed annual revenue of 73M€ in 2019).

8.4.3 Conclusion

Table 8.5 provides a summary of the revenues simulated in the different energy scenarios. Despite the uncertainty surrounding the future generation costs of gas-fired power plants, the revenues of PHS plants are projected to rise with the integration of renewable energy sources. This rise is mainly driven by the increased variability of power prices, which enables PHS plants to earn more in the energy market. The relative share of revenues from providing FCR and aFRR services is expected to decrease, aligning with findings from other studies (Chyong et al., 2022). Nevertheless, it remains uncertain whether these projected revenues will be sufficient to cover the annualized investment cost, estimated at 84.4 €/kW (see section 8.2.1). Moreover, it is important to note that revenues from the tertiary reserve are not considered here, while there are found to constitute the majority of the current PHS revenues in the UK, for instance (Chyong et al., 2022).

This study presents also other limitations. First, significant uncertainties surround the regulatory evolution of the different market mechanisms, such as ancillary services and capacity market, especially due to the growing integration of batteries and other

	2019 scenario	2050 ref scenario	2050 unchanged costs
Revenue from reserves (€/kW)	2.48	6.08	1.76
Revenue from energy market (€/kW)	26.7	332	37.9
Total (€/kW)	**29.4**	**334.9**	**39.9**

Table 8.5: Total revenues of PHS plants simulated in the different energy scenarios, in the *Hydrolim* case.

flexibility options like demand-side management. Additionally, the costs of the future PHS projects are also highly uncertain, as they will depend on their location and the potential use of preexisting reservoirs.

While the need for support mechanisms has been identified in multiple studies, future research should focus the design of these mechanisms. In France, the government is considering a support mechanism in the form of a tariff supplement based on market price fluctuations between the purchase and resale of electricity. This mechanism would guarantee an annual income to PHS operators, with the State committing to pay the supplement relative to the theoretical maximum income of the PHS plant given the actual price variations. The advantage of this approach is that it mitigates the risks linked to price fluctuations while still incentivizing PHS plants to be operated optimally for grid balancing.

CHAPTER 9

Conclusions and perspectives

During this thesis, I developed an integrated modeling framework to explore the impact of various climate change and power system scenarios on hydropower production within a regional power grid. Using France as a case study, I introduced the framework (Chapters 2 and 5), validated it against historical data (Chapters 3, 4, and 5), and applied it to analyze the effects of climate change and renewable energy penetration (Chapters 6 and 8). The analysis highlighted the uncertainties surrounding these results (Chapter 7). In this final chapter, I summarize the main findings of my work (Section 9.1), propose directions for future research (Section 9.2) and conclude by outlining some broader implications for future French hydropower stakeholders (Section 9.3).

Contents

9.1 Main findings 152

9.1.1 How to represent hydropower operation in a climate model considering the needs for power system balancing? 152

9.1.2 How to represent dynamic hydropower constraints in power system models? 152

9.1.3 How will hydropower production evolve in the future French power system under climate change? 153

9.2 Perspectives for future research 154

9.2.1 Towards a better assessment of climate change impacts on power systems 154

9.2.2 Enhancing the representation of water management in land surface models (LSMs) 155

9.2.3 Dealing with climate uncertainties 157

9.3 Broader implications 157

9.1 Main findings

Section 1.3.1 introduced the three main questions addressed in this manuscript. Below, I summarize the work conducted and the key findings for each of these questions.

9.1.1 How to represent hydropower operation in a climate model considering the needs for power system balancing?

As outlined in Chapter 1, anthropogenic water management has become a critical component of the continental hydrological cycle and must be integrated in land surface models (LSMs). The work conducted in Part I contributes to this goal in two ways.

Firstly, I have developed an algorithm to accurately locate infrastructures on the LSM grid, consistently with sub-grid hydrology and topography. This development facilitates several processes, such as positioning gauging stations for model calibration and validation against observed river discharges (Huang et al., 2024), and integrating water management within the model by locating infrastructures such as dams and power plants on the model grid.

Leveraging this work, I have implemented a reservoir module within the ORCHIDEE model. This module provides a framework to simulate the multipurpose operation of reservoirs, accounting for ecological, irrigative, touristic, and hydroelectric needs. Additional features such as direct evaporation, spillage, and dynamic water levels are also introduced.

In this thesis, I have focused on the representation of hydropower operations. Reservoir releases for hydropower generation are determined based on the needs for power system balancing. However, this link had yet not be accounted for in hydrological models or LSMs. I show that demand-driven algorithms, typically used for irrigation, can also be effective to represent water management for hydropower and capture this link. Such a methodology relies then on three main points: connecting each demand point (power plant) to a supplying reservoir, having an aggregate time-series of production to serve as aggregate demand - which can be built by power system models if observations are not available -, and defining a prioritization rule for the operation of individual plants.

A main limitation to this approach is the scarcity of detailed data on the hydroelectric network, particularly in mountainous regions where hydropower plants are fed by multiple water sources, including reservoirs, rivers, and snowpacks. While databases for reservoir and power plants are accessible in many regions, comprehensive data on water inputs for each hydropower plant is lacking, making the accurate estimation of hydropower potential difficult. However, I propose a solution to overcome this issue, provided that some production data are available at the resolution of individual power plants. Such data are published in databases such as European Commission et al. (2019) or Global Energy Observatory et al. (2019), but all countries are not evenly documented.

Non-energy water uses, such as irrigation or tourism, are described simplistically in this model version and could be further enhanced in further studies (see Section 9.2.2.1).

9.1.2 How to represent dynamic hydropower constraints in power system models?

Hydropower production is determined by the needs for power system balancing and the hydrological conditions. These two factors must therefore be properly accounted for in power system models (PSMs). However, PSMs typically use fixed constraints for reservoir

production, overlooking potential changes due to evolving climate conditions or shifts in power system needs.

In Part II, I show that coupling PSMs with a hydrological model (or LSM) such as ORCHIDEE can help to account for evolving conditions. This coupled framework ensures that the simulated hydropower schedule simultaneously adheres to water availability constraints and the power system's cost minimization objective. Furthermore, this approach enables the incorporation of additional constraints on reservoir production within PSMs. By comparing outputs from the EOLES-Dispatch model, both coupled and uncoupled with ORCHIDEE, against observed data, I show that accounting for these additional constraints improves the representation of hydropower plant flexibility. Accurately capturing this flexibility is particularly valuable for examining the reliability of power mixes with a high share of variable renewable energy, where flexibility becomes increasingly precious.

However, the coupling performed in Part II involves several iterations of the two models, which are computationally intensive and time-consuming. This iterative process is impractical for every simulation of the EOLES-Dispatch model, and even more so for the EOLES model, in which technology capacities are optimized in addition to the dispatch. A viable alternative is to develop a set of reference time series derived from coupled ORCHIDEE_EOLES-Dispatch simulations under several climate and power mix scenarios. The adequate time series can then be used as exogenous inputs for PSMs. This approach has already been implemented in the main version of the EOLES model[1].

In such an approach, the monthly production of reservoir plants is still optimized by the model, while the other constraints become static. However, since these constraints are derived from coupled simulations under climate and power system conditions close to those in the new experiment, they remain consistent with the hydropower operations simulated in the new context.

9.1.3 How will hydropower production evolve in the future French power system under climate change?

Thanks to the development of an interdisciplinary framework based on the first two parts of the manuscript, Part III explores the future of French hydropower production across various temporal and spatial scales, ranging from inter-annual variations to hourly dynamics, and from the national to the individual plant level. The main findings are summarized below.

First, I find a limited change in the annual French hydropower production by 2050, even under scenarios projecting the highest levels of global warming. By the end of the century, the evolution of the annual production is uncertain due to the variability in precipitation projections over France. Under the highest global warming scenario, 2 out of 4 climate models considered do not project a significant change, while the other two project a decrease by about 15%. Changes at the local scale are also inconsistent across models, except for the power plants in the Pyrenees and southeastern France where all models project a significant decrease.

Besides, climate change is projected to induce significant changes in the seasonality of streamflow. This results in significant impacts on run-of-river production and reservoir inflows, which are both expected to increase in winter and decrease in summer, at the national level.

Regarding the production by reservoir plants, I find that planned changes in the

[1] https://github.com/CIRED/EOLES/tree/v1.0.1

power system are expected to have a greater impact than climate change on intra-annual distribution by 2050. In power systems with a higher share of renewables, the distribution of reservoir production over the year is modified in response to the changes in the net load, with less production in November and more in January. The integration of more variable renewable energy sources into the grid is also found to increase the variability of power prices. This would increase the value of flexibility options such as reservoir or pumped hydro storage (PHS) plants and enhance the benefits they could generate in the energy market.

9.2 Perspectives for future research

The work described in this manuscript also highlights key directions for future research, which are presented below.

9.2.1 Towards a better assessment of climate change impacts on power systems

While this thesis focuses on the impacts of climate change on hydropower production, other components of the power system may also be affected by climate change, as explored in other studies. Future research could aim to provide a more comprehensive understanding of the overall effects of climate change on the power system. Below are some suggestions for future work in this direction.

9.2.1.1 Relying on consistent climate inputs for power supply and demand

This thesis has developed a method for constructing time series to constrain hydropower generation within PSMs based on climate projections, such as those from the EURO-CORDEX project. The analyses presented in this manuscript are based on simulations of EOLES-Dispatch informed by such constraints. However, these simulations used capacity factors for solar and wind, as well as demand time series, based on historical data. These inputs were therefore not meteorologically and climatologically consistent with the hydrological conditions simulated.

To better investigate the impacts of extreme events or climate change on the power system, it would be insightful to derive these capacity factors and demand time series from the same climate projections used for the hydropower constraints. Tantet et al. (2019) developed a method to build time series for solar and wind capacity factors and power demand based on EURO-CORDEX simulations. This approach offers a way to build consistent inputs across all components of the power system.

9.2.1.2 Changes in water resources may also affect other power supply technologies

Furthermore, the climate-induced hydrological changes discussed in this manuscript may also impact power supply by other technologies, namely nuclear power plants and power-to-gas-to-power storage. The ORCHIDEE model provides a promising tool to investigate these issues, as detailed below.

Nuclear power plants

The French nuclear fleet is composed of 56 reactors, located either by the sea or near rivers for cooling purposes. Two cooling technologies are used: open-loop or closed-loop

systems. In open-loop systems, the water pumped for cooling is discharged back into the river or sea, leading to increased water temperature but minimal water consumption through evaporation. In closed-loop systems, the warmed water passes through a cooling tower before being discharged, which increases water consumption but results in a lower temperature rise in the river.

At each nuclear plant site, specific regulations are in place to protect the ecosystem by setting thresholds for downstream flow, water temperature, and water heating. Climate change is projected to reduce river flows and increase water temperatures in France during the summer, which could constrain nuclear plant production.

The ORCHIDEE model could be used to assess how these constraints might evolve with climate change, as it simulates both river flows and water temperature (Polcher et al., 2023). However, our assessment of ORCHIDEE's performance in various French catchments with nuclear plants revealed a variable accuracy in simulating historical river discharges and water temperature. Additionally, new nuclear plants are planned to use closed-loop systems, which will reduce their risk of being constrained by thermal regulation. Regulatory thresholds may also evolve in the future and are not always strictly enforced, as the nuclear power producers often receive exemptions in practice.

Hydrogen production for power-to-gas storage

Most scenarios for the future French power system rely on power-to-gas storage, with hydrogen being generated through water electrolysis during periods of excess power supply, and then consumed in thermal plants to produce power during periods of high demand. The production of hydrogen requires however water, both as an input for production and a cooling medium (IRENA, 2023). RTE (2021) projects that by 2050, the total volume of hydrogen produced by electrolysis in France will range between 35 and 65 TWh PCI, corresponding to a water consumption of between 9.5 and 17.7 million cubic meters - relatively low compared to the 164 million cubic meters consumed by industry, as illustrated in Figure 1.7. However, depending on the locations of hydrogen production facilities, this could create additional pressure on the French water resources. According to IRENA (2023), 23% of Europe's green hydrogen projects are likely to be in areas under high or extremely high water stress by 2040.

Furthermore, RTE (2021) simulations indicate that hydrogen production would peak during the daytime in summer, in order to store the excess power generated by solar plants. This could enhance competition for water use during the summer months.

The first studies to explore this issue have mainly focused on the annual scale (Shi et al., 2020; Tonelli et al., 2023). However, a more detailed intra-annual analysis could provide more insightful results. The ORCHIDEE and EOLES-Dispatch models are promising tools for such an analysis. In particular, coupling these two models offers a method to evaluate the simultaneous availability of water and excess low-cost power generation.

9.2.2 Enhancing the representation of water management in land surface models (LSMs)

9.2.2.1 Improving the representation of other water uses

The reservoir operations module described in Chapter 2 provides a framework for accounting for competitive water uses. However, non-energy water uses are represented in a simplified manner in this model version, and further improvements are needed to explore these issues more thoroughly.

Irrigation

In this manuscript, irrigation is represented in a simplified way, with constant withdrawals during summer regardless of climate conditions. However, if we assume that irrigation requirements are based on the deficit between actual and potential transpiration (Yin et al., 2020; Zhou et al., 2021), these requirements are expected to increase in France, driven by the projected rise in potential evapotranspiration (Fig. C.1), especially in summer. Future irrigation requirements will also depend on agricultural policy choices.

Zhou et al. (2021) developed and validated a detailed method to incorporate reservoir management for irrigation within the ORCHIDEE model. Although this method was not included in the model version used in this thesis for computational reasons, ongoing technical improvements will soon enable its integration alongside hydropower operations. This method relies on four main steps: (i) defining irrigation areas on the model grid; (ii) linking each irrigation point with a river abstraction point; (iii) computing irrigation demand at each irrigation point; (iv) propagating water demands upstream and determining required withdrawals from reservoirs accordingly.

Ecological requirements

Our current modeling framework only accounts for environmental flow requirements (EFRs) directly downstream of reservoirs. However, similar requirements may also exist at other locations (Pastor et al., 2014). In the French regulations, river flows are subject to legal obligations at nodal points, which correspond to key points for water management defined in the water management schemes of each French watershed. Two requirements are defined at those points:

- **Low-water target flow**, defined as the target above which it is considered that all downstream uses are in equilibrium with the proper functioning of the aquatic environment.
- **Crisis flow**, defined as the target below which drinking water supply and species survival are threatened. During such conditions, water consumption is restricted to essential needs including health, public safety, civil security, drinking water supply, and environmental needs.

Accounting for these additional EFRs within our model would modify the computed releases from the reservoirs, especially during the summer, which is the low-flow season for most French rivers.

Incorporating ecological requirements and irrigation more comprehensively into the model would provide insights into how minimal release requirements from hydropower reservoirs will evolve during summer. Increased demands for other uses can lead to higher summer withdrawals, potentially reducing the water available for more valuable winter production, which is critical for optimizing the power grid.

9.2.2.2 Using SWOT data to validate reservoir operation

One of the difficulties encountered in Chapter 3 to validate the simulated reservoir operations was the lack of available data on the operation of individual hydroelectric reservoirs, as this information is kept confidential by energy producers. However, the SWOT mission, which was launched in 2021, provides a valuable resource to overcome this limitation. SWOT satellites collect data on water levels in rivers and reservoirs, offering

an instrumental tool for monitoring actual water storage in reservoirs (Bonnema et al., 2019; Nair et al., 2022) and comparing it to the simulations.

9.2.3 Dealing with climate uncertainties

Throughout the manuscript, significant climate uncertainties have been highlighted, both in observations and future projections. In particular, mountain precipitation has been identified as a source of substantial uncertainty at various levels, with large impacts on estimated hydropower production.

First, Chapter 3 has underlined significant differences in observed precipitation in mountainous regions when comparing different data sources. These discrepancies arise from two main factors. On the one hand, the observation network in mountainous areas is sparse, especially at higher altitudes, which leads to a skewed representation of precipitation, as most data are collected at lower elevations. This introduces biases that, despite correction efforts, remain difficult to fully eliminate. On the other hand, radar observations in mountainous regions may be compromised by orographic barriers that block radar beams. Addressing these challenges could involve increasing station density, especially in high altitudes, or using local observations from communities to fill data gaps in mountainous areas. Additionally, observations of streamflow, snowpack, or even hydropower production can be used to assess the validity of precipitation products (Lundquist et al., 2019).

Furthermore, Chapters 6 and 7 show that, when focusing on France, precipitation over mountainous areas is the most variable factor across climate simulations using different GCMs or under different RCPs. Several factors contribute to the difficulty in accurately modeling mountain precipitation. First, the spatial resolution of climate models is typically too coarse to capture the fine-scale topographic features that are crucial for accurate precipitation simulations in mountainous regions. Then, models rely on parameterization to represent small-scale processes like cloud formation or convection, which are critical in generating precipitation. These parameterizations may not fully capture the complexities of atmospheric processes in mountainous regions, especially convective precipitation.

Convection-permitting regional climate models (CPRCM) offer a promising strategy to overcome these limitations. CPRCMs operate at finer resolutions than usual RCMs, allowing them to reproduce mesoscale atmospheric structures and explicitly resolve deep convection. The explicit simulation of deep convection, coupled with finer and more accurate topographic details, enhances the ability to model precipitation characteristics (Lucas-Picher et al., 2021).

9.3 Broader implications

In conclusion, although the development of new large reservoirs is not planned in France, existing hydropower plants will play a precious role in the transition to a more renewable electricity mix. Despite significant intra-annual variability in precipitation, their annual output is not expected to be significantly affected by 2050.

Given these challenges, it is important to modernize existing hydropower plants to extend their lifespan and enhance their efficiency. This modernization should also incorporate the restoration of ecological continuity and ensure compliance with environmental regulations, which may, in some cases, reduce power generation. The methodology developed in this thesis provides a framework for quantifying the impact of these changes on the electrical system, which is needed to be able to assess the socio-economic benefits

of such projects by considering investment costs and ecological impacts.

However, two main obstacles currently impede these necessary investments. On the one hand, the current legal framework only permits minor modifications without re-opening the competition for hydropower concessions. The French government however opposes such opening to competition, potentially to foreign companies, as this would raise concerns about national sovereignty. Transitioning to an authorization regime, as advocated by major French hydropower producers and the government, could resolve this issue but requires a decision by the European Commission. On the other hand, as highlighted in this thesis, significant uncertainties surround the future production in some French water catchments, raising questions about the appropriate sizing of facilities.

Furthermore, we have highlighted significant uncertainty regarding future electricity prices, which will determine the future revenues of hydropower plants. If prices are low, revenues may be insufficient to recoup investments, particularly for new PHS plants. Conversely, high prices could lead to substantial profits for certain dam operators, at consumers' expense. To mitigate these risks, carefully defining contracts is crucial, in order to fairly distribute risks between the state, investors, and consumers. PSMs like EOLES-Dispatch can be useful tools to assess various contract designs and their sensitivity to the different kinds of uncertainties.

Finally, although this thesis primarily focuses on the French case, the challenges related to the future of hydropower production are relevant to many countries with diverse contexts. In each of these countries, the future value of hydropower will depend on changes in precipitation within water catchments and the transformation of the energy mix. In some regions, climate trends are clear (e.g., increasing precipitation in Norway and Canada, decreasing in Spain and Brazil), while in others, such as France, they remain uncertain (e.g., California, Italy). The framework developed in this thesis could be extended to other European countries, given that climate projections and hydropower databases are available at the European level. Moreover, existing PSMs like PyPSA (Hörsch et al., 2018) are well-suited to cover the entire European power grid, and could provide insights into how power exchanges between countries could adjust to compensate for climatic contrasts between regions.

APPENDIX A

Supplementary data for Part I

This chapter presents supplementary data that provide further details to the presentation and validation of the modeling approach presented in Part I. This data is included in the Appendices of the article submitted to HESS.

Contents

A.1 Building the routing network 159
A.1.1 Locating hydroelectric infrastructures on the river network . . 159
A.1.2 Adduction network 160
A.2 Alternative precipitation datasets 160
A.2.1 Presentation of the datasets 160
A.2.2 Simulation of hydropower production under SAF_SPAZM . . 161
A.2.3 Simulation of hydropower production under SAF_COM 161
A.3 Conversion factors for hydropower generation 164

A.1 Building the routing network

A.1.1 Locating hydroelectric infrastructures on the river network

Dams and hydropower plants are located on the MERIT grid based on georeferenced and upstream area information provided in the databases. The infrastructure datasets used for our study over France are presented in Section 3.1.2. The location procedure is done following these steps:

1. The initial location is identified based on geographical coordinates.
2. A search area is defined around this initial location (typically 10km in radius)
    - If the upstream area of the infrastructure is included in the databases, we identify all the pixels in the search area with an upstream area that is close enough to the area being searched (typically +/- 20%). Among these eligible pixels, the one closest to the initial location is selected. If no pixel meets this criteria, the infrastructure is not placed.

- If no upstream area data is included in the databases, we look for the closest pixel to the initial location that is likely to be situated on a river. To do this, the maximum upstream area of the pixels in the search area is identified (U_{max}) and the closest pixel to the first guess pixel satisfying ($U > \frac{U_{max}}{10}$) is selected, with U being the upstream area of the pixel.

Note that each vertex and edge can respectively contain only one dam or hydropower plant. If several reservoirs are placed on the same HTU during pixel aggregation, their respective volumes for the different uses are summed. If two plants are placed on the same edge, their installed power capacity and head are summed only if both plants have the same input point. Otherwise, only the plant with the highest installed capacity is kept. As in other studies (Abeshu et al., 2023), all the reservoir attributes are associated with the HTU of the dam (even if its water surface can be larger than the HTU area and its geometry is different from the HTU geometry).

A.1.2 Adduction network

Poundage and reservoir plants generate electricity from the water released from the upper reservoirs. To explicitly represent this adduction network in our model, we have to identify such connections between a feeding reservoir and a power plant. Since datasets describing these connections are rarely available, we use an algorithm to identify these connections. For each poundage or reservoir plant, we thus select as the feeding reservoir the one that maximizes the potential function $\phi = \frac{U*V*h}{d}$, where U is the upstream area of the dam, V is the storage capacity of the reservoir, h is the elevation difference between the plant and the reservoir and d is the horizontal distance between them. The definition of these potential functions is inspired by similar works aiming to connect an irrigated area to a water supply point (Neverre, 2015; Zhou et al., 2021).

This position algorithm relies on the assumption that each plant is fed by only one reservoir. This assumption is however debatable, especially for plants in mountain areas that may be connected to several reservoirs. In this case, our choice of the potential function ϕ privileges the reservoir with the largest upstream area since it is likely to determine the production potential of the plants. During calibration (see Sect. 2.2.5), plants for which the identification of a single reservoir conducts to a significant misrepresentation of the plant's hydropower potential are identified and a correction is made by moving the withdrawal point so that it gathers enough water to ensure the observed production is possible.

A.2 Alternative precipitation datasets

A.2.1 Presentation of the datasets

A.2.1.1 COMEPHORE

COMEPHORE (COmbinaison en vue de la Meilleure Estimation de la Précipitation HOraiRE) dataset provides observations of surface precipitation accumulation over metropolitan France at an hourly and kilometric resolution based on a synthesis of radar and rain gauge data. A specific processing chain has been implemented in order to address the various sources of error affecting radar data, in particular its low quality in high altitude mountainous areas like the Alps or the Pyrenees (Fumiére et al., 2020). The final database is nevertheless assumed to be the best representation of surface precipitation over metropolitan France (Fumiére et al., 2020).

We build a meteorologic dataset SAF_COM by replacing precipitation data in SAFRAN with data from COMEPHORE. As COMEPHORE does not distinguish solid and liquid precipitations, we keep SAFRAN's hourly ratio of solid/liquid precipitations when possible and discriminate based on the air temperature otherwise.

The differences in annual mean precipitation are generally small between SAFRAN and COMEPHORE, with an average deviation inferior to 1.0% in COMEPHORE compared to SAFRAN (Fig. 3.1). However, we find a small seasonal bias as this average deviation goes from -2.0% for the Winter period to +1.9% in the Summer. Moreover, discrepancies increase dramatically in mountainous regions, especially in the Alps and the Pyrenees. For grid points with an average elevation above 1000m, the annual mean precipitation in COMPEHORE is, on average, 10.4% lower.

A.2.1.2 SPAZM

SPAZM (SPAtialisation des précipitations en Zone de Montagne) is a daily reanalysis of precipitation at the kilometer scale, developed by EDF, the main electricity producer in France. SPAZM specifically covers the southern half of the French territory, where a large majority of hydroelectric power plants are located (Gottardi et al., 2008). Climatological precipitation outlines are first constructed based on daily precipitation observations categorized by types of oceanic circulation (weather patterns) (Garavaglia et al., 2011). These outlines are then spatially interpolated onto the kilometer-scale grid and deformed daily according to available observations. In addition to Météo-France's observations, which are also used to construct SAFRAN, EDF's measurement network is utilized. We interpolate the daily precipitation data from SPAZM to the hourly scale and merge it with SAFRAN data to create the alternative forcing dataset SAF_SPAZM. As for SAF_COM, we keep SAFRAN's hourly ratio of solid/liquid precipitations when possible. Compared to SAFRAN, precipitations are in average 2.7% higher in SPAZM with an average bias of 7.0% in Summer, against 2.1% in Winter. Bias is heterogeneously spread over France (Fig. 3.1) with bigger differences on the highest reliefs, without a clear sign (average deviation of +3.9% for grid points above 1000m).

A.2.2 Simulation of hydropower production under SAF_SPAZM

A.2.3 Simulation of hydropower production under SAF_COM

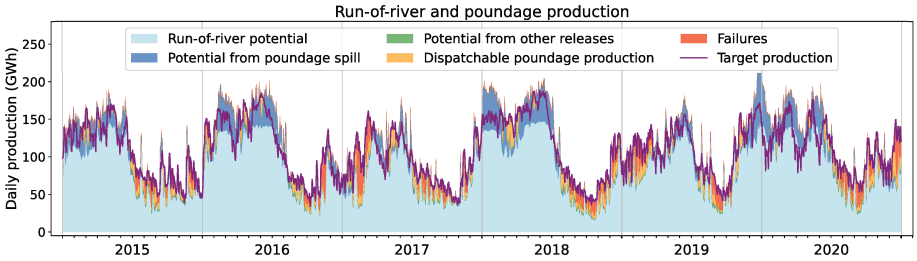

Figure A.1: National run-of-river plant production simulated in the model when forced by SAF_SPAZM. The purple line indicates the production that has been prescribed to the model and the red shows the difference between this production and the one simulated in the model when forced by SAF_SPAZM. The other colors refer to the nature of the flow that contributes to the production in the model. Light blue represents the gross potential of run-of-river plants, dark blue represents the potential of spill from poundage reservoir (water overflowing from the reservoir), green represents the potential from constrained releases of poundage reservoirs and lastly orange represents the dispatchable production, generated by the water specifically released from the poundage reservoirs for power generation.

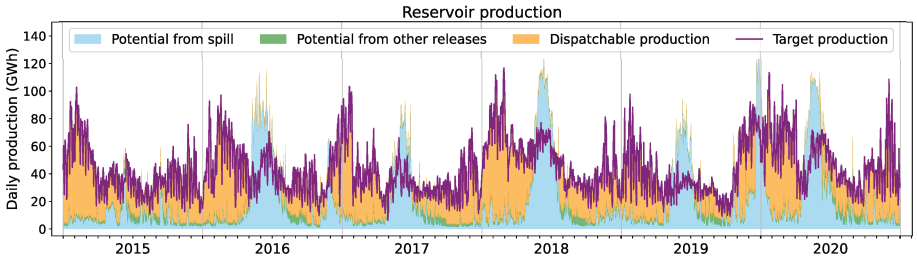

Figure A.2: National reservoir plant production simulated in the model when forced by SAF_SPAZM
The purple line indicates the production that has been prescribed to the model.The other colors refer to the nature of the flow that contributes to this production. Blue represents the gross potential from reservoir spill (water overflowing from the reservoir), green represents the potential from constrained releases of the reservoirs and lastly orange represents the production by the water that is specifically released from the reservoir for hydropower purposes.

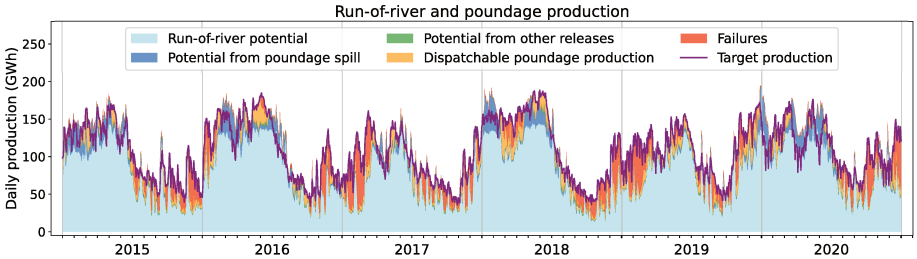

Figure A.3: National run-of-river plant production simulated in the model when forced by SAF_COM. The purple line indicates the production that has been prescribed to the model and the red shows the difference between this production and the one simulated in the model when forced by SAF_COM. The other colors refer to the nature of the flow that contributes to the production in the model. Light blue represents the gross potential of run-of-river plants, dark blue represents the potential of spill from poundage reservoir (water overflowing from the reservoir), green represents the potential from constrained releases of poundage reservoirs and lastly orange represents the dispatchable production, generated by the water specifically released from the poundage reservoirs for power generation.

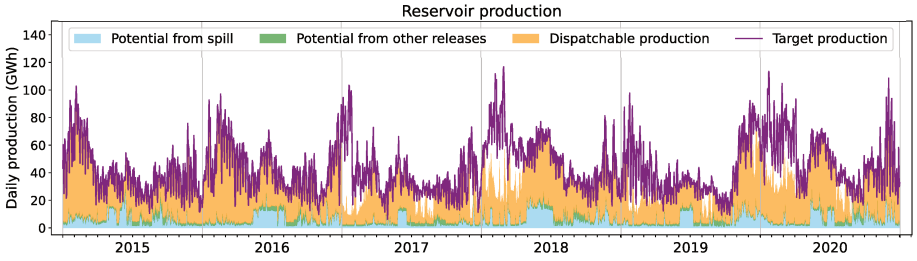

Figure A.4: National reservoir plant production simulated in the model when forced by SAF_COM
Purple line indicates the production that has been prescribed to the model.The other colors refer to the nature of the flow that contributes to this production. Blue represents the gross potential from reservoir spill (water overflowing from the reservoir), green represents the potential from constrained releases of the reservoirs and lastly orange represents the production by the water that is specifically released from the reservoir for hydropower purpose.

A.3 Conversion factors for hydropower generation

As presented in Table 3.1, our final dataset does not include all the hydropower plants installed in France. However, using annual production data of each plant provided by ODRÉ (2015, 2016, 2018), we can quantify the share of the national production provided by the power plants in our database. This enables us to compute a factor to convert the actual production of national time series (RTE, 2023b) into representative production in our model both for prescribing the production demand and comparing the results. The computation of such conversion factors is presented in Table A.1. It relies on the assumption that within each category of power plant, the geographical distribution of plants in our database is representative of all French power plants so that production ratios remain constant over time. This assumption is debatable as our database includes the largest power plants in terms of installed capacity, which are predominantly concentrated in certain regions, while smaller-scale plants may be located in watersheds not represented in our database (e.g., run-of-river plants on the River Seine for instance). However, as the missing plants have, by definition, a lower installed capacity than those in our database, their contribution to national production is lower and can reasonably be neglected.

	Total	Run-of-river	Poundage	Reservoir
National production in 2016 (RTE et al., 2016)	62.6	31.6	9.4	15.8
Total production from plants in national register in 2016 (ODRÉ, 2016)	57.6	27.5	9.0	15.6
compared to RTE et al. (2016)	*92.0%*	*87.0%*	*95.7*	*98.7%*
Total production from plants in the database in 2016 (based on ODRÉ (2016))	47.9	22.4	5.5	14.1
Coefficients 2016		70.9%	58.5%	89.3%
National production in 2018 (RTE et al., 2018)	66.9	31.3	10.9	18.8
Total production from plants in national register in 2018 (ODRÉ, 2018)	60.7	26.4	10.0	18.3
compared to RTE et al. (2018)	*90.7%*	*84.3%*	*91.7%*	*97.3%*
Total production from plants in the database in 2016 (based on ODRÉ (2018))	48.1	20.5	6.0	16.2
Coefficients 2018		65.5%	55.0%	86.1%
Conversion factors		**68.2%**	**56.8%**	**87.7%**

Table A.1: Comparison of the different available databases in terms of annual production (TWh) and calculation of conversion factors. n.a.=not available

APPENDIX B

Supplementary data for Part II

This chapter gathers supplementary data that provide more details to the work presented in Part II. This data is included in the Appendices of the article submitted to Applied Energy.

Contents

B.1 Convergence of the iterations 165
B.2 Thermal plants assumptions 169
B.3 2050 power mix 169
B.3.1 Power demand 169
B.3.2 Interconnections 170

B.1 Convergence of the iterations

Figure B.1 details the successive outputs of ORCHIDEE and EOLES-Dispatch models during the iterative process conducted in the ORCH_EOLES_res version for the 2019 weather year in the case of the 2019 power mix.

The simulation process begins with a first run of ORCHIDEE (referred to as *ORCHIDEE 0*), where no demand for reservoir production is prescribed. This initial run generates the first set of constraint time series - net inflow, maximum potential of spillage, constrained release, maximum potential of constrained release, and maximum capacity. These time series are then used as inputs for the first run of EOLES-Dispatch (*EOLES-Dispatch 1*). Reservoir production and initial reservoir stock simulated by EOLES-Dispatch are then provided to ORCHIDEE for the first simulation with hydropower operation (simulation *ORCHIDEE 1*). During this run, ORCHIDEE fails to fulfill the entire production simulated by EOLES-Dispatch, especially when it anticipates producing at full capacity during the summer. This is because the net inflows and spillages were overestimated in *ORCHIDEE 0*, as it was a "natural" simulation without operation of reservoirs, and therefore the actual storage and head could not be accounted for. New time series - for net inflow, maximum potential of spillage, constrained release, maximum potential of constrained release, and maximum capacity - are obtained from this simulation and are once again provided to the EOLES-Dispatch model, resulting in a new generation pattern (simulation *EOLES-Dispatch 2*). This revised production pattern can be almost fully satisfied by the ORCHIDEE model but does not meet the minimal production requirements of this new iteration.

Several iterations are conducted until the differences in dispatch cost and generation profiles obtained for two consecutive iterations of EOLES-Dispatch become sufficiently small, as depicted in Figure B.2. The convergence criteria we define is that the mean absolute difference in production between two consecutive iterations should be inferior to 10% of the mean production.

Figure B.3 illustrates the convergence of stock simulations. In the initial iteration, there is a significant disparity between the stock values simulated by EOLES-Dispatch and ORCHIDEE. This discrepancy arises primarily because the generation pattern simulated in EOLES-Dispatch cannot be fully met by ORCHIDEE. Additionally, the actual head levels simulated in ORCHIDEE lead to inflow computations that differ substantially from those transmitted to EOLES-Dispatch in the previous iteration. However, as the iterations progress, the disparity between the models reduces. By the last iteration (*EOLES 5* and *ORCHIDEE 5*), the difference is negligible, and the end-of-year storage values are comparable in both simulations.

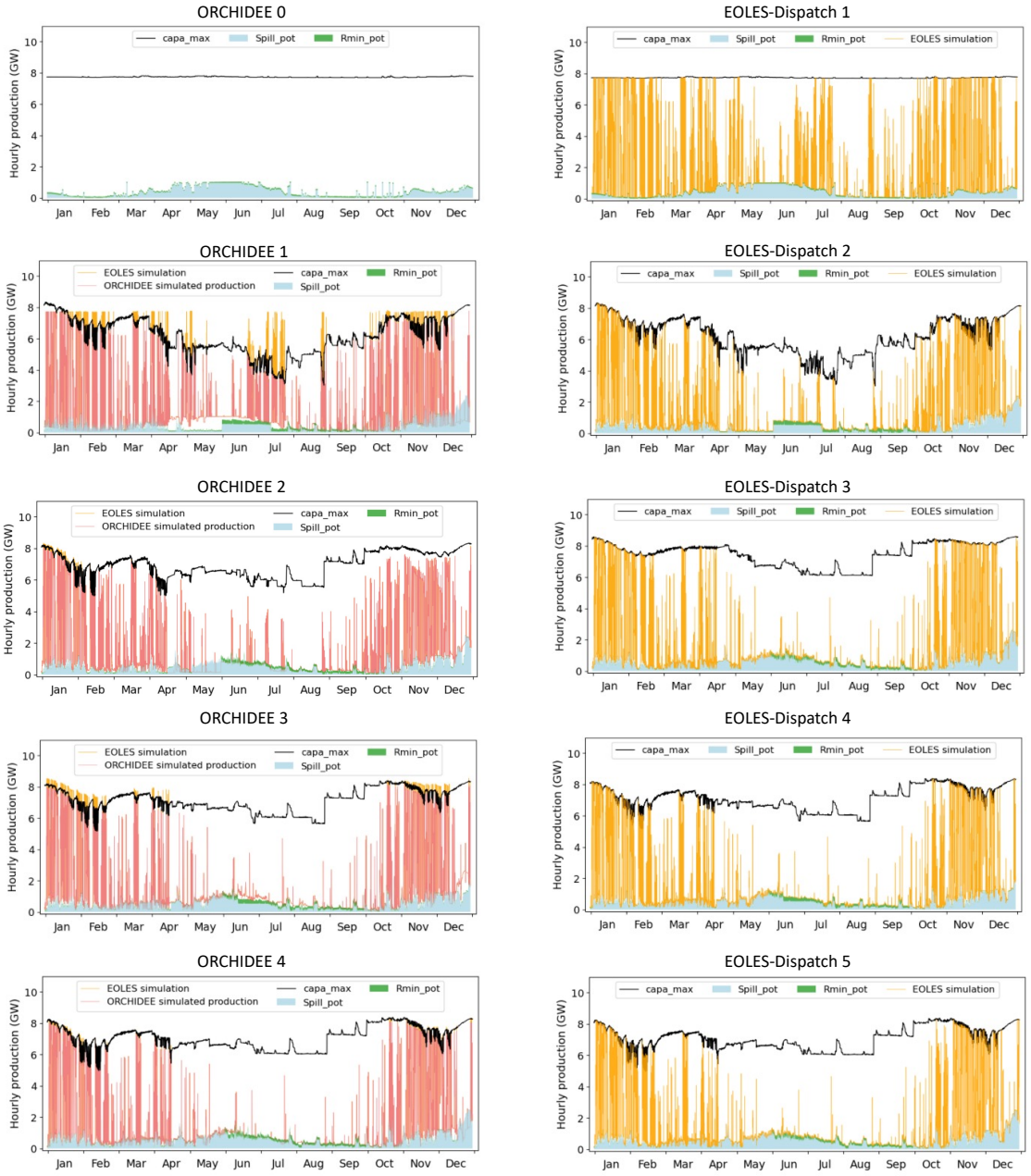

Figure B.1: Illustrative model outputs obtained for 2015 in successive iterations. Left: Outputs from the ORCHIDEE model. The orange line represents the prescribed demand time series (obtained from the previous run of EOLES-Dispatch), while the red line represents the reservoir production simulated by ORCHIDEE. The other colors represent constraint variables derived from ORCHIDEE simulations to constrain future EOLES simulations: the maximum capacity (black line), the generation potential from spillage (in blue), and the generation potential from constrained releases for irrigation and ecological flow (in green). Right: Outputs from EOLES-Dispatch model. The orange line is the simulated production.

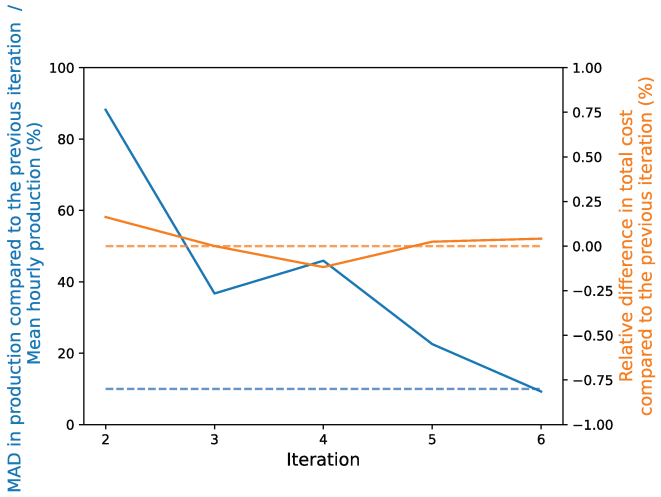

Figure B.2: Convergence of the dispatch cost and reservoir production across the iterations. The blue line shows the ratio, expressed in percentage, of the mean absolute difference (MAD) in hourly reservoir production between two consecutive iterations relative to the mean hourly production. The orange line indicates the relative difference in dispatch cost between two consecutive iterations.

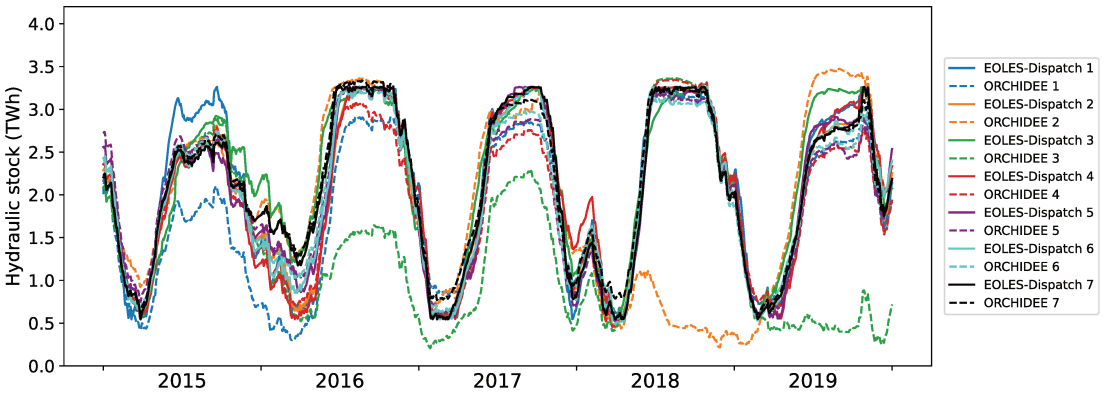

Figure B.3: Comparison of the hydraulic stock simulated over the 5 years in both models across the iterations of the coupling.

B.2 Thermal plants assumptions

Costs and operation constraints of thermal plants are taken from Leblanc (2023). We assume that gas plants run on hydrogen in the 2050 scenario mix and follow the assumption from RTE (2021) for the cost of hydrogen production.

Technology	Generation cost (€/MWh)	Start-up cost (€/MWh)	Ramping cost (€/MWh)	Min. off-time (h)
Nuclear	14.1	27.6	0.24	12
Coal (2019 mix)	37.2	120.4	1.58	8
CCGT - 2019 mix	45.1	78.4	0.49	2
OCGT - 2019 mix	61.8	21.8	0.63	1
CCGT - 2050 mix	250	78.4	0.40	2
OCGT - 2050 mix	270	21.8	0.63	1

Table B.1: Assumptions on generation, start-up and ramping costs, and minimum time-off periods for thermal technologies in the two power mix under study.

B.3 2050 power mix

B.3.1 Power demand

RTE (2021) provides assumptions about the evolution of annual demand in France, Italy, Spain, Germany, and the UK. An overall increase in electricity demand of 45% is assumed, with small disparities between countries (from +35% in France to +60% in the UK). This increase results from massive electrification, particularly in three sectors: transport, industry, and building.

However, no detail is provided about the hourly demand profiles. To construct hourly demand profiles for our 2050 scenario, we apply the annual increase factor to the hourly demand observed between 2015 and 2019. Since electricity consumption for transport and industry is relatively flexible, we assume that peak consumption does not increase as much as annual demand. We set the increase factor of peak demand at 40% of the initial factor (see B.4 for an illustration of this method in the case of France).

We use the same methodology to build hourly demand profiles in Switzerland and Belgium, based on the assumptions of annual changes from ENTSO-E (2011).

In addition to this demand increase, RTE (2021) also projects a power-to-gas demand to produce hydrogen through electrolysis as an end-use energy vector for industry or transports or as a fuel for thermal plants. This demand is assumed to be completely flexible. Our assumptions concerning hydrogen production are presented in Table B.2.

	France	Belgium	Germany	Switzerland	Italy	Spain	UK
Power-to-gas demand (TWh/year)	50	30	150	20	177	125	177
Electrolysis capacity (GW)	15	10	30	10	40	30	40

Table B.2: Assumptions regarding hydrogen production in the 2050 energy scenario. Source: ENTSO-E, 2011; RTE, 2021

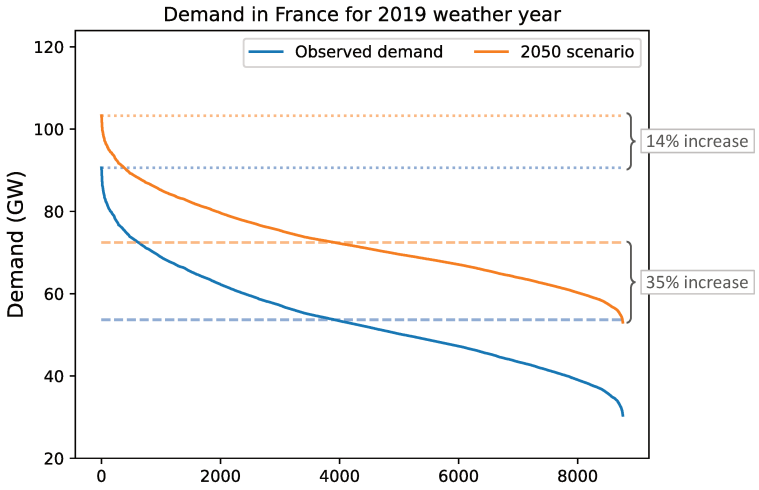

Figure B.4: Duration curves of observed demand and 2050 power demand scenario for the 2019 weather year in France.

B.3.2 Interconnections

RTE (2021) assume an increase in interconnection capacities between European countries. Assumptions taken in this study are presented in Tables B.3 and B.4.

	France →	Belgium →	Germany →	Switzerland →	Italy →	Spain →	UK →
→ France	-	1.8	1.5	3.4	0.4	3.8	2.6
→ Belgium	2.2	-	0	0	0	0	0.2
→ Germany	5	0	-	2	0	0	0
→ Switzerland	3	0	2.8	-	0	0	0
→ Italy	3	0	0	2.4	-	0	0
→ Spain	3	0	0	0	0	-	0
→ UK	3	0.7	0	0	0	0	-

Table B.3: Interconnections capacities in 2019 power mix.

	France →	Belgium →	Germany →	Switzerland →	Italy →	Spain →	UK →
→ France	-	3.6	3	6.8	4	7.6	5.2
→ Belgium	4.4	-	0	0	0	0	1.4
→ Germany	10	0	-	4	0	0	0
→ Switzerland	6	0	5.6	-	4.8	0	0
→ Italy	6	0	0	4.8	-	0	0
→ Spain	6	0	0	0	0	-	0
→ UK	6	1.4	0	0	0	0	-

Table B.4: Interconnections capacities in 2050 power mix scenario.

APPENDIX C

Supplementary data for Part III

This chapter gathers supplementary data that provide more details to the work presented in Part III.

Contents

C.1 Climate simulations 173
C.2 Simulation of electricity prices 177
C.3 Net load pattern 178

C.1 Climate simulations

Potential and effective evapotranspiration simulated by ORCHIDEE under the different climate scenarios are presented here.

Seasonal changes in river discharges simulated by ORCHIDEE under the different climate scenarios are presented in Fig. C.3.

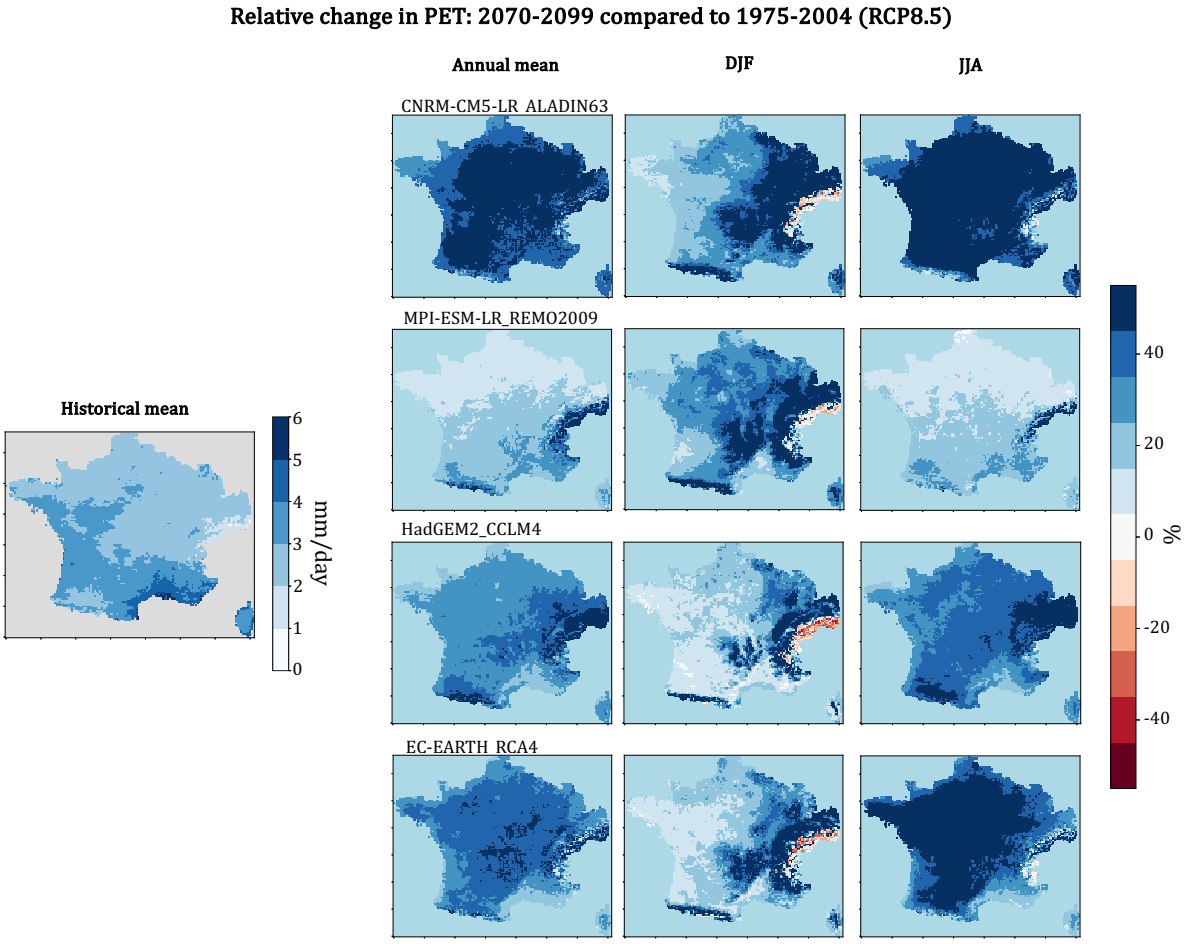

Figure C.1: Relative change in potential evapotranspiration (PET): 2070-2099 compared to 1975-2004 (RCP8.5). The changes are statistically significant everywhere (Student test with a p-value of 0.05).

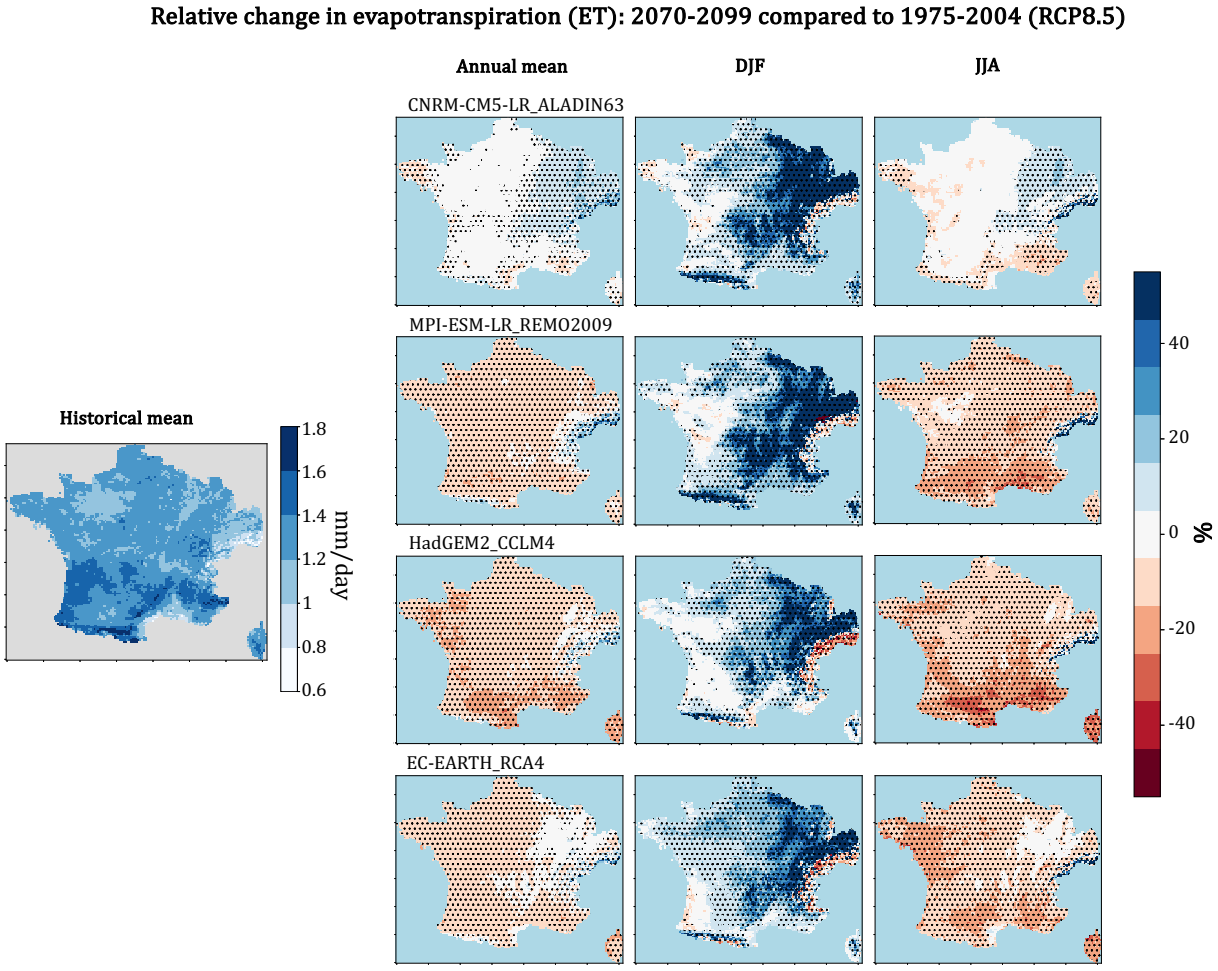

Figure C.2: Relative change in evapotranspiration (ET): 2070-2099 compared to 1975-2004 (RCP8.5). Black dots indicate the areas where the changes are statistically significant, which is assessed through a Student test (p-value of 0.05).

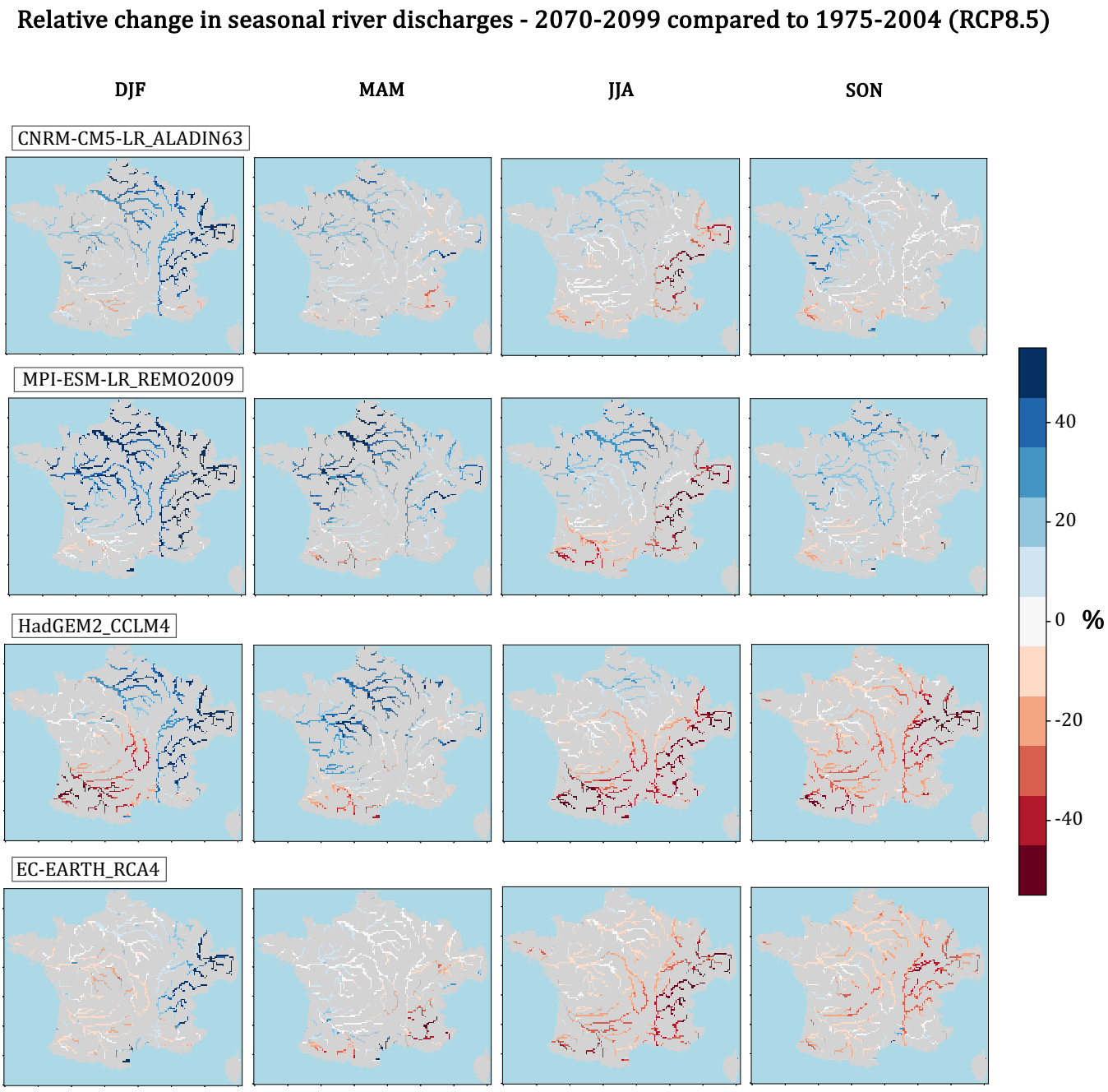

Figure C.3: Relative change in mean seasonal river discharge: 2070-2099 compared to 1975-2005 (RCP8.5). The discharges are shown for all grid points with an upstream area greater than 1000 km^2.

C.2 Simulation of electricity prices

Figure C.4 illustrates the hourly and daily power prices simulated by EOLES-Dispatch for the climate scenario EC-EARTH_RCA4 and the 2020 climatic period for the two power scenarios and compares these simulations with the power price observed in 2019 (data taken from ENTSO-E (2023)). We set 400€/MWh as the hourly power price if some unsatisfied demand occurs during the timestep.

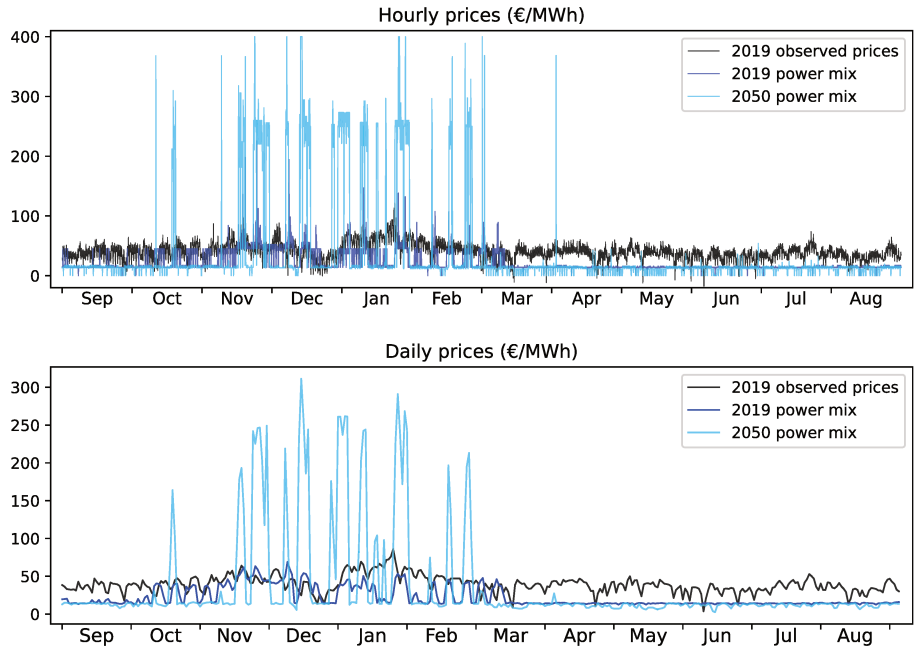

Figure C.4: Top: Hourly electricity price simulated by EOLES-Dispatch for the 2028-2029 hydrological year (EC-EARTH_RCA4 scenario) in both power scenarios and hourly observations of electricity price in 2019. Bottom: Daily electricity prices simulated by EOLES-Dispatch for the 2028-2029 hydrological years (EC-EARTH_RCA4 scenario) in both power scenarios and daily observations of electricity prices in 2019.

While the simulated price for the 2019 electricity mix in winter is in the same order of magnitude as the observed price in 2019, there are major differences in spring and summer. These discrepancies are due to the spatial scale of the model, which does not include exchanges with neighboring countries. During winter, the electricity produced by nuclear power plants in France may be exported to other European countries where the power price is higher, so gas power plants become the marginal technology in France, which increases the electricity price (see Section 5.7.1).

C.3 Net load pattern

The 2019 and 2050 power scenarios are distinguished by their net load pattern. Figure C.5 compares the net load (demand minus fatal production from solar PV, wind, and run-of-river) and the net-of-nuclear load, defined as the net load minus nuclear production potential, in both power scenarios. As a direct consequence of the integration of renewables, the net load is significantly lower in the 2050 power scenario. Additionally, the daily variability of net load is significantly higher in the 2050 scenario.

In the 2019 scenario, the peak in the net-of-nuclear load occurs in November, while in the 2050 power scenario, it occurs in January. This seasonal change is due to the limit on the availability of nuclear plants, which is higher in January than in November.

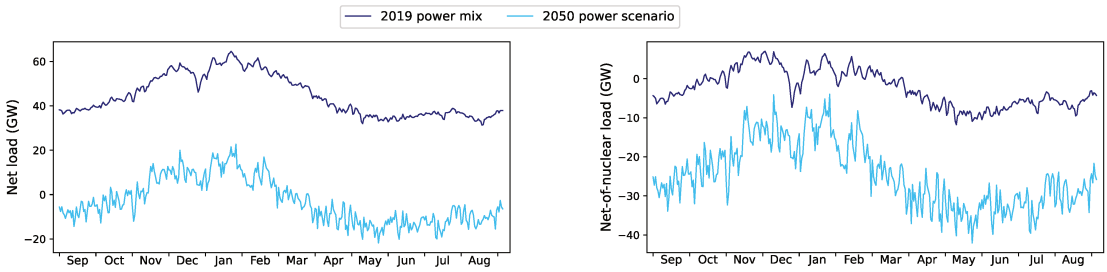

Figure C.5: Left: 2010-2029 interannual average of mean daily net load in both power scenarios. Right: 2010-2029 interannual average of mean daily net-of-nuclear load in both scenarios.

Bibliography

Abbott, Benjamin W. et al. (2019). "Human Domination of the Global Water Cycle Absent from Depictions and Perceptions". In: *Nature Geoscience* 12.7, pp. 533–540.

Abeshu, Guta Wakbulcho et al. (2023). *Enhancing the Representation of Water Management in Global Hydrological Models*. Preprint. Hydrology, pp. 1–41.

Allen Jr, LH (1990). "Plant responses to rising carbon dioxide and potential interactions with air pollutants". In: *Journal of Environmental Quality* 19.1, pp. 15–34.

Ambec, Stefan et al. (2003). "Decentralizing Hydro Power Production". In: *Canadian Journal of Economics/Revue canadienne d'économique* 36.3, pp. 587–607.

Baratgin, Laure et al. (2024 (submitted)[a]). "Coupling a power system model with a hydrological model improves the representation of hydropower flexibility". In: *Applied Energy*.

Baratgin, Laure et al. (2024 (submitted)[b]). "Modeling Hydropower Operations at the Scale of a Power Grid: A Demand-Based Approach". In: *EGUsphere*, pp. 1–52.

Barella-Ortiz, A. et al. (2013). "Potential Evaporation Estimation through an Unstressed Surface-Energy Balance and Its Sensitivity to Climate Change". In: *Hydrology and Earth System Sciences* 17.11, pp. 4625–4639.

Bassett, Kyle et al. (2018). "Energy Arbitrage and Market Opportunities for Energy Storage Facilities in Ontario". In: *Journal of Energy Storage* 20, pp. 478–484.

Biemans, H. et al. (2011). "Impact of Reservoirs on River Discharge and Irrigation Water Supply during the 20th Century". In: *Water Resources Research* 47.3.

Birman, Camille et al. (2017). "Precipitation analysis over the French Alps using a variational approach and study of potential added value of ground-based radar observations". In: *Journal of Hydrometeorology* 18.5, pp. 1425–1451.

Blakers, Andrew et al. (2021). "A Review of Pumped Hydro Energy Storage". In: *Progress in Energy* 3.2, p. 022003.

Boé, J. et al. (2009). "Projected Changes in Components of the Hydrological Cycle in French River Basins during the 21st Century". In: *Water Resources Research* 45.8.

Bonnema, Matthew et al. (2019). "Assessing the Potential of the Surface Water and Ocean Topography Mission for Reservoir Monitoring in the Mekong River Basin". In: *Water Resources Research* 55.1, pp. 444–461.

Boroomandnia, Arezoo et al. (2024). "Eco-economic comparison of batteries and pumped-hydro systems at the micro scale in buildings". In: *Energy Conversion and Management* 312, p. 118527.

Boßmann, Tobias et al. (2015). "The shape of future electricity demand: Exploring load curves in 2050s Germany and Britain". In: *Energy* 90, pp. 1317–1333.

Brandão, Joao Luiz B. (2010). "Performance of the Equivalent Reservoir Modelling Technique for Multi-Reservoir Hydropower Systems". In: *Water Resources Management* 24.12, pp. 3101–3114.

Brinkerink, Maarten et al. (2021). "Building and Calibrating a Country-Level Detailed Global Electricity Model Based on Public Data". In: *Energy Strategy Reviews* 33, p. 100592.

Brown, Tom et al. (2017). "PyPSA: Python for Power System Analysis". In: *Journal of open research software*.

Cattiaux, Julien et al. (2013). "European Temperatures in CMIP5: Origins of Present-Day Biases and Future Uncertainties". In: *Climate Dynamics* 41.11, pp. 2889–2907.

CFBR (2021). *Les barrages en France*.

Chowdhury, A. F. M. Kamal et al. (2021). "The Greater Mekong's Climate-Water-Energy Nexus: How ENSO-Triggered Regional Droughts Affect Power Supply and CO2 Emissions". In: *Earth's Future* 9.3, e2020EF001814.

Christidis, Nikolaos et al. (2022). "Human Influence on Seasonal Precipitation in Europe". In: *Journal of Climate* 35.15, pp. 5215–5231.

Chyong, Chi Kong et al. (2022). "A Unit Commitment and Economic Dispatch Model of the GB Electricity Market – Formulation and Application to Hydro Pumped Storage". In: *Energy Policy* 170, p. 113213.

Cloke, Hannah L. et al. (2013). "Modelling Climate Impact on Floods with Ensemble Climate Projections". In: *Quarterly Journal of the Royal Meteorological Society* 139.671, pp. 282–297.

Collignan, Julie et al. (2024 (submitted)). "Identifying and Quantifying the Impact of Climatic and Non-Climatic Drivers on River Discharge in Europe". In.

Coron, L et al. (2014). "On the lack of robustness of hydrologic models regarding water balance simulation: a diagnostic approach applied to three models of increasing complexity on 20 mountainous catchments". In: *Hydrology and Earth System Sciences* 18.2, pp. 727–746.

Corre, Lola et al. (2023). "Storylines to synthesize the range of future plausible climates over France for hydrological studies". In: *AG EURO-CORDEX 2023*.

Crampes, Claude (2014). *Les stations de transfert d'énergie par pompage (STEP)*. Tech. rep.

Cronin, Jennifer et al. (2018). "Climate Change Impacts on the Energy System: A Review of Trends and Gaps". In: *Climatic Change* 151.2, pp. 79–93.

Damm, Andrea et al. (2017). "Impacts of +2°C Global Warming on Electricity Demand in Europe". In: *Climate Services* 7, pp. 12–30.

Dang, Thanh Duc et al. (2020). "On the Representation of Water Reservoir Storage and Operations in Large-Scale Hydrological Models: Implications on Model Parameterization and Climate Change Impact Assessments". In: *Hydrology and Earth System Sciences* 24.1, pp. 397–416.

De Felice, Matteo (2021). *ENTSO-E Pan-European Climatic Database (PECD 2021.3) in Parquet format*.

Dimanchev, Emil G. et al. (2021). "The Role of Hydropower Reservoirs in Deep Decarbonization Policy". In: *Energy Policy* 155, p. 112369.

Döll, P. et al. (2012). "Impact of Water Withdrawals from Groundwater and Surface Water on Continental Water Storage Variations". In: *Journal of Geodynamics* 59–60, pp. 143–156.

Duethmann, Doris et al. (2020). "Why does a conceptual hydrological model fail to correctly predict discharge changes in response to climate change?" In: *Hydrology and Earth System Sciences* 24.7, pp. 3493–3511.

EDF (2017). *LES STEP : PERSPECTIVES DE DÉVELOPPEMENT*. Tech. rep. EDF.

Ehret, U. et al. (2012). “HESS Opinions "Should We Apply Bias Correction to Global and Regional Climate Model Data?"” In: *Hydrology and Earth System Sciences* 16.9, pp. 3391–3404.

Ek Fälth, Hanna et al. (2022). *Exploring Trade-Offs between Aggregated and Turbine-Level Representations of Hydropower in Optimization Models*. SSRN Scholarly Paper. Rochester, NY.

Emmanuel, Michael et al. (2020). “A Review of Power System Planning and Operational Models for Flexibility Assessment in High Solar Energy Penetration Scenarios”. In: *Solar Energy*. Special Issue on Grid Integration 210, pp. 169–180.

ENTSO-E (2011). *TYNDP 2022, Scenario Report*. Tech. rep. ENTSO-E.

— (2023). *Transparency platform*.

European Commission et al. (2019). *JRC Hydro-power database*. Tech. rep. JRC.

Evin, Guillaume et al. (2021). “Balanced Estimate and Uncertainty Assessment of European Climate Change Using the Large EURO-CORDEX Regional Climate Model Ensemble”. In: *Earth System Dynamics* 12.4, pp. 1543–1569.

Fatichi, S. et al. (2015). “High-Resolution Distributed Analysis of Climate and Anthropogenic Changes on the Hydrology of an Alpine Catchment”. In: *Journal of Hydrology* 525, pp. 362–382.

Fekete, Balázs M. et al. (2010). “Millennium Ecosystem Assessment Scenario Drivers (1970–2050): Climate and Hydrological Alterations”. In: *Global Biogeochemical Cycles* 24.4.

France Stratégie (2024). *Prélèvements et consommations d’eau : quels enjeux et usages ?* Tech. rep. France Stratégie.

François, Baptiste (2013). “Gestion optimale d’un réservoir hydraulique multiusages et changement climatique. Modéles, projections et incertitudes: Application á la réserve de Serre-Ponçon”. PhD thesis. Université de Grenoble.

Fumiére, Quentin et al. (2020). “Extreme Rainfall in Mediterranean France during the Fall: Added Value of the CNRM-AROME Convection-Permitting Regional Climate Model”. In: *Climate Dynamics* 55.1, pp. 77–91.

Gaudard, Ludovic (2014). “The Future of Hydropower in Europe: Interconnecting Climate, Markets and Policies”. In: *environmental science*, p. 10.

Global Energy Observatory et al. (2019). *Global Power Plant Database v1.2.0*. Tech. rep. GEO.

Gøtske, Ebbe Kyhl et al. (2021). “Future Operation of Hydropower in Europe under High Renewable Penetration and Climate Change”. In: *iScience* 24.9, p. 102999.

Gottardi, Frédéric et al. (2008). “Régionalisation des précipitations sur les massifs montagneux français á l’aide de régressions locales et par types de temps”. In: *Climatologie* 5, pp. 7–25.

Habets, Florence et al. (1999). “Simulation of the water budget and the river flows of the Rhone basin”. In: *Journal of Geophysical Research: Atmospheres* 104.D24, pp. 31145–31172.

Haddeland, Ingjerd et al. (2006). “Anthropogenic Impacts on Continental Surface Water Fluxes”. In: *Geophysical Research Letters* 33.8, p. L08406.

Haddeland, Ingjerd et al. (2014). “Global Water Resources Affected by Human Interventions and Climate Change”. In: *Proceedings of the National Academy of Sciences* 111.9, pp. 3251–3256.

Hagemann, Stefan et al. (2011). “Impact of a Statistical Bias Correction on the Projected Hydrological Changes Obtained from Three GCMs and Two Hydrology Models”. In: *Journal of Hydrometeorology* 12.4, pp. 556–578.

Hamududu, Byman et al. (2012). "Assessing Climate Change Impacts on Global Hydropower". In: *Energies* 5, pp. 305–322.

Hanasaki, N. et al. (2008). "An Integrated Model for the Assessment of Global Water Resources – Part 1: Model Description and Input Meteorological Forcing". In: *Hydrology and Earth System Sciences* 12.4, pp. 1007–1025.

Hanasaki, Naota et al. (2006). "A Reservoir Operation Scheme for Global River Routing Models". In: *Journal of Hydrology* 327.1-2, pp. 22–41.

Hanasaki, Naota et al. (2018). "A Global Hydrological Simulation to Specify the Sources of Water Used by Humans". In: *Hydrology and Earth System Sciences* 22.1, pp. 789–817.

Hausfather, Zeke et al. (2020). "RCP8.5 Is a Problematic Scenario for near-Term Emissions". In: *Proceedings of the National Academy of Sciences of the United States of America* 117.45, pp. 27791–27792.

Hawkins, Ed et al. (2009). "The Potential to Narrow Uncertainty in Regional Climate Predictions". In.

Hendrickx, F. et al. (2013). "Impact of Warming Climate on Water Management for the Ariége River Basin (France)". In: *Hydrological Sciences Journal* 58.5, pp. 976–993.

Hill, Joy et al. (2021). "The Effects of Climate Change on Interregional Electricity Market Dynamics on the U.S. West Coast". In.

Hörsch, Jonas et al. (2018). "PyPSA-Eur: An Open Optimisation Model of the European Transmission System". In: *Energy Strategy Reviews* 22, pp. 207–215.

Huang, Peng et al. (2022). "Vulnerability of Water Resource Management to Climate Change: Application to a Pyrenean Valley". In: *Journal of Hydrology: Regional Studies* 44, p. 101241.

Huang, Peng et al. (2024). *Multi-Objective Calibration and Evaluation of the ORCHIDEE Land Surface Model over France at High Resolution.*

Huertas-Hernando, Daniel et al. (2017). "Hydro Power Flexibility for Power Systems with Variable Renewable Energy Sources: An IEA Task 25 Collaboration". In: *WIREs Energy and Environment* 6.1, e220.

Huss, Matthias et al. (2018). "Global-Scale Hydrological Response to Future Glacier Mass Loss". In: *Nature Climate Change* 8.2, pp. 135–140.

Ibanez, Eduardo et al. (2014). "Enhancing Hydropower Modeling in Variable Generation Integration Studies". In: *Energy* 74, pp. 518–528.

IEA (2021). *Conditions and requirements for the technical feasibility of a power system with a high share of renewables in France towards 2050.* Tech. rep. IEA.

— (2023). *Managing Seasonal and Interannual Variability of Renewables.* Tech. rep. IEA.

IPCC (2021a). *Climate Change 2021: The Physical Science Basis. Contribution of Working Group I to the Sixth Assessment Report of the Intergovernmental Panel on Climate Change.* Ed. by V. Masson-Delmotte et al. Cambridge, UK and New York, NY, USA: Cambridge University Press.

— (2021b). "Summary for Policymakers". In: *Climate Change 2021: The Physical Science Basis. Contribution of Working Group I to the Sixth Assessment Report of the Intergovernmental Panel on Climate Change.* Ed. by V. Masson-Delmotte et al. Cambridge, UK and New York, NY, USA: Cambridge University Press.

— (2022a). *Climate Change 2022: Impacts, Adaptation and Vulnerability. Contribution of Working Group II to the Sixth Assessment Report of the Intergovernmental Panel on Climate Change.* Ed. by H. O. Pörtner et al. Cambridge, UK and New York, NY, USA: Cambridge University Press.

— (2022b). *Climate Change 2022: Mitigation of Climate Change. Contribution of Working Group III to the Sixth Assessment Report of the Intergovernmental Panel on Climate Change*. Ed. by P.R. Shukla et al. Cambridge, UK and New York, NY, USA: Cambridge University Press.

IRENA (2023). *Water for hydrogen production*. Tech. rep. IRENA.

Kintner-Meyer, Michael CW et al. (2012). *National assessment of energy storage for grid balancing and arbitrage: Phase 1, WECC*. Tech. rep. Pacific Northwest National Lab.(PNNL), Richland, WA (United States).

Krinner, Gerhard et al. (2005). "A Dynamic Global Vegetation Model for Studies of the Coupled Atmosphere-Biosphere System". In: *Global Biogeochemical Cycles* 19.1, p. 1015.

Larsen, M. A. D. et al. (2020). "Climate Change Impacts on Trends and Extremes in Future Heating and Cooling Demands over Europe". In: *Energy and Buildings* 226, p. 110397.

Laurent, Léa et al. (2020). "The Impact of Climate Change and Glacier Mass Loss on the Hydrology in the Mont-Blanc Massif". In: *Scientific Reports* 10.1, p. 10420.

Leblanc, Clément (2023). "Microeconomic analysis of subsidy mechanisms for power generation from wind and solar sources". PhD thesis. Marne-la-vallée, ENPC.

Lehner, Bernhard et al. (2005). "The Impact of Global Change on the Hydropower Potential of Europe: A Model-Based Analysis". In: *Energy Policy*, p. 17.

Lehner, Bernhard et al. (2011). "High-resolution Mapping of the World's Reservoirs and Dams for Sustainable River-flow Management". In: *Frontiers in Ecology and the Environment* 9.9, pp. 494–502.

Lehner, Flavio et al. (2020). "Partitioning Climate Projection Uncertainty with Multiple Large Ensembles and CMIP5/6". In: *Earth System Dynamics* 11.2, pp. 491–508.

Lemaitre-Basset, Thibault et al. (2022). "Evapotranspiration in Hydrological Models under Rising CO2: A Jump into the Unknown". In: *Climatic Change* 172.3, p. 36.

Liu, Hailiang (2019). "A High-Resolution Hydro Power Time-Series Model for Energy Systems Analysis: Validated with Chinese Hydro Reservoirs". In: *Applied Energy* 239, p. 9. arXiv: 1810.10347.

Loisel, Rodica et al. (2021). "Market Strategies for Large-Scale Energy Storage: Vertical Integration versus Stand-Alone Player". In: *Energy Policy* 151, p. 112169.

Lucas-Picher, Philippe et al. (2021). "Convection-Permitting Modeling with Regional Climate Models: Latest Developments and next Steps". In: *WIREs Climate Change* 12.6, e731.

Lund, Jay et al. (1999). "Derived Operating Rules for Reservoirs in Series or in Parallel". In: *Journal of Water Resources Planning and Management-asce - J WATER RESOUR PLAN MAN-ASCE* 125.3, pp. 143–153.

Lundquist, Jessica et al. (2019). "Our Skill in Modeling Mountain Rain and Snow Is Bypassing the Skill of Our Observational Networks". In.

Macian-Sorribes, Hector et al. (2020). "Inferring Efficient Operating Rules in Multireservoir Water Resource Systems: A Review". In: *WIREs Water* 7.1, e1400.

Magand, Claire et al. (2018). "Hybridation de réanalyses météorologiques de surface pour les zones de montagne: exemple du produit DuO sur le bassin de la Durance". In: *La Houille Blanche* 3, pp. 77–85.

Marshall, Adrienne M et al. (2022). "Hydroelectricity Modeling for Low-Carbon and No-Carbon Grids: Empirical Operational Parameters for Optimization and Dispatch Models". In: *Earth's Future* 10.8, e2021EF002503.

Marson, Paola et al. (2024). "Explore2 – Rapport de synthése sur les projections climatiques régionalisées". report. METEO FRANCE ; INRAE ; Institut Pierre-Simon Laplace.

Maurer, E. P. et al. (2014). "Bias Correction Can Modify Climate Model Simulated Precipitation Changes without Adverse Effect on the Ensemble Mean". In: *Hydrology and Earth System Sciences* 18.3, pp. 915–925.

McManamay, R. A. et al. (2016). "Classification of US Hydropower Dams by Their Modes of Operation". In: *River Research and Applications* 32.7, pp. 1450–1468.

Nair, Akhilesh S. et al. (2022). "Exploring the Potential of SWOT Mission for Reservoir Monitoring in Mahanadi Basin". In: *Advances in Space Research* 69.3, pp. 1481–1493.

Nazemi, A. et al. (2015a). "On inclusion of water resource management in Earth system models, Part 1: Problem definition and representation of water demand". en. In: *Hydrology and Earth System Sciences* 19.1, pp. 33–61.

— (2015b). "On inclusion of water resource management in Earth system models, Part 1: Problem definition and representation of water demand". en. In: *Hydrology and Earth System Sciences* 19.1, pp. 33–61.

— (2015c). "On inclusion of water resource management in Earth system models, Part 2: Representation of water supply and allocation and opportunities for improved modeling". en. In: *Hydrology and Earth System Sciences* 19.1, pp. 63–90.

Neverre, Noeḿie (2015). "Rareté de l'eau et relations interbassins en Méditerranée sous changements globaux. Développement et application d'un modéle hydroéconomique á large échelle". PhD thesis. Université Paris-Saclay (ComUE).

Newman, Andrew J. et al. (2017). "Benchmarking of a Physically Based Hydrologic Model". In: *Journal of Hydrometeorology* 18.8, pp. 2215–2225.

Nguyen-Quang, Trung et al. (2018). "ORCHIDEE-ROUTING: Revising the River Routing Scheme Using a High-Resolution Hydrological Database". In: *Geoscientific Model Development* 11.12, pp. 4965–4985.

Noilhan, J et al. (1996). "The ISBA land surface parameterisation scheme". In: *Global and planetary Change* 13.1-4, pp. 145–159.

O'Connell et al. (2019). "Sensitivity of Western US power system dynamics to droughts compounded with fuel price variability". In: *Applied Energy* 247, pp. 745–754.

ODRÉ (2015). *Registre 2015 des installations de production raccordées au réseau de transport d'électricité.*

— (2016). *Registre 2016 des installations de production raccordées au réseau de transport d'électricité.*

— (2018). *Registre national des installations de production et de stockage d'électricité (au 31 décembre 2018).*

— (2022). *Registre 2022 des installations de production raccordées au réseau de transport d'électricité.*

Oikonomou, Konstantinos et al. (2022). "Core Process Representation in Power System Operational Models: Gaps, Challenges, and Opportunities for Multisector Dynamics Research". In: *Energy* 238, p. 122049.

Oleson, Keith W (2010). "Technical description of version 4.0 of theCommunity Land Model (CLM)". In: *NCAR Technical Note*, p. 257.

Oudin, Ludovic et al. (2008). "Spatial Proximity, Physical Similarity, Regression and Ungaged Catchments: A Comparison of Regionalization Approaches Based on 913 French Catchments". In: *Water Resources Research* 44.3.

Pastor, A. V. et al. (2014). "Accounting for Environmental Flow Requirements in Global Water Assessments". In: *Hydrology and Earth System Sciences* 18.12, pp. 5041–5059.

Perera, A. T. D. et al. (2020). "Quantifying the Impacts of Climate Change and Extreme Climate Events on Energy Systems". In: *Nature Energy* 5.2, pp. 150–159.

Perez-Diaz, Juan I. et al. (2020). "Medium-Term Scheduling of a Hydropower Plant Participating as a Price-Maker in the Automatic Frequency Restoration Reserve Market". In: *106399*.

Perrin, Charles et al. (2003). "Improvement of a parsimonious model for streamflow simulation". In: *Journal of hydrology* 279.1-4, pp. 275–289.

Pokhrel, Yadu N. et al. (2016). "Recent Progresses in Incorporating Human Land–Water Management into Global Land Surface Models toward Their Integration into Earth System Models". In: *WIREs Water* 3.4, pp. 548–574.

Pokhrel, Yadu Nath et al. (2008). "A Grid Based Assessment of Global Theoretical Hydropower Potential". In: *Proceedings of Hydraulic Engineering* 52, pp. 7–12.

Polcher, Jan et al. (2023). "Hydrological modelling on atmospheric grids; using graphs of sub-grid elements to transport energy and water". In: *EGUsphere*, pp. 1–34.

Quintana-Segui, Pere et al. (2008). "Analysis of near-surface atmospheric variables: Validation of the SAFRAN analysis over France". In: *Journal of applied meteorology and climatology* 47.1, pp. 92–107.

Ralston Fonseca, Francisco et al. (2021). "Effects of climate change on capacity expansion decisions of an electricity generation fleet in the Southeast US". In: *Environmental Science & Technology* 55.4, pp. 2522–2531.

Reynolds, CA et al. (2000). "Estimating soil water-holding capacities by linking the Food and Agriculture Organization soil map of the world with global pedon databases and continuous pedotransfer functions". In: *Water Resources Research* 36.12, pp. 3653–3662.

Rheinheimer, David E. et al. (2023). "Hydropower Representation in Water and Energy System Models: A Review of Divergences and Call for Reconciliation". In: *Environmental Research: Infrastructure and Sustainability* 3.1, p. 012001.

Richter, Brian D et al. (2007). "Restoring environmental flows by modifying dam operations". In: *Ecology and society* 12.1.

Robin, Yoann et al. (2023). *PROJECTIONS CLIMATIQUES RÉGIONALISÉES : CORRECTION DE BIAIS ET CHANGEMENTS FUTURS*. Tech. rep.

RTE (2021). *Futurs énergétiques 2050*.

— (2023a). *BILAN ÉLECTRIQUE 2023*.

— (2023b). *Generated power aggregated by sector*.

— (2023c). *Generated power aggregated by unit*.

— (2023d). *Hydraulic stock*.

— (2024a). *Balancing capacity - Procured reserves*.

— (2024b). *Balancing energy - Volumes per energy type*.

RTE et al. (2016). *Panorama de l'électricité renouvelable en 2016*.

— (2018). *Panorama de l'électricité renouvelable en 2018*.

Sauquet, Eric et al. (2022). *Points et supports de simulation des projections hydrologiques*. Tech. rep. INRAE ; BRGM.

Schaefli, Bettina et al. (2019). "The Role of Glacier Retreat for Swiss Hydropower Production". In: *Renewable Energy* 132, pp. 615–627.

Schapi (2022). *HydroPortail*.

Scharff, Richard et al. (2014). "A Description of the Operative Decision-Making Process of a Power Generating Company on the Nordic Electricity Market". In: *Energy Systems* 5.2, pp. 349–369.

Shaad, Kashif (2018). "Evolution of River-Routing Schemes in Macro-Scale Models and Their Potential for Watershed Management". In: *Hydrological Sciences Journal* 63.7, pp. 1062–1077.

Sheng, Mingyang et al. (2017). "Evaluation of the Runoff and River Routing Schemes in the Community Land Model of the Yellow River Basin". In: *Journal of Advances in Modeling Earth Systems* 9.8, pp. 2993–3018.

Shi, Xunpeng et al. (2020). "Quantification of Fresh Water Consumption and Scarcity Footprints of Hydrogen from Water Electrolysis: A Methodology Framework". In: *Renewable Energy* 154, pp. 786–796.

Shirizadeh, Behrang et al. (2021). "Low-Carbon Options for the French Power Sector: What Role for Renewables, Nuclear Energy and Carbon Capture and Storage?" In: *Energy Economics* 95, p. 105004.

Shirizadeh, Behrang et al. (2022). "How sensitive are optimal fully renewable power systems to technology cost uncertainty?" In: *The Energy Journal* 43.1, pp. 43–75.

Siala, Kais et al. (2021). "Solar energy and regional coordination as a feasible alternative to large hydropower in Southeast Asia". In: *Nature Communications* 12.1, p. 4159.

Soubeyroux, Jean-Michel (2023). *Impact du changement climatique sur l'eau en France.*

Staffell, Iain et al. (2016). "Maximising the Value of Electricity Storage". In: *Journal of Energy Storage* 8, pp. 212–225.

Staffell, Iain et al. (2023). "A Global Model of Hourly Space Heating and Cooling Demand at Multiple Spatial Scales". In: *Nature Energy* 8.12, pp. 1328–1344.

Stahl, K. et al. (2010). "Streamflow Trends in Europe: Evidence from a Dataset of near-Natural Catchments". In: *Hydrology and Earth System Sciences* 14.12, pp. 2367–2382.

Stephens, Graeme et al. (2023). "The First 30 Years of GEWEX". In: *Bulletin of the American Meteorological Society* 104.1, E126–E157.

Sterl, Sebastian et al. (2020). "Smart Renewable Electricity Portfolios in West Africa". In: *Nature Sustainability* 3.9, pp. 710–719.

Stoft, Steven (2002). *Power system economics: designing markets for electricity.* Vol. 468. IEEE press Piscataway.

Su, Yufei et al. (2020). "An Open Source Model for Quantifying Risks in Bulk Electric Power Systems from Spatially and Temporally Correlated Hydrometeorological Processes". In: *Environmental Modelling & Software* 126.C, p. 104667.

Sutanudjaja, Edwin H. et al. (2018). "PCR-GLOBWB 2: A 5 Arcmin Global Hydrological and Water Resources Model". In: *Geoscientific Model Development* 11.6, pp. 2429–2453.

Tabary, Pierre et al. (2012). "A 10-year (1997—2006) reanalysis of Quantitative Precipitation Estimation over France: methodology and first results". In: *IAHS-AISH publication* 351, pp. 255–260.

Takata, Kumiko et al. (2003). "Development of the minimal advanced treatments of surface interaction and runoff". In: *Global and planetary Change* 38.1-2, pp. 209–222.

Tamang, Sagar K. et al. (2020). "Linking Global Changes of Snowfall and Wet-Bulb Temperature". In: *Journal of Climate* 33.1, pp. 39–59.

Tantet, Alexis et al. (2019). "E4clim 1.0: The Energy for a Climate Integrated Model: Description and Application to Italy". In: *Energies* 12.22, p. 4299.

Tarroja, Brian et al. (2019). "Implications of Hydropower Variability from Climate Change for a Future, Highly-Renewable Electric Grid in California". In: *Applied Energy* 237, pp. 353–366.

Telteu, Camelia-Eliza et al. (2021). "Understanding Each Other's Models: A Standard Representation of Global Water Models to Support Improvement, Intercomparison, and Communication". In: p. 56.

Tobin, I et al. (2018). "Vulnerabilities and Resilience of European Power Generation to 1.5 °C, 2 °C and 3 °C Warming". In: *Environmental Research Letters* 13.4, p. 044024.

Tonelli, Davide et al. (2023). "Global Land and Water Limits to Electrolytic Hydrogen Production Using Wind and Solar Resources". In: *Nature Communications* 14.1, p. 5532.

Tour, Marie-Alix Dupré la (2023). "Towards a decarbonized energy system in Europe in 2050: impact of vector coupling and renewable deployment limits". PhD thesis. Paris, EHESS.

Turner, S. W. D. et al. (2019). "Compound Climate Events Transform Electrical Power Shortfall Risk in the Pacific Northwest". In: *Nature Communications* 10.1, p. 8.

Turner, Sean W.D. et al. (2017). "Examining Global Electricity Supply Vulnerability to Climate Change Using a High-Fidelity Hydropower Dam Model". In: *Science of The Total Environment* 590–591, pp. 663–675.

Turner, Sean WD et al. (2022). "Simulation of hydropower at subcontinental to global scales: a state-of-the-art review". In: *Environmental Research Letters*.

Van Stiphout, Arne et al. (2017). "The Impact of Operating Reserves on Investment Planning of Renewable Power Systems". In: *IEEE Transactions on Power Systems* 32.1, pp. 378–388.

van Vliet, Michelle T H et al. (2013). "Water Constraints on European Power Supply under Climate Change: Impacts on Electricity Prices". In: *Environmental Research Letters* 8.3, p. 035010.

van Vliet, Michelle T. H. et al. (2016a). "Power-Generation System Vulnerability and Adaptation to Changes in Climate and Water Resources". In: *Nature Climate Change* 6.4, pp. 375–380.

van Vliet, M.T.H. et al. (2016b). "Multi-Model Assessment of Global Hydropower and Cooling Water Discharge Potential under Climate Change". In: *Global Environmental Change* 40, pp. 156–170.

Verfaillie, Deborah et al. (2017). "The Method ADAMONT v1.0 for Statistical Adjustment of Climate Projections Applicable to Energy Balance Land Surface Models (GMD Discussions)". In: *Geoscientific Model Development Discussions* 10, pp. 1–42.

Vicente-Serrano, S. M. et al. (2019). "Climate, Irrigation, and Land Cover Change Explain Streamflow Trends in Countries Bordering the Northeast Atlantic". In: *Geophysical Research Letters* 46.19, pp. 10821–10833.

Voisin, N. et al. (2016). "Vulnerability of the US Western Electric Grid to Hydro-Climatological Conditions: How Bad Can It Get?" In: *Energy* 115, pp. 1–12.

Voisin, N. et al. (2018). "Opportunities for Joint Water–Energy Management: Sensitivity of the 2010 Western U.S. Electricity Grid Operations to Climate Oscillations". In: *Bulletin of the American Meteorological Society* 99.2, pp. 299–312.

Voisin, Nathalie et al. (2020). "Impact of Climate Change on Water Availability and Its Propagation through the Western U.S. Power Grid". In: *Applied Energy* 276, p. 115467.

Wagner, T. et al. (2017). "Impacts of Climate Change on Stream Flow and Hydro Power Generation in the Alpine Region". In: *Environmental Earth Sciences* 76.1, p. 4.

Wasti, Asphota et al. (2022). "Climate Change and the Hydropower Sector: A Global Review". In: *WIREs Climate Change* 13.2, e757.

Wessel, Michael et al. (2020). “Economic feasibility of semi-underground pumped storage hydropower plants in open-pit mines”. In: *Energies* 13.16, p. 4178.

Wood, Allen J et al. (2013). *Power generation, operation, and control*. John Wiley & Sons.

Yalew, Seleshi G. et al. (2020). “Impacts of Climate Change on Energy Systems in Global and Regional Scenarios”. In: *Nature Energy* 5.10, pp. 794–802.

Yamazaki, Daiki Ikeshima et al. (2019). “MERIT Hydro: A high-resolution global hydrography map based on latest topography datasets”. In: *Water Resources Research* 55.6, pp. 5053–5073.

Yin, Z. et al. (2020). “Improvement of the Irrigation Scheme in the ORCHIDEE Land Surface Model and Impacts of Irrigation on Regional Water Budgets Over China”. In: *Journal of Advances in Modeling Earth Systems* 12.4, e2019MS001770.

Zakeri, Behnam et al. (2015). “Electrical Energy Storage Systems: A Comparative Life Cycle Cost Analysis”. In: *Renewable and Sustainable Energy Reviews* 42, pp. 569–596.

Zemp, M. et al. (2006). “Alpine Glaciers to Disappear within Decades?” In: *Geophysical Research Letters - GEOPHYS RES LETT* 331.

Zerrahn, Alexander et al. (2017). “Long-Run Power Storage Requirements for High Shares of Renewables: Review and a New Model”. In: *Renewable and Sustainable Energy Reviews* 79, pp. 1518–1534.

Zhang, Yongqiang et al. (2016). “Multi-Decadal Trends in Global Terrestrial Evapotranspiration and Its Components”. In: *Scientific Reports* 6.1, p. 19124.

Zhou, Jian et al. (2022). “Why the Effect of CO2 on Potential Evapotranspiration Estimation Should Be Considered in Future Climate”. In: *Water* 14.6, p. 986.

Zhou, Tian et al. (2018). “Non-Stationary Hydropower Generation Projections Constrained by Environmental and Electricity Grid Operations over the Western United States”. In: *Environmental Research Letters* 13.7, p. 074035.

Zhou, Xudong et al. (2021). “Representing Human Water Management in a Land Surface Model Using a Supply/Demand Approach”. In: *Water Resources Research* 57.4, e2020WR028133.

ECOLE DOCTORALE

Titre : L'hydroélectricité à l'épreuve du changement climatique : modélisation couplée des systèmes hydrologiques et électriques pour l'adaptation et l'atténuation

Mots clés : Hydroélectricité, Changement climatique, Énergies renouvelables, Gestion de l'eau

Résumé : La production hydroélectrique française sera exposée à d'importants changements dans les années à venir. D'une part le réchauffement climatique accentue les contrastes saisonniers de précipitations et augmente la demande évaporative, modifiant les débits des rivières et donc la ressource disponible pour les centrales hydroélectriques. D'autre part, l'intégration croissante d'énergies renouvelables variables prévue par les politiques d'atténuation des émissions modifie les besoins de flexibilités du système électrique. Enfin, la gestion des réservoirs hydroélectriques dépend également des autres usages de l'eau et sera donc influencée par leur évolution. Dans cette thèse, nous proposons une approche intégrée de modélisation pour quantifier et analyser ces différents effets et leur interaction. Notre approche repose sur le couplage d'un modèle climatique de surface continentale (LSM) et d'un modèle d'optimisation du système électrique (PSM), qui nous permet de représenter conjointement les contraintes liées au climat et au système électrique. Nous représentons l'opération multi-objectifs des réservoirs hydroélectriques dans le LSM et utilisons la production simulée par le PSM comme cible pour guider l'opération des réservoirs. Inversement, les contraintes de production hydroélectriques du PSM sont définies à partir des simulations du LSM. Nous montrons que cette approche intégrée améliore à la fois la modélisation de l'écoulement des rivières dans le modèle climatique et celle du dispatch de la production dans le modèle électrique. Surtout, cela permet de simuler la réponse de la production hydroélectrique à différents scénarios de changement climatique et de système électrique. Concernant le futur de la production hydroélectrique en France, nous trouvons un effet limité du changement climatique à l'échelle annuelle mais des contrastes saisonniers plus marqués avec une augmentation de la production en hiver et une diminution en été. Par ailleurs, l'intégration d'énergies renouvelables variables modifie le profil de production des centrales réservoirs et augmente la valeur de la flexibilité offerte par les réservoirs hydroélectriques. Toutefois, notre étude met aussi en évidence une importante incertitude sur les niveaux futurs de production hydroélectrique liée aux projections climatiques, et sur les prix de l'électricité liée aux coûts de production des centrales thermiques décarbonées.

Title : Hydropower in a changing climate: coupled modeling of hydrological and electricity systems for adaptation and mitigation

Keywords : Hydropower, Climate change, Renewable energy, Water management

Abstract : French hydropower production is expected to undergo major changes in the coming years. On the one hand, global warming intensifies seasonal precipitation contrasts and increases evaporative demand, altering river flows and, consequently, the water resources available for hydropower plants. On the other hand, the growing integration of variable renewable energies, encouraged by CO2 emission mitigation policies, changes the flexibility requirements of the electrical system. Finally, the management of hydropower reservoirs also depends on the evolution of other water uses. In this thesis, we propose an integrated modeling approach to simulate and quantify these different effects and their interaction. Our approach is based on the coupling of a land surface model (LSM) and a power system optimization model (PSM), enabling us to jointly represent the constraints related to climate and the electrical system. We represent the multipurpose operation of hydropower reservoirs in the LSM and use the power generation time series simulated by the PSM as a target to guide reservoir operations. Conversely, the hydropower production constraints used in the PSM are defined based on LSM simulations. We show that this integrated approach enhances both the representation of river flows in the climate model and of production dispatch in the PSM. Most importantly, it allows us to simulate the response of hydropower production to different scenarios of climate change and power system configurations. Regarding the future of hydropower production in France, we find a limited impact of climate change at the annual scale but more pronounced seasonal contrasts, with increased production in winter and decreased production in summer. Besides, the integration of variable energy modifies the production pattern of reservoir power plants and increases the value of the flexibility provided by hydropower reservoirs. However, our study also highlights significant uncertainty in future production levels and electricity prices, linked to uncertainties in climate projections and the future cost of decarbonized thermal power plants.

Institut Polytechnique de Paris
91120 Palaiseau, France